Electronic Thesis and Dissertation Repository

3-21-2022 3:15 PM

The Bio-Mechanical Development and Kinematic Evaluation of Zone I and Zone II Injuries and their Corresponding Surgical Repair Techniques using an In-Vitro Active Finger Motion Simulator: A Cadaveric Study

Mohammad Haddara, *The University of Western Ontario*

Follow this and additional works at: https://ir.lib.uwo.ca/etd

Part of the Biomechanics and Biotransport Commons, and the Biomedical Devices and Instrumentation Commons

Abstract

Research development involving large scale joint mechanics and biomechanical adaptations is growing. However, interest in smaller scale joints, such as the fingers, is limited. Thus, the present work describes the enhancement and clinical application of a previously designed *in-vitro* active finger motion simulator in measuring and assessing intrinsic joint kinematics and tissue biomechanics including load transfer and strains induced tissues within the finger. Accuracy of electromagnetic tracking (EM) systems were evaluated compared to the standard optical tracking systems and used to develop motion derived finger joint coordinate systems. Moreover, minute strain gauges were utilized to measure strains induced by the volar plate. Multiple *in-vitro* studies involving zone I and II injuries and repairs were evaluated where joint motion kinematics, tendon loads, work of flexion (WOF), and volar plate strains were measured. Strains, tendon load, and WOF increased with each progressive injury simulation. Joint kinematics were also significantly influenced with each injury simulation. Subsequent repair of the injuries restored metrics to the near-normal state. The active motion system and the present work advances the knowledge on finger biomechanics and provides researchers with a more detailed and refined insight on the overall effect of different innovate surgical techniques, rehabilitation protocols, and traumatic injuries on the biomechanics of single, or multiple, internal structures.

Keywords

Active Motion Simulator, Tendon, Strain, Biomechanics, Joint Kinematics, *In-vitro*, Cadavers, Force, Volar Plate.

Summary for Lay Audience

The finger is composed of a series of small delicate group of bones, soft tissues, and joints that function together to simulate smooth motion. They are subjected to injuries every day and thus, proper knowledge of the internal structural integrity and the biomechanics of the finger is important for the further development of more advanced and reliable surgical and rehabilitation protocols. There is currently limited advanced research on the biomechanics of the finger, despite how susceptible they are to injury. Previous studies have used different passive and active-assisted motion methods to study the impact of different surgical techniques or suture types. However, the use of a well enhanced device for mimicking and controlling true active finger motion in the literature is lacking. A rigorous framework and understanding of how metrics are biomechanically influenced by different injury conditions and motions is vital. Misguided information or lack of knowledge can result in the overall diminishing of a patient's quality of care and life. In addition, the use of a standardized design for biomechanical and joint testing will result in more reliable findings between different groups. The purpose of this work is to further enhance a previously developed fully simulated active motion system capable of quantifying and accurately assessing finger motion and load transfers across tissues in order to contribute to the ongoing research in finger biomechanics.

Co-Authorship Statement

Chapter 1 – Introduction and Literature Review

Sole Authorship: Mohammad Haddara

Chapter Review: Louis M. Ferreira

Chapter 2 - Assessment of Spatial Tracking Technology for In-Vitro Finger Motion Studies (Optical vs. Electromagnetic tracking)

Study Design: Mohammad Haddara, Louis M. Ferreira, Ovidiu-Remus Tutunea-Fatan

Data Collection and Analysis: Mohammad Haddara

Chapter Review: Louis M. Ferreira

Chapter 3 - The Effect of Flexor Digitorum Profundus Repair Position Relative to Camper's Chiasm on Tendon Biomechanics

Study Design: Mohammad Haddara, Eric Mitchell, Louis M. Ferreira, Joshua Gillis

Data Collection and Analysis: Mohammad Haddara

Manuscript Preparation: Mohammad Haddara, Eric Mitchell

Manuscript Review: Louis M. Ferreira, Joshua Gillis

Chapter 4 - Development of an In-Vitro Swan Neck Deformity Biomechanical Model

Study Design: Mohammad Haddara, Bogdan A. Matache, Louis M. Ferreira, Nina Suh

Data Collection and Analysis: Mohammad Haddara

Manuscript Preparation: Mohammad Haddara

Manuscript Review: Stacy Fan, Bogdan A. Matache, Shrikant J. Chinchalkar, Louis M. Ferreira, Nina Suh

Chapter 5 - The Effect of a Flexor Digitorum Superficialis Hemitenodesis on Reducing Volar Plate Strains for Swan Neck Deformities

Study Design: Mohammad Haddara, Louis M. Ferreira, Nina Suh

Data Collection & Analysis: Mohammad Haddara

Manuscript Preparation: Mohammad Haddara

Manuscript Review: Assaf Kadar, Louis M. Ferreira, Nina Suh

Chapter 6 - Evaluation and Comparison of *In-vitro* Joint Kinematics using Motion-Based Coordinate System vs. Anatomical Landmarks

Study Design: Mohammad Haddara, David Axford, Louis M. Ferreira

Data Analysis: Mohammad Haddara

Manuscript Review: David Axford, Louis M. Ferreira

Chapter 7 - The Evaluation of a Novel FDP-to-Volar Plate Zone I Repair Versus Button Repair: An In-Vitro Biomechanics Study

Study Design: Mohammad Haddara, Louis M. Ferreira, Nina Suh, Joshua Gillis

Data Collection & Analysis: Mohammad Haddara

Manuscript Preparation: Mohammad Haddara

Manuscript Review: Eric Mitchell, Louis M. Ferreira, Joshua Gillis, Nina Suh

Chapter 8 – Conclusions and Future Work

Sole Authorship: Mohammad Haddara

Chapter Review: Louis M. Ferreira

Acknowledgments

I would like to begin my acknowledging my supervisor, Dr. Louis Ferreira, for allowing me to be part of such incredible work here at the lab. Thank you for the unwavering supporting me throughout my academic journey and ensuring that a clear and bright future is paved right ahead for me. You always managed to push me to limits I never thought I could reach and for that, I am beyond grateful. Working with you closely throughout my masters and my PhD has been an honour.

To Dr. Mitchell, Dr. Fan, and Dr. Kadar, thank you all for the time and effort that you put into our studies. Your hard work and dedication to these studies means a lot. If it wasn't for you, my thesis would not be where it is now so thank you. To Dr. Gillis and Dr. Suh, your contribution to this work has been extremely valuable. Your continuous support throughout all of it has not gone unnoticed. Thank you for all the long hours and mountains of emails you had to go through to ensure that my work gets recognized. I appreciate the time an efforts you both put towards my success and my future.

To Raneem, my sister and my whole heart. Thank you so much for always being there for me. Whether it was endless nights of editing or just tough days, you have always been there by my side supporting me through it all. You never fail to recognize my achievements and celebrate them. I am so incredibly proud of the woman you have become. I am beyond grateful to call you my sister, my rock, my heart. Also to the little bun in the oven, I love you so much already. Uncle can't wait to meet you.

Finally, to my parents, Moustafa Haddara and Sahar El-Arousy. Where can I even begin. Dad, thank you for always supporting me throughout all my personal and academic related decisions. Also thank you for always providing me with the upmost valuable advice throughout my life. You have always been there for me since day one helping me through the challenges I face and following up on my achievements. You will always be my role model. Mama, you're my entire life. I can't imagine how my life and state of mental health would have been if it weren't for you by my side. I thank you from the bottom of my heart. Thank you for giving me endless support and love. You gave me the confidence that I needed the most when I was down so thank you for everything you do for me. I love you.

Table of Contents

List of Tables

List of Figures

Nomenclature

$G_0(x_0,y_0,z_0)$ — Global frame and associated axes (World)

$G_R^F(x_R^F, y_R^F, z_R^F)$ — Local frame and associated axes of segment 'R' obtained with respect to a local frame definition 'F'.

S_x^y — Motion tracking sensor x about sensor y of interest (where 'x' and 'y' are defined as sensors 1, 2, 3, or 4 representing the sensors in the distal, middle, proximal, and metacarpal finger segments, respectively).

R_x^y — Rotation matrix of segment x about segment y, where x and y denote the tracking sensor associated with the segment of interest.

$\hat{u}_x^y$ — Unit direction vector computed using helical axes of segment x about segment y, where x and y denote the motion sensor associated with the segment of interest.

O_j — The origin of joint 'j' or the point midway between the center of the distal and proximal epiphysis (variable 'j' can be defined as DIPJ, PIPJ, MCPJ, and CMCJ)

Chapter 1

1   Introduction and Literature Review

OVERVIEW: This chapter begins with a review of the basic anatomy and biomechanics of the finger and then continues with an overview of injuries induced by flexor tendons, extensor mechanism, volar plate, and surrounding ligaments. Literature review regarding joint coordinate frame quantification and the various joint motion and kinematics tracking systems is discussed. This is followed by the literature review of state-of-the-art past and ongoing biomechanics simulators. This chapter concludes with the purpose behind the work and the objective toward enhancing the previously validated active finger motion simulator and its use in analyzing finger joint kinematics and measuring forces and strains induced by the tendons and tissues within the finger.

1.1   Overview of the Human Hand

The hand is one of the most intricate and significant components of the human body. It represents a mechanism of great complexity and is intimately concomitant with the human brain and the development of an individual.[1] With any mechanism, whether active or passive, functional capabilities often relate both to structural characteristics and function. Similarly, the hand functions as a product of multiple complex interactions between the motion simulated by different musculature and tendons, the stability provided by delicate ligaments, and the assembly formed by different bone and joint structures.[2] Therefore, the hand, amongst all other body parts, is an assembly that is heavily reliant on the proper and composed integrity and the flexibility of its surrounding joints, tissues, and driving mechanisms. Variations in its true anatomical structure through injuries or disorders can negatively affect the overall function of the hand. Therefore, fine understanding of the hand anatomy is important before assessing the root cause of structural variability. This research chapter will provide a detailed description of the skeletal anatomy of the human hand; including a thorough bone, tendon, and ligament focus on their contribution to certain disorders such as swan neck deformities and pulley loss. In addition, due to slight anatomical variations in the first and fifth digits (thumb and the small finger), both structures and their individual functions were omitted from this research.

1.2   Structure of the Hand

1.2.1 Bones

The bone structure of the hand is comprised of two groups; carpal bones, consisting of eight bones that make up the wrist and root of the hand, and the digit bones, or fingers, each comprised of its metacarpal and their individual phalangeal segments (Figure 1.1) [3]. The carpal bones are effective for the flexion and extension of the hand, allowing for both precise and powerful grasping. Traditionally, the carpal bones are considered part of the wrist joint as they contribute to the stability and motion of the wrist in the sagittal and coronal planes [2]. The phalanges and metacarpals however, move relative to one other and are effective for individual finger motion in the sagittal plane. There are three phalanges

that make up the structure of the finger; the proximal, middle, and distal phalanges[4]. Each with varying lengths but similar in their structural organization and function.
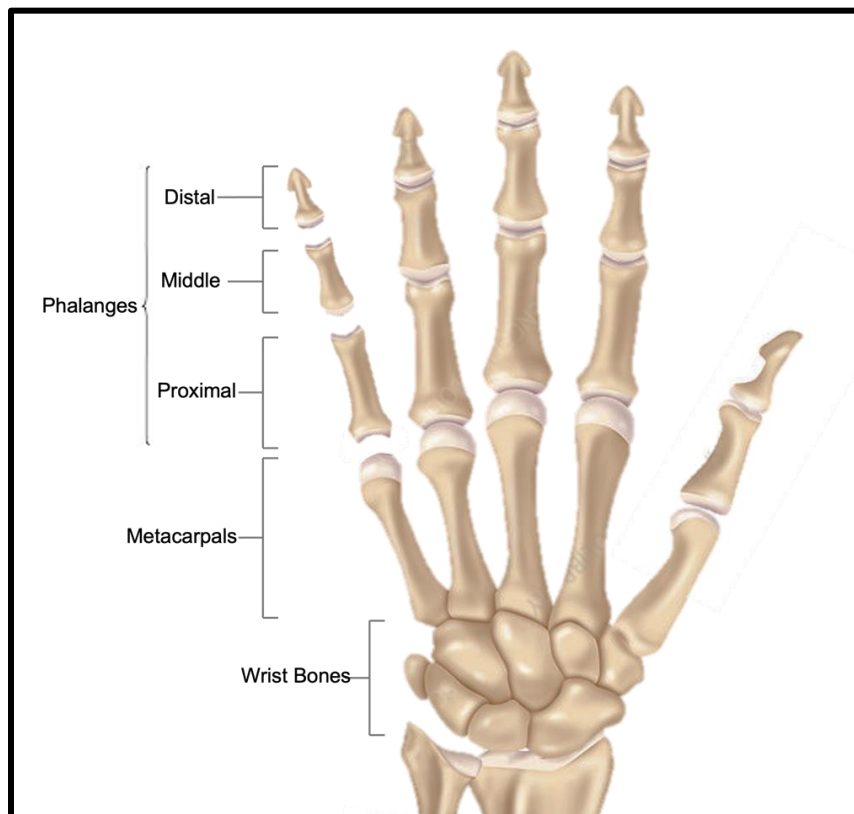
Figure 1.1 - Bone Anatomy of Hand

The bone structure of the hand including the wrist, metacarpals, and the individual phalanges are illustrated.

1.2.2 Interphalangeal Joints

The gaps formed between the second to fifth metacarpal base and phalangeal articulate with each other by small, self-lubricating cartilage covered surfaces, connected and supported by surrounding ligaments forming joints. There are three joints that form the finger; the metacarpophalangeal joint (MCPJ), proximal interphalangeal joint (PIPJ), and the distal interphalangeal joint (DIPJ) (Figure 1.2)[5]. Finger joints allow for the smooth and controlled flexion and extension of the fingers. The maximum flexion angle achieved by

joints is considerable yet vary with joints having a more extensive range between the first and second phalanges than between the second and third.

1.2.2.1 Metacarpophalangeal joints (MCPJ)

The MCPJ, commonly referred to as the knuckle, is the first and most proximal joint where the base of the metacarpals meets with the proximal phalanx. The structure of the joint allows for an average palmar flexion of 90° to 120° respectively from the index finger to the little finger. Such range of motion (ROM) of the joint permits the dorsal tip of the finger to reach the palm of the hand [6].

1.2.2.2 Proximal Interphalangeal Joints (PIPJ)

The PIPJ joint is the second, and middle joint, formed between the distal end of the proximal phalanx and the proximal end of middle phalanx. The joint allows for an ample palmar flexion of approximately 110° on each finger [6].

1.2.2.3 Distal Interphalangeal Joints (DIPJ)

The DIPJ is the third, and most distal, joint. Anatomically, the proximal and distal interphalangeal articulations are very similar with some minor differences in the structure of the surrounding ligaments and tissues that stabilize the joint; leading to smaller dimension and reduced palmar flexion of approximately 70° on each finger [6,7].
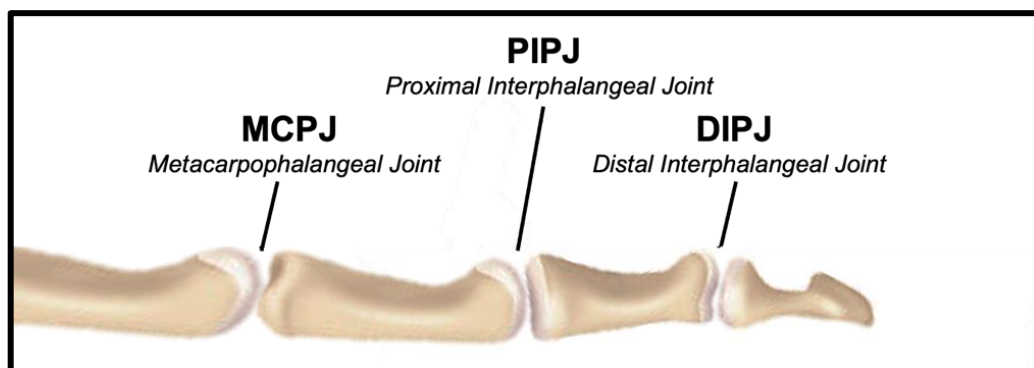
Figure 1.2 - Finger Joints

The three joints of the finger that form between the different bone segments are illustrated.

1.2.3 Muscle and Tendons

Most of the muscles responsible for wrist and finger motion originate in the forearm. Anatomically, the forearm can be divided into two compartments: anterior and posterior [8]. The anterior sector contains the group of muscles responsible for the flexion of the wrist and digits, and the supination of the forearm. The muscles that flex the digits include the flexor digitorum profundus (FDP), flexor digitorum superficialis (FDS), and the flexor pollicis longus (FPL). Structurally, The FPL muscle attaches to the thumb as it inserts into the distal phalanx, flexing the interphalangeal and the metacarpophalangeal joints of the thumb [9]. In contrast to the anterior subgroup, the posterior sector contains the subset of extensor muscle that assist in the pronation of the forearm and counteract the flexion motion achieved by the flexor muscles in the digits. Such muscles include the extensor digitorum muscle, more commonly referred to as extensor digitorum communis (EDC) [10].

Both sets of muscles, either located anteriorly or posteriorly, are adjoined to the individual digits, or bone segments, by fibrous connective tissues known as tendons. Tendons are thin and delicate structures that function by continuously transmitting forces from muscle to bone [11]. Similar to the muscle groups, tendons within the hand run along the palmar and dorsal side of the hand and are subcategorized into two tendon groups: flexor and extensor tendons, each with distinct lengths, insertion points, and function but work collectively to achieve digit flexion and extension (Figure 1.3)[12,13].
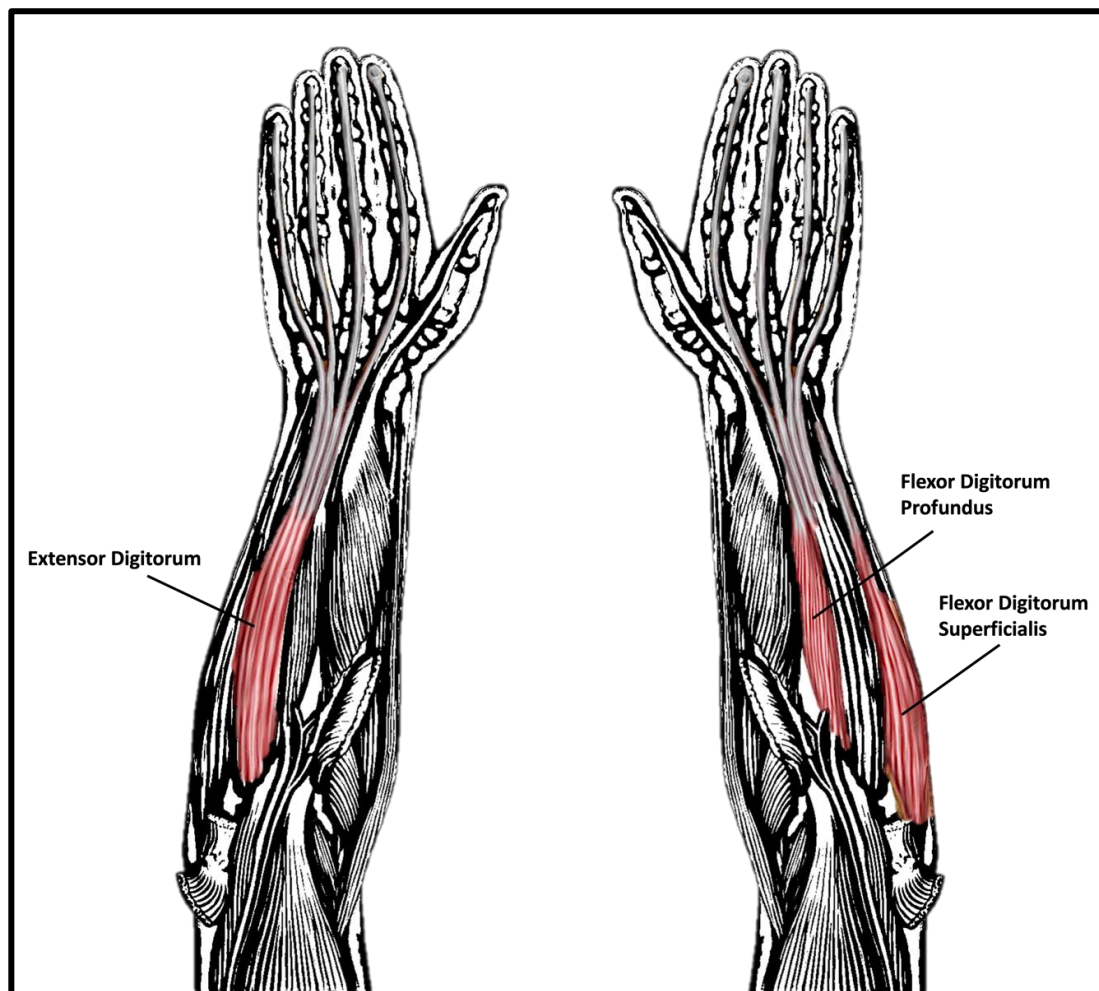
Figure 1.3 - Flexor and Extensor Muscles

A posterior view (left) and anterior view (right) of the forearm are illustrated where the extensor and flexor digitorum muscles are highlighted in red.

1.2.3.1   Extensor Digitorum Communis Tendon

The extensor digitorum communis tendon, or EDC tendon, is the primary source of digit extension for the second to fourth digits (index to ring). The tendon arises posteriorly from the EDC muscle and extends distally to the distal phalanx; inserting at multiple points along the digit [10].

1.2.3.2 Flexor Digitorum Profundus Tendon

The flexor digitorum profundus tendon, or FDP tendon, arises from the FDP muscle in the forearm and extends anteriorly and distally to its insertion point at the tip of the distal phalanx (Figure 1.4), primarily flexing the PIPJ and DIPJ along the way [14].

1.2.3.3 Flexor Digitorum Superficialis Tendon

The flexor digitorum superficialis tendon, or FDS tendon, is the second anterior flexor tendon that arises from the FDS muscle in the forearm. Unlike the FDP , FDS's insertion point extends only as far as the middle phalanx, primarily flexing the PIPJ only along its line of action [14].
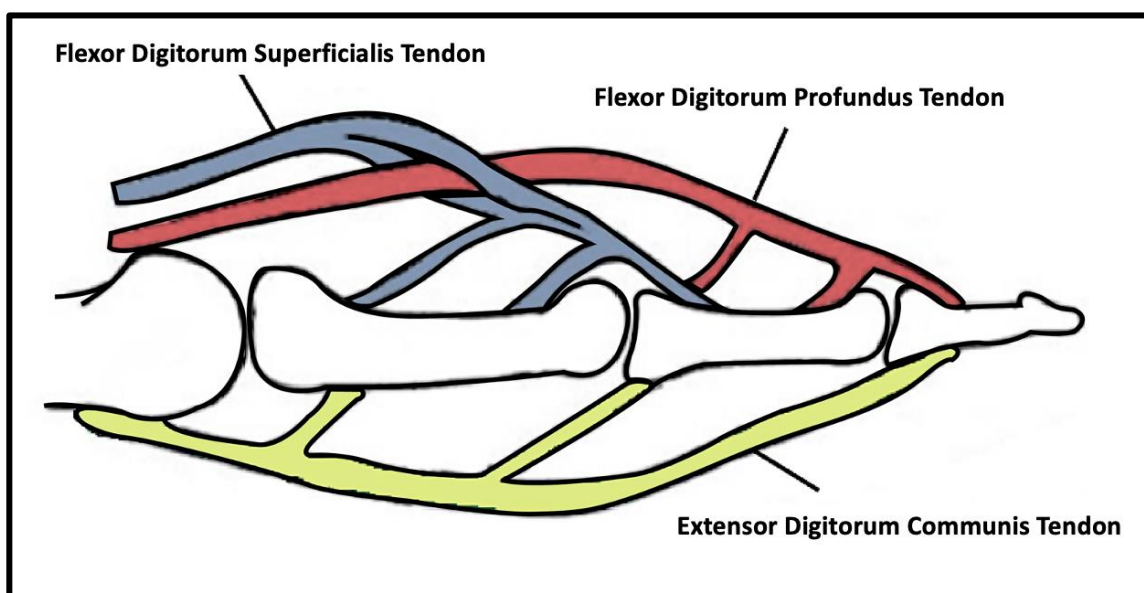
Figure 1.4 - Flexor and Extensor Tendons

The tissue and sheath are excluded to illustrate the complexity of the flexor (red: profundus, blue: superficialis) and extensor (yellow) tendon mechanism in the finger.

1.2.4 Flexor Tendon Zones

The anatomical relationship of the flexor tendons is usually discussed in terms of zones, shown in figure 1.5 below. The five zones shown were classified as distal to proximal boundaries in which prognosis is most influenced by following flexor tendon injury and repair [15–17]. Zone I consists of the FDP tendon only and is bounded proximally by the insertion of the FDS tendon and distally by the insertion of the FDP tendon into the distal phalanx. Zone II involves the proximal third of the proximal phalanx and the site where FDS tendons split into two slips allowing the FDP to pass through. These slips then divide around the FDP tendon and reunite on the dorsal aspect of the FDP, inserting into the distal end of the middle phalanx [18]. The site of bifurcation is referred to as 'Camper chiasm'. Moreover, zone II is commonly referred to as 'no man's land'; a term indicating the frequent occurrence of complications and restrictive adhesion bands that develop around lacerations in this area [19]. Proximal to zone II, the FDS tendons lie superficial to the FDP tendons. Zone III extends from the distal edge of the wrist to the proximal edge of the MCPJ, which is the entrance of the tendon sheath. Zone IV includes the wrist carpal and its contents, and Zone V extends from the origin of the flexor tendons at their respective muscle bellies to the proximal edge of the wrist [20].
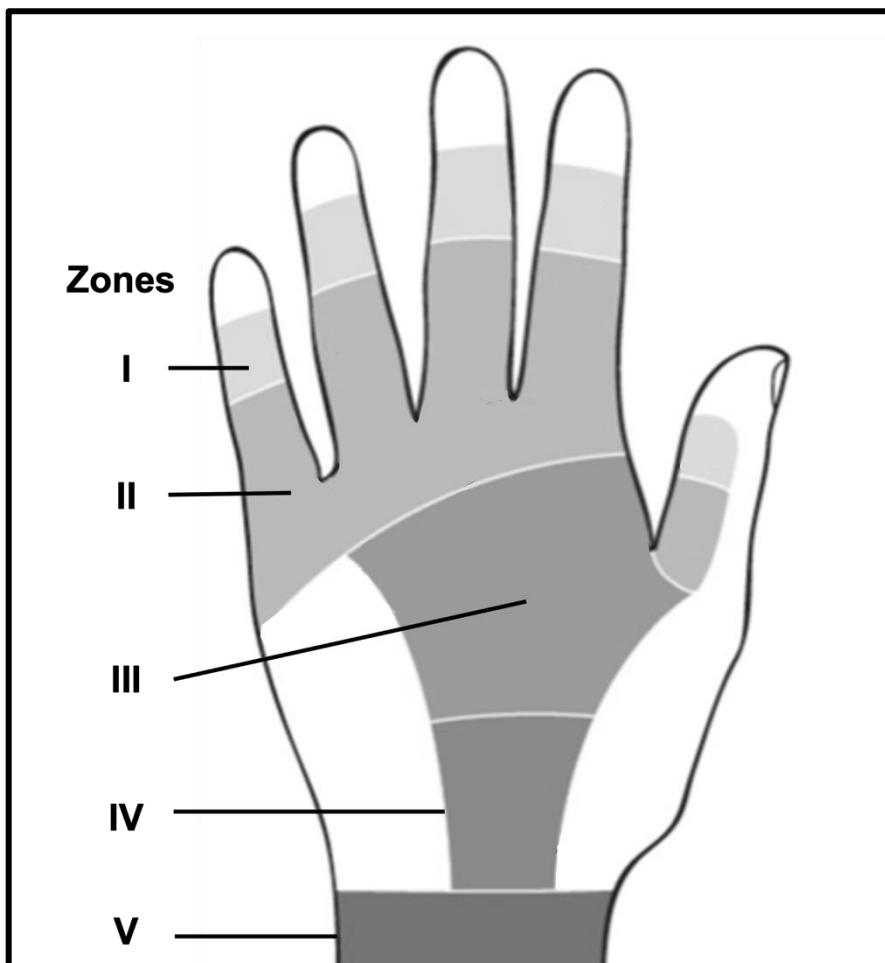
Figure 1.5 - Zones of Hand

The degree or site of injury in the hand is commonly represented by zones from 1 to 5.

1.2.5 Flexor Pulleys

The digital flexor pulley system is a complex structure composed of pulleys made of fibrous tissue condensations, encircling the flexor tendons through fibro-osseous channels that function by maintaining flexor tendons close to bone [21]. Thus, enabling the linear forces developed in the flexor muscle–tendon unit to be converted into rotation and torque at the finger joints [22]. There are five annular (A1–A5) pulleys that run along the digit in descending order from proximal to distal, each with distinct insertion points and size (Figure 1.6) [23]. The A1, A3, and A5 pulleys originate from the volar plate and adjacent bony surface of the MCPJ, PIPJ and DIPJ, respectively. The A2 and A4 pulleys originate

from, and insert directly onto the bone surface of the proximal and middle phalanges, respectively [24,25]. Loss of one or multiple pulleys through injury or rupture can lead to tendon bowstringing [26]. Tendon bowstringing is a condition where the tendon that was previously held adjacent to bone, translates away from the center of rotation of the joint; altering the flexion moment arm of the joint and therefore, resulting in a loss of strength and a decreased range of motion [27] . Mechanically, the A2 and A4 pulleys are recognized to be strongest and stiffest pulleys than the A1, A3, and A5 pulleys. [28,29]. In addition, the A2 and A4 pulleys are clinically known to be the most important pulleys for ensuring optimal transmission of forces, therefore, critical for the prevention of bowstringing [30–32]. The A3 pulley also serves an important role in regulating the degree of tendon bowstringing, as well as, it is essential in maintaining the tendons adjacent to bone due to its close positioning at the PIPJ [33].
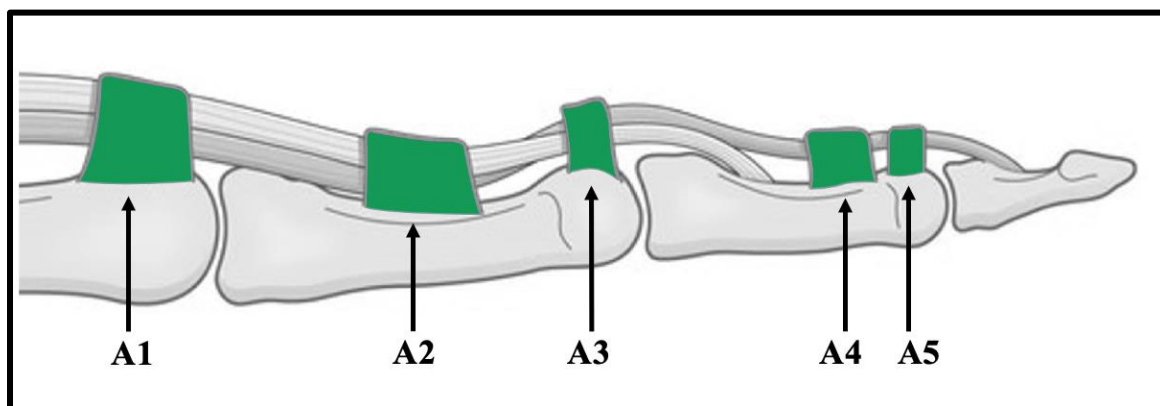
Figure 1.6 - Flexor Pulleys

The five flexor pulley (highlighted in green: A1 – A5) that hold the flexor tendons in place as illustrated along the finger.

1.2.6 Ligaments

Ligaments are strong bands comprised of fibrous connective tissues that function by maintaining close connection of bone for join stability [34]. The ligaments in the hand and wrist are categorized into intrinsic and extrinsic groups and are also placed into broader categories such as: radiocarpal, ulnocarpal, distal radioulnar, intercarpal, and

carpometacarpal ligaments. However, for the sake of relevancy, there are two ligaments, 1) the retinacular ligaments, and 2) the volar plate that play an important role in the proper stabilization of the PIPJ and thus, will be discussed.

1.2.6.1   Retinacular Ligaments

The retinacular ligaments, or commonly known as Landsmeer retinacular ligament, is small and has two bands; the oblique and transverse ligaments [35]. The oblique originates on the lateral volar side of the proximal phalanx and attaches dorsally to the common extensor tendon [36]. The transverse ligament however has a shorter course and originates and attaches closer to the joint line and inserts on the lateral side of the proximal phalanx. Mechanically, both ligaments aid in the smooth motion of the PIPJ with respect to the DIPJ during digit flexion and extension. Their anatomical structure and elasticity allows for the reinforcement of surrounding tissues; ensuring proper PIPJ stabilization during extension [35]. Contracture of the ligaments would lead to the volar translation of the lateral bands, resulting in a boutonniere deformity [37].

1.2.6.2   Volar plate

The volar plate is the strongest ligament in the finger. By forming the floor of the PIPJ, the volar plate (1) provides crucial stability against hyperextension, lateral displacement, and torsional forces that act on the PIPJ; (2) acts as a meniscus between the middle phalangeal base and proximal phalangeal head; (3) forms part of the lining of the PIP joint; and (4) provides a smooth gliding surface for the flexor tendon over the joint [38–41]. Loss or injury to the volar plate can lead to laxity and hyperextension of the PIPJ. Left untreated, and it can ultimately lead to a swan neck deformity.

1.3   Traumatic Injuries

Injuries pertaining to the hand due to trauma are common and in some cases, difficult to overcome. In fact, hand injuries account for approximately 20% of patient visits to the emergency room [42]. As a result, they impose a large economic burden of $740 million U.S. dollar annually and rank first in the order of most expensive injury types [42]. Hand or finger

pain is an enervating health concern and depending on the degree of severity, can result in an overall decrease in the quality of life and independence of those affected. Four of the most common traumatic injuries to the hand or finger include: flexor tendon laceration, flexor pulley rupture, extensor tendon tears at the distal joint resulting in mallet finger, and when left untreated, develops into a swan neck deformity.

1.3.1 Flexor Tendon Tear

Tendon injuries in general are relatively common, significantly disabling greater than 100,000 people in the United States annually and incurring a cost of up to $409 million U.S. annually for tendon injuries alone [43,44]. An estimated 24.9% of acute traumatic tendon injuries occur due to work-related injuries, 14.4% due to food preparation and serving related incidences, and 12.5% due to transportation and material moving occupations [45,46]. Flexor tendon injuries remain a formidable challenge for surgeons due to three main reasons. Firstly, flexor tendons have limited vascularity and are nourished mainly by synovial fluid. Hence, unlike other tendons in the body, flexor tendons are among the body's tissues with the poorest healing potential [47]. Therefore, surgical intervention where the two ends of the tendons are surgically brought together for healing is imperative for proper tendon repair. Secondly postoperative management needs to be carefully planned as mobilization has shown to be essential to prevent scar tissue, or adhesions, from forming; risking chances of post-op tendon rupture [48–50]. Lastly due to the unique anatomy of the tendons running through flexor pulleys to function, surgeons need to avoid increasing the bulkiness of the tendon through its sheath, which is not always possible from scarring as this affects the functional outcome of the tendon [51,52].

1.3.2 Flexor Pulley Rupture

Injuries sustained by pulleys are quite common and occur more frequently within rock climbers than other sports or activities. These injuries are the result of slips or falls in which body weight was abruptly transferred to the flexed pulley system [53,54]. Approximately 40% of all climbing injuries clinically documented involve the fingers, where 20-26% of which are directly related to pulley injuries [55,56]. Injuries can include full or partial tears of one or

more annular pulleys; significantly impacting digital performance. Biomechanical disorders can include bowstringing, decreased ROM of joints, and flexion contractures [57–61]. Many previous studies have delineated the importance of the A2 and A4 pulleys in maintaining proper finger biomechanics and reducing tendon bowstringing [62–66]. Anatomically, these pulleys shield a proportionally large area of the flexor tendons and therefore, preserving the integrity of both pulleys is important for healthy joint motion. Surgical reconstruction of pulleys generally involve harvesting a tendon graft from the same specimen and using a single, double, or triple loop technique to construct artificial pulleys around the proximal and middle phalanges [67–70].

1.3.3 Mallet Finger

Commonly referred to as mallet finger, drop finger, or baseball finger, terminal extensor tendon injuries are one of the more common types of hand injuries [71,72]. The deformity is generally a high energy injury sustained in sports and elicited by the accidental laceration or rupture of the extensor tendon at the DIPJ [73,74]. Due to the impairment of the extensor tendon mechanism, active extension of the distal phalanx is constrained and depending on the severity of the laceration, a patient can suffer from acute (0-10°) or severe (>25°) loss of DIPJ extension. The resulting imbalance between the flexor and extensor tendon mechanism can eventually lead to an early or late swan-neck deformity which can result in further loss of function [75–77]. Therefore, once induced, it is crucial for the integrity of the extensor tendon mechanism at the DIP joint to be restored. Surgical intervention to correct chronic mallet fingers is highly dependent on the severity of the deformity and can range from a conservative approach using a cast or splint therapy to help regain loss, to a more invasive approach involving surgical repair of damaged tissues or a full joint arthroplasty [78–84].

1.3.4 Swan Neck Deformity

Swan neck deformity, or SND, is a condition characterized by the permanent hyperextension of the PIPJ and the flexion of the DIPJ within a finger (Figure 1.7)[85–87]. There are several triggers that provoke the joints into a 'swan neck' state. Such causes

include neurological conditions, autoimmune disorders, rheumatoid arthritis, or other disorders and can originate at MCPJ, the PIPJ, or the DIPJ [88–93]. The imbalance within the internal structures of the digit results in the weakening of the volar plate ligament shielding the PIPJ and the translation of the retinacular ligaments which overtime, develops into the characteristic deformity [94,95]. Similar to mallet finger, SND correction can be made through a variety of nonsurgical and surgical treatment modalities used to rebalance the forces and restore the motion of the impacted joints [96,97].
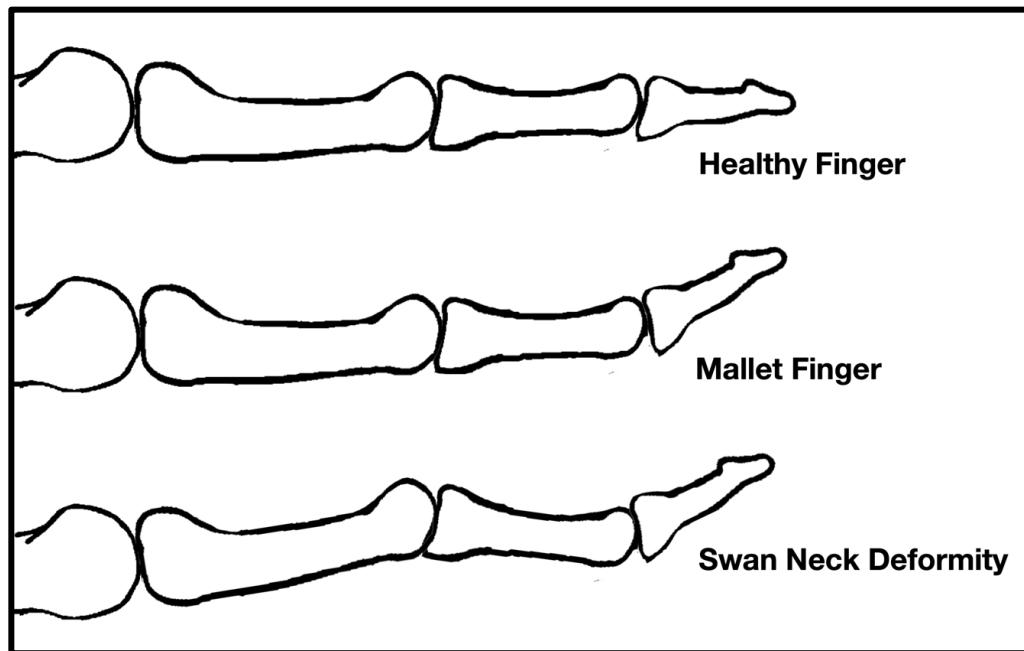
Figure 1.7 - Mallet and Swan Neck Deformity

The progression of a swan neck deformity as a result of an untreated mallet finger injury. In contrast to the healthy finger, a swan neck results in a hyperextension of the PIPJ and a flexion of the DIPJ.

1.4   Finger Joint Kinematics

1.4.1 Overview

The range of motion achieved by the different interphalangeal joints are dictated by the type of joint. The DIP and PIP joints are simple hinge joints that allow for only pure

flexion-extension of the joint with small deviations in the lateral and axis rotations [98]. The MCP joint however is a diarthrodial joint where the large convex head of the distal aspect of the metacarpals articulate with the concave-shaped proximal aspect of each phalange allowing for movement beyond flexion-extension such as abduction, adduction, and limited circumduction [99].

1.4.2 Coordinate System Definitions

Assessment of finger kinematics is relevant to many domains in biomechanics such as hand rehabilitation and finger modelling[100,101]. To measure joint kinematics, a clear and accurate assignment of a cartesian coordinate frame describing the joint's absolute and relative position and orientation within all three axes is required. Generally, joint kinematics are deduced using the relative motions between the distal and proximal segments of the finger. Once a local frame has been established for each segment, the three commonly used methods in biomechanics for dynamic finger kinematic measurement include using: i) reference frames, ii) anatomical frames, and iii) functional frames [102]. However, because the hand is composed of many relatively small segments, consensus on the most accurate method for representing joint kinematics is still being evaluated.

1.4.2.1   Reference Frame

The reference frame definition corresponds to the static alignment of the anatomical axes with an external global axes frame [102].

1.4.2.2   Anatomical Frames

The anatomical frame definition corresponds to the building of the anatomical axes using specific palpated bony landmarks and the global axes. Similar to references frames, anatomical frames are done in the static postural pose of the interphalangeal segments of interest [102]. The implementation of this definition has been used widely across finger kinematic studies and was first adapted from the proposition of the International Society of Biomechanics (ISB) [103].

1.4.2.3   Functional Frames

The functional frame definition corresponds to the implementation of a function flexion-extension axes and global axes. In contrast to the reference and anatomical frame definitions, functional frames are implemented using dynamic motion where the flexion-extension axes are quantified as the helical axes, or the relative orientation of the proximal and distal markers, during motion [102].

1.4.3 Tracking Systems

With the advancement and increase in tracking technology, there are a variety of methods currently adopted for measuring and reporting *in-vivo* and *in-vitro* joint kinematics of which most predominately include, but are not limited to, inertial sensors, goniometers, image-based tracking, electromagnetic tracking, and optical tracking.

1.4.3.1   Inertial Measurement Units

Inertial measurement units (IMU) are common and deemed well suited for motion measurements in clinical settings in comparison to other tracking methods, as they are small in size, wearable, and capable of long-term data collection, whilst preserving power consumption and minimizing cost [104–107]. IMUs are composed of accelerometers and gyroscopes to provide a direct estimate of joint angles in a three-dimensional space [108]. However, accurate estimation of joint angles is, in some case challenging due to drifting of the gyroscope, sensor to segment misalignment, and motion artifacts [109]. In addition, IMU sensors readings are noisy and may have bias. Drift can lead to physically unrealizable joint angle estimates. To avoid this, a common method used in many studies to correct gyroscope drift include introducing and applying additional kinematic constraints to the estimation model [110–112]. However, this method would require additional parameters such as sensor position and limb length to be known. Another major issue with IMUs is their sensitivity to misalignment. Joint angles should be measured in the anatomical joint coordinate system; any misalignment between the sensor local frame and the anatomical joint frame may lead to error. An exact positioning of the sensor or a calibration procedure is needed for best results [113]. Although these methods can improve accuracy, they are time

consuming and the precision depends on the accuracy of the motion executed by the subject [114].

1.4.3.2 Goniometer

A common method of joint mobility assessment is the measurement of joint range of motion, or flexibility, using a universal goniometers [115]. Goniometers measure both passive and active joint ranges by comparing the angle of two bones relative to one another [116]. Joints measured can range from larger extremities, such as a shoulder or knee, to smaller and more delicate joints such as the elbow or finger [117–119]. By aligning the stationary and movable arms of the device with specific bony landmarks on either side of the joint, the full extent of joint mobility can be measured in degrees. This method allows for a simple means to measure joint angle for *in-vitro* specimens since calibration is not required for the instrument. The largest drawback of using a goniometer is the substantial estimation errors of the position of the joint segments by the operator. In addition, some of the center of motion of some joints tend to translate with flexion/extension, however, this is usually not a concern when dealing with joints as small as the finger.

1.4.3.3 Computed Tomography

Computed Tomography, or more commonly known as CT, is a computerized x-ray imaging procedure that uses motorized x-ray beams that are aimed at a patient and quickly rotated around a section of the body to generate static cross sectional images or 'slides' of the body [120]. Each image taken is transmitted to a computer, and when digitally stacked with a number of successive others, generates a clear three-dimensional image of the segment of the patient that was intended to be captured. With every full rotation of the beam, the computer in which the CT relays information to, uses complex mathematical techniques to construct an individual 2D image slide of the patient [121]. Once one slide is accurately constructed, the x-ray scanning process is then repeated to produce another image slide. This process is repeated until the desired number of slides to properly construct a three-dimensional image is collected. The use of CT imaging in studies measuring joint kinematic is currently on the rise [122,123]. With a proper joint motion protocol conducted,

joint ranges of motion and angles can be determined by recording two separate static joint positions and subsequently, using a computer to measure the change in joint angle between the two individual images [124]. Although more time consuming, CT scans provide a high standard in imaging quality, accuracy, and repeatability. However, the biggest drawback of CT imaging is the exposure of high amounts of ionizing radiation that over time, can cause threating biological and mutational effects in living tissue [121].

1.4.3.4   Image Based Tracking

Similar to CT imaging, image based tracking, or video tracking, is the procedure in which a sequence of images or slides are taken from a video source through small skin markers attached to a portion of the body of interest, and stitched to one another to track the overall kinematics of the joint motion and trajectories [125]. However, unlike CTs, image-based tracking rely on dynamic captured motion of a patient or body segment throughout a selected course of time. Although used for joint kinematic analysis, this method of motion tracking is more commonly intended for studies involving gait analysis [126]. In addition, the risk of losing image quality can arise from loss of image depth and scale, reflective ambiguities where multiple poses produce similar images, and lost observations due to occlusions of limbs during motion

1.4.3.5   Electromagnetic Tracking Systems

Electromagnetic tracking using miniaturized electromagnetic sensors is widely used in current clinical practice [127–129]. Examples include surgical interventions, motion tracking, and implant reconstruction studies [130–135]. Electromagnetic tracking, or EM for short, is a system that functions by emitting electromagnetic fields through a transmitter, which is then captured and read by receiving coils located in minute 6 degree-of-freedom (DOF) sensors. By locating the sensors, the EM system can calculate and determine the position and orientation in real time, with respect to the position of the transmitter [136]. Unlike most other tracking methods, EM does not require direct interface between the receiver (sensor) and the transmitter to correctly locate its whereabouts in space. However, as the tracking system depends on an electromagnetic field, the tracking accuracy is heavily affected by

excessive electrical noise and magnetic field distortion [137]. The cause of noise can be from both internal and external sources. Internal sources can include variations in measurement timing, algorithm errors, etc. External sources tend to have a larger effect on the measurement noise as they include metallic objects within the field, noise generated by electrical circuits, fluorescent lighting, power supplies, and wiring with current that varies over time [135,138]. In addition, magnetic field strength decreases with distance from the generator. Therefore, as the distance between the EM transmitter and the EM sensor increases, the uncertainties including bias and jitter error of the EM system measurement become bigger [135,139].

1.4.3.6 Optical Tracking Systems

Unlike EM systems, optical tracking systems rely on infrared waves emitted by at least two cameras as a source of communication between its sensors and its system unit [140]. There are two forms of sensors associated with optical tracking: passive and active sensors. Passive sensors are generally spheres or surfaces that reflect infrared light emitted from the cameras without the need of an external power source. Therefore, direct contact between the cameras and the sensors is required for the retrieval of the position and orientation of the sensors, with respect to a fixed frame of reference. However, there is a risk of error due to potential unwanted noise from reflective surfaces in the field of view of the camera which requires filtering from the data collected. Active markers however, contain light emitting diodes (LEDs) that emit their own infrared light requiring a power source from either a battery or the terminal [141]. The intensity of light from an LED allows the point of recognition to be much smaller than a passive marker and therefore, lowering the risk of relative error when recording. By linking multiple sensors and assignment them to specific bones or important bony landmarks, joint motion and kinematics can be determined using relevant body segment coordinate systems and inverse kinematics within a computer program to determine the accurate 6D position and orientation of the joints [142,143]. With such configuration, the system is able to correctly generate and display the position and orientation of a joint or bone of interest to the user.

1.4.4 Joint Frame Quantification

Joint rotations are typically quantified using Euler angles where each angle corresponds to motions observed along its assigned axis[144–146]. As per ISB's recommendation, the origin of a coordinate system is defined as the center point along the bone segment; midway between the center of the distal and proximal heads of the bone[103]. The common +Z-axis is derived as the flexion-extension axis of the finger segment and is directed radially[103]. The +Y-axis is derived as the line parallel to the line from the center of the distal head to the midpoint of the metacarpal and is directed proximally down the bone segment[103]. Finally, the +X-axis is defined such that the X-Y plane creates a sagittal plane that splits the metacarpal bone into mirror images and is directed volarly[103].

1.4.4.1   Challenges

Quantification of a standard and accurate finger joint kinematic definition is a challenge. As previously mentioned, the finger is made up of very delicate and small structures that are easily influenced by small changes in motion. Unlike other larger scale joints such as the elbow or knee, tracking finger motion is heavily limited due to the size of the individual phalangeal segments and overall stability of the joints. In addition, the lack of having a clear and standardized method of frame definitions that can be used across all research groups is limiting. Historically, the implementation of landmark-based definition has been widely used to quantify kinematics *in-vitro*, despite the challenge of anatomy-based frames. The choice to denude segments in order to locate small anatomical features poses a large source of error and introduces both intra- and inter-user variabilities that hamper reproducibility across research groups. Moreover, the need to denude specimens often limits the ability to perform testing protocols *in-vivo*, which leads to modifications in the anatomy digitizing methods used and thus, departures from standardized approaches.

An alternative approach to bone digitization without the need to denude and adopted by research groups Coupier *et al*. and Ishii *et al.* is through coordinate registration of CT scanned skeletal models[144,147]. This approach requires the digitization of bone segments using the same motion tracking decide used to measure the kinematic of interest. This

approach has been used by multiple research studies to track joint kinematics in-vivo and in-vitro, however this extra digitization, and the corresponding transformation algebra also introduces registration errors that negatively impact the measured kinematics.

1.5   Biomechanical Testing & Motion Simulators

The investigation and treatment of finger-related pathologies require a thorough knowledge and understanding of the proper biomechanical behaviour of the individual structures of the finger such as the bones, ligaments, tendons, and soft tissues. Several methodologies, by means of biomechanical testing, have been developed and enhanced over the years to deepen the biomechanical knowledge of the finger, allowing for an advancement of surgical techniques and therapy protocols. Although many static 2D and 3D imaging modalities such as X-rays and CT images have provided sufficient information on soft tissues surrounding bones, they commonly lack the ability of providing dynamic and functional analysis on finger structures and joint kinematics. In recent years, many researchers have adopted the use of novel biomechanical simulators complimented by 3D motion capture systems, such as electromagnetic tracking or optical tracking to study dynamic finger function and joint motion.

The evolution of *in-vitro* passive and active finger motion simulators to reanimate near-normal *in-vivo* articulation through the use of cadaver specimens as musculoskeletal models has opened many doors to attaining reliable and in-depth quantitative analysis for the investigation of joint and finger kinematics. Passive motion generally involves the physical interaction of a joint or structure along its course of motion or function by an external source and with little to no effort from the patient whereas, active motion involves the use of a motorized system to simulate true near-normal structural motion. *In-vitro* experimentation provides researchers with a standardized test allowing for the simulation of highly repeatable testing protocols that effectively reduces intra-specimen variability. As such, the effects of different clinical injuries and surgical interventions can be studied, while neglecting patient-specific compensation approaches.

1.5.1 Passive Motion Simulators

Passive motion is a commonly adopted therapeutic technique that involves the movement of a joint through a desired range of motion without the patient's use of the involved extremity [148]. This motion is typically accomplished by human interaction or by the use of a machine, primarily to reduce stresses within a joint or surrounding structures post-surgery or for the sole purpose of clinical research [149]. In rehabilitation therapy, passive motion is strongly encouraged as it facilitates recovery by significantly reducing pain and increasing active joint range of motion; allowing the patient to continue an active lifestyle [150–152]. However, although effective in therapy exercise, the use of passive motion protocols in *in-vitro* finger studies are not as encouraged due to certain limitations that can affect the quality of produced results and reliability of the test. As human or motorized engagement is required to induce motion to certain finger structures, true anatomical mimicking of the finger *in-vitro* is therefore not properly replicated and can also result in unrepeatable motion, diminishing the quality of the study and the results. In addition, the lack of replicating a true in-vivo scenario during passive motion can significantly alter the internal biomechanics, resulting in slightly inaccurate findings in comparison to active motion protocols.

Sapienza *et al.* conducted a cadaveric study evaluating and comparing the flexor tendon load and excursion during passive and active motion of the index, middle, and ring fingers [153]. The cadaveric specimen was secured to a fabricated fiberglass splint with Velcro on a flat table and measurements were performed during five different simulated exercises All movements started from a resting hand position where passive exercises were performed by the examiner's hand manipulating the specimen to maintain the positions and active movements were simulated by pulling on the zone V tendon suture-loop. The tensions on the FDS or FDP tendons were measured respectively in each tendon using a pull-meter in each movement. The tension recorded for the active motions was the minimum tension necessary to perform the simulated exercise. Each measurement was performed in triplicate with the average of these values recorded for data analysis. Mean tendon forces were higher in all active versus passive movements. In addition, active motion resulted in higher tendon excursion than did passive motion. These findings further

support the inconsistency in findings between both methods in the same hand model during post-operative exercise therapy regimen.

1.5.2 Passive Motion Against Active Resistance Simulators

Human interaction in cadaveric studies is not the only approach to achieving passive motion of the finger. For example, an actuator or dead weight attached externally at the tip of the distal phalanx intended to simulate finger extension while an opposing actuator attached to the flexor tendons is simulating active finger flexion would be considered a form of passive motion against active resistance. However, unlike human interface, electrical actuators are considered more accurate as their motions are repeatable and concise with previous motion runs; providing more reliable results but are still subjected to errors if the line of action of the force applied is not aligned with the anatomy. An *in-vitro* study conducted by Yamaguchi *et al.* compared motions of these tissues in an intact and open carpal tunnel condition [154]. Using cadaver upper extremities mounted onto a motion fixture, Yamaguchi followed a passive protocol against an active resistance by fixing the proximal ends of the finger FDS tendons with sutures and connecting them to an electric motor for finger flexion simulation. In response, a 0.1 N weight was attached to the fingertips to maintain finger extension. Tendon excursion was measured using relative motion markers measured directly and captured on a digital video recording.

Another study conducted by Schweizer *et al.* evaluated the influence of a preceding flexion or extension movement on the static interaction of human finger flexor tendons and pulleys concerning flexion torque being generated. Six human fresh frozen cadaver long fingers were mounted in an isokinetic movement device for the PIPJ powered by a torque of 30 Nm. A piezoelectric force transducer was positioned at the pulp of the finger in the middle between the distal finger flexion crease and the tip of the finger. Both flexor tendons, FDP and FDS, were equally loaded with 40 N against the isokinetic movement device. This resulted in a PIP joint flexion working against the external force generated from the isokinetic movement device.

1.5.3 Active Motion Simulators

Active *in-vitro* simulation of a joint is a common methodological approach implemented in many finger related studies. Despite the use of human interaction during passive motion, *in-vivo* active motion is affected by the patient themselves, unaided by external influences. Mirroring the movement in a cadaveric specimen typically incorporate the loading of internal structures, such as muscles or tendons, through the use of a motorized system. Active motion simulators in *in-vitro* finger studies are currently on the rise [154–159]. Anatomically, they are deemed more accurate as they encompass the use of the surrounding tissues in the movement of the joints; partially replicating near-normal functional conditions of a finger *in-vivo*. In addition, the use of free weight or accurate motorized systems can result in highly repeatable motion; positively affecting the quality and reliability of the study and its results.

Deml *et al.* conducted a biomechanically cadaveric study comparing two common surgical techniques used in correcting a chronic mallet deformity: fowler central slip tenotomy vs. spiral oblique retinacular ligament reconstruction [160]. Fingers from 6 specimens were positioned in a custom setup where 4 pulleys were attached at the rear end for loading the flexors (FDP and FDS), and extensor tendons. To simulate a controlled active extension of the fingers, the extrinsic extensor tendons were loaded with a 500g mass, and the flexor tendons were loaded with 50g. Active extension using weights was carried out and constantly replicated in the same fashion from a maximally flexed finger position.

An alternative *in-vitro* finger study conducted by Cheng *et al.* involved the development of a comprehensive trigger finger cadaveric model by characterizing tendon mechanical properties such as gliding behaviors [161]. Cheng used a custom-designed frame for specimen mounting and used a 200 g free weight applied to the distal end of each flexor tendon for pre-tension purposes. However, the proximal ends of the two flexor tendons were attached to a motor system with a ring load cell in between. Motors were used to guide the tendons from full flexion to extension through a desired amount of excursion. Results obtained from this study, such as tendon and pulley gliding resistance, were used

to strengthen the knowledge of the internal characteristics and biomechanics of a finger model. Limitations of the study however include the choice of singling out the proximal bone for testing through the detachment of the metacarpal bones and the disarticulation of the finger at the PIPJ.

Both forms of joint simulation, whether through a motor or free weights, tend to achieve the same overall function. However, some differences between the two results in motors being a more favorable choice of simulation. The most relevant and significant difference is the motor's ability, more specifically servo motors, to control its position as well as the load applied onto the structure of interest. Although motors more expensive and require excessive coding and tuning to sync the motor with the simulator, they are anatomically more suitable for *in-vitro* studies and for measuring tendon excursions as they are not subjected to position error.

1.6   Thesis Rationale

Kinematic analysis and biomechanical modelling of upper limb joints has been proven valuable in clinical analysis. Assessment of hand and finger kinematics is relevant for many domains, including surgical and rehabilitation purposes. Although there is a current ongoing interest into the development of reliable and advanced upper limb models, the hand imposes a challenging obstacle due to its relatively small scale segments and joints. Providing objective measurement to better understand the relationship between bone segments and the corresponding load transfers that occur during finger motion can help clinicians establish proper patient specific therapeutic decisions and functional capabilities.

Despite the abundance of different finger frame construction methodologies, global standardization, especially for clinical applications and motion evaluation, is made difficult. The current lack of a consensus about motion representations or a standardized joint frame definition related to finger motion introduces a source of error between group findings, more prominently in cross talk errors. In addition, further refinement of a previously designed and validated *in-vitro* active finger motion simulator will allow for a more comprehensive understanding of finger biomechanics following trauma and their subsequent forms of treatment.

Therefore, the purpose of this thesis was to further develop and enhance the finger motion simulator to allow for a comprehensive and reliable measure of finger joint motion along with the quantification of intrinsic metrics of interests such as tendon loads, work of flexion, strains induced by the surrounding tissues under the influence of several clinically relevant conditions. Moreover, to propose an accurate and standardized joint frame definition that will help unite researchers in their experimental methodologies and provide valuable knowledge of healthy and pathological conditions.

1.7   Thesis Objectives and Hypothesis

1. **Objective:** Evaluating the rotational and translational accuracy and reliability of using electromagnetic tracking for joint motion tracking compared to optical tracking.

   Hypothesis: The rotational accuracy of optical tracking will be equal to, or smaller than 0.5°. Rotational accuracy of electromagnetic tracking will be within ±0.8° of optical tracking. Moreover, depth will have a more notable influence on the accuracy of optical tracking with errors as high as 0.5 mm and 0.3° in translational and rotational accuracies, respectively, compared to electromagnetic tracking.

2. **Objective:** To study the impact of injury and effectiveness of surgical treatments on finger biomechanics *in-vitro* by establishing:

   a. Distinct tendon-to-load and work of flexion relationships following the re-routing of the profundus tendon within zone II and;

   b. A finger biomechanical model using volar plate strain, tendon load, and joint range of motion following the simulation, and treatment, of a swan neck deformity.

   Hypothesis:

   a. Tendons will exhibit a linear increase in load with increasing tendon excursion. Moreover, rerouting of the tendon will decrease the gliding resistance of the repair going through the chiasm; decreasing loads in the zone.

   b. The sensitivity of the gauge will be high enough to detect changes in volar plate strain with each progression level of a swan neck deformity. Moreover, metrics measured will be repeatable to within 5%; allowing for sufficient signal to noise ratio to achieve distinguishing clinical relevant changes.

3. **Objective:** Development of novel motion derived based coordinate frame definitions for finger joint kinematic analysis.

   Hypothesis: Analysis of joint kinematics using helical axes will result in similar discrepancies (within 10°) in joint kinematic data between subjects, compared to ISB's anatomical frame definitions. Moreover, repeatability metrics made from repeated motion cycles will not exceed 5° between trials.

4. **Objective:** To combine the individually developed and enhanced biomechanical tools developed throughout this thesis, and apply them within an *in-vitro* cadaveric test where tendon load, excursions, volar plate strain, and joint kinematics metrics are evaluated simultaneously.

   Hypothesis: Advancements in the finger motion system will allow for a comprehensive evaluation of multiple discrete metrics within the finger.

1.8   Thesis Overview

The structure of the following chapters is as follows:

- **Chapter 2**: Evaluation and assessment of the translational and rotational accuracy of electromagnetic tracking compared to optical tracking.
- **Chapter 3**: Zone II Tendon Study; an *in-vitro* study investigating the effects of repairing a lacerated flexor profundus tendon within-chiasm vs. outside-chiasm. Flexor tendon loads, work of flexion, finger joint ROM, and tendon excursion are evaluated and compared between conditions.
- **Chapter 4**: Swan Neck Model; an *in-vitro* study involving the development of a swan neck deformity biomechanical model using tendon loads, joint ROM, and volar plate strains as metrics of analysis.
- **Chapter 5**: FDS Hemitenodesis Repair; an *in-vitro* study where two different SND repair techniques are simulated and biomechanically compared using tendon loads, tendon excursion, joint ROM, and volar plate strains

- **Chapter 6**: Helical Axes; motion derived finger coordinate system frames are applied, examined, and compared to the standard ISB recommended definition in reproducibility and repeatability of each selected joint coordinate system during finger flexion and extension motion.
- **Chapter 7**: Strain Gauge Refinement and Volar Plate Repair Study; a benchmark test is conducted to increase the sensitivity of the strain gauge and then applied *in-vitro* in a study investigating the reliability of a novel volar plate technique in restoring tendon load, work of flexion, and joint kinematics following zone 1 tendon avulsion, compared to the standardly used pull-out button technique.
- **Chapter 8**: Summary, conclusions and future work

1.9   References

1.   Taylor CL, Schwarz RJ. The Anatomy and Mechanics of the Human Hand. *Artif Limbs*. 1955;2(2):22-35.

2.   Panchal-Kildare S, Malone K. Skeletal Anatomy of the Hand. *Hand Clin*. 2013;29(4):459-471. doi:10.1016/j.hcl.2013.08.001

3.   Ombregt L. Applied anatomy of the wrist, thumb and hand. In: *A System of Orthopaedic Medicine*. Elsevier; 2013:e102-e111. doi:10.1016/b978-0-7020-3145-8.00072-7

4.   Taghinia AH, Talbot SG. Phalangeal and Metacarpal Fractures. *Clin Plast Surg*. 2019;46(3):415-423. doi:10.1016/j.cps.2019.02.011

5.   Doyle JR, Botte MJ. *Surgical Anatomy of the Hand and Upper Extremity*. Lippincott Williams & Wilkins; 2003. https://books.google.ca/books?id=96jG5n-vmPcC&dq=Anatomy+of+the+hand&lr=&source=gbs_navlinks_s. Accessed April 13, 2017.

6.   Vargas A, Chiapas-Gasca K, Hernández-Díaz C, et al. Clinical Anatomy of the Hand. *Reumatol Clin*. 2012;8(SUPPL.2):25-32. doi:10.1016/j.reuma.2012.10.004

7.   Fontaine C, Wavreille G, Chantelot C, Prodhomme G. Surgical anatomy of the dorsal face of the hand and the wrist. *Chir Main*. 2005;24(2):64-78. doi:10.1016/j.main.2005.01.007

8.   Zajac FE. Muscle and tendon: properties, models, scaling, and application to biomechanics and motor control. *Crit Rev Biomed Eng*. 1989;17(4):359-411.

9.   Boles CA, Kannam S, Cardwell AB. The Forearm: Anatomy of Muscle Compartments and Nerves. *Am J Roentgenol*. 2000;174(1):151-159. doi:10.2214/ajr.174.1.1740151

10.   Hirai Y, Yoshida K, Yamanaka K, Inoue A, Yamaki K, Yoshizuka M. An anatomic study of the extensor tendons of the human hand. *J Hand Surg Am*. 2001;26(6):1009-1015. doi:https://doi.org/10.1016/S0363-5023(01)70045-7

11.   Kannus P. Structure of the tendon connective tissue. *Scand J Med Sci Sport*. 2000;10(6):312-320. doi:10.1034/j.1600-0838.2000.010006312.x

12.   Elliott DH. Structure and Function of Mammalian Tendon. *Biol Rev Camb Philos Soc*. 1965;40:392-421. doi:10.1111/j.1469-185x.1965.tb00808.x

13.   Wehbé MA, Hunter JM. Flexor tendon gliding in the hand. Part I. In vivo excursions. *J Hand Surg Am*. 1985;10(4):570-574. doi:10.1016/S0363-5023(85)80085-X

14.   Idler RS. Anatomy and biomechanics of the digital flexor tendons. *Hand Clin*. 1985;1(1):3-11.

15.   Strickland JW. Flexor tendon repair. *Hand Clin*. 1985;1(1):55-68.

16.   Venkatramani H, Varadharajan V, Bhardwaj P, Vallurupalli A, Sabapathy SR. Flexor tendon injuries. *J Clin Orthop trauma*. 2019;10(5):853-861. doi:10.1016/j.jcot.2019.08.005

17.   Klifto CS, Capo JT, Sapienza A, Yang SS, Paksima N. Flexor Tendon Injuries. *J*

Am Acad Orthop Surg. 2018;26(2):e26-e35. doi:10.5435/JAAOS-D-16-00316

18. Asmus A, Kim S, Millrose M, Jodkowski J, Ekkernkamp A, Eisenschenk A. [Rehabilitation after flexor tendon injuries of the hand]. *Orthopade*. 2015;44(10):786-802. doi:10.1007/s00132-015-3160-6

19. Bunnell S. *Surgery of the Hand*. 2nd ed. Philadelphia : J.B. Lippincott Co.; 1948.

20. Collocott SJF, Kelly E, Foster M, Myhr H, Wang A, Ellis RF. A randomized clinical trial comparing early active motion programs: Earlier hand function, TAM, and orthotic satisfaction with a relative motion extension program for zones V and VI extensor tendon repairs. *J hand Ther Off J Am Soc Hand Ther*. March 2019. doi:10.1016/j.jht.2018.10.003

21. Zafonte B, Rendulic D, Szabo RM. Flexor Pulley System: Anatomy, Injury, and Management. *J Hand Surg Am*. 2014;39(12):2525–2532.

22. Lin GT, Amadio PC, An KN, Cooney WP. Functional anatomy of the human digital flexor pulley system. *J Hand Surg Am*. 1989;14(6):949-956.

23. Godfrey J, Rayan GM. Anatomy of the Volar Retinacular Elements of the Hand: A Unified Nomenclature. *J Hand Surg Am*. 2018;43(3):260-270. doi:10.1016/j.jhsa.2017.12.015

24. Dy CJ, Daluiski A. Flexor Pulley Reconstruction. *Hand Clin*. 2013;29(2):235-242. doi:https://doi.org/10.1016/j.hcl.2013.02.005

25. Clark T, Skeete K, Amadio P. Flexor tendon pulley reconstruction. *J Hand Surg Am*. 2010;35(10):9.

26. Doyle JR. Anatomy of the finger flexor tendon sheath and pulley system. *J Hand Surg Am*. 1988;13(4):473-484. doi:10.1016/S0363-5023(88)80082-0

27. Schöffl I, Oppelt K, Jüngert J, et al. The influence of concentric and eccentric loading on the finger pulley system. *J Biomech*. 2009;42(13):2124-2128.

doi:10.1016/j.jbiomech.2009.05.033

28. Lin GT, Cooney WP, Amadio PC, An KN. Mechanical properties of human pulleys. *J Hand Surg Br*. 1990;15(4):429-434. doi:10.1016/0266-7681(90)90085-i

29. Jones MM, Amis AA. The fibrous flexor sheaths of the fingers. *J Anat*. 1988;156:185-196.

30. Chow JC, Sensinger J, McNeal D, Chow B, Amirouche F, Gonzalez M. Importance of proximal A2 and A4 pulleys to maintaining kinematics in the hand: a biomechanical study. *Hand (N Y)*. 2014;9(1):105-111. doi:10.1007/s11552-013-9547-0

31. Amadio PC, Lin GT, An K-N. Anatomy and pathomechanics of the flexor pulley system. *J Hand Ther*. 1989;2(2):138-141. doi:https://doi.org/10.1016/S0894-1130(89)80051-1

32. Dunlap J, McCarthy JA, Joyce ME, Manske PR. Biomechanical and histologic evaluations of pulley reconstructions in nonhuman primates. *J Hand Surg Am*. 1990;15(1):57-63. doi:https://doi.org/10.1016/S0363-5023(09)91106-6

33. Roloff I, Schöffl VR, Vigouroux L, Quaine F. Biomechanical model for the determination of the forces acting on the finger pulley system. *J Biomech*. 2006;39(5):915-923. doi:10.1016/j.jbiomech.2005.01.028

34. Leggit JC, Meko CJ. Acute finger injuries: part I. Tendons and ligaments. *Am Fam Physician*. 2006;73(5):810-816.

35. Leis VM, Kasdan ML. Examination and anatomy of the hand. *Occup Med*. 1998;13(3):475-488.

36. El-Gammal TA, Steyers CM, Blair WF, Maynard JA. Anatomy of the oblique retinacular ligament of the index finger. *J Hand Surg Am*. 1993;18(4):717-721. doi:10.1016/0363-5023(93)90326-X

37.   Adkinson JM, Johnson SP, Chung KC. The clinical implications of the oblique
        retinacular ligament. *J Hand Surg Am*. 2014;39(3):535-541.
        doi:10.1016/j.jhsa.2013.12.011

38.   Williams EH, McCarthy E, Bickel KD. The histologic anatomy of the volar plate.
        J Hand Surg Am. 1998;23(5):805-810. doi:10.1016/S0363-5023(98)80154-8

39.   Bowers WH, Wolf JWJ, Nehil JL, Bittinger S. The proximal interphalangeal joint
        volar plate. I. An anatomical and biomechanical study. *J Hand Surg Am*.
        1980;5(1):79-88.

40.   Gad P. The anatomy of the volar part of the capsules of the finger joints. *J Bone
        Joint Surg Br*. 1967;49(2):362-367.

41.   Watanabe H, Hashizume H, Inoue H, Ogura T. Collagen framework of the volar
        plate of human proximal interphalangeal joint. *Acta Med Okayama*.
        1994;48(2):101-108. doi:10.18926/AMO/31103

42.   de Putter CE, Selles RW, Polinder S, Panneman MM, Hovius SR, van Beeck EF.
        Economic Impact of Hand and Wrist Injuries: Health-Care Costs and Productivity
        Costs in a Population-Based Study. *J Bone Jt Surgery-American Vol*.
        2012;94(9):e56-1-7. doi:10.2106/JBJS.K.00561

43.   Mehrzad R, Mookerjee V, Schmidt S, Jehle CC, Kiwanuka E, Liu PY. The
        Economic Impact of Flexor Tendon Lacerations of the Hand in the United States.
        Ann Plast Surg. 2019;83(4):419-423. doi:10.1097/SAP.0000000000001950

44.   Griffin M, Hindocha S, Jordan D, Saleh M, Khan W. An overview of the
        management of flexor tendon injuries. *Open Orthop J*. 2012;6:28-35.
        doi:10.2174/1874325001206010028

45.   de Jong JP, Nguyen JT, Sonnema AJM, Nguyen EC, Amadio PC, Moran SL. The
        incidence of acute traumatic tendon injuries in the hand and wrist: a 10-year
        population-based study. *Clin Orthop Surg*. 2014;6(2):196-202.

doi:10.4055/cios.2014.6.2.196

46.   Clayton RAE, Court-Brown CM. The epidemiology of musculoskeletal tendinous and ligamentous injuries. *Injury*. 2008;39(12):1338-1344. doi:10.1016/j.injury.2008.06.021

47.   Boyer MI. Flexor tendon biology. *Hand Clin*. 2005;21(2):159-166. doi:10.1016/j.hcl.2004.11.009

48.   Samora JB, Klinefelter RD. Flexor Tendon Reconstruction. *J Am Acad Orthop Surg*. 2016;24(1):28-36. doi:10.5435/JAAOS-D-14-00195

49.   Moore T, Anderson B, Seiler JG 3rd. Flexor tendon reconstruction. *J Hand Surg Am*. 2010;35(6):1025-1030. doi:10.1016/j.jhsa.2010.03.042

50.   Khor WS, Langer MF, Wong R, Zhou R, Peck F, Wong JKF. Improving Outcomes in Tendon Repair: A Critical Look at the Evidence for Flexor Tendon Repair and Rehabilitation. *Plast Reconstr Surg*. 2016;138(6):1045e-1058e. doi:10.1097/PRS.0000000000002769

51.   Matarrese MR, Hammert WC. Flexor tendon rehabilitation. *J Hand Surg Am*. 2012;37(11):2386-2388. doi:10.1016/j.jhsa.2012.07.020

52.   Thomopoulos S, Parks WC, Rifkin DB, Derwin KA. Mechanisms of tendon injury and repair. *J Orthop Res Off Publ Orthop Res Soc*. 2015;33(6):832-839. doi:10.1002/jor.22806

53.   Bollen SR. Soft tissue injury in extreme rock climbers. *Br J Sports Med*. 1988;22(4):145-147. http://www.ncbi.nlm.nih.gov/pubmed/3228682. Accessed July 17, 2017.

54.   Bollen SR, Gunson CK. Hand injuries in competition climbers. *Br J Sports Med*. 1990;24(1):16-18. doi:10.1136/bjsm.24.1.16

55.   Schöffl V, Hochholzer T, Winkelmann HP, Strecker W. Pulley injuries in rock

climbers. *Wilderness Environ Med*. 2003;14(2):94-100. http://www.ncbi.nlm.nih.gov/pubmed/12825883. Accessed July 17, 2017.

56. Rohrbough JT, Mudge MK, Schilling RC. Overuse injuries in the elite rock climber. *Med Sci Sports Exerc*. 2000;32(8):1369-1372. http://www.ncbi.nlm.nih.gov/pubmed/10949000. Accessed July 17, 2017.

57. Hume EL, Hutchinson DT, Jaeger SA, Hunter JM. Biomechanics of pulley reconstruction. *J Hand Surg Am*. 1991;16(4):722-730. http://www.ncbi.nlm.nih.gov/pubmed/1880373. Accessed September 20, 2018.

58. Bowers WH, Kuzma GR, Bynum DK. Closed traumatic rupture of finger flexor pulleys. *J Hand Surg Am*. 1994;19(5):782-787. doi:10.1016/0363-5023(94)90183-X

59. Strickland JW. Management of acute flexor tendon injuries. *Orthop Clin North Am*. 1983;14(4):827-849.

60. Mehta V, Phillips C. Flexor tendon pulley reconstruction. *Hand Clin*. 2005;21(2):245-251.

61. Manske PR, Lesker PA. Palmar aponeurosis pulley. *J Hand Surg Am*. 1983;8(3):259-263. doi:10.1016/s0363-5023(83)80154-3

62. Rispler D, Greenwald D, Shumway S, Allan C, Mass D. Efficiency of the flexor tendon pulley system in human cadaver hands. *J Hand Surg Am*. 1996;21(3):444-450. doi:10.1016/S0363-5023(96)80361-3

63. Kwai Ben I, Elliot D. "Venting" or partial lateral release of the A2 and A4 pulleys after repair of zone 2 flexor tendon injuries. *J Hand Surg Br*. 1998;23(5):649-654. http://www.ncbi.nlm.nih.gov/pubmed/9821612. Accessed July 24, 2017.

64. Mitsionis G, Fischer KJ, Bastidas JA, Grewal R, Pfaeffle HJ, Tomaino MM. Feasibility of Partial A2 and A4 Pulley Excision: Residual Pulley Strength. *J Hand Surg Am*. 2000;25(1):90-94. doi:10.1054/jhsb.1999.0332

65. Lister GD. Reconstruction of pulleys employing extensor retinaculum. *J Hand Surg Am*. 1979;4(5):461-464.

66. Manske PR, Lesker PA. Strength of human pulleys. *Hand*. 1977;9(2):147-152. doi:10.1016/s0072-968x(77)80009-0

67. Lin GT, Amadio PC, An KN, Cooney WP, Chao EY. Biomechanical analysis of finger flexor pulley reconstruction. *J Hand Surg Br*. 1989;14(3):278-282.

68. LITTLER JW. Free tendon grafts in secondary flexor tendon repair. *Am J Surg*. 1947;74(3):315-321. doi:10.1016/0002-9610(47)90118-9

69. Boyes JH, Stark HH. Flexor-tendon grafts in the fingers and thumb. A study of factors influencing results in 1000 cases. *J Bone Joint Surg Am*. 1971;53(7):1332-1342.

70. Landsmeer JM. A report on the coordination of the interphalangeal joints of the human finger and its disturbances. *Acta Morphol Neerl Scand*. 1958;2(1):59-84.

71. Oravcová D. Injury of the extensor mechanism in the zone I - mallet deformity. *Rozhl Chir*. 2014;93(3):117-122. http://www.ncbi.nlm.nih.gov/pubmed/24720714. Accessed July 18, 2017.

72. Ramponi DR, Hellier SD. Mallet Finger. *Adv Emerg Nurs J*. 2019;41(3):198-203. doi:10.1097/TME.0000000000000251

73. Stark HH, Boyes JH, Wilson JN. Mallet Finger. *JBJS*. 1962;44(6). https://journals.lww.com/jbjsjournal/Fulltext/1962/44060/Mallet_Finger.2.aspx.

74. Bendre AA, Hartigan BJ, Kalainov DM. Mallet Finger. *JAAOS - J Am Acad Orthop Surg*. 2005;13(5). https://journals.lww.com/jaaos/Fulltext/2005/09000/Mallet_Finger.7.aspx.

75. Okafor B, Mbubaegbu C, Munshi I, Williams DJ. Mallet Deformity of the Finger. *Bone Joint J*. 1997;79-B(4). http://bjj.boneandjoint.org.uk/content/79-

B/4/544.short. Accessed July 18, 2017.

76. Lamaris GA, Matthew MK. The Diagnosis and Management of Mallet Finger Injuries. *Hand (N Y)*. 2017;12(3):223-228. doi:10.1177/1558944716642763

77. Rosinsky P, Sarig O, David Y, Oron A. [MALLET FINGER - DIAGNOSIS, CLASSIFICATION AND TREATMENT]. *Harefuah*. 2018;157(2):104-107.

78. Yan H, Tan Q, Zhou S, et al. [Short-term effectiveness of Kirschner wire elastic fixation in treatment of Doyle type and mallet finger]. *Zhongguo Xiu Fu Chong Jian Wai Ke Za Zhi*. 2017;31(11):1287-1290. doi:10.7507/1002-1892.201706051

79. Crawford GP. The Molded Polythene Splint for Mallet Finger Deformities. *J Hand Surg Am*. 1984;9(2):231-237. http://www.ncbi.nlm.nih.gov/pubmed/6715831. Accessed July 18, 2017.

80. Warren RA, Norris SH, Ferguson DG. Mallet finger: a Trial of Two Splints. *J Hand Surg Br*. 1988;13(2):151-153. http://www.ncbi.nlm.nih.gov/pubmed/3385289. Accessed July 18, 2017.

81. Lin JS, Samora JB. Surgical and Nonsurgical Management of Mallet Finger: A Systematic Review. *J Hand Surg Am*. 2018;43(2):146-163.e2. doi:10.1016/j.jhsa.2017.10.004

82. Smit JM, Beets MR, Zeebregts CJ, Rood A, Welters CFM. Treatment Options for Mallet Finger: A Review. *Plast Reconstr Surg*. 2010;126(5). https://journals.lww.com/plasreconsurg/Fulltext/2010/11000/Treatment_Options_for_Mallet_Finger__A_Review.24.aspx.

83. Patel MR, Desai SS, Bassini-Lipson L. Conservative management of chronic mallet finger. *J Hand Surg Am*. 1986;11(4):570-573. doi:10.1016/S0363-5023(86)80202-7

84. Kalainov DM, Hoepfner PE, Hartigan BJ, Carroll C, Genuario J. Nonsurgical Treatment of Closed Mallet Finger Fractures. *J Hand Surg Am*. 2005;30(3):580-

586. doi:https://doi.org/10.1016/j.jhsa.2005.02.010

85. Ridley WE, Xiang H, Han J, Ridley LJ. Swan neck deformity. *J Med Imaging Radiat Oncol*. 2018;62:159-160. doi:10.1111/1754-9485.31_12786

86. Elzinga K, Chung KC. Managing Swan Neck and Boutonniere Deformities. *Clin Plast Surg*. 2019;46(3):329-337. doi:10.1016/j.cps.2019.02.006

87. Lane R, Nallamothu S V. Swan-Neck Deformity. In: Treasure Island (FL); 2019.

88. Dreyfus JN, Schnitzer TJ. Pathogenesis and differential diagnosis of the swan-neck deformity. *Semin Arthritis Rheum*. 1983;13(2):200-211. doi:10.1016/0049-0172(83)90007-0

89. Carlson EJ, Carlson MG. Treatment of swan neck deformity in cerebral palsy. *J Hand Surg Am*. 2014;39(4):768-772. doi:10.1016/j.jhsa.2014.01.039

90. Nalebuff EA. The rheumatoid swan-neck deformity. *Hand Clin*. 1989;5(2):203-214. http://www.ncbi.nlm.nih.gov/pubmed/2661576. Accessed November 6, 2019.

91. Bullock J, Rizvi SAA, Saleh AM, et al. Rheumatoid arthritis: A brief overview of the treatment. *Med Princ Pract*. 2019;27(6):501-507. doi:10.1159/000493390

92. Vigneron AM, Lioté F. Marfan syndrome. *Rev du Rhum Monogr*. 2019;86(2):113-119. doi:10.1016/j.monrhu.2019.02.004

93. Erçöçen AR, Yenidünya MO, Yilmaz S, Ozbek MR. Dynamic swan neck deformity in a patient with Ehlers-Danlos syndrome. *J Hand Surg Br*. 1997;22(1):128-130. doi:10.1016/s0266-7681(97)80039-3

94. Vedel PN, Tranum-Jensen J, Dahlin LB, Brogren E, Soe NH. [Deformities of the finger joints]. *Ugeskr Laeger*. 2017;179(48).

95. Lane R, Nallamothu S V. Swan-Neck Deformity. In: Treasure Island (FL); 2020.

96. Fox PM, Chang J. Treating the Proximal Interphalangeal Joint in Swan Neck and

Boutonniere Deformities. *Hand Clin*. 2018;34(2):167-176. doi:10.1016/j.hcl.2017.12.006

97. Vishwanathan K, Ganjiwale D. A novel surgical correction and innovative splint for swan neck deformity in hypermobility syndrome. *J Fam Med Prim Care*. 2018;7(1):242. doi:10.4103/jfmpc.jfmpc_14_17

98. Gupton M, Munjal A, Terreberry RR. Anatomy, Hinge Joints. *StatPearls*. July 2021. https://www.ncbi.nlm.nih.gov/books/NBK518967/. Accessed October 19, 2021.

99. Benson DC, Graefe S, Varacallo M. Anatomy, Shoulder and Upper Limb, Metacarpophalangeal Joints. *StatPearls*. August 2021. https://www.ncbi.nlm.nih.gov/books/NBK538428/. Accessed October 19, 2021.

100. Carpinella I, Mazzoleni P, Rabuffetti M, Thorsen R, Ferrarin M. Experimental protocol for the kinematic analysis of the hand: Definition and repeatability. *Gait Posture*. 2006;23(4):445-454. doi:10.1016/J.GAITPOST.2005.05.001

101. Sancho-Bru JL, Pérez-González A, Vergara-Monedero M, Giurintano D. A 3-D dynamic model of human finger for studying free movements. *J Biomech*. 2001;34(11):1491-1500. doi:10.1016/S0021-9290(01)00106-3

102. Goislard de Monsabert B, Visser JMA, Vigouroux L, Van der Helm FCT, Veeger HEJ. Comparison of three local frame definitions for the kinematic analysis of the fingers and the wrist. *J Biomech*. 2014;47(11):2590-2597. doi:10.1016/j.jbiomech.2014.05.025

103. Wu G, van der Helm FCT, Veeger HEJD, et al. ISB recommendation on definitions of joint coordinate systems of various joints for the reporting of human joint motion--Part II: shoulder, elbow, wrist and hand. *J Biomech*. 2005;38(5):981-992. doi:10.1016/j.jbiomech.2004.05.042

104. Fong DT-P, Chan Y-Y. The use of wearable inertial motion sensors in human

lower limb biomechanics studies: a systematic review. *Sensors (Basel)*. 2010;10(12):11556-11565. doi:10.3390/s101211556

105. Valldeperes A, Altuna X, Martinez-Basterra Z, et al. Wireless inertial measurement unit (IMU)-based posturography. *Eur Arch oto-rhino-laryngology Off J Eur Fed Oto-Rhino-Laryngological Soc Affil with Ger Soc Oto-Rhino-Laryngology - Head Neck Surg*. 2019;276(11):3057-3065. doi:10.1007/s00405-019-05607-1

106. Kianifar R, Joukov V, Lee A, Raina S, Kulić D. Inertial measurement unit-based pose estimation: Analyzing and reducing sensitivity to sensor placement and body measures. *J Rehabil Assist Technol Eng*. 2019;6:2055668318813455. doi:10.1177/2055668318813455

107. Byun S, Lee HJ, Han JW, Kim JS, Choi E, Kim KW. Walking-speed estimation using a single inertial measurement unit for the older adults. *PLoS One*. 2019;14(12):e0227075. doi:10.1371/journal.pone.0227075

108. Yoon T-L, Kim H-N, Min J-H. Validity and Reliability of an Inertial Measurement Unit-based 3-Dimensional Angular Measurement of Cervical Range of Motion. *J Manipulative Physiol Ther*. 2019;42(1):75-81. doi:10.1016/j.jmpt.2018.06.001

109. Seel T, Raisch J, Schauer T. IMU-based joint angle measurement for gait analysis. *Sensors (Basel)*. 2014;14(4):6891-6909. doi:10.3390/s140406891

110. Slajpah S, Kamnik R, Munih M. Kinematics based sensory fusion for wearable motion assessment in human walking. *Comput Methods Programs Biomed*. 2014;116(2):131-144. doi:10.1016/j.cmpb.2013.11.012

111. Bonnet V, Mazzà C, Fraisse P, Cappozzo A. A least-squares identification algorithm for estimating squat exercise mechanics using a single inertial measurement unit. *J Biomech*. 2012;45(8):1472-1477. doi:10.1016/j.jbiomech.2012.02.014

112. Lin JFS, Kulić D. Human pose recovery using wireless inertial measurement units. *Physiol Meas*. 2012;33(12):2099-2115. doi:10.1088/0967-3334/33/12/2099

113. Cho Y-S, Jang S-H, Cho J-S, et al. Evaluation of Validity and Reliability of Inertial Measurement Unit-Based Gait Analysis Systems. *Ann Rehabil Med*. 2018;42(6):872-883. doi:10.5535/arm.2018.42.6.872

114. Koska D, Gaudel J, Hein T, Maiwald C. Validation of an inertial measurement unit for the quantification of rearfoot kinematics during running. *Gait Posture*. 2018;64:135-140. doi:10.1016/j.gaitpost.2018.06.007

115. Norkin C, White D. *Measurement of Joint Motion : A Guide to Goniometry*. 5th ed. Jaypee Brothers Medical Publishers; 2009. https://archive.org/details/MeasureOfJointRomsGuideToGoniometry. Accessed March 2, 2017.

116. Gajdosik RL, Bohannon RW. Goniometry Emphasizing Reliability and Validity Clinical Measurement of Range of Motion: Review of Clinical Measurement of Range of Motion Review of Goniometry Emphasizing Reliability and Validity. *PHYS THER*. 1987;67:1867-1872. http://ptjournal.apta.org/content/67/12/1867. Accessed April 16, 2017.

117. Dos Santos RA, Derhon V, Brandalize M, Brandalize D, Rossi LP. Evaluation of knee range of motion: Correlation between measurements using a universal goniometer and a smartphone goniometric application. *J Bodyw Mov Ther*. 2017;21(3):699-703. doi:10.1016/j.jbmt.2016.11.008

118. Svensson M, Lind V, Löfgren Harringe M. Measurement of knee joint range of motion with a digital goniometer: A reliability study. *Physiother Res Int J Res Clin Phys Ther*. 2019;24(2):e1765. doi:10.1002/pri.1765

119. Soucie JM, Wang C, Forsyth A, et al. Range of motion measurements: reference values and a database for comparison studies. *Haemophilia*. 2011;17(3):500-507. doi:10.1111/j.1365-2516.2010.02399.x

120. Buzug TM. Computed Tomography BT - Springer Handbook of Medical Technology. In: Kramme R, Hoffmann K-P, Pozos RS, eds. Berlin, Heidelberg: Springer Berlin Heidelberg; 2011:311-342. doi:10.1007/978-3-540-74658-4_16

121. Brenner DJ, Hall EJ. Computed Tomography — An Increasing Source of Radiation Exposure. *N Engl J Med*. 2007;357(22):2277-2284. doi:10.1056/NEJMra072149

122. Lalone EA, McDonald CP, Ferreira LM, Peters TM, King GW, Johnson JA. Development of an image-based technique to examine joint congruency at the elbow. *Comput Methods Biomech Biomed Engin*. 2013;16(3):280-290. doi:10.1080/10255842.2011.617006

123. Kelly PM, Hopkins JG, Furey AJ, Squire DS. Dynamic CT Scan of the Normal Scapholunate Joint in a Clenched Fist and Radial and Ulnar Deviation. *Hand (N Y)*. 2018;13(6):666-670. doi:10.1177/1558944717726372

124. Vetter SY, Privalov M, Beisemann N, et al. Influence of ankle joint position on angles and distances of the ankle mortise using intraoperative cone beam CT: A cadaveric study. *PLoS One*. 2019;14(5):e0217737. doi:10.1371/journal.pone.0217737

125. Queirós S, Morais P, Barbosa D, Fonseca JC, Vilaça JL, D'Hooge J. MITT: Medical Image Tracking Toolbox. *IEEE Trans Med Imaging*. 2018;37(11):2547-2557. doi:10.1109/TMI.2018.2840820

126. Balkovec C, Veldhuis J, Baird JW, Wayne Brodland G, McGill SM. Digital tracking algorithm reveals the influence of structural irregularities on joint movements in the human cervical spine. *Clin Biomech (Bristol, Avon)*. 2018;56:11-17. doi:10.1016/j.clinbiomech.2018.04.015

127. Franz AM, Haidegger T, Birkfellner W, Cleary K, Peters TM, Maier-Hein L. Electromagnetic tracking in medicine--a review of technology, validation, and applications. *IEEE Trans Med Imaging*. 2014;33(8):1702-1725.

doi:10.1109/TMI.2014.2321777

128. Cherpak A, Ding W, Hallil A, Cygler JE. Evaluation of a novel 4D in vivo dosimetry system. *Med Phys*. 2009;36(5):1672-1679. doi:10.1118/1.3100264

129. Kickuth R, Reichling C, Bley T, Hahn D, Ritter C. C-Arm Cone-Beam CT Combined with a New Electromagnetic Navigation System for Guidance of Percutaneous Needle Biopsies: Initial Clinical Experience. *Rofo*. 2015;187(7):569-576. doi:10.1055/s-0034-1399313

130. Narsule CK, Sales Dos Santos R, Gupta A, et al. The efficacy of electromagnetic navigation to assist with computed tomography-guided percutaneous thermal ablation of lung tumors. *Innovations (Phila)*. 2012;7(3):187-190. doi:10.1097/IMI.0b013e318265b127

131. Lei P, Moeslein F, Wood BJ, Shekhar R. Real-time tracking of liver motion and deformation using a flexible needle. *Int J Comput Assist Radiol Surg*. 2011;6(3):435-446. doi:10.1007/s11548-010-0523-7

132. Zhou J, Sebastian E, Mangona V, Yan D. Real-time catheter tracking for high-dose-rate prostate brachytherapy using an electromagnetic 3D-guidance device: a preliminary performance study. *Med Phys*. 2013;40(2):21716. doi:10.1118/1.4788641

133. Poulin E, Racine E, Binnekamp D, Beaulieu L. Fast, automatic, and accurate catheter reconstruction in HDR brachytherapy using an electromagnetic 3D tracking system. *Med Phys*. 2015;42(3):1227-1232. doi:10.1118/1.4908011

134. Bharat S, Kung C, Dehghan E, et al. Electromagnetic tracking for catheter reconstruction in ultrasound-guided high-dose-rate brachytherapy of the prostate. *Brachytherapy*. 2014;13(6):640-650. doi:10.1016/j.brachy.2014.05.012

135. Kellermeier M, Herbolzheimer J, Kreppner S, Lotter M, Strnad V, Bert C. Electromagnetic tracking (EMT) technology for improved treatment quality

assurance in interstitial brachytherapy. *J Appl Clin Med Phys*. 2017;18(1):211-222. doi:10.1002/acm2.12021

136.   Qi Y, Sadjadi H, Yeo CT, Hashtrudi-Zaad K, Fichtinger G. Electromagnetic tracking performance analysis and optimization. *Conf Proc . Annu Int Conf IEEE Eng Med Biol Soc IEEE Eng Med Biol Soc Annu Conf*. 2014;2014:6534-6538. doi:10.1109/EMBC.2014.6945125

137.   Xiao G, Bonmati E, Thompson S, et al. Electromagnetic tracking in image-guided laparoscopic surgery: Comparison with optical tracking and feasibility study of a combined laparoscope and laparoscopic ultrasound system. *Med Phys*. 2018;45(11):5094-5104. doi:10.1002/mp.13210

138.   Geisbüsch A, Auer C, Dickhaus H, Niklasch M, Dreher T. Electromagnetic bone segment tracking to control femoral derotation osteotomy-A saw bone study. *J Orthop Res Off Publ Orthop Res Soc*. 2017;35(5):1106-1112. doi:10.1002/jor.23348

139.   Kügler D, Krumb H, Bredemann J, et al. High-precision evaluation of electromagnetic tracking. *Int J Comput Assist Radiol Surg*. 2019;14(7):1127-1135. doi:10.1007/s11548-019-01959-5

140.   Dorfmuller-Ulhaas K, Schmalstieg D. Finger tracking for interaction in augmented environments. In: *Proceedings IEEE and ACM International Symposium on Augmented Reality*. IEEE Comput. Soc; :55-64. doi:10.1109/ISAR.2001.970515

141.   Khadem R, Yeh CC, Sadeghi-Tehrani M, et al. Comparative Tracking Error Analysis of Five Different Optical Tracking Systems. *Comput Aided Surg*. 2000;5(2):98-107. doi:10.3109/10929080009148876

142.   Ribo M, Pinz A, Fuhrmann AL. A new optical tracking system for virtual and augmented reality applications. In: *IMTC 2001. Proceedings of the 18th IEEE Instrumentation and Measurement Technology Conference. Rediscovering Measurement in the Age of Informatics (Cat. No.01CH 37188)*. Vol 3. ;

2001:1932-1936 vol.3. doi:10.1109/IMTC.2001.929537

143.   Kim A, Golnaraghi MF. Initial calibration of an inertial measurement unit using an optical position tracking system. In: *PLANS 2004. Position Location and Navigation Symposium (IEEE Cat. No.04CH37556)*. ; 2004:96-101. doi:10.1109/PLANS.2004.1308980

144.   Coupier J, Moiseev F, Feipel V, Rooze M, Van Sint Jan S. Motion representation of the long fingers: a proposal for the definitions of new anatomical frames. *J Biomech*. 2014;47(6):1299-1306. doi:10.1016/j.jbiomech.2014.02.017

145.   Coupier J, Hamoudi S, Telese-Izzi S, Feipel V, Rooze M, Van Sint Jan S. A novel method for in-vivo evaluation of finger kinematics including definition of healthy motion patterns. *Clin Biomech*. 2016;31:47-58. doi:10.1016/j.clinbiomech.2015.10.002

146.   Metcalf CD, Notley S V., Chappell PH, Burridge JH, Yule VT. Validation and application of a computational model for wrist and hand movements using surface markers. *IEEE Trans Biomed Eng*. 2008;55(3):1199-1210. doi:10.1109/TBME.2007.908087

147.   Ishii K, Oki S, Iwamoto T, et al. Quantitative analysis of metacarpophalangeal joints during active flexion using four-dimensional computed tomography. *Clin Biomech*. 2020;80. doi:10.1016/j.clinbiomech.2020.105188

148.   Rex C. Continuous passive motion therapy after total knee arthroplasty. *Nursing2020*. 2018;48(5). https://journals.lww.com/nursing/Fulltext/2018/05000/Continuous_passive_motion_therapy_after_total_knee.15.aspx.

149.   Chaudhry H, Bhandari M. Cochrane in CORR (®): Continuous Passive Motion Following Total Knee Arthroplasty in People With Arthritis (Review). *Clin Orthop Relat Res*. 2015;473(11):3348-3354. doi:10.1007/s11999-015-4528-y

150. Herbold JA, Bonistall K, Blackburn M, et al. Randomized controlled trial of the effectiveness of continuous passive motion after total knee replacement. *Arch Phys Med Rehabil*. 2014;95(7):1240-1245. doi:10.1016/j.apmr.2014.03.012

151. Boese CK, Weis M, Phillips T, Lawton-Peters S, Gallo T, Centeno L. The efficacy of continuous passive motion after total knee arthroplasty: a comparison of three protocols. *J Arthroplasty*. 2014;29(6):1158-1162. doi:10.1016/j.arth.2013.12.005

152. Tanaka T, Amadio PC, Zhao C, Zobitz ME, An K-N. Flexor Digitorum Profundus Tendon Tension during Finger Manipulation A Study in Human Cadaver Hands. doi:10.1197/j.jht.2005.04.001

153. Sapienza A, Yoon HK, Karia R, Lee SK. Flexor tendon excursion and load during passive and active simulated motion: a cadaver study. *J Hand Surg Eur Vol*. 2013;38(9):964-971. doi:10.1177/1753193412469128

154. Yamaguchi T, Osamura N, Zhao C, An K-N, Amadio PC. Relative longitudinal motion of the finger flexors, subsynovial connective tissue, and median nerve before and after carpal tunnel release in a human cadaver model. *J Hand Surg Am*. 2008;33(6):888-892. doi:10.1016/j.jhsa.2008.02.017

155. Schweizer A, Moor BK, Nagy L, Snedeker JG. Static and dynamic human flexor tendon-pulley interaction. *J Biomech*. 2009;42(12):1856-1861. doi:10.1016/j.jbiomech.2009.05.025

156. Qiu D, Kamper DG. Orthopaedic applications of a validated force-based biomechanical model of the index finger. *Conf Proc . Annu Int Conf IEEE Eng Med Biol Soc IEEE Eng Med Biol Soc Annu Conf*. 2014;2014:4013-4016. doi:10.1109/EMBC.2014.6944504

157. Buonocore S, Sawh-Martinez R, Emerson JW, Mohan P, Dymarczyk M, Thomson JG. The effects of edema and self-adherent wrap on the work of flexion in a cadaveric hand. *J Hand Surg Am*. 2012;37(7):1349-1355. doi:10.1016/j.jhsa.2012.03.038

158. Lee SW, Chen H, Towles JD, Kamper DG. Effect of finger posture on the tendon force distribution within the finger extensor mechanism. *J Biomech Eng*. 2008;130(5):51014. doi:10.1115/1.2978983

159. Greenwald D, Shumway S, Allen C, Mass D. Dynamic analysis of profundus tendon function. *J Hand Surg Am*. 1994;19(4):626-635. doi:10.1016/0363-5023(94)90272-0

160. Deml C, Baradaran A, Chen N, Nasr M, Kachooei AR. Fowler Central Slip Tenotomy or Spiral Oblique Retinacular Ligament Reconstruction? A Cadaveric Biomechanical Study in Swan-Neck Deformity. *Hand (N Y)*. March 2019:1558944719834643. doi:10.1177/1558944719834643

161. Cheng Y-S, Chieh H-F, Lin C-J, Kuo L-C, An K-N, Su F-C. Comprehensive simulation on morphological and mechanical properties of trigger finger - A cadaveric model. *J Biomech*. 2018;74:187-191. doi:10.1016/j.jbiomech.2018.03.043

Chapter 2

2   Assessment of spatial tracking technology for in-vitro finger motion studies (Optical vs. Electromagnetic tracking)

OVERVIEW: The use of electromagnetic tracking for joint motion kinematic analysis is currently on the rise however, its inferior manufacturer's accuracy and resolution compared to optical tracking raises minor concerns. This chapter presents a quantitative accuracy assessment experiment where the rotational and translational accuracy of electromagnetic tracking is compared to optical tracking, under the same setting. Moreover, research and clinical-oriented applications are described for both technologies. Finally, a critical comparative analysis of the state of the art which highlights the potentialities and the limitations of each tracking system is provided.

2.1   Introduction

Upper limb joint kinematics is a common and evolving area of interest within the literature. Although several motion capture systems have been established, researchers tend to advocate for the use of optical and electromagnetic systems when reporting *in-vivo* and *in-vitro* human motion kinematics due their reliability and accuracies compared to other tracking methodologies[1–5]

As discussed in chapter 1, optical tracking uses infrared cameras to record the position of reflective markers placed on the body, whereas the electromagnetic tracking (EM) systems utilize receivers within an electromagnetic field to compute the position and orientation of body segments in space[6]. Such need of a continuous line of sight by the optical camera is challenging when involving a large set of rigid bodies moving in complex motion pathways. Nonetheless, many previous studies have relied on optical tracking to measure finger kinematics despite said limitations[7–9]. In addition, unlike EM, the rotational accuracy of optical systems, more specifically the Optotrak Certus, has not yet been formally reported. This lack in knowledge limits the support for using optical tracking since the rotational accuracy of a system is deemed more important than the translation accuracy when evaluating kinematics of joint rotation angles.

Therefore, the purpose of this study was to directly compare the Optotrak Certus system to a trakSTAR electromagnetic tracking device under the same measurement settings to (1) measure and understand the rotational accuracy of the Certus and, (2) to validate the rotational accuracy of trakSTAR.

2.2   Materials and Methods

2.2.1 Equipment

Two motion tracking systems, Optotrak Certus motion capture system (Manufacturer position accuracy = 0.1 mm RMS) (Northern Digital, Waterloo, Ontario, Canada) derived of three components; the camera, the control unit, and the markers, and an Electromagnetic tracking system (Manufacturer position accuracy = 1.4 mm RMS and rotational accuracy

= 0.5° RMS) (Northern Digital, Waterloo, Ontario, Canada), consisting of a mid-range transmitter, the control unit, and the sensors (M180) were evaluated using two motion systems: a Coordinate Measuring Machine (CMM) (CM - Global Measurement Solutions, Topsfield, MA, United States), and a Rotary Computer Numerical Control (CNC) machine. The frame rate of measurement was selected as 20Hz and the data collection process was set to be in real time, where each frame is separately conveyed to the computer as it is completed.

A Coordinate Measuring Machine is a gold standard tool that relies on a very sensitive electronic probe to measure a series of discrete points from the geometry of a solid part in an X-Y-Z coordinate plane. All of the motions of the gantry and probe can be controlled manually via a joystick or programmed automatically. A Rotary CNC machine is also an automated machining mainly used for milling and other purposes by means of a computer. It is capable of rotating in different variations and degree increment to meet user specifications by following a coded programmed instruction.

2.2.2 Setup and Protocol

Each protocol was run consecutively between both systems. A 20cm^2 Delrin block was used to mount 9 individual trackers (Certus and trakSTAR) at fixed and equal distances from one another (Figure 2.1).
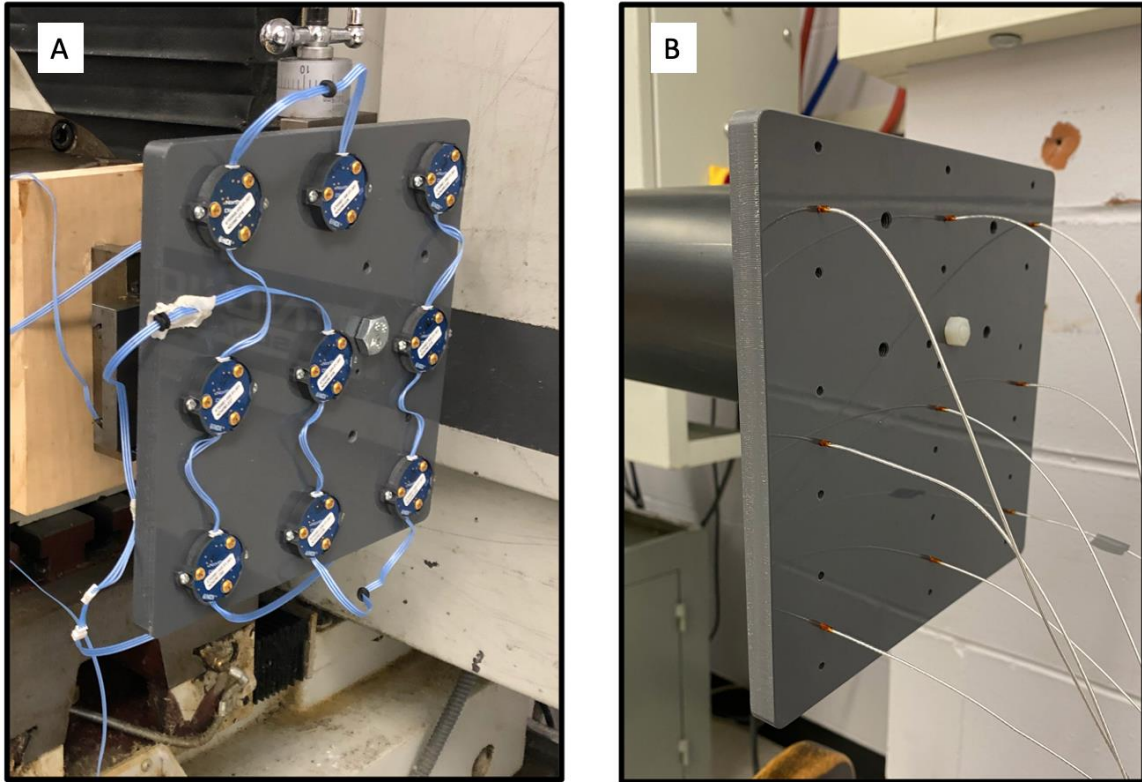
Figure 2.1 – Certus and trakSTAR Sensors Mounted onto Delrin Plate

A Delrin plate (grey) showcasing (a) 9 optical trackers (blue with yellow markers) and (b) 9 electromagnetic trackers. The plate was designed for the rigid mounting of the trackers for accuracy evaluation purposes where both optical and electromagnetics trackers were mounted at an equal distances from one another.

A separate optical reference tracker in which all 9 trackers rotated and translated with respect to was mounted firmly onto a stable and rigid base within the system's field of vision. The performance of both systems were evaluated under two separate test conditions: A and B (Figure 2.2). Session A involved tests carried out using the CMM while session B involved experiments using the rotary CNC. Both, translational and rotational, errors were measured in each test condition. A standard test method[10] (ASTM) for evaluating the performance of systems that measure static, 6DOF measurements, was followed and used as a guideline for accurately collecting, computing, and evaluating the performance of both systems. Prior to testing, the Certus and trakSTAR systems were both initially transformed to a common coordinate system as guided by the ASTM.
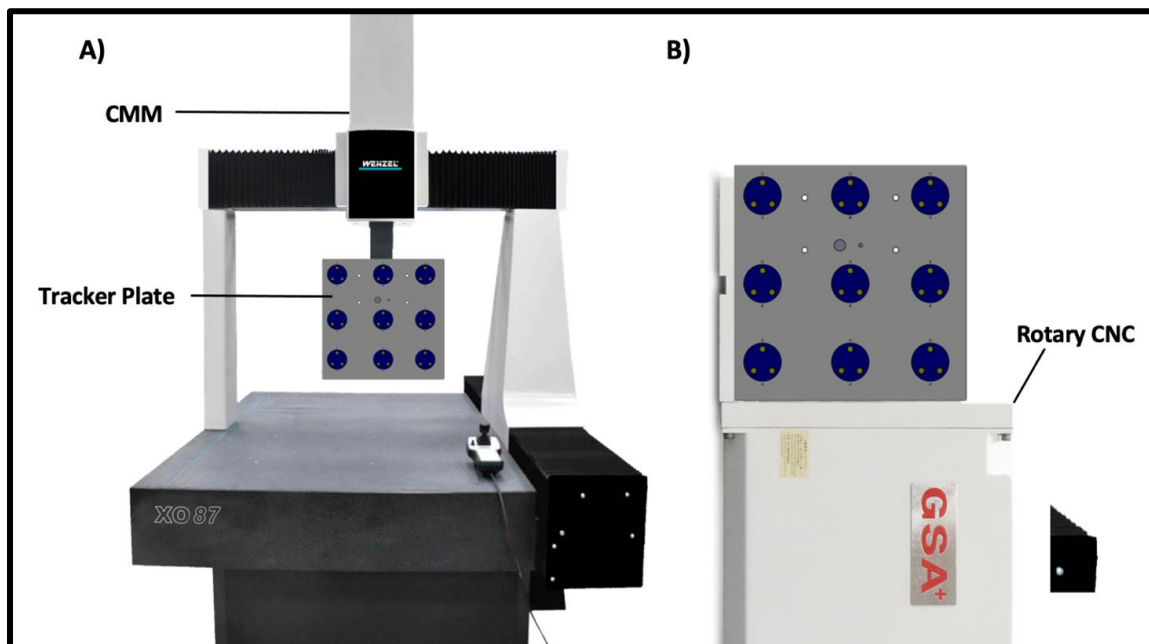
Figure 2.2 - CMM and Rotary CNC: Experimental Setup

Translational and rotational accuracy of the tracker plate was quantified under two separate sessions; (A) using the CMM and (B) the rotary CNC.

2.2.3 Certus Tracking under CMM

For the CMM measurements, the tracker block was driven to several positions around an arbitrary 64 x 24 x 43 cm^3 cube in small 10 mm increments with a 1 second delay between each increment; encompassing the total workplace of the CMM (N ≈ 10,00,000 sample per tracker). Within the same volume, a smaller 30 x 30x 22 cm^3 cube in the center was selected in which finer 5 mm increments were chosen for tracking within the Certus' field of vision (Figures 2.3 and 2.4). The size of the smaller cube or "inner volume" was determined based on the size of the average hand in upper arm in-vivo and in-vitro research; mimicking a true finger joint or wrist tracking scenario. The system was run with the camera set a fixed distance of 3m away from the center of the CMM's volume. The camera depth was predominantly chosen based on findings from previously reported studies supporting the accuracy of Certus tracking at different depths from the camera[12]. Moreover, the accuracy of the Certus within the smaller cube were evaluated at an

additional 2 depth levels from the sensor: (a) 1.5m and (b) 4.5m. All depth levels were chosen based off the maximum possible allowable distance within the space tested, while maintaining and ensuring that the trackers are constantly within the camera's field of vision.
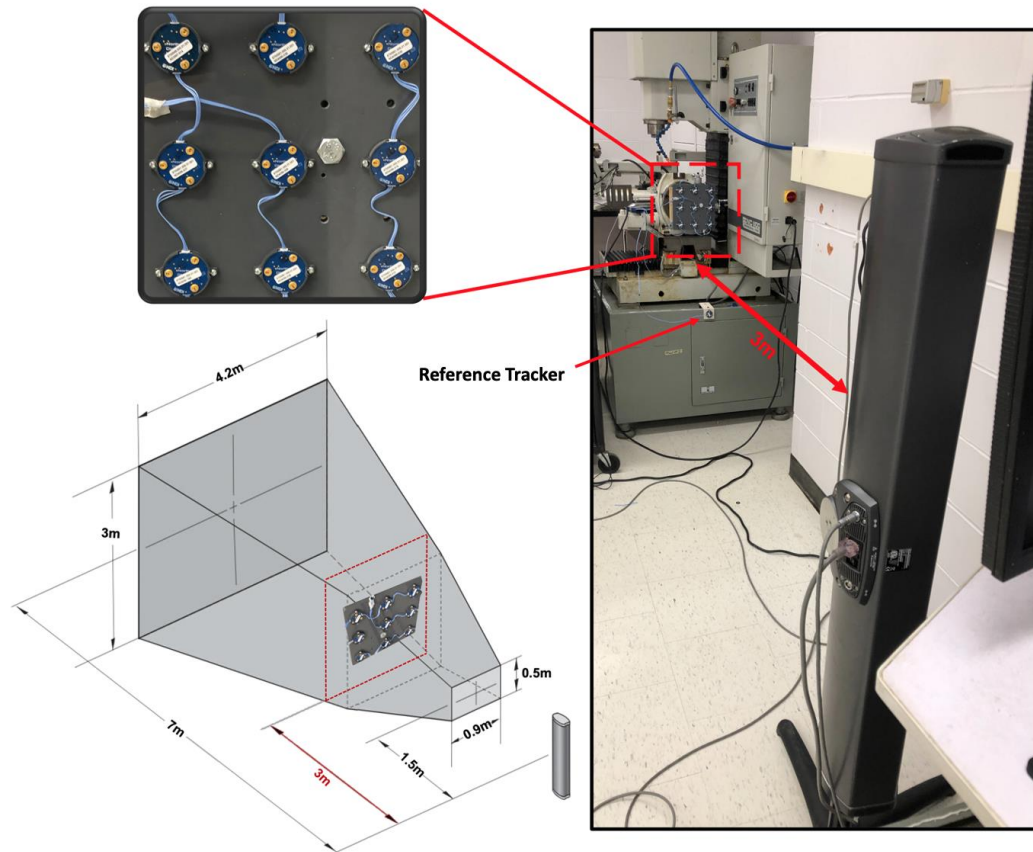
Figure 2.3 – Certus' Field of Vision

Measurements made using the Certus were recorded at a fixed distance of 3m away from the tracker plate. The image on the bottom left illustrates the maximum field of vision allowed by the Certus where the red dotted box highlights the 3m mark within the workspace. In addition, the Certus was also evaluated at 1.5m and 4.5m away from the camera.
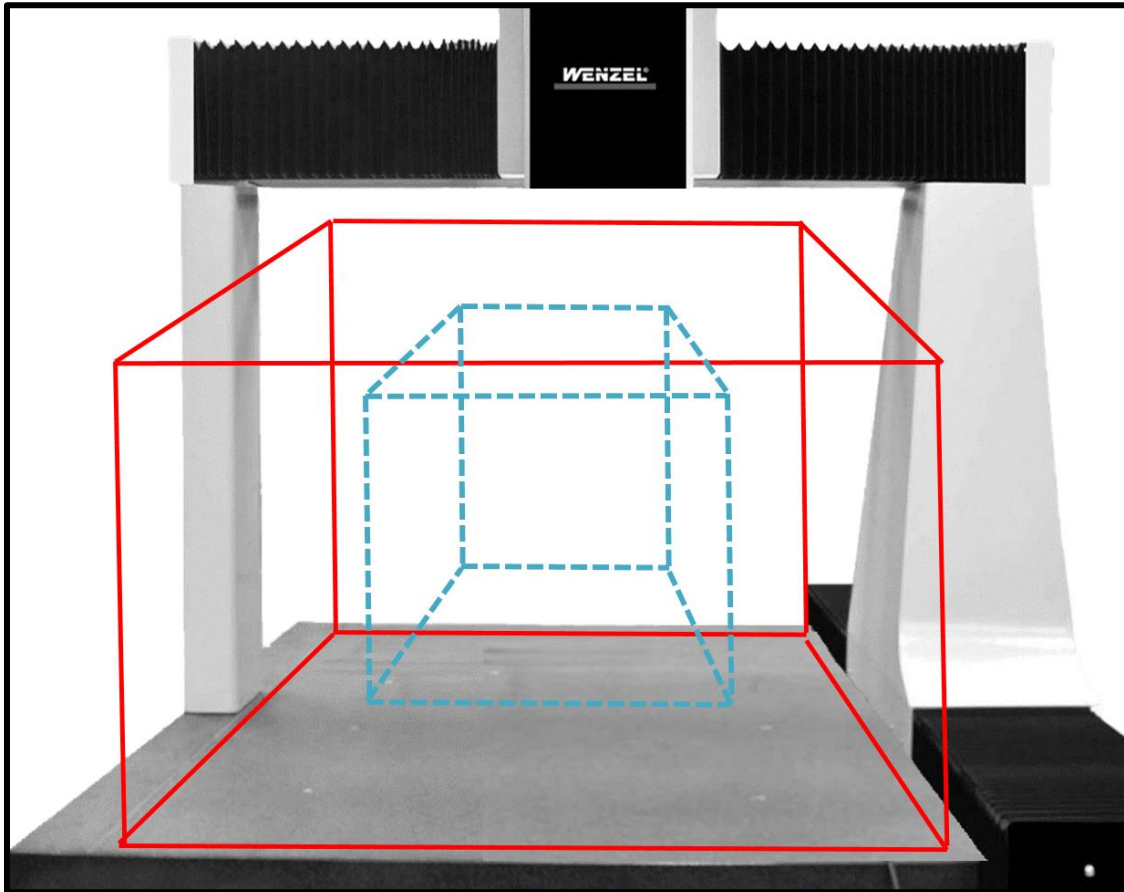
Figure 2.4 - CMM's Volume Workspace

The motion pathway volumes tested by the Certus is illustrated above where the outer (64 cmx43 cmx24 cm) and inner (30 cmx30 cmx20 cm) volumes are highlighted in red and blue, respectively. The EM was tested in the inner volume only.

2.2.4 trakSTAR under CMM

The electromagnetic transmitter was placed 0.43 m away from the center of the CMM's volume, which lies in the middle of the transmitter's functional workspace (figure 2.5). Unlike the Certus, trakSTAR does not require a direct line of sight to function and therefore, depth of the system is thought to not directly affect the accuracy of the system. In addition, due to the vast increase in ferromagnetic material encompassing the trackers in the CMM, the protocol for trakSTAR under the CMM only included motion of finer 5 mm increments within the inner volume space alone; the volume furthest away from

possible magnetic interference. Furthermore, depth tests at 0.2 m and 0.66 m, similar to the ones conducted for the Certus were replicated for trakSTAR trackers to evaluate the possible effects of depth on technical accuracy.
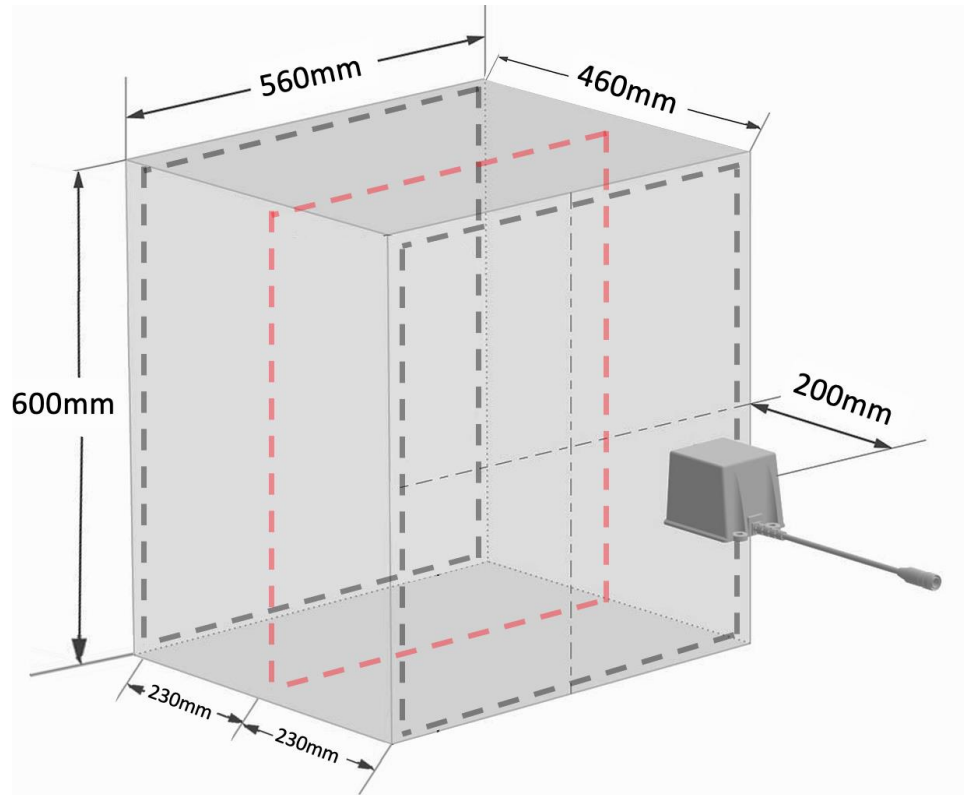
Figure 2.5 - trakSTAR Field of Vision

The minimum and maximum allowable field of the tracking of the electromagnetic transmitter. All measurements conducted by the EM system were done 0.43 m away from the transmitter; in the center of the field (along the red dotted frame). Moreover, two more depth levels were evaluated along at the two grey dotted frames at 0.2 m and 0.66 m.

2.2.5 Rotary CNC

The rotary CNC followed a selected pathway identical to both Certus and trakSTAR, where the tracker block itself was rotated at absolute 1° degree increments until full rotation (360°) with a 3s delay between each rotation, at 9 different static positions along the CNC's

workplace for rotational and translational measurements (Figure 2.6) (N = 14,400 samples per tracker per position).
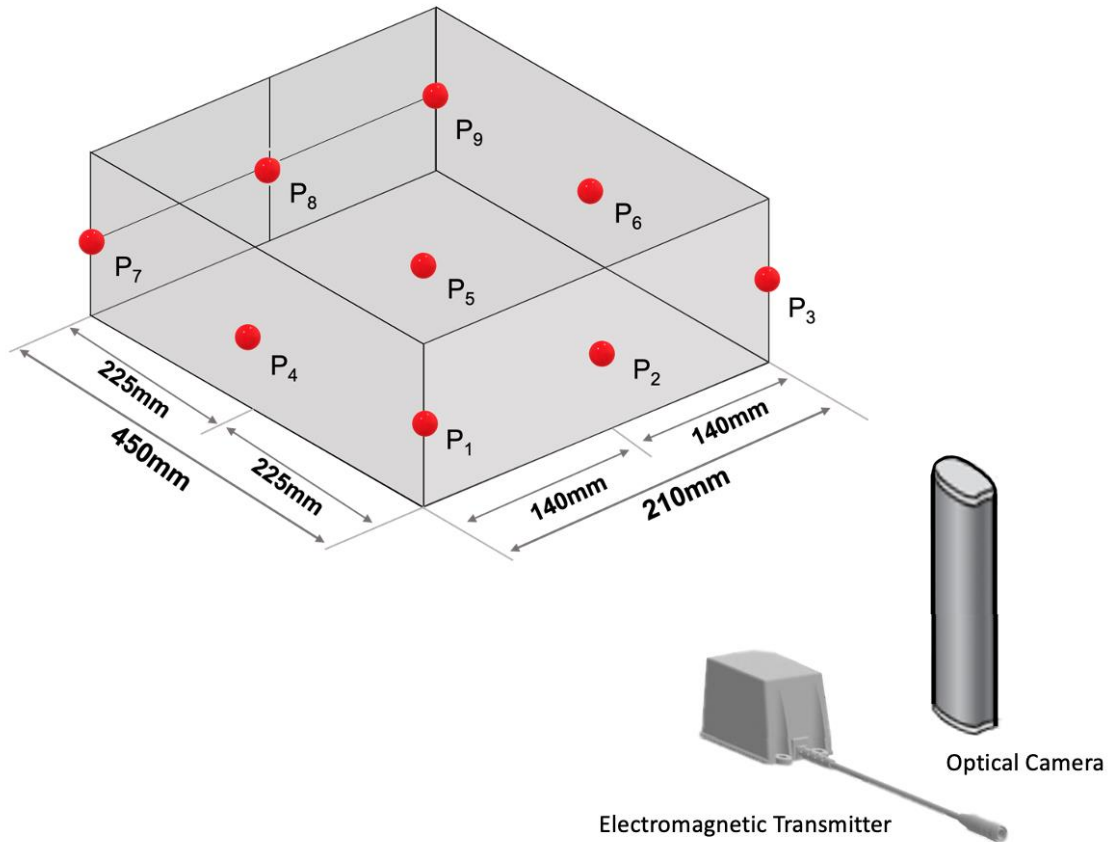
Figure 2.6 - CNC Pathway

The pattern followed by the CNC is illustrated above where the red dots denote the 9 positions, moving from position 1 (p1) to position 9 (p9) in numerical order. Rotations of 1° increments to full rotation (360°) were conducted at each of the 9 positions under both optical and EM tracking.

The different positions were chosen arbitrarily, however, enclosed the entire accessible workplace area of the CNC machine. The tracker block for the Certus test was mounted firmly onto the rotary CNC and the reference tracker as previously mentioned, was rigidly mounted on a surface nearby. The trakSTAR setup however incorporated a 1.5m hollow plastic tube between the fixed ends of the CNC and the tracker block (Figure 2.7). This

offset caused by the cylinder ensured that the metal within the machine did not affect the accuracy and quality of the trackers during simulation.
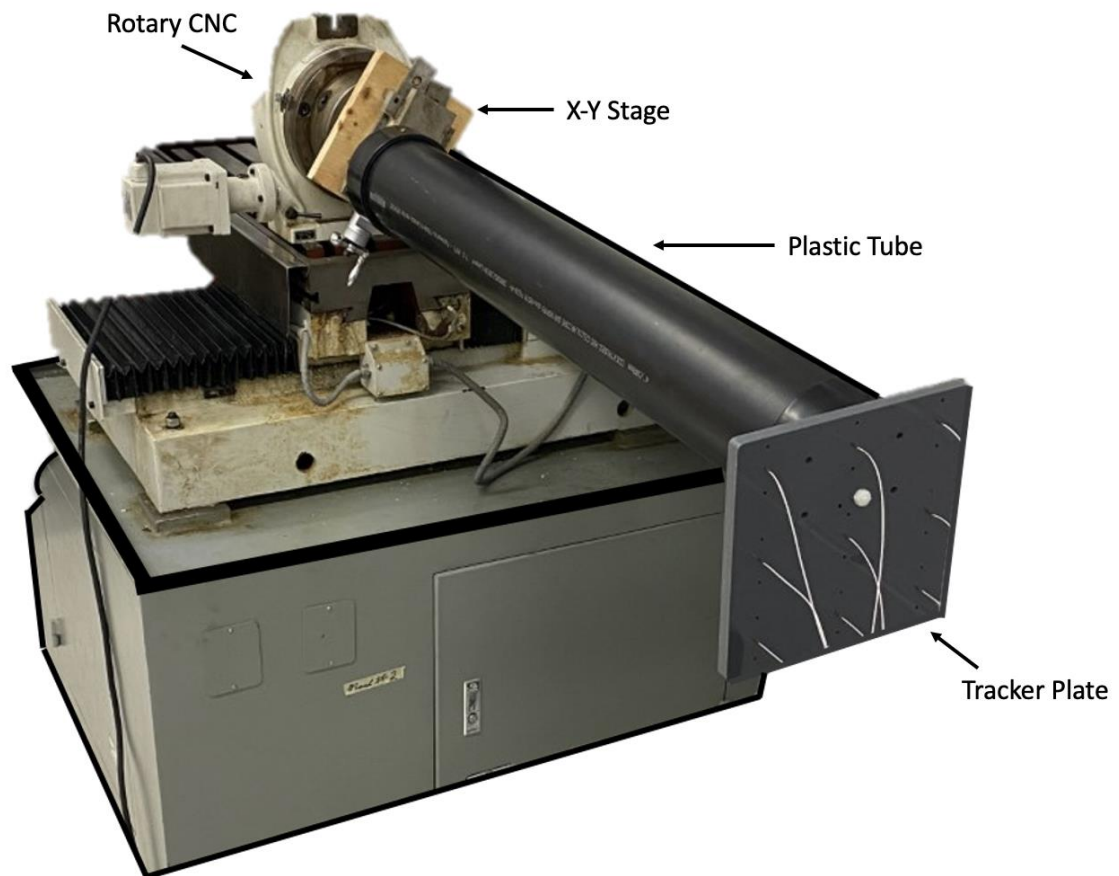
Figure 2.7 – Rotary CNC Setup with trakSTAR

The mounting process of the tracker plate onto the rotary CNC is illustrated where the plate was fixed onto one end of a 1.5m long plastic tube that was then fixed directly onto the rotary CNC machine.

In addition, the effect of depth on the technical accuracy of the Certus and trakSTAR were also assessed at all three different depth levels from the center of the CNC's workspace; Certus: (a) 1.5m; (b) 3m; and (c) 4.5m and EM: (a) 0.2m; (b) 0.43m; and (c) 0.66m. Unlike the Certus, the tracking volume of trakSTAR is much smaller and thus, depth (c) was chosen as the maximum range in which the system can track its sensors.

2.2.6 Data Analysis

The translational and rotational measurement errors were calculated for each system at each accuracy assessment point using,

$$e_{Trans\ error,k} = \sqrt{(x_{SUT,k} - x_{RS,k})^2 + (y_{SUT,k} - y_{RS,k})^2 + (z_{SUT,k} - z_{RS,k})^2} \quad (1)$$

$$e_{Rot\ error,k} = \cos^{-1}\left(\frac{trace\ (R_k)-1}{2}\right) \quad (2)$$

where SUT is used to denote the measurements from the system under test (SUT) in its own coordinate frame, RS represents a measurement from the reference system (RS) coordinate frame transformed to the SUT system coordinate frame, and $R_k = R_{RS,k}$ x $R_{SUT,k}^{T}$ [10].

The mean error, E_{mean}, was obtained using (3), the RMS error, E_{RMS} using (4):

$$E_{Mean} = \frac{1}{N}\sum_{k=1}^{N} e_{Trans\ error,k} \quad (3)$$

$$E_{RMS} = \sqrt{\frac{1}{N}\sum_{k=1}^{N}(e_{Trans\ error,k})^2} \quad (4)$$

Where $e_{Trans\ error,k}$ indicates the mean error at each corresponding accuracy assessment point gained using (1), and N indicates the number of points/samples tests[10].

In addition, a one-way repeated-measures ANOVA was performed to assess the accuracy of the Certus within 3 camera depth levels (close, middle, and far). Within-subject effects and pairwise comparisons were also examined, with significance set at $p<0.05$. Repeatability of each individual tracker was assessed by the standard deviation taken over 3 repeated trials.

2.3   Results

2.3.1 Translational Error

2.3.1.1   CMM (Certus vs. trakSTAR)

With the CMM moving in 10 mm increments in the outer volume and 5 mm increments in the inner volume, the average translational error ($E_{Trans,Mean}$) measured for all 9 trackers (N ≈ 200,000 samples per tracker per volume) was 0.23 ± 0.04 mm and 0.10 ± 0.02 mm respectively for Certus (E_{RMS} of 0.14 mm and 0.09 mm respectively) (Figure 2.8). Moving the trakSTAR in the inner volume only however resulted in an average translational error ($E_{Trans,Mean}$) of 1.71 ± 0.57 mm, with an E_{RMS} of 1.23 mm for all 9 trackers, compared to the Certus (Figure 2.9).
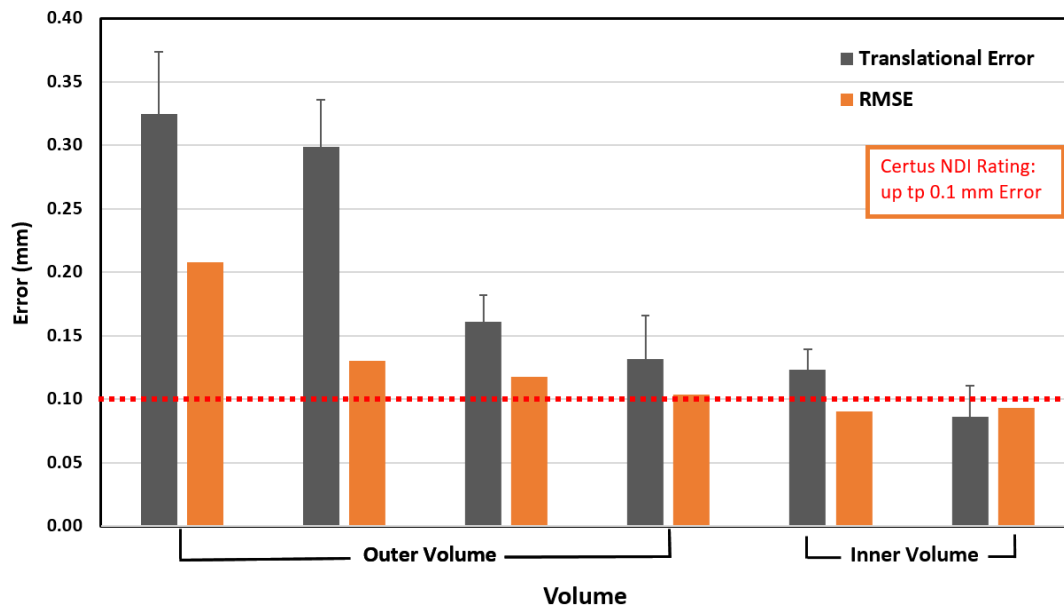
Figure 2.8 - Translation Accuracy of Certus under CMM

Translational error is plotted as a function of CMM's volume, where whiskers denote standard deviations of all 9 trackers and the red dotted line represents the error of the system as reported by the manufacturer. With the CMM moving in the outer volume and in the inner volume, the average translational errors measured for all 9 trackers was 0.23 ± 0.04 mm and 0.10 ±0.02 mm respectively.
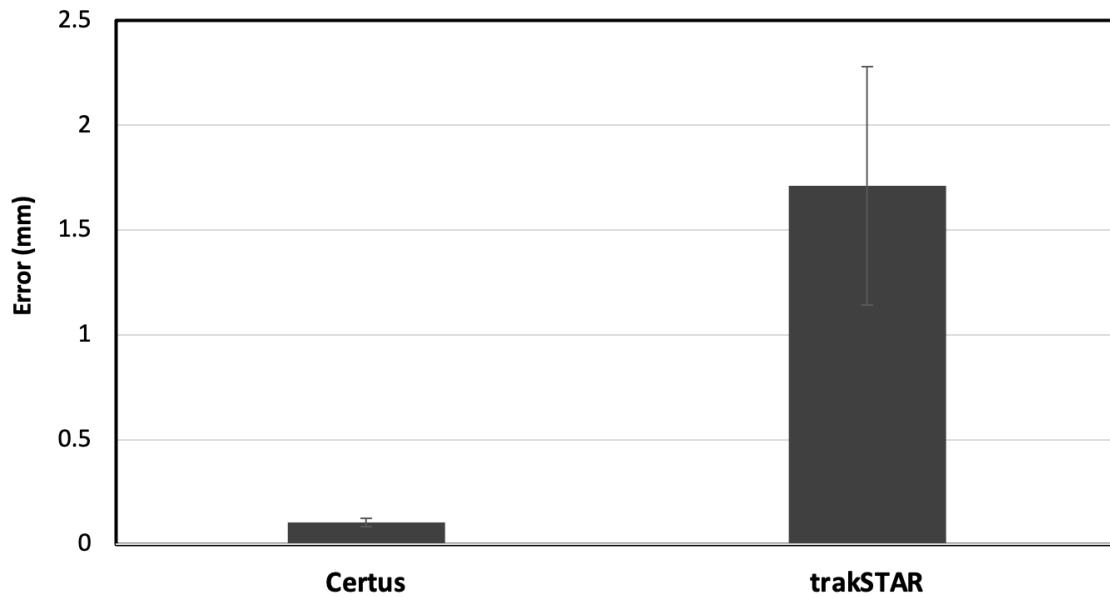
Figure 2.9: Direct Comparison of the Translational Accuracy of Certus vs. trakSTAR under CMM

At 5 mm X-Y-Z increments, the translational error is plotted for both systems under test where whiskers denote standard deviations of all 9 tracker. The average translational error measured for all 9 Certus trackers was 0.10 ±0.02 mm. Replacing the Certus with trakSTAR resulted in a 1.61mm increase in error compared to the Certus..

2.3.1.2 Rotary CNC (Certus vs. trakSTAR)

With the rotary CNC rotating in $1°$ increments, the $E_{Trans,Mean}$ measured within all 9 selected positions for all 9 Certus and trakSTAR trackers were 0.77 ± 0.4 mm and 1.58 ± 0.36 mm, respectively (Figure 2.10).
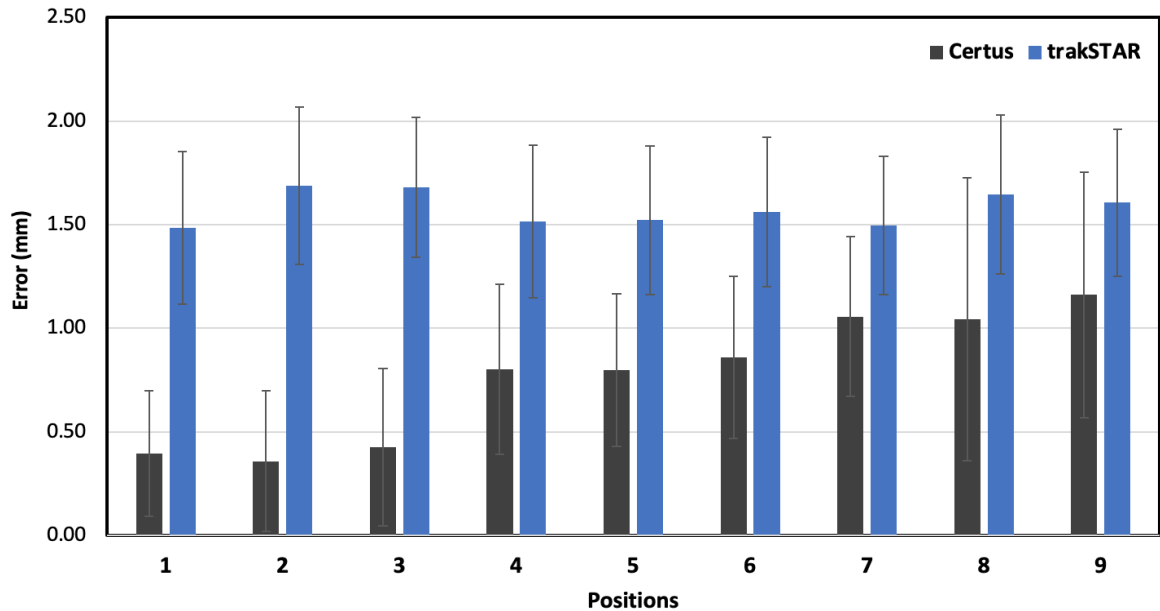
Figure 2.10: Direct Comparison of the Translational Accuracy of Certus vs. trakSTAR under Rotary CNC

At $1°$ increment rotations, the translational error is plotted as a function of the 9 positions achieved by the rotary CNC, where whiskers denote standard deviations of all 9 trackers. The overall average translational errors between all 9 selected positions for the Certus and trakSTAR were 0.77 ± 0.43 mm and 1.88 ± 0.66 mm, respectively.

2.3.2 Rotational Error

2.3.2.1 CMM (Certus vs. trakSTAR)

Similar to the translational test, the average rotational error ($E_{Rot,Mean}$) for all 9 trackers in the CMM moving in 10 mm increments in the outer volume and 5 mm increments in the inner volume (N ≈ 200,000 per tracker per volume) was measured to be 0.41 ± 0.03 deg and 0.21 ± 0.03 deg respectively for the Certus (E_{RMS} of 0.24 deg and 0.12 deg respectively) (Figure 2.11). In terms of trakSTAR, The $E_{Rot,Mean}$ for all 9 trackers in the CMM moving in 5 mm increments in the inner volume only was measured to be 0.30 ± 0.01 deg (E_{RMS} of 0.52 deg) compared to the Certus (Figure 2.12).
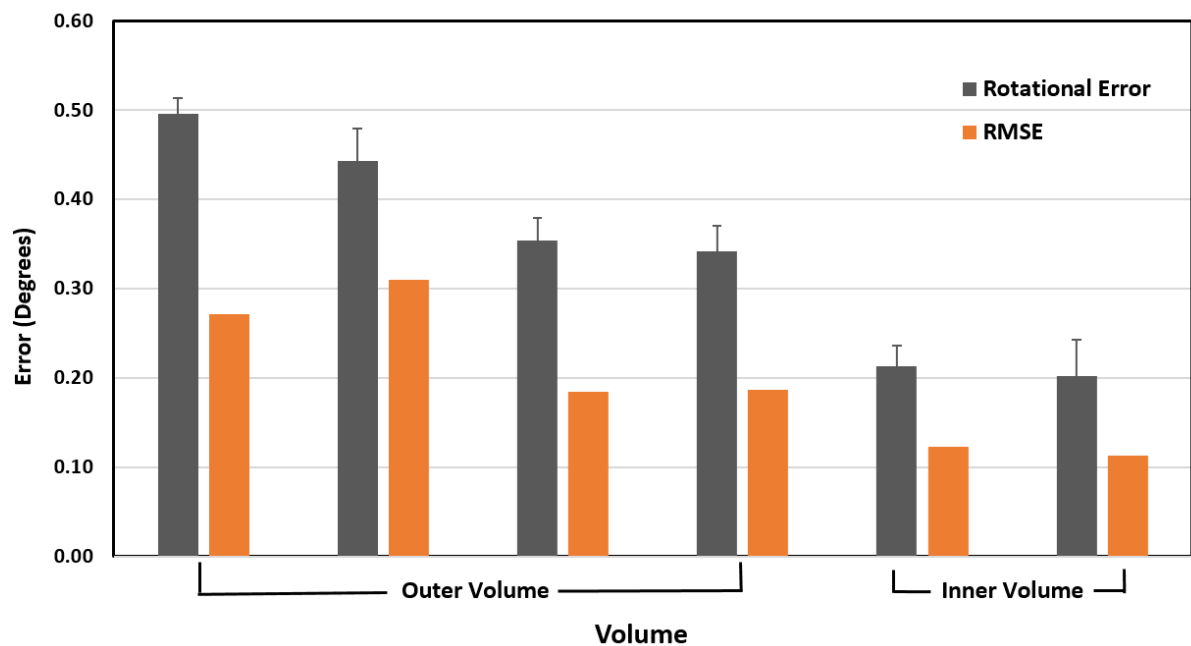
Figure 2.11 - Rotational Accuracy of Certus under CMM

At 10 mm and 5 mm incremented X-Y-Z motion, the translational error is plotted as a function of CMM's volume, where whiskers denote standard deviation of 9 trackers. With the CMM moving in the outer volume and in the inner volume, the average rotational errors for all 9 trackers was measured to be 0.41 ± 0.03 deg and 0.21 ± 0.03 deg respectively.
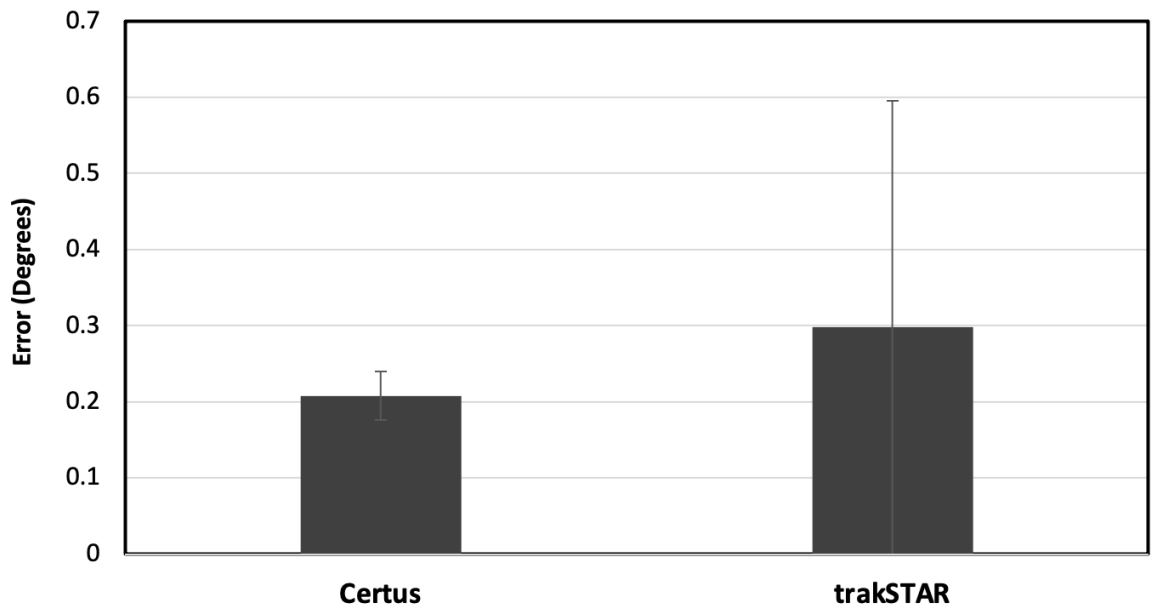
Figure 2.12 - Direct Comparison of the Rotational Accuracy of Certus vs. trakSTAR under CMM

At 10 mm and 5 mm incremented X-Y-Z motion, the rotational error is plotted as a function of CMM's volume, where whiskers denote standard deviation of 9 trackers. With the CMM moving in the inner volume, the average rotational errors for the Certus for all 9 trackers was 0.21 ± 0.03 deg. Using trakSTAR resulted in a minor increase of 0.09 deg in rotational error compared to Certus.

2.3.2.2   Rotary CNC (Certus vs. trakSTAR)

With the CNC rotating in $1°$ increments, the $E_{Rot,Mean}$ measured within all 9 selected positions for all 9 Certus and trakSTAR trackers were 0.23 ± 0.1 deg and 0.59 ± 0.24 deg, respectively (Figure 2.13).
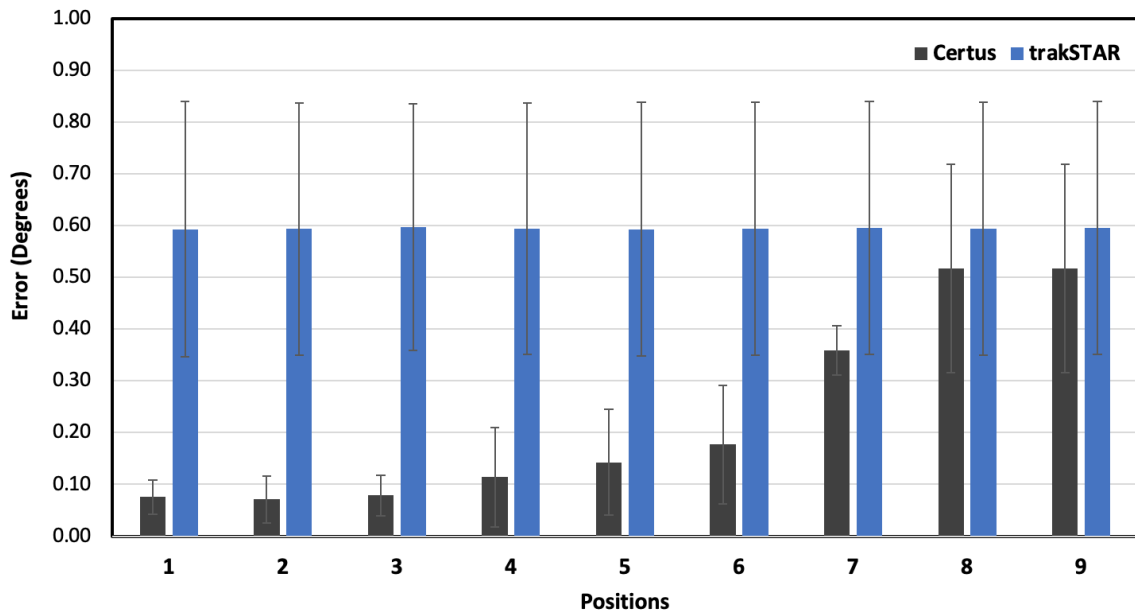
Figure 2.13 - Direct Comparison of the Rotational Accuracy of Certus vs. trakSTAR under Rotary CNC

At $1°$ increment rotations, the rotational error is plotted as a function of the 9 positions achieved by the CNC, where whiskers denote standard deviations of all 9 trackers. The overall average rotational errors measured while the machine was rotating for all 9 trackers for the Certus and trakSTAR were 0.23 ± 0.1 deg and 0.59 ± 0.24 deg, respectively.

Table 2.1 - Summary of Results for Certus and trakSTAR Systems

	Optical (Certus)		Electromagnetic (trakSTAR)	
	CMM (InnerVol)	CNC	CMM (InnerVol)	CNC
Translational Accuracy ($E_{Trans,Mean}$) (mm)	0.10 ± 0.02	0.77 ± 0.4	1.71 ± 0.57	1.58 ± 0.36
RMSE (E_{RMS}) (mm)	0.09	0.14	1.23	1.38
Rotational Accuracy ($E_{Rot,Mean}$) (deg)	0.21 ± 0.03	0.23 ± 0.1	0.30 ± 0.01	0.59 ± 0.24
RMSE (E_{RMS}) (deg)	0.12	0.2	0.52	0.56

2.3.3 Repeatability

The repeatability of all 9 individual trackers of the Certus and trakSTAR were each measured to be 0.047 mm and 0.024 mm, respectively. This degree of repeatability was sufficient to detect changes in measurement accuracy within statistical significance.

2.3.4 Depth

The distance between the camera and tracker plate had a significant effect on the accuracy of the Certus at further depths, relative to the nearest (1.5m) baseline distance. In the case of the CMM, the 3m (middle) depth caused a significant reduction of 0.14 ± 0.03 mm (48%) (p<0.001) in translational error of the trackers, compared to the close (1.5m) depth. Placing the camera at the farthest depth (4.5m) however had an opposite effect as it caused for a significant increase of 0.08 ± 0.4 mm (27%) (p<0.001) in translational error, compared to the native close depth. Similarly, depth of the tracker plate also seemed to have a significant effect on the rotational accuracy of the trackers. Placing the plate in the middle (3m) depth and the furthest depth (4.5m) caused a significant reduction of 0.12 ± 0.08° (29%) (p<0.001) and a significant increase of 0.19 ± 0.12° (49%) (p<0.001) respectively in error compared to the native close (1.5m) depth.

2.4   Discussion

The aim of this study was to quantify the rotational accuracy of the Certus and directly compare the technical accuracies of trakSTAR to the Certus under the same test setting. For the rotational accuracy of the Certus, we decided to proceed with using 0.22° as it is in agreement with both mean error and RMSE results. The 0.12° RMSE obtained in the CMM test is given less weight because this was a translation only test and therefore, is less relevant for joint angle kinematics application. In terms of TrakSTAR, 0.50° was chosen as that is the same value that was formally reported by the manufacturer as well as what the study also found. Additionally, it is almost centrally between the mean errors for the CMM and CNC tests; thus, 0.50 deg is in good agreement despite the limitations of the CNC test.

The translational accuracy also appears to be comparable to the information provided by the manufacturer, although in the case of the Certus, only the translational accuracy was reported in its manual, rather than both rotational and translational accuracy. For translational accuracy of the Certus, we decided to proceed with 0.1 mm as that is the RMSE reported by the manufacturer as well as the RMSE reported during the CNC test. Similarly, 1.4mm RMSE was selected for trakSTAR as it was also the value reported by both the manufacturer and this study. The purely translational CMM test produced a lower RMSE for both systems, however, as discussed earlier, pure translations are not relevant to joint biomechanics studies; thus, the CNC result is selected. Unlike the Certus, a notable difference was the increase in trakSTAR's mean translational error for the CMM, compared to the CNC . Metal artefact may have contributed to this.

Findings obtained within this study have shown to reflect similar or better accuracy results than most studies of motion analysis systems[12–19]. Groups assessing the translational accuracy of optical compared to electromagnetic tracking have reported technical accuracies in the range of 0.1 mm to 1.4 mm, and 0.17 mm to 2.0 mm respectively, depending on the assessed device and methodology followed[20–25]. Other studies evaluating rotational accuracy reported results as low as 0.1 degrees; which prominently compliments the findings in this study[26]. Additional studies such as the ones conducted by Barnes *et*

al.[27], Sugano *et al.*[28] and Li *et al.*[29]*,* all evaluated the accuracy of the Certus tracker in real in-vivo bone and other medical and mechanical cases. Sugano's study resulted in an average RMS error of 1.3 mm and 0.5 degrees, whereas findings by Li and Barnes resulted in errors as low as 0.76 mm and 0.2 mm both respectively. Goislard de Monsabert *et al.*[30] also conducted a biomechanical study using Cetus optical tracking to compare the effects of local frame definitions on local axis orientations and joint angles of the fingers and the wrist in which a nominal translational accruacy of 0.3 mm was reported.

There are two main drawbacks in using optical tracking for biomechanics studies. The accuracy of optical systems is related to tracker size; the trackers themselves tend to be large and bulky. The second major problem with optical systems is that they require a direct optical path between the position sensor system and the three or more targets that are being tracked. This is fairly more difficult to achieve with smaller joints as the fingers tend to obstruct one another while moving. In contrast, minute electromagnetic sensors, like the ones used in this study, allow for greater accessibility for soft-tissue interventions. In addition, the ability of electromagnetic systems to track without requiring a direct line of sight to the instrumentation is a great advantage of this technology; however, these systems have smaller tracking volumes and are quite sensitive to ferromagnetic surroundings.

Table 2.2 - Comparison between Optical and Electromagnetic Tracking Systems

Attribute	Optical	Electromagnetic
Translational Accuracy	+	0
Rotational Accuracy	+	+
Line of Sight	-	0
Working Volume	+	0
Metal Sensitivity	0	-
Tracker Size	-	+
Depth Sensitivity	-	+

* + = superior, 0=acceptable, and - = inferior

Although optical tracking is known to be more accurate than electromagnetic tracking, some studies have reported and argued that the accuracy of both systems are in fact comparable and can be used interchangeably. One study performed a direct comparison evaluation using a mechanical articulator to assess the accuracy of EM tracking when compared to digital optical tracking. The examiners used the gold standard known ranges of motion to compare both the optical and EM trackers. From their results, they determined that measurements from both systems are clinically comparable[31]. It is important to note, however, that they were using an articulator designed to simulate the elbow, so the magnitude of the acceptable accuracy and precision may be different than those required for the finger. The investigation also mimicked bone fixation and did not consider skin motion.

Several of past studies, as well as our results, reveal that precision of optical sensors is commonly negatively affected at increasing depths from the camera itself. States *et al.* used a repeated measures design study to evaluate the precision and repeatability of the Optotrak 3020 motion measurement system at different depths and concluded that the most optimal depth for preserving precision should be confined within a 2m-4m distance[11]. Furthermore, Maletsky *et al.* also concluded that the precision was seen to decrease as the camera distance grew larger and should be confined within a 1.75m - 3.25m distance[32]. These findings and their effects were found evident when measuring the trasnaltional and rotational accuracy of the trackers in this study. Although, all three distances revelead to have a sigificant effect on accuracy, the middle depth (3m) however caused the least increase in error compared to other distances. Placing the tracker plate at the 3m mark resulted in a sigificant 48% decrease in trasnlational error and a 29% in rotational error compared to the 1.5m mark. Similarly, placing the trackers at 3m caused an overal sigificant 59% decrease in translational error and a 51% in rotational error compared to the 4.5m mark; further supporting the conclusion that a direct linear correlation between distance from the camera and accuracy measurement is evident.

In contrast, the electromagnetic tracking system revealed no significant effect of depth on the accuracy of the system. In fact, placing the trackers at its maximum tracking depth resulted in a 7% decrease and a 0.6% increase in translational and rotational accuracies,

respectively, compared to the minimum tracking depth, further supporting the hypothesis made in chapter 1. Therefore, these results reveal that the optical tracking system is significantly more sensitive to depth than electromagnetic trackers. In addition, the most optimal depth for optical tracking should be conducted relatively around the 3m distance mark from the camera.

Our study was conducted despite three limitations. The Optotrak Certus system has not been calibrated within the 5 year time frame, as recommended by the manufactured. Therefore, the trackers and camera were set to their default settings, rather than being optimized for this specific study setting. Secondly, although properly calibrated, the rotary CNC machine used not of a gold standard method of rotational or translational measurement, unlike the CMM. Therefore, errors in accuracy within the machine may have contributed to an increase in error in the results. Lastly, external noise from the surroundings such as thermal, light, or metal disturbances may have contributed to errors for either system.

2.5   Conclusion

Quantification and direct comparison of the accuracy and repeatability of electromagnetic tracking to optical tracking was evaluated in this chapter. Findings from our study revealed differences as small as 0.4° in the rotational accuracies of the Optotrak Certus compared to trakSTAR. Moreover, findings showed a larger and more significant impact on the accuracy of the Certus at different depth levels, compared to the trakSTAR; supporting the hypothesis made in chapter 1. In conclusion, these results support the use of electromagnetic tracking as a reliable and accurate modality for kinematic tracking and quantification for clinical and research purposes.

2.6   References

1.   Degeorges R, Parasie J, Mitton D, Imbert N, Goubier J-N, Lavaste F. Three-dimensional rotations of human three-joint fingers: an optoelectronic measurement. Preliminary results. *Surg Radiol Anat*. 2005;27(1):43-50. doi:10.1007/s00276-004-0277-4

2.   Sorriento A, Porfido MB, Mazzoleni S, et al. Optical and Electromagnetic Tracking Systems for Biomedical Applications: A Critical Review on Potentialities and Limitations. *IEEE Rev Biomed Eng*. 2020;13:212-232. doi:10.1109/RBME.2019.2939091

3.   Du T, Yanai T. Accuracy and reliability of a method for measuring three-dimensional articular motions of the shoulder complex during swimming. *Sport Biomech*. February 2020:1-13. doi:10.1080/14763141.2019.1702089

4.   Tung WL, Kuo LC, Lai KY, Jou IM, Sun YN, Su FC. Quantitative evidence of kinematics and functional differences in different graded trigger fingers. *Clin Biomech*. 2010;25(6):535-540. doi:10.1016/j.clinbiomech.2010.02.009

5.   Magit DP, McGarry M, Tibone JE, Lee TQ. Comparison of cutaneous and transosseous electromagnetic position sensors in the assessment of tibial rotation in a cadaveric model. *Am J Sports Med*. 2008;36(5):971-977. doi:10.1177/0363546507312639

6.   Dorfmuller-Ulhaas K, Schmalstieg D. Finger tracking for interaction in augmented environments. In: *Proceedings IEEE and ACM International Symposium on Augmented Reality*. IEEE Comput. Soc; :55-64. doi:10.1109/ISAR.2001.970515

7.   Coupier J, Hamoudi S, Telese-Izzi S, Feipel V, Rooze M, Van Sint Jan S. A novel method for in-vivo evaluation of finger kinematics including definition of healthy motion patterns. *Clin Biomech (Bristol, Avon)*. October 2015. doi:10.1016/j.clinbiomech.2015.10.002

8.   Nataraj R, Li ZM. Robust identification of three-dimensional thumb and index finger kinematics with a minimal set of markers. *J Biomech Eng*. 2013;135(9). doi:10.1115/1.4024753

9.   Zhang X, Lee SW, Braido P. Determining finger segmental centers of rotation in flexion-extension based on surface marker measurement. *J Biomech*. 2003;36(8):1097-1102. doi:10.1016/S0021-9290(03)00112-X

10.   ASTM E2919-14. *Standard Test Method for Evaluating the Performance of Systems That Measure Static, Six Degrees of Freedom (6DOF), Pose*. West Conshohocken, PA; 2014.

11.   States RA, Pappas E. Precision and repeatability of the Optotrak 3020 motion measurement system. *J Med Eng Technol*. 2006;30(1):11-16. doi:10.1080/03091900512331304556

12.   Helmer RJN, Farrow D, Ball K, Phillips E, Farouil A, Blanchonette I. A pilot evaluation of an electronic textile for lower limb monitoring and interactive biofeedback. In: *Procedia Engineering*. Vol 13. Elsevier Ltd; 2011:513-518. doi:10.1016/j.proeng.2011.05.123

13.   Schulze M, Hartensuer R, Gehweiler D, Hölscher U, Raschke MJ, Vordemvenne T. Evaluation of a robot-assisted testing system for multisegmental spine specimens. *J Biomech*. 2012;45(8):1457-1462. doi:10.1016/j.jbiomech.2012.02.013

14.   Schulze M, Trautwein F, Vordemvenne T, Raschke M, Heuer F. A method to perform spinal motion analysis from functional X-ray images. *J Biomech*. 2011;44(9):1740-1746. doi:10.1016/j.jbiomech.2011.03.040

15.   Rudolph T, Ebert L, Kowal J. Comparison of three optical tracking systems in a complex navigation scenario. *Comput Aided Surg*. 2010;15(4-6):104-109. doi:10.3109/10929088.2010.530793

16. Morasiewicz P, Filipiak J, Krysztoforski K, Dragan S. Biomechanical aspects of lower limb torsional deformation correction with the ilizarov external fixator. *Ann Biomed Eng*. 2014;42(3):613-618. doi:10.1007/s10439-013-0911-6

17. McLachlin SD, Ferreira LM, Dunning CE. A Refined Technique to Calculate Finite Helical Axes from Rigid Body Trackers. *J Biomech Eng*. 2014;136(12). doi:10.1115/1.4028413

18. Faria C, Sadowsky O, Bicho E, et al. Validation of a stereo camera system to quantify brain deformation due to breathing and pulsatility. *Med Phys*. 2014;41(11). doi:10.1118/1.4897569

19. Maletsky LP, Sun J, Morton NA. Accuracy of an optical active-marker system to track the relative motion of rigid bodies. *J Biomech*. 2007;40(3):682-685. doi:10.1016/j.jbiomech.2006.01.017

20. Simon DA. *Intra-Operative Position Sensing and Tracking Devices*. http://www.ndigital.com/. Accessed May 17, 2021.

21. Wiles AD, Thompson DG, Frantz DD. Accuracy assessment and interpretation for optical tracking systems. In: *Medical Imaging 2004: Visualization, Image-Guided Procedures, and Display*. Vol 5367. SPIE; 2004:421. doi:10.1117/12.536128

22. Krücker J, Xu S, Glossop N, et al. Electromagnetic Tracking for Thermal Ablation and Biopsy Guidance: Clinical Evaluation of Spatial Accuracy. *J Vasc Interv Radiol*. 2007;18(9):1141-1150. doi:10.1016/j.jvir.2007.06.014

23. Mascott CR. Comparison of magnetic tracking and optical tracking by simultaneous use of two independent frameless stereotactic systems. *Neurosurgery*. 2005;57(4 SUPPL.). doi:10.1227/01.NEU.0000176411.55324.1E

24. De Lambert A, Esneault S, Lucas A, Haigron P, Cinquin P, Magne JL. Electromagnetic tracking for registration and navigation in endovascular aneurysm repair: A phantom study. *Eur J Vasc Endovasc Surg*. 2012;43(6):684-689.

doi:10.1016/j.ejvs.2012.03.007

25. Schicho K, Figl M, Donat M, et al. Stability of miniature electromagnetic tracking systems. *Phys Med Biol*. 2005;50(9):2089-2098. doi:10.1088/0031-9155/50/9/011

26. Evers J, Lakemeier M, Wähnert D, et al. 3D Optical Investigation of 2 Nail Systems Used in Tibiotalocalcaneal Arthrodesis: A Biomechanical Study. *Foot Ankle Int*. 2017;38(5):571-579. doi:10.1177/1071100717690805

27. Barnes PJ, Baldock C, Meikle SR, Fulton RR. Benchmarking of a motion sensing system for medical imaging and radiotherapy. *Phys Med Biol*. 2008;53(20):5845-5857. doi:10.1088/0031-9155/53/20/019

28. Sugano N, Sasama T, Sato Y, et al. Accuracy evaluation of surface-based registration methods in a computer navigation system for hip surgery performed through a posterolateral approach. *Comput Aided Surg*. 2001;6(4):195-203. doi:10.1002/igs.10011

29. Q L, L Z, Z J, et al. Effect of Optical Digitizer Selection on the Application Accuracy of a Surgical Localization System-A Quantitative Comparison Between the OPTOTRAK and Flashpoint Tracking Systems. *Comput Aided Surg*. 1999;4(6). doi:10.1002/(SICI)1097-0150(1999)4:6<314::AID-IGS3>3.0.CO;2-G

30. Goislard de Monsabert B, Visser JMA, Vigouroux L, Van der Helm FCT, Veeger HEJ. Comparison of three local frame definitions for the kinematic analysis of the fingers and the wrist. *J Biomech*. 2014;47(11):2590-2597. doi:10.1016/j.jbiomech.2014.05.025

31. Hassan EA, Jenkyn TR, Dunning CE. Direct comparison of kinematic data collected using an electromagnetic tracking system versus a digital optical system. *J Biomech*. 2007;40(4):930-935. doi:10.1016/j.jbiomech.2006.03.019

32. Maletsky LP, Sun J, Morton NA. Accuracy of an optical active-marker system to track the relative motion of rigid bodies. *J Biomech*. 2007;40(3):682-685.

Chapter 3

3 **The Effect of Flexor Digitorum Profundus Repair Position Relative to Camper's Chiasm on Tendon Biomechanics**

OVERVIEW: This chapter introduces an in-vitro cadaveric study evaluating the impact of altering the repair site of the profundus tendon within zone II of the finger. The chapter begins with a brief overview on the challenges faced with tendon injuries and continues to introduce the experimental protocol followed and the results of the metrics of interests that were measured. The chapter then concludes with a proposed clinical message and recommendations made based on the study and its relevance within literature.[*]

3.1   Introduction

The presence of both flexor digitorum superficialis (FDS) and flexor digitorum profundus (FDP) tendons within the narrow zone II flexor tendon sheath of the hand presents a unique challenge in repair. Due to the complex anatomy, injuries in this zone often have relatively poor post-operative outcomes[1]. Two goals of ideal repair include ensuring adequate strength while optimizing tendon gliding[2]. Various solutions to improve FDP gliding have been examined in the literature, including partial or complete excision of the FDS tendon, pulley resection or venting, and repair of FDS outside of the A2 pulley[3–8]. However, there are drawbacks to these methods, as FDS integrity is thought to be important to prevent hyperextension of the proximal interphalangeal joint (PIPJ) with forceful pinch and allow stronger flexion force, while native position of the flexor tendons relative to the pulleys helps prevent bowstringing[9,10].

Tang *et al.*[4] found that removal of FDS under the A2 pulley resulted in decreased work of flexion of the FDP, whereas removal of FDS distal to the pulley did not significantly change FDP work of flexion, suggesting that the area under the A2 pulley has the greatest impact on FDP gliding. In this area, instead of partial or complete excision of FDS under the pulley or venting the pulley, the path of FDP after repair could be altered so that it lies outside the FDS slips.

The level where FDS divides into slips and then unites into terminal tendons, commonly referred to as Camper's Chiasm, is thought to not only provide a pathway for FDP to move from its dorsal to palmar position, but also to act as a pulley system and increase balance stability of the PIPJ[10]. However, it is an area thought to negatively impact gliding after tendon repair[3,4]. Thus, the purpose of this study was to determine whether repair of a zone II FDP laceration inside Camper's Chiasm versus outside would impact tendon loads.

3.2   Materials and Methods

Eight fresh-frozen upper extremities were utilized (4 male, 2 female; age: 65.6 ± 6.8 years). Twenty digits, consisting of the index, long, ring, and small fingers were tested. Specimens were excluded from the study if their computed tomography (CT) scans showed the presence of osteoarthritis or any other visible deformities at the finger joints. All screened specimens were amputated 15 cm proximal to the wrist, then thawed overnight (approximately 16 hours) at room temperature prior to simulation and checked for normal passive range of motion (ROM).

3.2.1 Specimen Preparation

Careful dissection of the wrists was performed to isolate the FDP, FDS, and the extensor digitorum communis (EDC) of each finger (Figure 3.1). Once isolated, each tendon was then sutured with a Krackow stitch and connected to a uni-axial load cell (Model 34; Honeywell, Charlotte, NC) using a 0-braided Vicryl suture (Ethicon, Somerville, NJ), which was mounted to the end-shaft of a linear servo-actuator (Figure 3.2). The dorsal skin was then re-approximated with a running closure prior to simulated active motion testing. Specimens were secured in the motion simulator in a supinated position using four transverse screws – two in the ulna and two in the radius. The second to fifth metacarpals were then cross-pinned using two 1.5 mm K-wires, and a 2 mm Dacron-braided cable (Melton International Tackle, Anaheim, CA) was used to constrain the metacarpal K-wires to secure the wrist during simulated active finger motions. Finally, a fixed rigid foam block was used to support the dorsum of the hand in a neutral wrist position.

Figure 3.1: Flexor Tendon Isolation and Suturing

Dissection of the wrists was performed to isolate and suture the flexor digitorum profundus (FDP), flexor digitorum superficialis (FDS), and the extensor digitorum communis (EDC) of each tested finger using 0-braided Vicryl in a locked Krackow fashion.
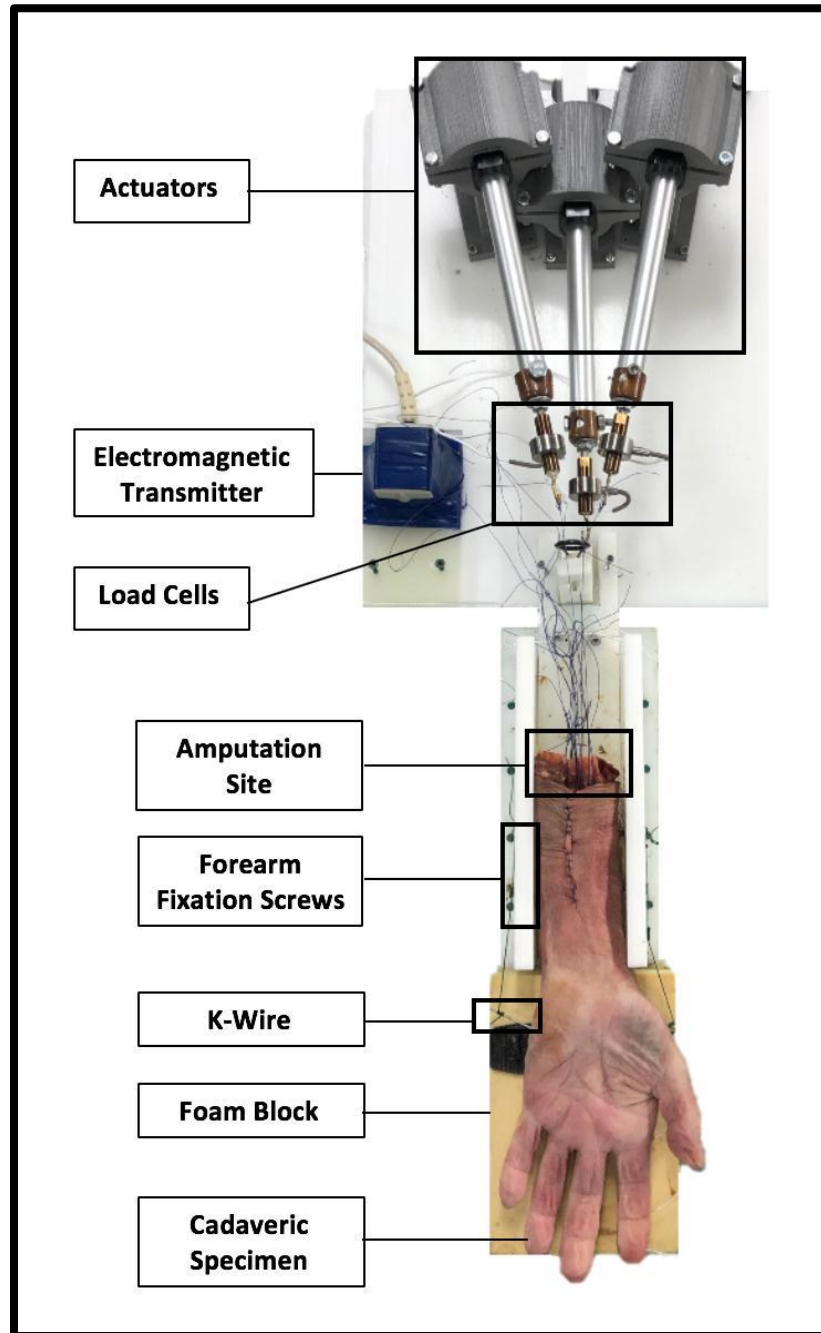
Figure 3.2 – Specimen Setup in Action Finger Motion Simulator

Linear servo-actuators were used to generate active finger motion. Tendon loads were controlled and measured using uni-axial load cell feedback, and finger motions were recorded by electromagnetic tracking.

3.2.2 In-Vitro Active Finger Motion Simulation

Simulated active finger flexion/extension was controlled using a previously reported finger motion simulation protocol[11]. In order to determine tendon excursion for each finger, a flexion trial in the intact tendon condition was initially performed by moving FDP and FDS in position control against a constant 10 N antagonist load on the extensor until full flexion ROM was achieved in all joints (MCP: $83 \pm 10°$, PIP: $101 \pm 13°$, DIP: $57 \pm 9°$). This was repeated for finger extension, with the extensor tendon in position control against a constant 5 N load on each flexor tendon. Subsequently, all motion trials for every tested surgical condition were performed with the same tendon excursions measured in the intact condition.

3.2.3 Tendon Repair Techniques

A longitudinal volar midline incision was carried out on the digit from 1 cm proximal to the MCPJ to the PIPJ. The flexor tendon sheath was exposed through an incision between A2 and A4 pulleys, involving the A3 pulley, to visualize Camper's Chiasm, taking care not to injure the A2 and A4 pulleys. The FDP tendon was then sharply incised with a scalpel in a transverse fashion 1 cm distal to the A2 pulley[12]. Once incised, the FDP tendon underwent two different repair techniques: inside- and outside-chiasm (Figure 3.3). Repairs were carried out in random order using 3-0 Ethibond Excel (Ethicon, Somerville, NJ) with a 4-strand Adelaide technique. Skin was then re-approximated to maintain specimen hydration during motion trials.
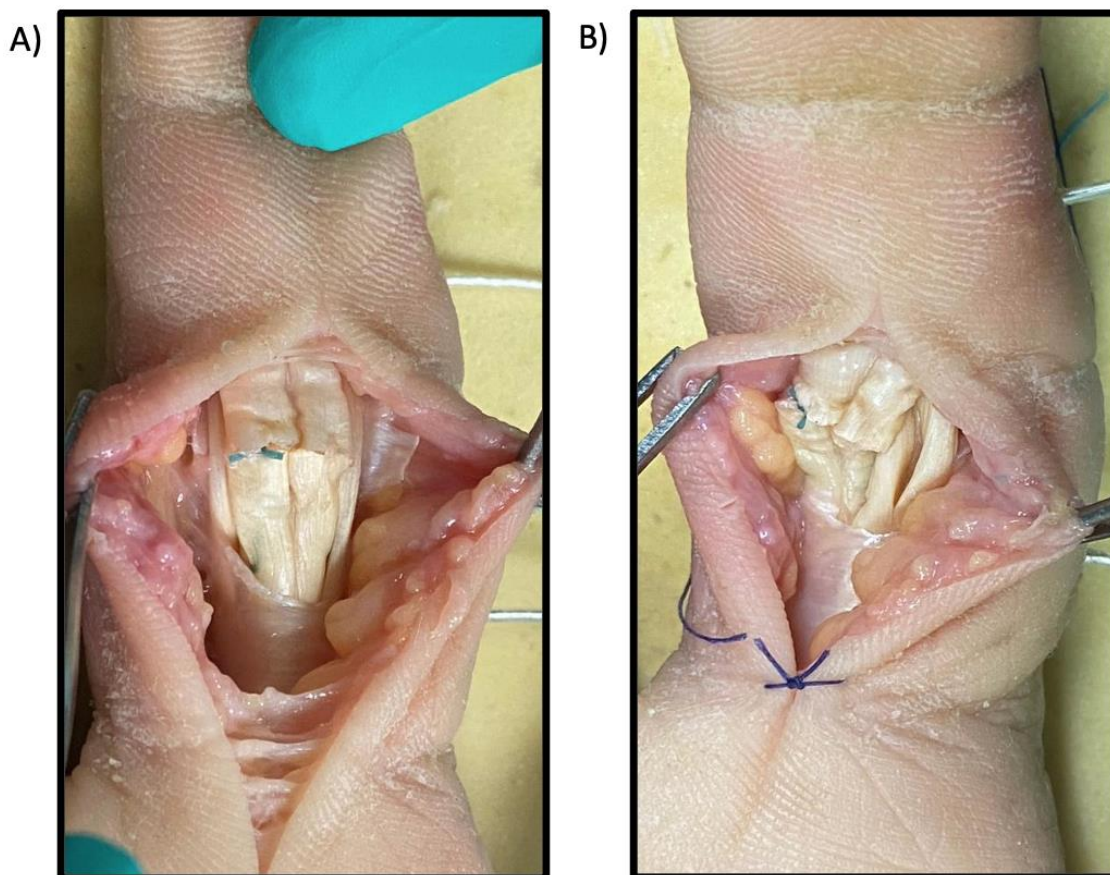
Figure 3.3: Chiasm Repair Techniques

The finger conditions following intact are illustrated, (a) inside-chiasm and (b) outside-chiasm. The divergence of the flexor digitorum profundus (FDP) tendon's anatomical line of action is characteristic of the two repair techniques.

3.2.4 Joint Angle Measurement

Joint angles were measured using the previously validated trakSTAR® (NDI, Waterloo, ON, Canada) electromagnetic tracking system in Chapter 2. To install the trackers, short lateral incisions were made along the finger to expose the lateral aspect of each bone segment. Three electromagnetic trackers (2 mm Ø, model M180, trakSTAR, NDI) were then press-fit into 2.1 mm drill holes made laterally at the center of each phalanx. A fourth reference tracker was similarly inserted into the metacarpal of the second digit. Total active

joint ROM was recorded as the collective angle achieved by the DIPJ, PIPJ, and MCPJ together.

3.2.5 Tendon Load and Work of Flexion Measurement

Flexor and extensor tendon load feedback was provided by the uni-axial load cells mounted to the end shaft of each linear servo actuator and closed-loop load control was achieved using custom code made in the LabVIEW programming environment (National Instruments, Austin, TX). The work of flexion (WOF) was calculated as the area under the tendon load versus tendon excursion curve[13]. WOF done by FDP and FDS was evaluated through the complete flexion range for each finger.

3.2.6 Motion Trial Protocols

Loads experienced by both flexor tendons, as well as joint angles, were collected under the three tested FDP tendon conditions: 1) intact; 2) inside-chiasm repair; and 3) outside-chiasm repair. All remaining tissues within the specimen were left intact and saline solution was used to maintain hydration throughout testing to prevent desiccation. All three conditions were tested in each finger in a repeated-measures model, with the repairs performed in random order. Each finger motion was repeated 3 times, and measurements from the 3rd motion trial were recorded for statistical analysis; the first 2 motions ensured that the finger was preconditioned following the prior surgical intervention.

3.2.7 Statistical Analysis

Two-way repeated-measures ANOVA models, with Bonferroni correction, were performed to analyze the effect of the two FDP repair techniques on tendon load, WOF and joint ROM within all three tested conditions of FDP(intact, inside-chiasm, and outside-chiasm). Within-subject effects and pairwise comparisons were also examined, with significance set at $p < 0.05$.

3.3   Results

3.3.1   Active Joint Motion

The repairs had no statistically significant effect on active joint ROM (p=0.256) (Figure 3.4). The change from intact ROM caused by the inside- and outside-chiasm repairs was +1.65 ± 0.74° (p=1.000) and -2.95 ± 0.50° (p=0.657), respectively. Thus, finger ROM was not altered by either repair.
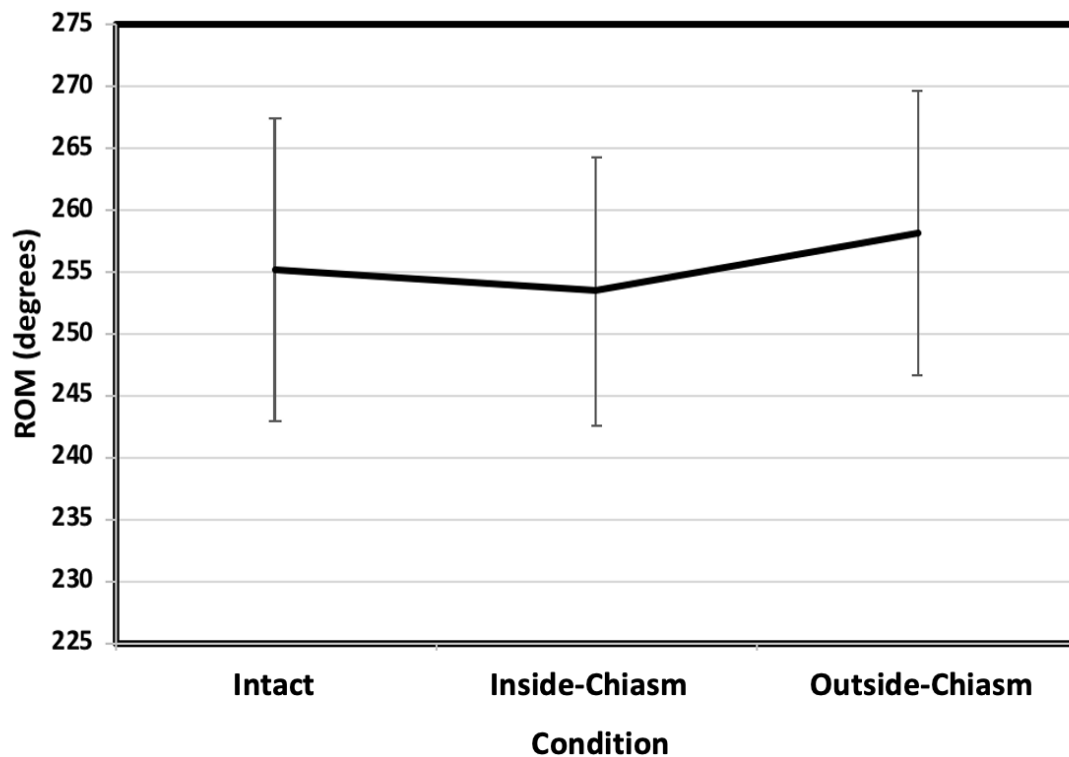
Figure 3.4: Total Active ROM

Total ROM was calculated as the sum of all finger joints, distal interphalangeal to the metacarpophalangeal (DIPJ to MCPJ) as a function of finger condition (*p<0.05), where whiskers denote one standard deviation of 20 finger specimens. No statistically significant difference in ROM was found. The inside-chiasm repair decreased ROM by 1.65 ± 0.74°, whereas the outside-chiasm repair increased ROM by 2.95 ± 0.5°, though not statistically significant.

3.3.2 Flexor Tendon Loads

Tendon loads increased significantly with flexion angle for every condition (p<0.001) (Figure 3.5). At full flexion, the outside-chiasm repairs significantly increased FDP loads by 3.8 ± 2.9 N (p=0.014) and reduced FDS loads by 1.5 ± 1.2 N (p=0.015) compared to the intact condition. These effects from outside-chiasm repair represent percent differences of +32% and -9% load changes to FDP and FDS load, respectively. Notably, the outside-chiasm repair increased FDP load in all 20 specimens. The inside-chiasm repairs had no significant effect on tendon loads; measured differences were $+0.9 \pm 1.5$ N (p=0.420) and -0.8 ± 1.1 N (p=0.168) for FDP and FDS, respectively. Comparing the two conditions, outside-chiasm repairs resulted in a significant increase of 3.8 ± 2.2 N (p=0.014) in FDP loads compared to inside-chiasm repairs.
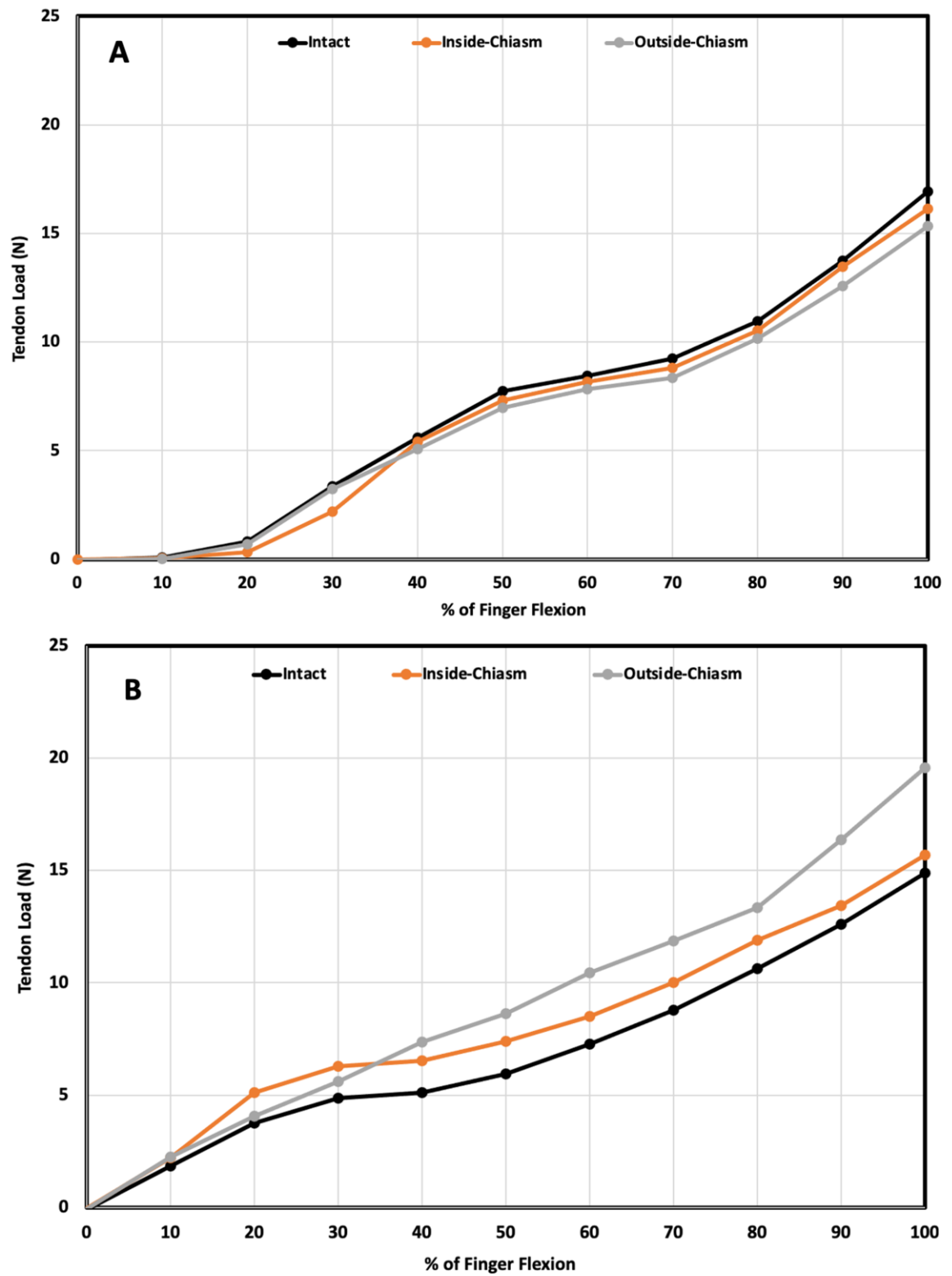
Figure 3.5: Tendon Load vs. Finger Flexion

Flexor tendon loads experienced by a) FDP and b) FDS as a function of percent flexion range. Tendon loads increased with flexion angle for every condition (p<0.001). At full flexion, the outside-chiasm repairs significantly increased FDP loads by 3.8 ± 2.9 N (p=0.014) and reduced FDS loads by 1.5 ± 1.2 N (p=0.015) compared to the intact condition.

3.3.3 Work of Flexion

From the intact condition, outside-chiasm repairs significantly increased the WOF for FDP by 115.3 ± 56.3 N.mm (p<0.001), while reducing WOF for FDS by 67.3 ± 111.2 N.mm (p=0.042) (Figure 3.5). The inside-chiasm repairs did not significantly affect WOF; measured differences were +26 ± 48.6 N.mm (p=0.082) and -31.6 ± 60.1 N.mm (p=0.089) for FDP and FDS, respectively. Comparing the two repairs, the WOF by FDP was 89.3 ± 65.1 N.mm greater with outside-chiasm than with inside-chiasm repair (p<0.001). The WOF by FDS was not affected by repair type (p=0.381).
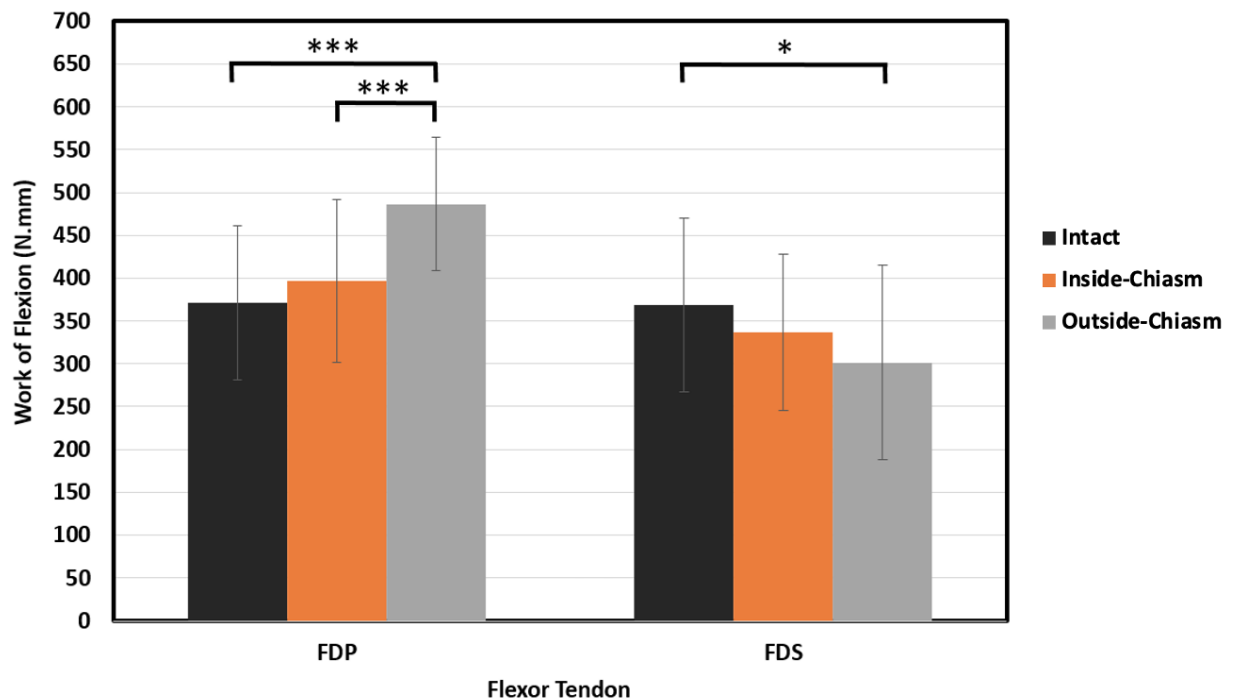
Figure 3.6: Work of Flexion

*Work of flexion summed over the full range (WOF) as a function of repair type (n=20; Mean ± 1 SD; *p<0.05; ***<0.001). The outside-chiasm repair significantly increased*

FDP's WOF by 115.3 ± 56.3 N.mm (p<0.001) and decreased FDS' WOF by 67.3 ± 111.2 N.mm (p=0.042) compared to the intact condition. Furthermore, the outside-chiasm repair resulted in 89.3 ± 65.1 N.mm greater WOF than the inside-chiasm repair (p<0.001). The inside-chiasm repair did not significantly affect WOF.

3.4   Discussion

The ideal treatment of tendon injuries restores functional stability and motion of the finger and alleviates pain; however, treatment of zone II flexor tendon injuries remains a challenge despite improvements in repair outcomes[14,15]. A common concern in zone II flexor tendon repair is tendon bulk, which in excess, can restrict tendon gliding through the pulley system and impede motion. In particular, repair bulk within the tendon sheath around the A2 pulley increases tendon resistance to glide but may reflect a stronger repair. Various methods have been used to decrease gliding resistance, however the influence of FDP tendon repair position relative to Camper's Chiasm on tendon load, digit work of flexion, and joint motion has not been previously reported[3–8]. The impact of varying FDP's line of action within the chiasm is unknown; therefore, this study focused on evaluating the biomechanics of varying FDP repair location, comparing inside versus outside chiasm repairs.

Using WOF, flexor tendon load, and ROM as measures for effectiveness of the repair placement[16,17], this *in-vitro* study found that performing an FDP tendon repair within the chiasm did not alter flexor tendon loads in either the FDP or FDS tendons. In contrast, FDP repairs done outside of the chiasm significantly increased FDP loads and WOF, reaching maximum increases at full flexion of +32% (p=0.014) and +31% (p<0.001), respectively. Moreover, FDS loads and WOF were significantly decreased by -9% (p=0.015) and -18% (p=0.042), respectively. This indicates that the outside-chiasm repair shifted the balance of shared tendon load from FDS to FDP, which is evidenced by their mirrored loading patterns (Figure 3.5). However, this redistribution did not conserve the total tendon load or WOF. Summing the tendon loads reveals that the inside-chiasm repair conserved the total sum of FDP+FDS load, whereas the outside-chiasm repair added more than 4 N (10%) to the sum total, with all of this additional tendon load placed on FDP.

Comparing repairs to each other, FDP load and WOF were 25% and 22% higher with outside-chiasm versus inside-chiasm repairs (p<0.001).

An important function of the chiasm is to provide a pathway for FDP to move from dorsal to palmar relative to FDS, while maintaining a midline pull. Rerouting FDP altered the axis of pull and may have introduced intertendinous wrapping as FDP came around the side of the FDS tendon, which likely reduced efficiency of excursion[18,19]. The change in axis can be appreciated in the resting position in Figure 3.2. The FDP tendon loads observed in Figure 3.5a followed the intact pattern with inside-chiasm repair, but not with outside-chiasm, indicating that FDP biomechanics were negatively impacted by removal from the chiasm. An interesting observation is that the inside- and outside-chiasm tendon load curves cross each other between 20% and 40% of the flexion range – the only sub-range where the repairs were not significantly different from each other (Figure 3.5). This phenomenon occurred in all fingers, and it was more pronounced in FDP than in FDS, once again owing to the FDP repairs.

The chiasm also provides a smooth gliding surface for FDP[4,20]; however, a rationale for rerouting FDP out of the chiasm is to avoid increased intertendinous gliding resistance caused by bulk of the FDP repair passing through the FDS slips. In addition, with finger flexion, the slips of FDS are thought to compress FDP, possibly causing more compression on a tendon repair site and thus increase loads[21]. These results, however, show that this alteration increased FDP loads and WOF significantly compared to both the intact condition and inside-chiasm repair, refuting part of the hypothesis made in chapter 1. However, in contrast to tendon gliding, a linear relationship between tendon load and excursion was established ($R^2 = 0.9915$) based on study findings; supporting the remaining part of the hypothesis made in chapter 1.

Limitations should be considered when interpreting the results: (1) the cadaveric specimens used were previously frozen and of advanced age; (2) the sacrificing of the tendon sheath and A3 pulley to gain access to the chiasm site was unavoidable and thus, may have altered the biomechanics of the finger, however the A2 and A4 pulleys were confirmed to be intact; and (3) amputation of the arm proximal to the wrist was necessary

to accommodate the simulator. However, a repeated-measures experimental design was employed, and thus, any changes in the biomechanics due to the amputation were applied to all tested conditions.

Despite these limitations, this study has important strengths: (1) the 4-core Adelaide tendon repair technique reflected standard clinical practice; and (2) the use of an advanced, repeatable, and validated *in-vitro* active motion simulator with position and load control of the tendons, which allowed biomechanical measurements of isolated conditions. This is evidenced by observations that the repair sequence did not affect tendon loads (p=0.309) or WOF (p=0.498), and ROM was not altered by either repair (p>0.05).

3.5   Conclusion

Findings from this study support the choice to repair FDP tendon lacerations within the chiasm as opposed to outside of the chiasm, given that out of chiasm repair increased FDP load by an average of 32%. Further clinical correlation is needed to determine the long-term effects of the changes in tendon loads reflected in our study.

3.6   References

1.   Kotwal PP, Ansari MT. Zone 2 flexor tendon injuries: Venturing into the no man's land. *Indian J Orthop*. 2012;46(6):608-615. doi:10.4103/0019-5413.104183

2.   Green DP, Scott W W. Green's Operative Hand Surgery. In: *Flexor Tendon Injury*. 6th ed. Philadelphia, PA: Elsevier/Churchill Livingstone; 2011:189-195.

3.   Zhao C, Amadio PC, Zobitz ME, An K-N. Resection of the flexor digitorum superficialis reduces gliding resistance after zone II flexor digitorum profundus repair in vitro. *J Hand Surg Am*. 2002;27(2):316-321. doi:10.1053/jhsu.2002.31729

4.   Tang JB, Xu Y, Chen F. Impact of flexor digitorum superficialis on gliding

function of the flexor digitorum profundus according to regions in zone II. *J Hand
Surg Am*. 2003;28(5):838-844. doi:10.1016/s0363-5023(03)00300-9

5.   Kwai Ben I, Elliot D. "Venting" or partial lateral release of the A2 and A4 pulleys

after repair of zone 2 flexor tendon injuries. *J Hand Surg Br*. 1998;23(5):649-654.

http://www.ncbi.nlm.nih.gov/pubmed/9821612. Accessed July 24, 2017.

6.   Tang JB. Indications, methods, postoperative motion and outcome evaluation of

primary flexor tendon repairs in Zone 2. *J Hand Surg Eur Vol*. 2007;32(2):118-

129. doi:10.1016/j.jhsb.2006.12.009

7.   Tang JB. New Developments Are Improving Flexor Tendon Repair. *Plast

Reconstr Surg*. 2018;141(6):1427-1437. doi:10.1097/PRS.0000000000004416

8.   Geary MB, English C, Yaseen Z, Stanbury S, Awad H, Elfar JC. Flexor digitorum

superficialis repair outside the A2 pulley after zone II laceration: gliding and

bowstringing. *J Hand Surg Am*. 2015;40(4):653-659.

doi:10.1016/j.jhsa.2014.12.045

9.   Tang JB, Zhou X, Pan ZJ, Qing J, Gong KT, Chen J. Strong Digital Flexor Tendon

Repair, Extension-Flexion Test, and Early Active Flexion: Experience in 300

Tendons. *Hand Clin*. 2017;33(3):455-463. doi:10.1016/j.hcl.2017.04.012

10.   Schmidt H-M, Zhang S-X, Zieseniss K. Clinical anatomy of the chiasma

tendlinum (camper) in the fingers. *Clin Anat*. 1994;7(2):65-71.

doi:https://doi.org/10.1002/ca.980070202

11.   Haddara MM, Byers B, Chinchalkar S, Ferreira LM, Suh N. The Effect of Wrist

Position on Finger Tendon Loads Following Pulley Sectioning and Operative Reconstruction. *J Hand Surg Glob Online*. 2019;1(3):154-160. doi:10.1016/j.jhsg.2019.04.002

12.   Gordon JA, Stone L, Gordon L. Surface markers for locating the pulleys and flexor tendon anatomy in the palm and fingers with reference to minimally invasive incisions. *J Hand Surg Am*. 2012;37(5):913-918. doi:10.1016/j.jhsa.2011.12.036

13.   Zhao C, Amadio PC, Berglund L, Zobitz ME, An K-N. A new testing device for measuring gliding resistance and work of flexion in a digit. *J Biomech*. 2003;36(2):295-299. doi:10.1016/s0021-9290(02)00300-7

14.   Gibson PD, Sobol GL, Ahmed IH. Zone II Flexor Tendon Repairs in the United States: Trends in Current Management. *J Hand Surg Am*. 2017;42(2):e99-e108. doi:10.1016/j.jhsa.2016.11.022

15.   Coats RW, Echevarría-Oré JC, Mass DP. Acute flexor tendon repairs in zone II. *Hand Clin*. 2005;21(2):173-179. doi:10.1016/j.hcl.2004.11.001

16.   Xie RG, Cao Y, Xu XF, Zhu B. The gliding force and work of flexion in the early days after primary repair of lacerated flexor tendons: An experimental study. *J Hand Surg Eur Vol*. 2008;33(2):192-196. doi:10.1177/1753193408087035

17.   Aoki M, Manske PR, Pruitt DL, Kubota H, Larson BJ. Work of flexion after flexor tendon repair according to the placement of sutures. *Clin Orthop Relat Res*. 1995;(320):205-210. doi:10.1097/00003086-199511000-00033

18.   Strickland J. Flexor tendon injuries: Foundations of treatment. *J Am Acad Ortho Surg*. 1995;3:44-45.

19.   Sapienza A, Yoon HK, Karia R, Lee SK. Flexor tendon excursion and load during passive and active simulated motion: a cadaver study. *J Hand Surg Eur Vol*. 2013;38(9):964-971. doi:10.1177/1753193412469128

20.   Pike JM, Gelberman RH. Zone II combined flexor digitorum superficialis and flexor digitorum profundus repair distal to the A2 pulley. *J Hand Surg Am*. 2010;35(9):1523-1527. doi:10.1016/j.jhsa.2010.06.024

21.   Walbeehm ET, McGrouther DA. An anatomical study of the mechanical interactions of flexor digitorum superficialis and profundus and the flexor tendon sheath in zone 2. *J Hand Surg Br*. 1995;20(3):269-280. doi:10.1016/s0266-7681(05)80077-4

Chapter 4

4   Development of an In-Vitro Swan Neck Deformity Biomechanical Model

OVERVIEW: Swan neck deformities are quite common yet challenging to treat. However, although various operative and post-operative management protocols have been investigated, complications that arise following a SND repair are common and not well understood. Hence, the basis of the proposed chapter introduces the use of strain gauges to measure strain induced by the PIPJ volar plate in an in-vitro cadaveric setting. This study will properly examine, evaluate, and design an advanced swan neck deformity finger model that can provide a clear and detailed understanding of how different stresses along the flexor/extensor tendons and strains induced by the volar plate can enhance the development of a SND. This chapter will then conclude with the relevance of such a model and how it will help reduce the risk of complication following a repair.[*]

4.1 Introduction

Swan neck deformity (SND) is a condition characterized by the hyperextension of the proximal interphalangeal joint (PIPJ) and the compensatory flexion of the distal interphalangeal joint (DIPJ) of the finger[1,2]. There are several pathoetiologies that produce the clinical phenotype of SND[3], and causes can originate at the metacarpophalangeal joint (MCPJ), the PIPJ, or the DIPJ. Examples of such etiologies include neurologic disorders that result in extensor hyperactivity (spinal cord injuries)[4], rheumatologic diseases that cause attritional tendon ruptures (rheumatoid or psoriatic arthritis)[3,5,6], connective tissue disorders including Ehlers-Danlos and Marfan's Syndrome that can cause PIPJ volar plate laxity[7,8], and post-traumatic causes (flexor or extensor tendon injuries)[9,10]. In this paper, we will focus on SND secondary to distal extensor tendon injury given its common clinical prevalence and ease of reproducibility in the cadaveric setting.

Laceration or rupture of the terminal extensor tendon, known as "mallet finger", results in a flexion deformity at the DIPJ due to the unopposed pull of flexor digitorum profundus (FDP) tendon. If left untreated, mallet finger becomes chronic and leads to PIPJ volar plate insufficiency as the lateral bands subluxate dorsally and centrally, limiting the power of extension at the DIPJ with subsequent hyperextension of the PIPJ, ultimately resulting in the characteristic "swan neck" deformity[11,12].

The development of an *in-vitro* cadaveric swan neck model would provide an important baseline for evaluating surgical treatments of SND. Therefore, the primary objective of this study was to design a clinically relevant and reproducible cadaveric SND model. The challenge is that PIPJ hyperextension is not immediately appreciable following mallet finger injury, even when it is thoroughly induced in a cadaver. However, the eventual volar plate insufficiency that occurs clinically suggests that an imbalance of soft tissue strain arises with the mallet finger injury, and that this persistent imbalance leads to attrition of the volar plate. Based on this rationale, we hypothesized that a sudden rise in volar plate strain would be detected upon creation of the simulated SND finger injury.

4.2   Materials and Methods

Eight fresh-frozen upper extremities were utilized (4 male, 4 female; age: 69.2 ± 2.4 years). Twenty-one digits, comprised of the index, long, and ring fingers were tested. Specimens were amputated 15 cm proximal to the wrist. All specimens underwent computed tomography (CT) scans and were excluded if any arthritic pathology was present. Specimens were thawed for 18 hours prior to biomechanical testing, then checked for normal digital passive range of motion (ROM). Simulated active flexion/extension was controlled using a previously reported finger motion simulator[13]. Specimens were transfixed in the motion simulator in a supinated position using four transverse screws – two in the ulna and two in the radius. The second to fifth metacarpals were then cross-pinned using two 1.5 mm Kirshner wires (K-wires), and a 2 mm Dacron-braided cable was used to constrain the metacarpal K-wires to secure the wrist during simulated active finger motions. Finally, a fixed rigid foam block supported the dorsum of the hand in a neutral wrist position, as previously reported[13].

Careful dissection of the specimens was performed by a hand surgery resident supervised by a fellowship-trained hand surgeon to isolate the flexor digitorum superficialis (FDS), flexor digitorum profundus (FDP), and extensor digitorum communis (EDC) tendons of the index, long, and ring fingers. A dorsal midline wrist incision was made through the skin and subcutaneous tissues. Dissection was carried down to the level of the extensor retinaculum, which was incised over the fourth dorsal compartment. The EDC tendon slips to the index, long, and ring fingers were identified and independently tagged with 0-Vicryl suture using a locking Krakow technique and connected to linear servo actuators for testing[13]. The retinaculum was then repaired and the dorsal skin was re-approximated with a running closure. Next, a midline volar skin incision was utilized to identify the FDS and FDP tendons, which were tagged in the same manner as above. Closure was performed in a standard fashion. Saline solution was used to maintain tissue hydration throughout simulation to prevent tendon desiccation.

4.2.1 PIPJ Extension Angle Measurement

Three, 2 mm diameter electromagnetic trackers (M180, trakSTAR, ON) were used to measure the terminal angles achieved by each joint (DIPJ, PIPJ and MCPJ). To install the trackers, short mid-lateral incisions were used along the finger to expose the lateral aspect of each bone segment. Then, 2.1 mm holes were drilled in the center of each phalanx, and a tracker was press-fit into each hole to sit flush within the bone. A fourth tracker was also inserted within the metacarpal of the second digit to confirm stable fixation of the hand.

4.2.2 Volar Plate Strain Measurement

A volar midline incision centered over the PIPJ was utilized, and full thickness radial and ulnar skin flaps were raised. The C1, A3, and C2 pulleys were incised, taking care to preserve the A2 and A4 pulleys. The flexor tendons were retracted ulnarly, exposing the underlying volar plate while ensuring that the integrity of the plate remains intact. Next, a small transverse incision was made at the distal edge of the volar plate down to bone, and a small uni-axial strain gauge (0.7 cm x 0.3 cm, Omega, CT, United States) was inserted deep to the volar plate and fixed using 4-0 Vicryl suture in a figure of 8 configuration. A small transverse incision was made at the level of the radial skin flap overlying the middle phalanx, and the wire of the strain gauge was passed through this split and secured with 0 Vicryl sutures (Figure 4.1). The longitudinal skin incision was closed, and the strain gauge wires were further secured to the palm of the hand using Mastisol (Ferndale Laboratories, Inc., MI, United States) and adhesive tape (Figure 4.2).
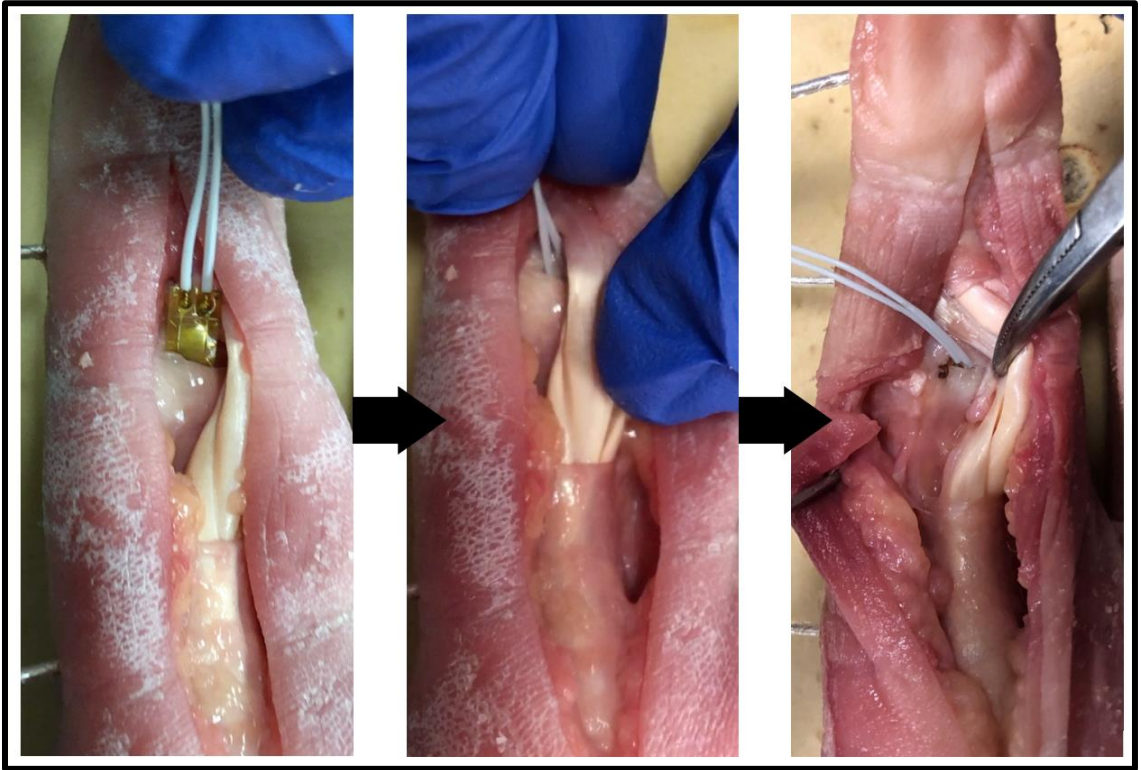
Figure 4.1: Volar Plate Strain Gauge Insertion

The PIPJ volar plate was identified and separated from bone. The strain gauge was inserted under the volar plate and secured with a suture.
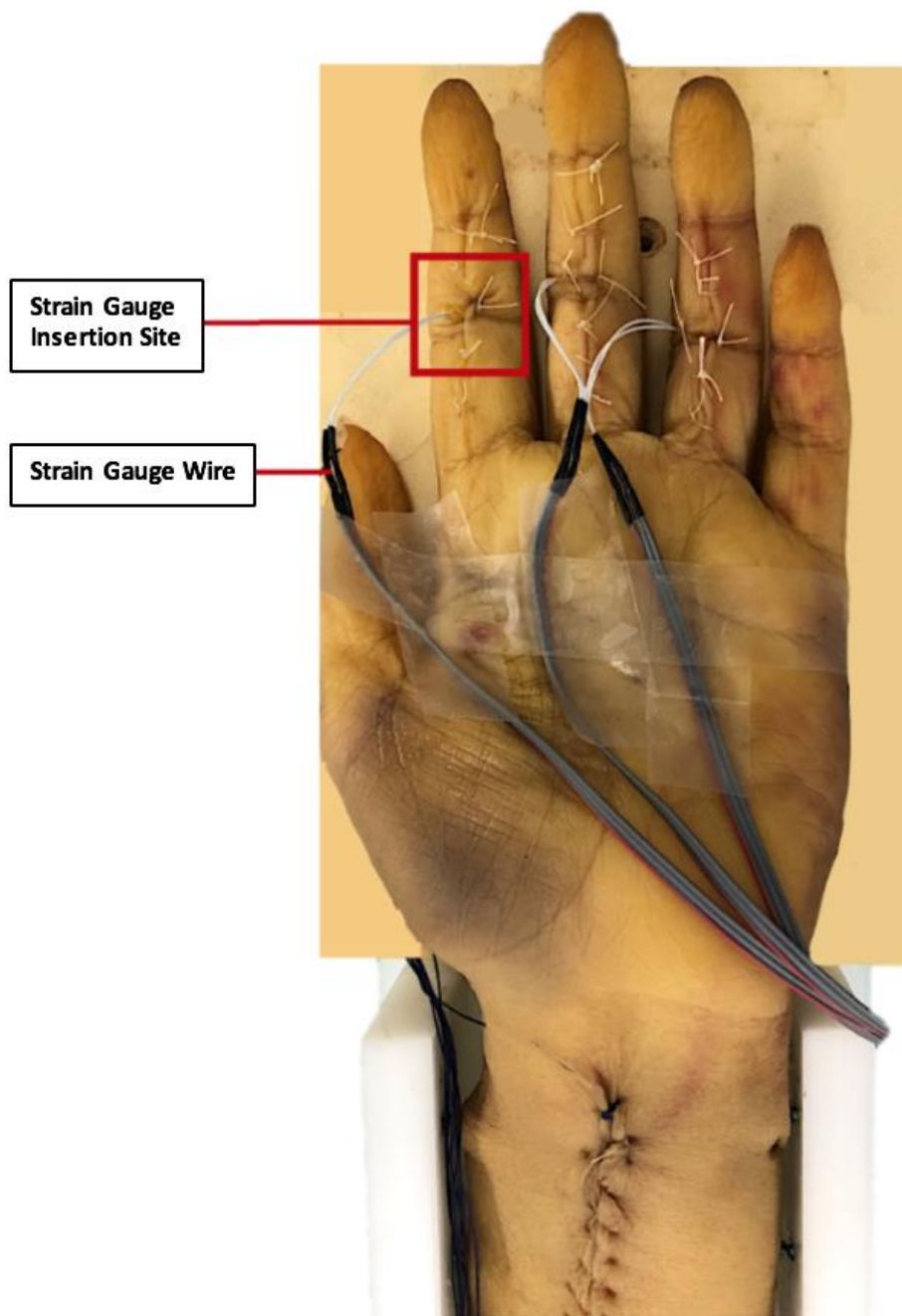
Figure 4.2: Volar Plate Strain Measurement

A uni-axial strain gauge was inserted under the volar plate of the index, middle and ring fingers to measure strain at full extension. The strain gauge wires were adhered onto the skin using Mastisol and reinforced by tape to secure them during motion trials.

4.2.3 Swan Neck Model

A mallet finger was created using a transverse incision along the dorsal aspect of the index, long, and ring finger DIP joints. The terminal extensor tendon was cut by dissecting to, but not through, the DIPJ capsule, and confirming that each digit assumed a position of resting flexion at the DIPJ after this dissection.

In order to complete the swan neck model, the previous volar skin incision was used, and skin flaps were further mobilized dorsally. Subsequently, a longitudinal incision along the radial and ulnar borders of the PIPJ, down to the joint capsule, was made to release the transverse retinacular ligaments to allow the lateral bands to subluxate dorsally (Figure 4.3). Skin was re-approximated.

4.2.4 Motion Control and Volar Strain Measurements

Motion control and data acquisition software was custom coded using the LabVIEW programming environment (National Instruments). Tendon excursions were closed-loop controlled with servo actuators using the same protocols established in a prior study[13]. Each motion cycle (full flexion followed by full extension) was repeated 5 times to assess repeatability. Volar strain values were collected under three finger conditions: 1) intact, 2) mallet finger, and 3) swan neck deformity (SND).

4.2.5 Data Analysis

A two-way repeated-measures ANOVA model, with a Bonferroni correction, was performed to analyze the effect of finger condition with 3 levels (intact, mallet, SND), as well as the effect of different fingers (index, long, and ring). Within-subject effects and pairwise comparisons were also examined, with significance set at $p < 0.05$. Repeatability of the strain gauge was assessed by the standard deviation taken over the 5 repeated trials in each condition. In addition, a correlation test was conducted to determine the relationship between volar plate strain and PIPJ terminal extension angle.
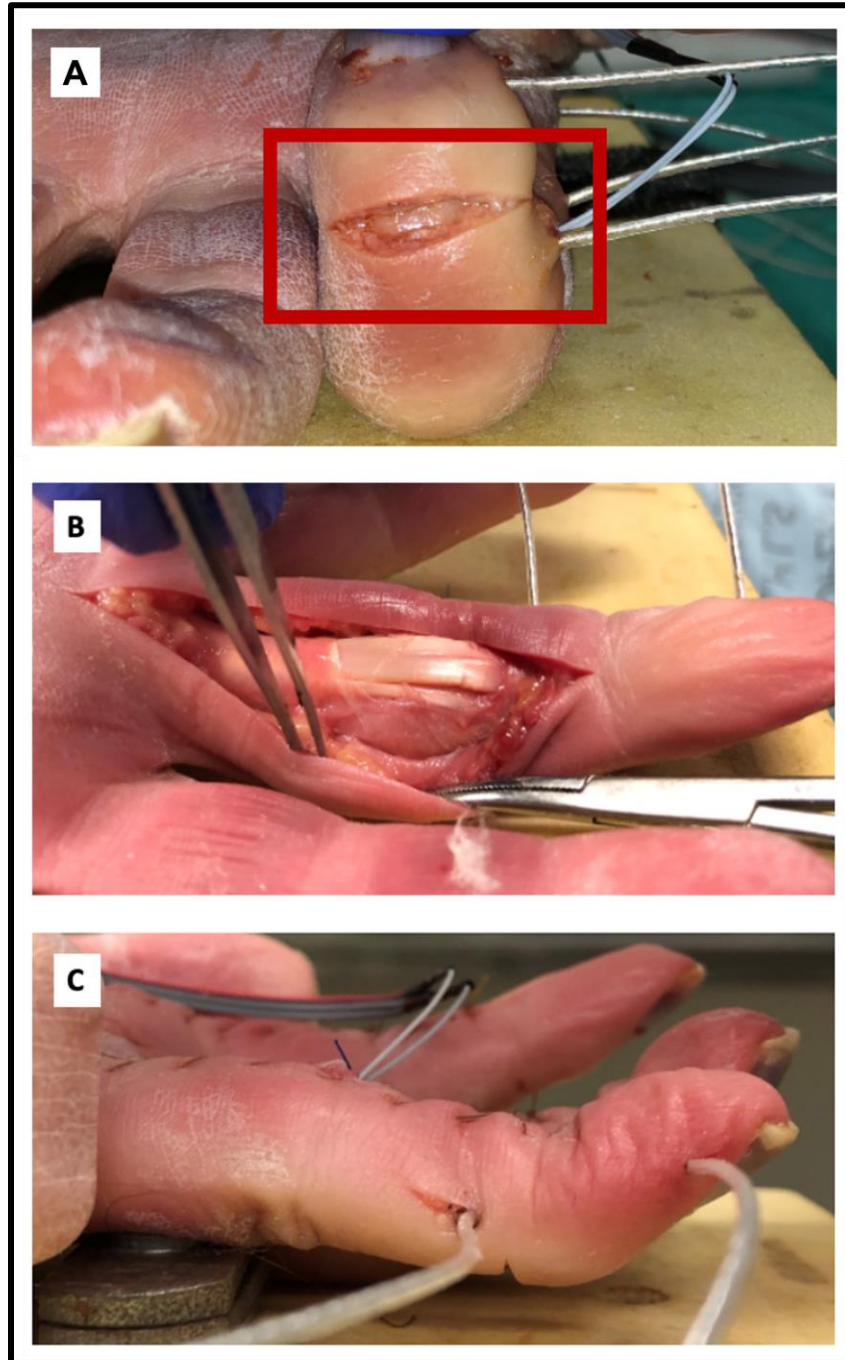
Figure 4.3: Mallet + TRL Release

The two finger conditions are illustrated: (a) simulated tear in the extensor mechanism at the DIPJ (mallet) and (b)TRL release at the PIPJ, resulting in (c) a swan neck deformity. Lead wires from electromagnetic trackers are seen protruding transversely from the bone segments, and the volar plate strain gauge lead wires protruding from the PIPJ.

4.3   Results

4.3.1 Volar Plate Strain

The intact condition at full extension served as the baseline for determination of delta strain (ΔStrain) measured at the volar plate, which represented the change in strain from the intact condition to the subsequent mallet and SND conditions (Figure 4.4). Strain in the volar plate increased progressively with creation of the mallet and SND conditions (p=0.015). At terminal extension, the mallet condition increased volar plate strain by 0.27±0.13 milli-strain over the intact condition (baseline), accounting for 26% of the overall increase; however, not statistically significant. Subsequent sectioning of the TRL to create the SND increased volar plate strain by an additional 0.58±0.18 milli-strain over the mallet (p=0.031), which accounted for 74% of the total increased strain. Repeatability of the strain gauge was 0.10, 0.07 and 0.06 milli-strain for the intact, mallet and SND conditions, respectively. This degree of variability was equivalent to 26% of the average change from intact to mallet conditions, and to 13% in the SND condition, which was sufficiently repeatable to detect the SND with statistical significance.

4.3.2 PIPJ Hyperextension

Hyperextension, defined as increased in PIPJ terminal extension angle, was calculated relative to the baseline intact condition (Figure 4.5). The mallet condition caused a 0.1±0.5% (0.1±0.1°) hyperextension, and the SND condition caused a 0.2±0.6% (0.2±0.1°) hyperextension. As predicted, neither was statistically significant; however, correlating the mean hyperextension with volar plate strain produced a strong positive linear correlation (R^2=1.0, p<0.001) (Figure 4.6).
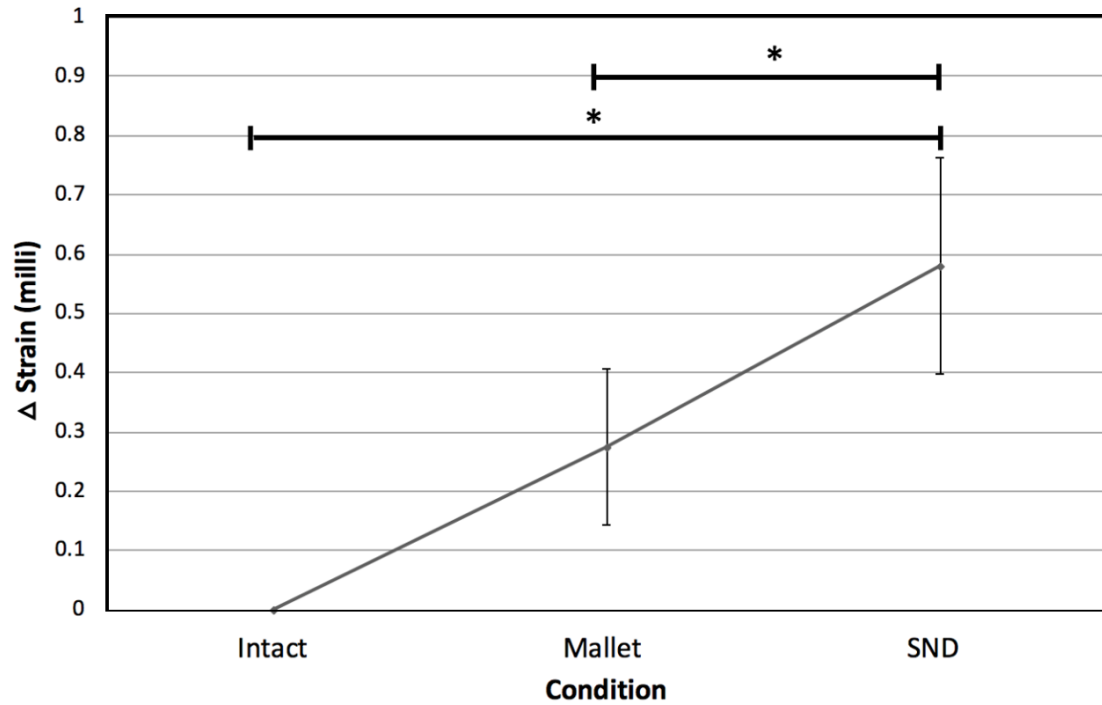
Figure 4.4: Change in Volar Plate Strain

At terminal extension, the change in strain is plotted as a function of finger condition (*p<0.05), where whiskers denote standard error from the RM-ANOVA model (n = 21). Inducing the SND condition significantly increased volar plate strain (p=0.015). The mallet condition accounted for 26% of the increase from the intact condition (baseline); however, not statistically significant. Subsequent creation of the SND accounted for 74% of the total increased volar plate strain (p=0.031).
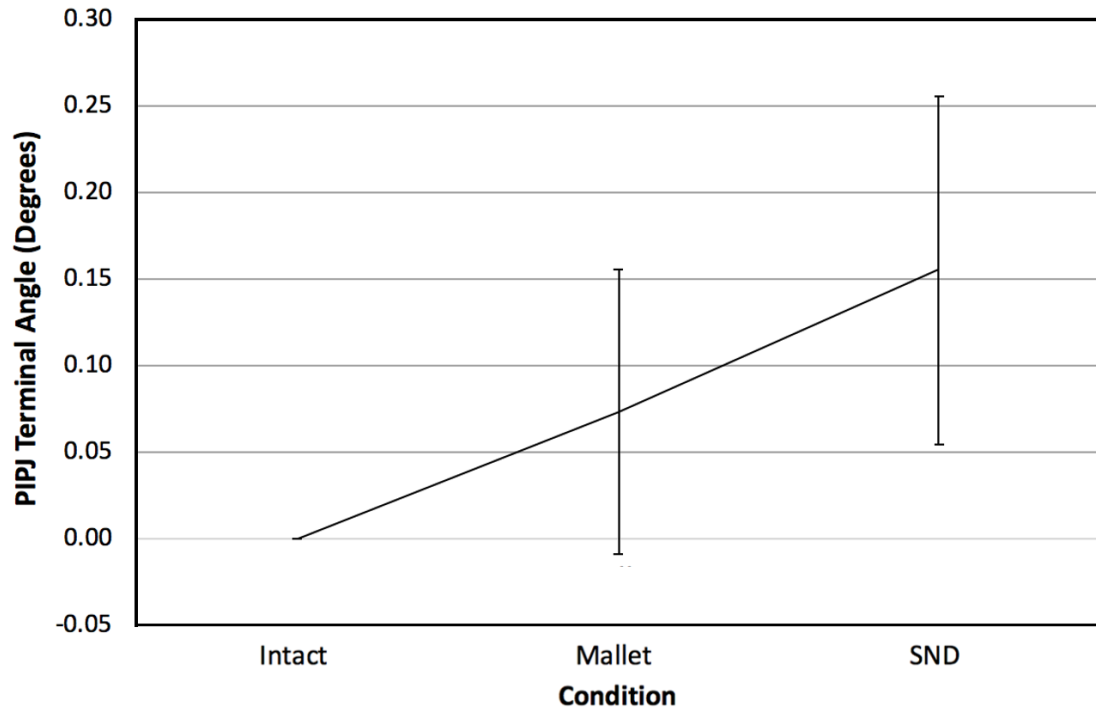
Figure 4.5: Change in PIPJ Angle at Terminal Extension

At terminal extension, the change in PIPJ's terminal angle is plotted as a function of finger condition, where whiskers denote standard error from the RM-ANOVA model (n = 21). The mallet and SND conditions caused an overall increase of 0.1±0.5% and 0.2±0.6%, respectively, in PIPJ's terminal angle compared to the intact condition; however, not statistically significant.
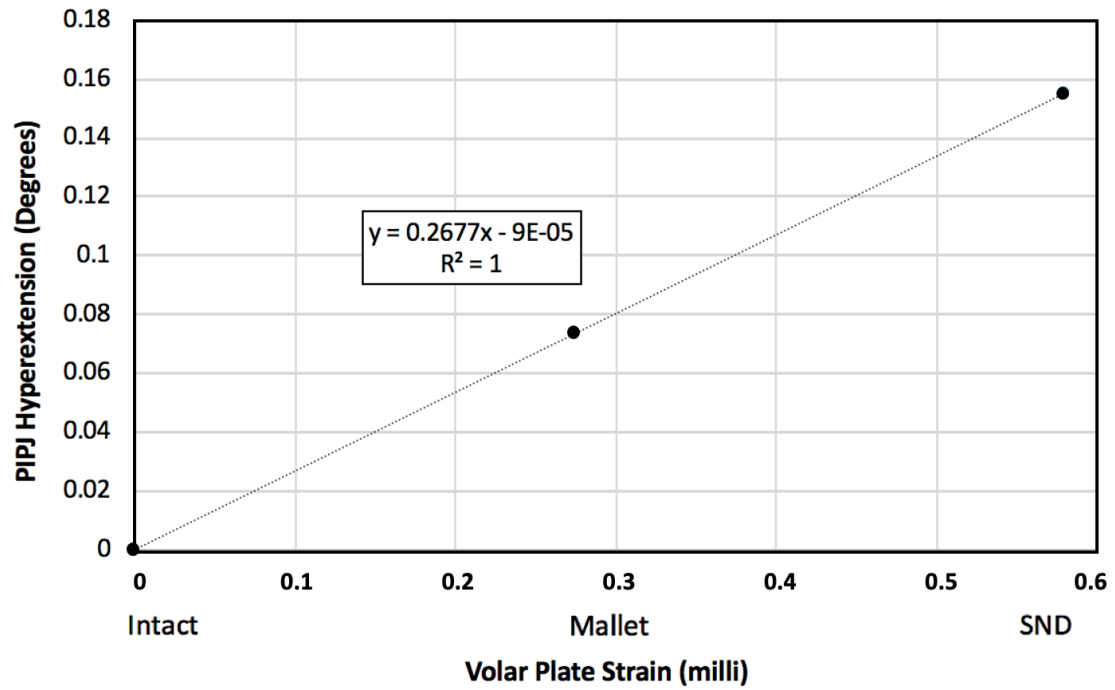
Figure 4.6: Correlation of PIPJ Hyperextension with Volar Plate Strain

At terminal extension, the relationship between strain and PIPJ's terminal angle is plotted for the mean of 21 digits ($R^2=1.0$, $p<0.001$).

4.4 Discussion

There is a vast pool of conceived surgical and non-surgical interventions aimed at restoring finger function following the progression to a SND from a chronic mallet finger injury. Although current treatment of SND is targeted to address the etiology of the deformity, there are still multiple repair techniques to be considered. For example, surgical options for SND secondary to chronic mallet deformity include tenodermodesis[5], Fowler central slip tenotomy, spiral oblique retinacular ligament (SORL) reconstruction[7], and salvage procedures (such as fusion). Current literature is inconclusive on which method of surgical intervention is superior. In order to examine this problem, clinicians must have a thorough understanding of digit biomechanics under normal and advanced injury conditions[14]. To our knowledge, this is the first study to directly examine the deformation of the volar plate, and to report a clear model of strain progression under both mallet finger and swan neck deformity finger conditions.

This study produced results that exhibited an increase in strains at the volar plate (from baseline) once a mallet finger was induced. Strain was further increased with release of the radial and ulnar TRL. Thus, with the simulated progression of a mallet deformity to a SND, strain at the volar plate further increased significantly. These results may suggest that clinical treatment of SND may involve enhancing the supportive role of the volar plate at the PIPJ. In addition, although changes with SND was observed, these results may also suggest that the sensitivity of the strain gauge was not ample enough to detect significant stain changes between the mallet finger condition and the intact condition, refuting the hypothesis made in chapter 1. Lastly, surgical intervention may need to address the increasing strain at the volar plate, which presumably worsens the deformity by causing volar plate laxity.

There are several limitations to this study. First, the cadaveric specimens used were previously frozen and of advanced age. The specimens also had to be amputated at the mid-to proximal forearm level (15 cm proximal to the carpus) in order to use the active motion simulator. Amputation at this level may have altered the biomechanics of the digit secondary to reduced friction and load on the tendons compared to an *in-vivo* state.

Additionally, in order to insert the strain gauge beneath the volar plate, the A3, C1, and C2 pulleys had to be sacrificed. This may have altered the biomechanics of the digit, although we ensured that the A2 and A4 pulleys, which have previously been shown to be the most important in flexor tendon function due to their osseous insertions[15], were left intact. Moreover, since sacrifice of those pulleys was made before the baseline condition, the application of a repeated-measures study design isolated the effect of the conditions tested.

Despite these limitations, this study has several strengths. The use of a highly sensitive strain gauge to measure deformation at the volar plate is a novel concept, which made it possible to detect the initiation of heightened tissue strains – an effect otherwise too small to be detected as PIPJ hyperextension using kinematic measurement devices. The strong positive correlation that was observed between PIPJ hyperextension and volar plate strain supports the use of strain as a surrogate measurement for hyperextension. The use of a validated finger motion simulator[13], provided highly repeatable motions and tendon loads, which further improved the sensitivity to detect minute changes in strain. Moreover, this study used a large sample size (n = 21) to develop this anatomic model of SND and to ensure statistical power was adequate.

4.5   Conclusion

In this study, we were able to detect a sudden increase in volar plate strain at the PIPJ with statistically significant and clinically significant increases above 20%. We believe that, in the *in-vivo* state, this heightened and persistent strain leads to attrition of the volar plate and surrounding soft tissues that are meant to resist hyperextension of the PIPJ. Moving forward, this swan neck strain model can be used in studies to evaluate the influence of different surgical interventions on the strain at the volar plate within a defective digit.

4.6   References

1.   Ridley WE, Xiang H, Han J, Ridley LJ. Swan neck deformity. *J Med Imaging Radiat Oncol*. 2018;62:159-160. doi:10.1111/1754-9485.31_12786

2.   Vishwanathan K. A novel surgical correction and innovative splint for swan neck deformity in hypermobility syndrome. *J Fam Med Prim care*. 2018;7(1):242-245. doi:10.4103/jfmpc.jfmpc_14_17

3.   Dreyfus JN, Schnitzer TJ. Pathogenesis and differential diagnosis of the swan-neck deformity. *Semin Arthritis Rheum*. 1983;13(2):200-211. doi:10.1016/0049-0172(83)90007-0

4.   Carlson EJ, Carlson MG. Treatment of swan neck deformity in cerebral palsy. *J Hand Surg Am*. 2014;39(4):768-772. doi:10.1016/j.jhsa.2014.01.039

5.   Nalebuff EA. The rheumatoid swan-neck deformity. *Hand Clin*. 1989;5(2):203-214. http://www.ncbi.nlm.nih.gov/pubmed/2661576. Accessed November 6, 2019.

6.   Bullock J, Rizvi SAA, Saleh AM, et al. Rheumatoid arthritis: A brief overview of the treatment. *Med Princ Pract*. 2019;27(6):501-507. doi:10.1159/000493390

7.   Vigneron AM, Lioté F. Marfan syndrome. *Rev du Rhum Monogr*. 2019;86(2):113-119. doi:10.1016/j.monrhu.2019.02.004

8.   Erçöçen AR, Yenidünya MO, Yilmaz S, Ozbek MR. Dynamic swan neck deformity in a patient with Ehlers-Danlos syndrome. *J Hand Surg Br*. 1997;22(1):128-130. doi:10.1016/s0266-7681(97)80039-3

9.   Vedel PN, Tranum-Jensen J, Dahlin LB, Brogren E, Soe NH. [Deformities of the finger joints]. *Ugeskr Laeger*. 2017;179(48).

10.   Lane R, Nallamothu S V. Swan-Neck Deformity. In: Treasure Island (FL); 2019.

11.   McKeon KE, Lee DH. Posttraumatic Boutonniere and Swan Neck Deformities. *J Am Acad Orthop Surg*. 2015;23(10):623-632. doi:10.5435/JAAOS-D-14-00272

12.   Bowers WH, Wolf JWJ, Nehil JL, Bittinger S. The proximal interphalangeal joint volar plate. I. An anatomical and biomechanical study. *J Hand Surg Am*.

1980;5(1):79-88.

13. Haddara M. Development of an Active Finger Motion Simulator: With In-Vitro Assessments of Tendon Loads and Joint Kinematics. [master's thesis]. London, Canada: Western University; 2017.

14. Shrewsbury MM, Johnson RK. Ligaments of the distal interphalangeal joint and the mallet position. *J Hand Surg Am*. 1980;5(3):214-216. doi:10.1016/s0363-5023(80)80004-9

15. Lin GT, Cooney WP, Amadio PC, An KN. Mechanical properties of human pulleys. *J Hand Surg Br*. 1990;15(4):429-434. doi:10.1016/0266-7681(90)90085-i

Chapter 5

5 The Effect of a Flexor Digitorum Superficialis Hemitenodesis on Reducing Volar Plate Strains for Swan Neck Deformities

OVERVIEW: *Flexor digitorum superficialis (FDS) hemitenodesis is a common procedure for treating chronic swan neck deformity yet lacks support due to the lack of literature assessing the biomechanical effectiveness of the repair. Hence, the basis of the proposed chapter is to evaluate the impact of a FDS hemitenodesis on joint ROM and strains induced by the volar plate. Furthermore, this chapter also discusses the effectiveness of combining a commonly used distal interphalangeal (DIP) fusion approach with the hemitenodesis.*[*]

5.1 Introduction

Treatment of swan neck deformities (SND) elicited by an injury or tear to the extensor mechanism at the DIP joint or mallet finger is common yet challenging. The choice of treatment selected is highly dependent on the severity of the deformity. It can range from a conservative approach using a cast or a blocking splint, to a more invasive approach such as fusion of joints using metal K-wires or a full joint arthroplasty[1–7].

Although various treatment methods are commonly used today, multiple studies have evaluated the effectiveness of surgical management versus non-surgical management in regards to repairing a SND condition[8–15]. Nearly all of the studies concluded that surgical intervention is a more favourable choice than conservative treatments, as complications that arise following SND treatment are less frequent with surgery (3-53%) compared to non-surgical treatments such as splinting (45%)[16].

A commonly practiced surgical approach used today for SND correction is through a flexor digitorum superficialis (FDS) hemitenodesis, using one slip of the FDS tendon looped around the A2 pulley[17–19]. Littler[20] first described the technique of superficialis tenodesis in 1959; however surprisingly little has been written about the biomechanical effects of the technique[21]. Ciclamini[22], Catalano[23], and Froelich[24] have all advocated for this technique for correction of supple swan-neck deformities, but with uncertainty on the biomechanical consequences.

Consequently, the optimal treatment choice for SND remains controversial. Therefore, the primary purpose of this study was to evaluate the effectiveness of the FDS hemitenodesis repair. The performance metrics were volar plate strain and flexor tendon loads, measured using a previously validated in-vitro swan neck model[25]. The secondary objective of this study was to evaluate the effectiveness of combining a distal interphalangeal (DIP) fusion with the hemitenodesis as an approach to providing additional stability and laxity correction in the proximal interphalangeal joint (PIPJ).

5.2   Materials and Methods

Fifteen digits, comprised of the index, long, and ring fingers were tested from five freshly frozen cadaveric specimens (age: 70 ± 10; 4 males, 1 female). Specimens were excluded from the study if their computed tomography scans showed the presence of osteoarthritis or any other visible deformities at the finger joints. All screened specimens were amputated 15 cm proximal to the wrist and then thawed overnight (approx. 16 hours) at room temperature prior to testing.

5.2.1 Specimen Preparation

The transversely sectioned distal radius and ulna were secured in the finger motion simulator using screws in each bone, with attention to maintaining neutral forearm rotation. Careful dissection of the specimens were performed by a hand fellowship-trained surgeon to isolate the flexor digitorum profundus (FDP), flexor digitorum superficialis (FDS), and the extensor digitorum communis (EDC) tendons of each finger. Once isolated, each tendon was subsequently sutured to linear servo actuators using 0-braided Vicryl (ETHICON®, Somerville, NJ, United States) in a locked Krakow fashion[26]. In addition, two K-wires were inserted transversely through the metacarpals to ensure stability during finger motion and a rigid foam block was placed below the hand to maintain a neutral wrist. The hand was then further stabilized using 2 mm Dacron braided cables (Melton International Tackle, Anaheim, CA, United States) to constrain the metacarpal K-wires and prevent movement of the wrist during simulated active finger motion.

5.2.2 In-Vitro Active Finger Motion Simulation

Finger flexion and extension motions were performed by controlling tendon excursions and loads. Tendon load feedback was provided by a uni-axial load cell (Model 34, Honeywell, Charlotte, NC, United States) mounted to the end shaft of each linear servo actuator and closed-loop load control was achieved with custom LabVIEW code. In order to determine tendon excursion for each finger, a flexion trial in the intact condition was initially performed by moving FDP and FDS in position control against a constant 10 N

antagonist load on the extensor until full flexion range of motion (ROM) was achieved in all joints (MCP: $83 \pm 10°$, PIP: $101 \pm 13°$, DIP: $57 \pm 9°$). Once determined, subsequent SND and repair conditions following intact were each tested with the same tendon excursion and motion sequence as the intact condition. This was repeated for finger extension, with the extensor tendon in position control against a constant 5 N load on each flexor tendon.

5.2.3 Swan Neck Deformity (SND) Model

A SND condition was created through a mallet finger followed by a transverse retinacular tear. Initially, a transverse incision just proximal to the dorsal aspect of the DIPJ was made, exposing the terminal extensor tendon. The tendon was incised transversely to create the mallet finger taking care not to violate the joint capsule. Once the tendon was incised, the digit assumed a position of resting flexion at the DIPJ, confirming the creation of a mallet finger. Subsequently, a longitudinal midline incision extending from the volar base of the finger to the distal interphalangeal joint volar crease was made. Soft tissues were elevated along the radial and ulnar borders of the PIPJ, exposing the transverse retinaculum ligament (TRL). The TRL was then sharply incised with a longitudinal lateral incision. Incising the TRL allowed the lateral bands to subluxate dorsally, thus completing the swan neck deformity model. Skin was then re-approximated to maintain specimen hydration.

5.2.4 Flexor Digitorum Superficialis (FDS) Hemitenodesis

FDS hemitenodesis was performed on all specimens (Figure 5.1). This technique employs one slip of the FDS as a static restraint against a flexible hyperextension of the PIPJ. Several variations of this technique have been described, differing mostly in the location where the tendon is secured[27]. We utilized tenodesis of one slip of the FDS to the A2 pulley. Following exposure of the A2, A3, A4 and cruciate pulleys through a central incision, we incised the cruciate pulley to expose the FDS tendon insertion. Traction on the ulnar slip of the FDS was then applied and pulled distally to incise it as proximal as possible. Caution was taken not to injure the radial slip of the FDS, which was kept intact.

A transverse incision in the distal third of the A2 pulley was then created, and a small tendon retriever was used to pull the ulnar slip through the incision in the pulley. Subsequently, we completed the tenodesis by suturing the slip onto itself with two figure of eight sutures using a 3-0 Vicryl[28] (ETHICON®). A 10° PIPJ flexion angle position was chosen for the tenodesis[23]. The skin was closed with interrupted 3-0 Nylon sutures (ETHICON®).

5.2.5 DIP Fusion

The distal interphalangeal joint, where we had previously induced a mallet finger, was fused in neutral position with a 0.062-inch Kirschner Wire inserted from the tip of the distal phalanx, retrograde across the joint and to the middle phalanx. It was confirmed that the K-Wire was not left protruding in any direction and that the joint was firmly fused.

5.2.6 Joint Angle Measurement

Joint angles were measured using a trakSTAR® (NDI, Waterloo, ON, Canada) electromagnetic tracking system. Small electromagnetic position and angle sensors recorded the terminal joint extension angle achieved by each joint (DIPJ, PIPJ, and MCPJ). To install the trackers, short lateral incisions were made along the finger to expose each bone segment. Three electromagnetic trackers (2 mm Ø, model M180, trakSTAR, NDI) were then press-fit into a drill hole made laterally at the center of each phalanx. A fourth tracker was also inserted in the metacarpal of the second digit to confirm stable fixation of the hand.
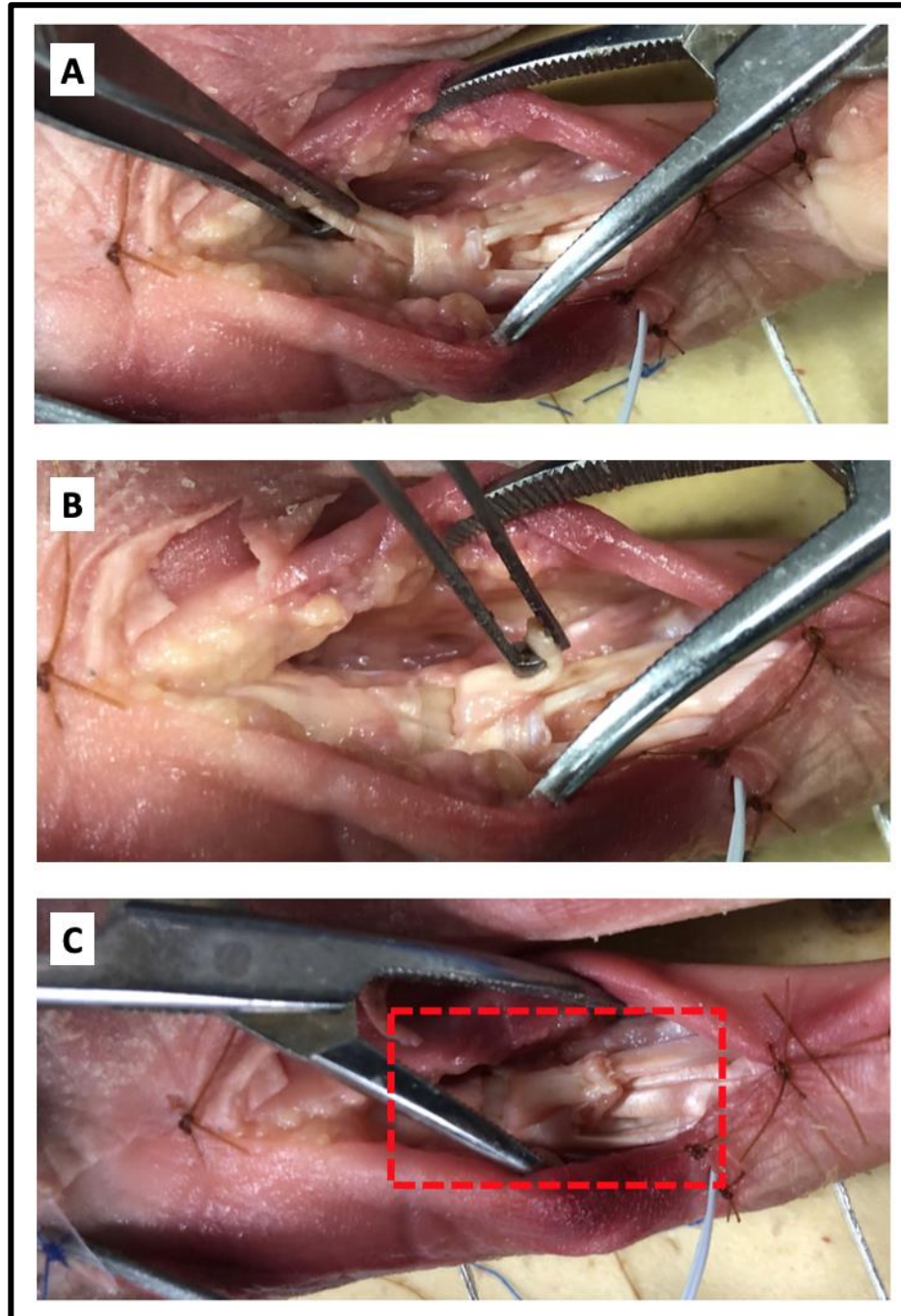
Figure 5.1: FDS Hemitenodesis Technique

One slip of the FDS was utilized as a static restraint secured to the A2 pulley. (a) A transverse incision in the distal third of the A2 pulley was created and a small tendon retriever was used to pull the ulnar slip through the incision. Subsequently, tenodesis was completed by (b) looping the slip over the A2 pulley and (c) suturing the slip onto itself with two figure of eight sutures.
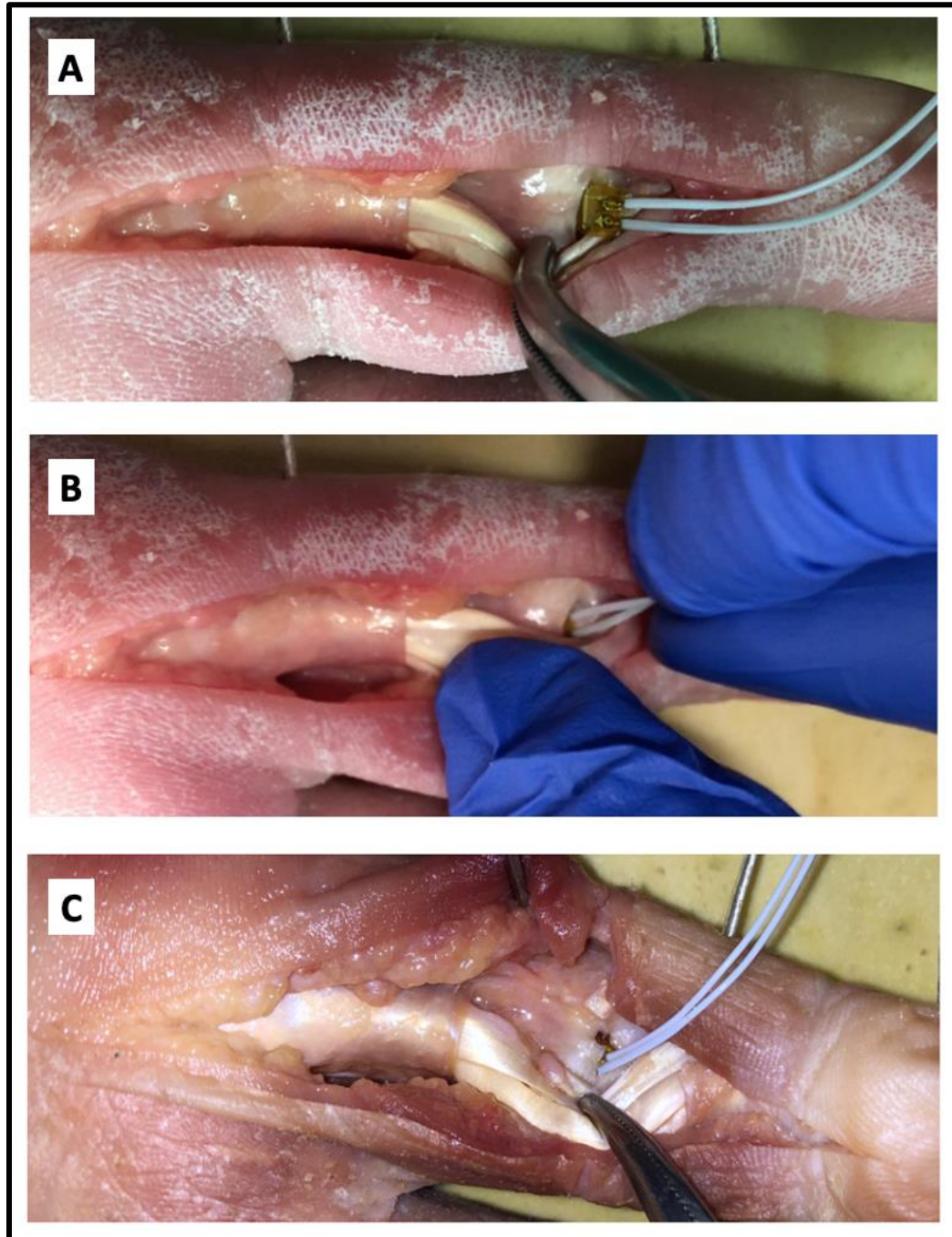
Figure 5.2: Strain Gauge Insertion Process

The volar plate was identified, and a 5 mm transverse incision was performed over its insertion to the middle phalanx. Astrain gauge was inserted underneath the volar plate (a, b) and secured with a suture (c).

5.2.7 Volar Plate Strain Measurement

Strain at the volar plate was measured to indicate the onset of strain imbalance caused by the simulated SND, and to evaluate the effect of each injury and repair condition against the baseline intact condition. To install the strain gauge, a mid-line incision was made along the length of the volar surface of each digit to locate and identify the volar plate. Sacrificing of the A3 pulley was necessary for gaining clear access to the volar plate. A strain gauge was inserted under the volar plate and secured using 4-0 Vicryl sutures in a figure of 8 configuration (Figure 5.2). A small transverse incision was made at the level of the radial skin flap overlying the middle phalanx, and the wire of the strain gauge was passed through this split and secured with 0-Vicryl sutures. The longitudinal skin incision was closed, and the strain gauge wires were further secured to the palm of the hand using Mastisol (Ferndale Laboratories, Inc., MI, United States) and adhesive tape. Strain measurements were collected with custom code made in the LabVIEW programming environment (National Instruments, Austin, TX, United States).

5.2.8 Motion Trial Protocols

All measurements of volar plate strain and joint angles were collected under four finger conditions (Figure 5.3): 1) intact; 2) swan neck deformity (SND); 3) FDS hemitenodesis; and 4) DIP fusion. All remaining tissues within the specimen were left intact and saline solution was used to maintain hydration throughout testing to prevent desiccation. All four conditions were tested in each finger in a repeated-measures model. Each finger motion was repeated 5 times to assess repeatability. Measurements from the 5th motion trial were recorded for statistical analysis, with the first 4 motions ensuring that the finger was preconditioned following the prior surgical intervention.

5.2.9 Statistical Analysis

A minimum sample size of n=6 was determined using G*Power software with a repeated-measures ANOVA model, set to achieve statistical significance with 80% power for an effect size of 1.098. The effect size was determined from pilot tests in four specimens. Multiple one-way and two-way repeated-measures ANOVA models, with

Bonferroni correction, were performed to analyze the effect of volar plate strain, tendon load, and PIPJ angle under all 4 conditions (intact, SND, FDS hemitenodesis, and DIP fusion). Within-subject effects and pairwise comparisons were also examined, with significance set at $p<0.05$.
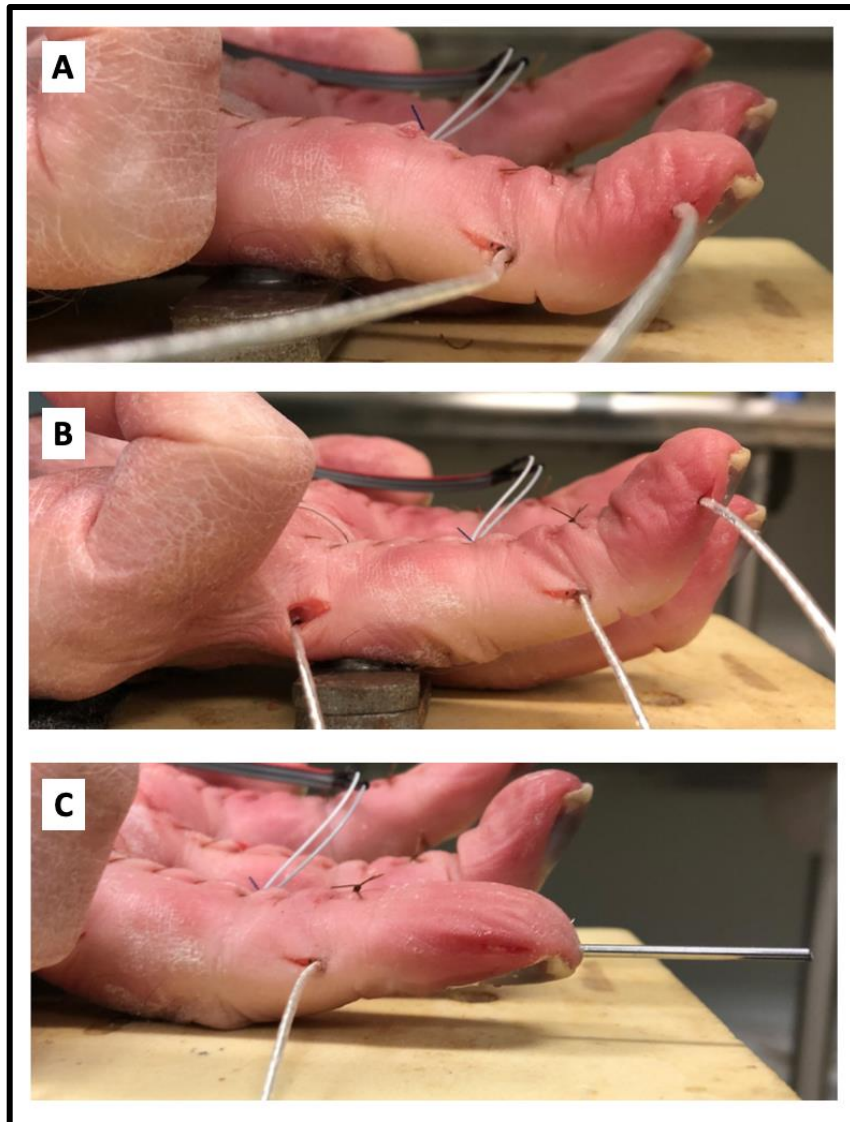
Figure 5.3: Finger Conditions

The three finger conditions following intact are illustrated, (a) swan neck deformity, (b) FDS Hemitenodesis and (c) DIP Fusion. The hyperextension of the PIPJ and the flexion of the DIPJ represent the characteristics of a true swan neck deformity case. A fulcrum in

(a) and (b) was used underneath the digit to illustrate the significant deformation and subsequent repair in the finger.

5.3   Results

5.3.1 PIPJ Terminal Extension Angle

For each condition, the change in PIPJ's range of motion, or delta PIPJ angle, was calculated as the maximum extension achieved in comparison to the intact condition. Thus, a positive value represents an increase in extension range (i.e. hyperextension), while a negative value represents a loss (Figure 5.4). The simulated SND increased the terminal extension angle by $0.2 \pm 0.6º$ compared to the intact condition, though not statistically significant. Repairing SND through FDS hemitenodesis caused a loss in terminal extension angle of $10.2 \pm 3.8º$ ($p<0.01$). Following the FDS hemitenodesis with a DIP fusion further reduced the extension range to a terminal extension angle of $10.7 \pm 4.2º$ compared to the intact condition ($p<0.01$).
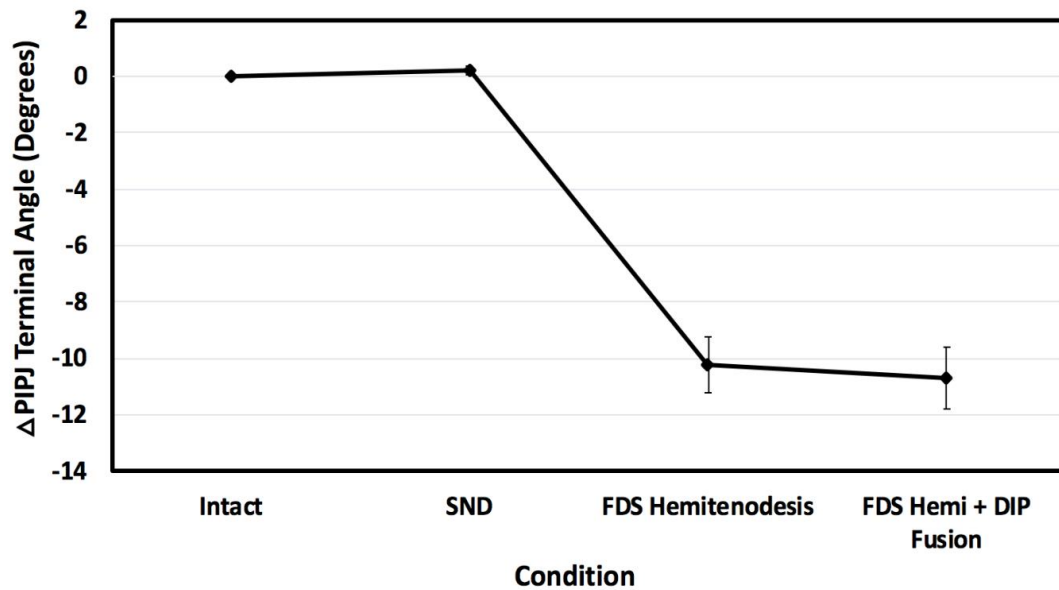
Figure 5.4: Change in PIPJ Angle at Terminal Extension

At terminal extension, the change in PIPJ's terminal angle is plotted as a function of finger condition, where whiskers denote standard error of 15 finger specimens. Simulation of a SND condition caused an overall increase of 0.2 ± 0.6 degrees in PIPJ extension (hyperextension) compared to the intact condition; however, not statistically significant. Repair using FDS Hemitenodesis and DIP Fusion caused an overall decrease of 10 ± 4 degrees and 11 ± 4 degrees, respectively.

5.3.2 Volar Plate Strain

In order to compare the four tested conditions by changes in PIPJ volar plate strain, a common maximal extension angle was selected. Since DIP fusion caused the greatest loss of extension range, strain measurements for all four conditions were extracted at the terminal extension angle of the DIP fusion condition. This terminal angle was determined individually for each finger, and the resulting volar plate strains are plotted in Figure 5.5. The SND condition significantly increased volar plate strains by 6.6 ± 4.0 milli-strain compared to the intact condition (p<0.001). Surgical correction of the deformity through a FDS hemitenodesis significantly reduced strains by 3.6 ± 2.5 milli-strain compared to the SND condition (p<0.001). This was a 50% reduction, which restored volar plate strain to within a statistically non-significant difference from the intact condition. Further correction of the deformity through a DIP fusion caused an additional reduction of 0.4 ± 1.0 milli-strain, which was also a statistically significant reduction from the SND condition (p<0.001), though not significantly different from the FDS hemitenodesis.

5.3.3 Flexor Tendon Loads

Flexor tendon loads were all evaluated at the full flexion range of each finger (Figure 5.6). From the intact condition, creation of the SND decreased FDP load by 0.6 ± 0.9 N (p=0.202) and decreased the FDS load by 1.2 ± 1.6 N (p=0.065), though these reductions were not statistically significant. Surgical repair with FDS hemitenodesis significantly decreased FDS load by 1.3 ± 1.3 N (p=0.012) from the SND and increased FDP load by 2.1 ± 1.5 N (p<0.001). Additional repair through a DIP fusion further decreased FDS load significantly by 0.8 ± 0.8 N (p=0.009) from the FDS hemitenodesis, whereas FDP load increased 0.6 ± 1.0 N, though not statistically significant (p=0.182).
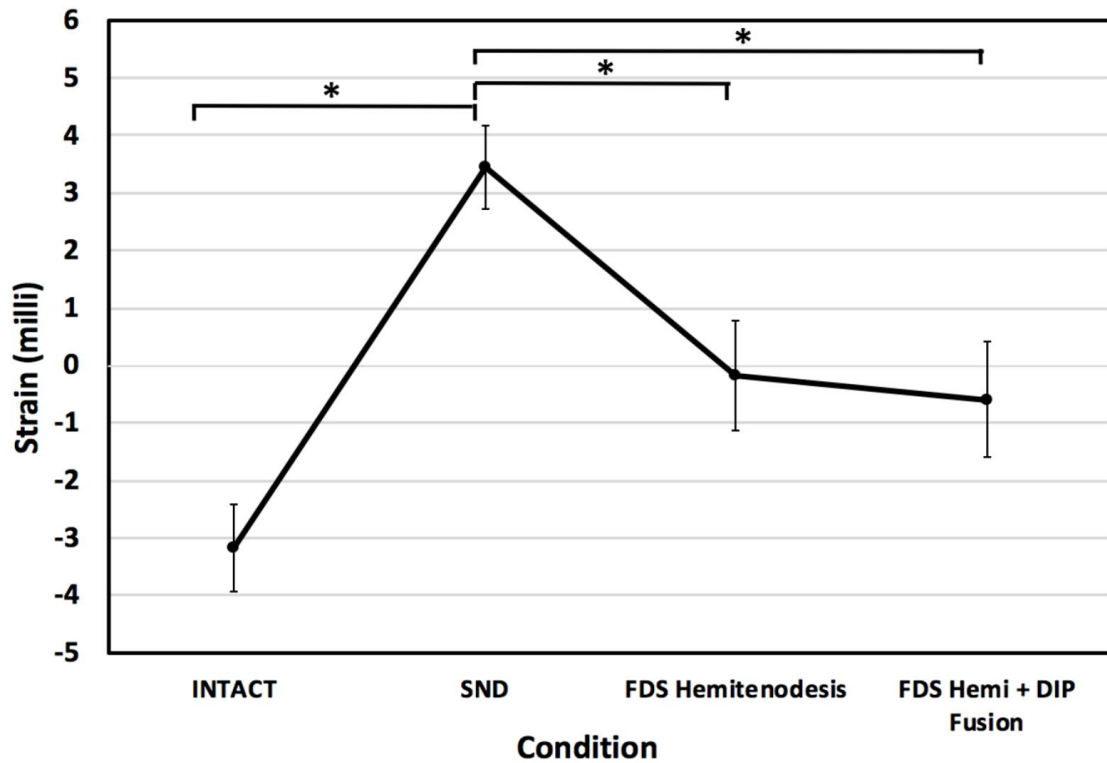
Figure 5.5: Volar Plate Strain

*At DIP Fusion's terminal extension, the volar plate strain is plotted as a function of finger condition (*p<0.05), where whiskers denote standard error of 15 finger specimens. The SND condition caused a 176 ± 95% increase of strain (p<0.001) compared to the intact condition. Subsequent repair with the hemitenodesis resulted in of 181 ± 523% significant reduction in strain compared to the SND condition, restoring strains to within 3.0 milli-strain of the intact condition (p=0.158). DIP fusion also produced an added apparent reduction of 87 ± 252% in strain compared to the hemitenodesis condition, though not statistically significant (p=0.776).*
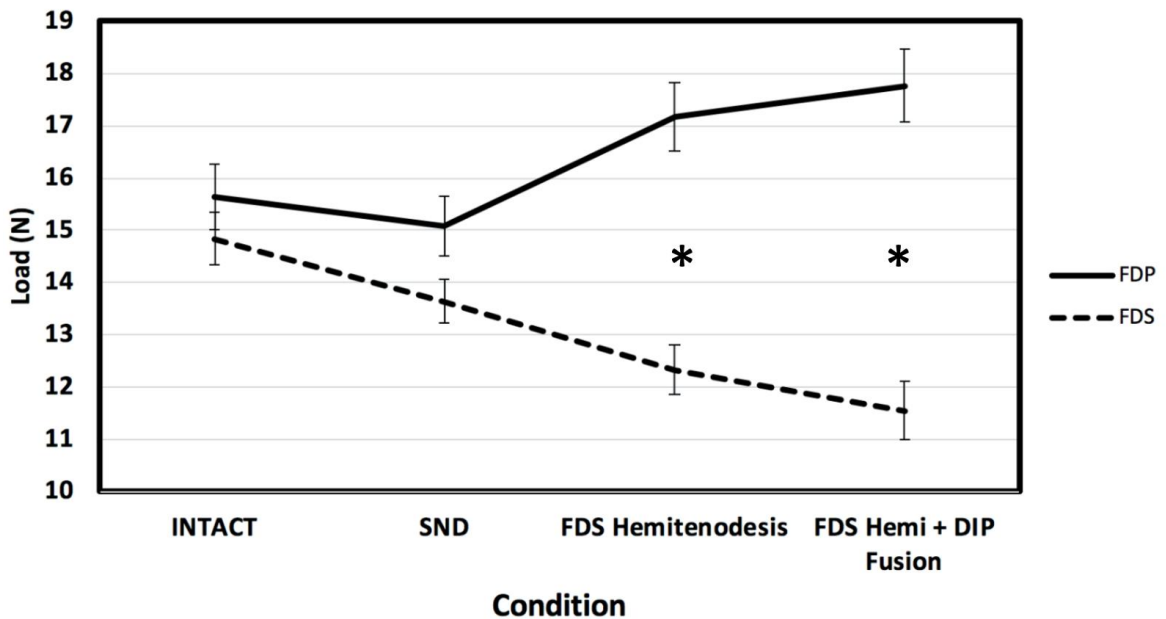
Figure 5.6: Flexor Tendon Loads

At full finger flexor, flexor loads, FDP and FDS, were plotted as a function of finger condition (*p<0.05), where whiskers denote standard error of 15 finger specimens. FDP and FDS load values diverged as a function of finger condition (p=0.001). With the hemitenodesis, FDP load caused a 99 ±12% increase where FDS load experiences an 77 ±10% decreased from the SND condition. Simulation of the DIP fusion continued to cause a divergence in tendon load further increase FDP load by 86 ±6% and decreasing FDS load by 81 ±7% compared to the hemitenodesis condition.

5.4   Discussion

Swan neck is a challenging deformity to treat. The goal of treatment of symptomatic chronic injuries is to restore functional stability of the PIPJ and alleviate any pain. A hemitenodesis using a slip of the FDS tendon is an established treatment option for PIPJ hyperextension correction. However, the influence in which hemitenodesis has on the changes in internal kinematics, such as strain at the volar plate and flexor tendon load, was never investigated[29]. Therefore, this study focused on evaluating the effect of a commonly performed FDS hemitenodesis approach, with the addition of a DIP fusion for further stability, on the changes in strain induced by the affected volar plate and the internal loads experienced by flexor tendons for the correction of chronic mallet deformity with resultant swan-neck deformity. To the best of our knowledge, this is the first study that directly examined the degree of deformation in the volar plate and the loads withstood by the flexor tendons in response to a swan neck simulation and subsequent repair.

Using flexor tendon load and strain as a surrogate measure for effectiveness of the repair, our study found that application of a hemitenodesis had a significant effect on volar plate strain and tendon load following SND correction, with the SND condition resulting in a 176% increase in volar plate strain compared to the intact condition. Subsequent repair with the hemitenodesis resulted in a 181% reduction of strain compared to the SND condition, restoring strains to within 3.0 milli-strain of the intact condition, which was not significantly different (p=0.158). DIP fusion also produced an added apparent reduction of 87% in strain compared to the hemitenodesis condition, though this did not reach statistical significance (p=0.776). These results support the use of FDS hemitenodesis to prevent the progression of a SND induced by increased strain across the PIPJ. The DIP fusion did not further reduce strain compared to FDS hemitenodesis, which was observed in every finger. This suggests that DIP fusion does not further protect the PIP joint from increased hyperextension stress; possibly a reason to not employ a DIP fusion.

In addition, FDP and FDS load values diverged as a function of finger condition (p=0.001). With the hemitenodesis, FDP load increased by 2.1 N (+13%) where FDS load decreased by 1.3 N (-11%) from the SND condition. Simulation of the DIP fusion

continued to cause a divergence in tendon load with FDP loads further increasing by 0.6 N (+5%) compared to the hemitenodesis condition and FDS load further decreasing by 0.8 N (-8%). The divergence in load following FDS hemitenodesis is significant and likely due to the nature of the repair; however, the further increase in divergence following a DIP fusion is likely due to an imbalance between flexor tendon loads. Thus, further strengthening the choice to not employ DIP fusion with a hemitenodesis in the correction of a SND. Our ability to place these findings in the context of the existing literature is limited by the lack of published biomechanical case reports following SND correction.

FDS hemitenodesis, as well as other procedures to limit hyperextension of the PIPJ (Volar plate advancement, oblique retinaculum ligament reconstruction) has been utilized to treat flexible SND with mixed outcomes. Catalano et al. reported overall favorable results with return to function and minimal pain for most of his case series of 12 patients[23]. The major complication reported in his cohort was flexion contracture of the PIPJ. Conversely, Ciclamini et al. recently reported less reliable outcomes of FDS hemitenodesis with a common major complication of PIPJ hyper-extension relapse. The authors of the latter study hypothesized that the FDS tendon used to limit strains across the PIPJ will ultimately fail due to the strain across a vulnerable soft tissue[22]. The premise of soft tissue procedures to treat SND is preventing the flexible form of SND from progressing to a fixed deformity with the associated pain and disability. Our study provides the biomechanical rational to this premise, namely, reducing the strain across the volar plate and keeping this important PIP stabilizer functional and robust. It should be noted that harvesting half of the FDS reduces its ability to share the loads on finger flexion and causes the FDP to carry more loads. The clinical correlation of this biomechanical finding is still unclear.

Surgical treatment of the DIP flexion deformity that is part of SND is a matter of debate. McKeon at al suggested that the addition of DIP fusion or arthrodesis should be left to the treating surgeon and patient discretion, and judged by the pain and functional limitation the DIP deformity creates[6]. Certainly, DIPJ fusion is not a routine part of repairing the PIPJ hyperextension and non-operative treatment of the DIPJ deformity is optional as an alternative to the surgical fixation[6]. From a biomechanical standpoint, our

findings suggest there are no additional benefits of fusing the DIPJ in reducing strain across the PIPJ. Moreover, fusion the DIPJ adds to the imbalance of the flexor tendon loads.

Limitations should be considered when interpreting the results: (1) The cadaveric specimens used were previously frozen and of advanced age; (2) the sacrificing of the A3 pulley to gain access to the volar plate site was inevitable and thus, the loss of the pulley may have altered the mechanics of the finger; and (3) amputation of each arm proximal to the wrist to accommodate for the simulator used. However, a repeated-measures experimental design was employed, and thus, any changes in the mechanics due to the amputation were applied to all tested conditions.

Despite limitations, a few important strengths should be considered within the study: (1) the use of an advanced, repeatable ,and validated active motion simulator with position and load control of the tendons, in comparison to previously reported in-vitro finger motion simulators; (2) the accurate measurement method of recording strain, load, and joint angle changes within the volar plate, tendons, and PIPJ respectively, (3) a large sample size where an analysis was performed to predict sufficient statistical power for the hypothesis test, which is an improvement compared to standard practice in upper extremity in-vitro motion testing; and (4) the routing of the FDS hemitenodesis technique was standard and reflected standard clinical practice.

5.5   Conclusion

Findings from this study support the use of FDS hemitenodesis to reduced strain across the PIPJ following swan neck deformity. The role of DIPJ fusion however, remains uncertain and showed no additional benefits in our biomechanical analysis. Further clinical correlation is needed to determine the long-term effects of the changes in tendon loads reflected in our study.

5.6 References

1. Fox PM, Chang J. Treating the Proximal Interphalangeal Joint in Swan Neck and Boutonniere Deformities. *Hand Clin*. 2018;34(2):167-176. doi:10.1016/j.hcl.2017.12.006

2. Yan H, Tan Q, Zhou S, et al. [Short-term effectiveness of Kirschner wire elastic fixation in treatment of Doyle type and mallet finger]. *Zhongguo Xiu Fu Chong Jian Wai Ke Za Zhi*. 2017;31(11):1287-1290. doi:10.7507/1002-1892.201706051

3. Crawford GP. The Molded Polythene Splint for Mallet Finger Deformities. *J Hand Surg Am*. 1984;9(2):231-237. http://www.ncbi.nlm.nih.gov/pubmed/6715831. Accessed July 18, 2017.

4. Bullock J, Rizvi SAA, Saleh AM, et al. Rheumatoid arthritis: A brief overview of the treatment. *Med Princ Pract*. 2019;27(6):501-507. doi:10.1159/000493390

5. Thompson JS, Littler JW, Upton J. The spiral oblique retinacular ligament (SORL). *J Hand Surg Am*. 1978;3(5):482-487. doi:10.1016/s0363-5023(78)80144-0

6. McKeon KE, Lee DH. Posttraumatic Boutonniere and Swan Neck Deformities. *J Am Acad Orthop Surg*. 2015;23(10):623-632. doi:10.5435/JAAOS-D-14-00272

7. Carlson EJ, Carlson MG. Treatment of swan neck deformity in cerebral palsy. *J Hand Surg Am*. 2014;39(4):768-772. doi:10.1016/j.jhsa.2014.01.039

8. Lane R, Nallamothu S V. Swan-Neck Deformity. In: Treasure Island (FL); 2019.

9. Vedel PN, Tranum-Jensen J, Dahlin LB, Brogren E, Soe NH. [Deformities of the finger joints]. *Ugeskr Laeger*. 2017;179(48).

10. Enriquez de Salamanca F. Swan-neck deformity: mechanism and surgical

treatment. *Hand*. 1976;8(3):215-221. doi:10.1016/0072-968x(76)90004-8

11. Renfree KJ, Odgers RA, Ivy CC. Comparison of Extension Orthosis Versus Percutaneous Pinning of the Distal Interphalangeal Joint for Closed Mallet Injuries. *Ann Plast Surg*. 2016;76(5):499-503. doi:10.1097/SAP.0000000000000315

12. Ozturk S, Zor F, Sengezer M, Isik S. Correction of bilateral congenital swan-neck deformity by use of Mitek mini anchor: A new technique. *Br J Plast Surg*. 2005;58(6):822-825. doi:10.1016/j.bjps.2005.01.017

13. De Bruin M, Van Vliet DC, Smeulders MJ, Kreulen M. Long-term results of lateral band translocation for the correction of swan neck deformity in cerebral palsy. *J Pediatr Orthop*. 2010;30(1):67-70. doi:10.1097/BPO.0b013e3181c6c363

14. Kiefhaber TR, Strickland JW. Soft tissue reconstruction for rheumatoid swan-neck and boutonniere deformities: Long-term results. *J Hand Surg Am*. 1993;18(6):984-989. doi:10.1016/0363-5023(93)90387-I

15. Brulard C, Sauvage A, Mares O, Wavreille G, Fontaine C. Treatment of rheumatoid swan neck deformity by tenodesis of proximal interphalangeal joint with a half flexor digitorum superficialis tendon. About 23 fingers at 61 months follow-up. *Chir Main*. 2012;31(3):118-127. doi:10.1016/j.main.2012.04.010

16. Salazar Botero S, Hidalgo Diaz JJ, Benaida A, Collon S, Facca S, Liverneaux PA. Review of Acute Traumatic Closed Mallet Finger Injuries in Adults. *Arch Plast Surg*. 2016;43(2):134-144. doi:10.5999/aps.2016.43.2.134

17. Vishwanathan K. A novel surgical correction and innovative splint for swan neck deformity in hypermobility syndrome. *J Fam Med Prim care*. 2018;7(1):242-245.

doi:10.4103/jfmpc.jfmpc_14_17

18. Hamada Y, Takai H, Satoh R, Hibino N, Ueda Y, Minamikawa Y. Swan neck deformity due to chronic radial collateral ligament injury of the little finger proximal interphalangeal joint. *J Hand Surg (European Vol*. 2018;43(5):513-517. doi:10.1177/1753193417739248

19. Nalebuff EA. The rheumatoid swan-neck deformity. *Hand Clin*. 1989;5(2):203-214. http://www.ncbi.nlm.nih.gov/pubmed/2661576. Accessed November 6, 2019.

20. Littler J. *The Hand and Wrist*. MB Howorth. (Droman S, ed.). CT: A textbook of orthopedics; 1959.

21. Deml C, Baradaran A, Chen N, Nasr M, Kachooei AR. Fowler Central Slip Tenotomy or Spiral Oblique Retinacular Ligament Reconstruction? A Cadaveric Biomechanical Study in Swan-Neck Deformity. *Hand (N Y)*. March 2019:1558944719834643. doi:10.1177/1558944719834643

22. Ciclamini D, Tos P, Monticelli A, Crosio A, De Blasi P, Battiston B. Flexor digitorum superficialis tenodesis for treatment of flexible swan neck deformity of fingers. Comparison between two surgical techniques to fix the tendon: A pilot study. *J Plast Reconstr Aesthetic Surg*. 2019;72(8):1418-1433. doi:10.1016/j.bjps.2019.04.006

23. Catalano LW, Skarparis AC, Glickel SZ, Barron OA, Malley D, Lane LB. Treatment of chronic, traumatic hyperextension deformities of the proximal interphalangeal joint with flexor digitorum superficialis tenodesis. *J Hand Surg Am*. 2003;28(3):448-452. doi:10.1053/jhsu.2003.50084

24. Froelich JM, Rizzo M. Reconstruction of swan neck deformities after proximal

interphalangeal joint arthroplasty. *Hand*. 2014;9(1):93-98. doi:10.1007/s11552-013-9571-0

25.   Haddara MM, Fan S, Matache BA, Chinchalkar SJ, Ferreira LM, Suh N. Development of an *In Vitro* Swan Neck Deformity Biomechanical Model. *Hand (N Y)*. 2020;1558944720966736. doi:10.1177/1558944720966736

26.   Haddara M. Development of an Active Finger Motion Simulator: With In-Vitro Assessments of Tendon Loads and Joint Kinematics. [master's thesis]. London, Canada: Western University; 2017.

27.   Boyer MI, Gelberman RH. Operative correction of swan-neck and boutonniere deformities in the rheumatoid hand. *J Am Acad Orthop Surg*. 1999;7(2):92-100. doi:10.5435/00124635-199903000-00002

28.   Wei DH, Terrono AL. Superficialis sling (flexor digitorum superficialis tenodesis) for swan neck reconstruction. *J Hand Surg Am*. 2015;40(10):2068-2074. doi:10.1016/j.jhsa.2015.07.018

29.   Shrewsbury MM, Johnson RK. Ligaments of the distal interphalangeal joint and the mallet position. *J Hand Surg Am*. 1980;5(3):214-216.

Chapter 6

6 **Evaluation and Comparison of *In-vitro* Joint Kinematics using Motion-Based Coordinate Frames vs. Anatomical Landmarks**

OVERVIEW: Despite the availability of the International Society of Biomechanics (ISB) recommendations for anatomical frame orientation, no consensus exists about motion representations related to finger kinematics. This chapter proposes the use of novel motion based coordinate frames to quantify finger joint kinematics. It begins with an review of current variations in joint coordinate systems (JCS) among studies followed by findings from different research groups. This chapter then evaluates the accuracy of the novel derived helical axes during finger motion and evaluates the reliability and accuracy of results in comparison to ISB's anatomical frame definitions.

6.1 Introduction

The interest in upper limb joint kinematics has provided valuable outcomes for clinical analysis and musculoskeletal modelling over the years[1–5]. However, to accurately represent joint motion, Joint Coordinate System (JCS) conventions must be applied. In an effort of standardization, recommendations on constructing anatomical frames for upper limb segments, including the fingers and wrist, have been previously proposed by the International Society of Biomechanics (ISB)[6]. Many authors have adopted the techniques as per ISB Recommendation[7–11]; however, a challenge and limitation of creating anatomy-based frames is the need to denude to locate and digitize unique features on bones, which is a large source of error introducing both intra- and inter-user variabilities that hamper reproducibility across research groups. Moreover, the need to denude specimens often interferes with the desired testing protocol, which limits testing conditions and encourages researchers to modify their anatomy digitizing method, leading to departures from standardized approaches.

Therefore, recent studies have investigated new alternatives to anatomical joint coordinate frames by using functional frames (i.e. helical axis)[12–16]. A thorough study conducted by Goislard de Monsabert *et al.* analyzed and compared the effect of both anatomical and functional frame definitions for the hand[10]. Their findings supported the use of functional frames when investigating complex three-dimensional movements, as the functional frame method reduced kinematics cross-talk on the secondary and tertiary Cardan angles by up to 20°. Various models, both conceptual and practical, have been proposed with an aim to accurately measure fine hand motion to address any cross validation analysis difficulties and allowing for post data processing compatibility[7,17,18]. This abundance of different methods for finger anatomical frame construction makes standardizations difficult in clinical applications and motion evaluation.

Therefore, the objective of this study was to quantify and validate the use of a new Motion-based Coordinate System (MCS) functional frame definition for finger joints using helical axes (HA) in an *in-vitro* setting. This model was directly compared to the

standardized ISB's recommendations for JCS anatomical frame (AF) construction within the same model.

6.2   Methods and Materials

Eleven digits, consisting of the index, long, and ring fingers from 4 fresh-frozen upper extremities were utilized (4 male; age: 66±4.7 years). Specimens were excluded if their computed tomography (CT) scans showed presence of osteoarthritis or any other deformities. All screened specimens were amputated 15 cm proximal to the wrist, then thawed overnight (approximately 16 hours) at room temperature prior to testing, and then checked for normal passive range of motion (ROM)[19–22].

6.2.1 Specimen Preparation

Prior to testing, each finger had undergone a simulated tear of the Flexor Digitorum Profundus tendon at the distal insertion with a surgical repair performed by an orthoplastic surgeon, which is a common pathology and clinically relevant condition. Dissection of the wrist was performed to isolate the Flexor Digitorum Profundus (FDP), Flexor Digitorum Superficialis (FDS), and the extensor digitorum communis (EDC) of each finger. Once isolated, each tendon was sutured with a Krackow stitch and connected to linear actuators of a previously reported active motion simulator[19–22]. Specimens were secured in the motion simulator in a supinated position using four transverse screws – two in the ulna and two in the radius. The dorsum of the hand was supported by a rigid foam block. The second to fifth metacarpals were cross-pinned with two 1.5 mm K-wires, and a 2 mm Dacron-braided cable was tied to the K-wires and wrapped around the foam block to secure the hand and prevent wrist flexion during simulated active finger motions. All thawing and specimen setup procedures were consistent with previously reported studies[19–22].

6.2.2 In-Vitro Active Finger Motion Simulation

Simulated active finger flexion/extension was controlled using a previously reported finger motion simulation protocol, which uses tendon displacement control in the

agonists and load control in the antagonists[20]. Flexion motions were performed by moving FDP and FDS in displacement control against a constant 10 N extensor antagonist load until full flexion ROM was achieved in all joints. This was repeated for finger extension, with the extensor tendon in displacement control against a constant 2 N load on each flexor tendon. Five full motion cycles were conducted for each finger. Tendon displacement was set to a rate of 0.6 in/sec [ref], and all motion trials were performed with consistent tendon excursions.

6.2.3 Motion Analysis

Finger segments were tracked using an electromagnetic transmitter system (trakSTAR, Northern Digital Inc., Canada) and four electromagnetic tracker sensors (Ø2 mm, model M180, trakSTAR, NDI, nominal accuracy: 1.4 mm). To install the trackers, short lateral incisions were made along the finger to expose the lateral aspect of each bone segment. Each tracker was then inserted laterally in a 2.1 mm hole at the center of each bone segment of interest (distal phalanx, middle phalanx, proximal phalanx, and metacarpal) (Figure 6.1). Rigid fixation was achieved by interference tolerance fit.
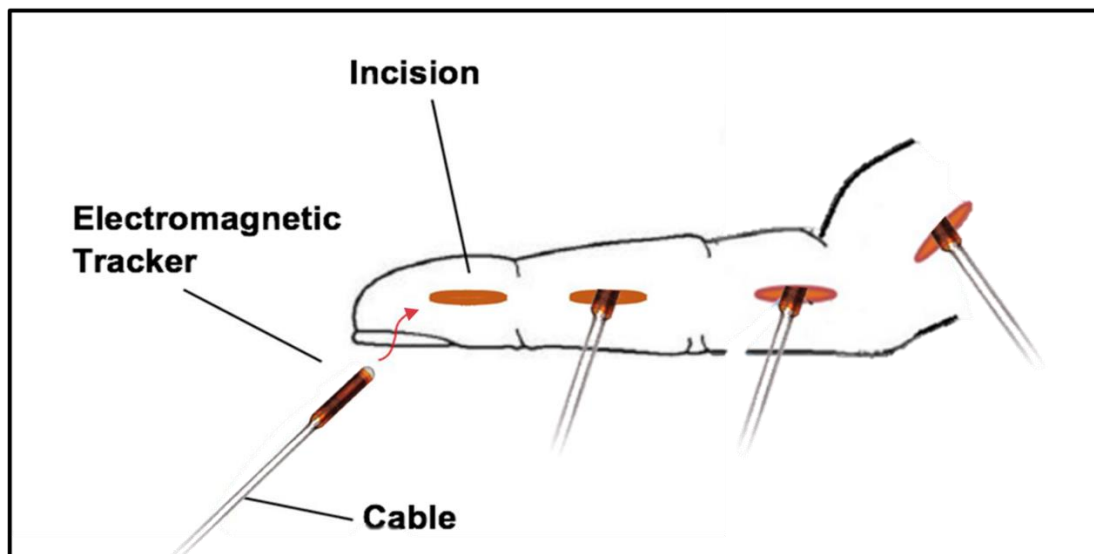
Figure 6.1: Electromagnetic Tracker Sensor Installation

Tracker sensors of diameter Ø2 mm were inserted into a hole drilled in each bone segment.

Kinematic analysis Data measured from the trackers were imported into a customized software program called The MotionMonitor xGEN (TMM, Innovative Sports Training Inc., Chicago). This dataset included the positions and orientation of the trackers during active functional movements which consisted of a repeated 5 flexion-extension motion trial of the long fingers from partial full extension to partial full flexion (limiting the finger from reaching maximum flexion-extension endpoints). Discrete motion pathways of each segment were dictated in each bone segment to obtain the associated mean helical axis orientations (direction cosines) required for coordinate system building. In addition, this software allows for a virtual construction of the finger segments using temporary palpated discrete points with a single electromagnetic tracker stylus to create a fully animated 3D virtual finger model for real-time finger motion purposes only.

6.2.4 Anatomical Landmark Digitization

To construct ISB's AF, a total of 16 anatomical landmarks (ALs) (4 for each finger segment) following ISB recommendations were used[6]. These landmarks were referenced as MC, PP, MP, and DP for metacarpal, proximal phalanx, middle phalanx, and distal phalanx, respectively where 'O' is for origin of the segment and each frame, 'H' is for center of the distal epiphysis (obtained by averaging coordinates of 15 palpated landmarks), 'B' is for the center of the proximal epiphysis (obtained the same way as H), and HM is for the center medial point to the distal epiphysis (Figure 6.2). ALs were taken by denuding each finger segment, while maintaining rigid fixation of trackers in bone, and importing palpated bony landmarks (Table 6.1).
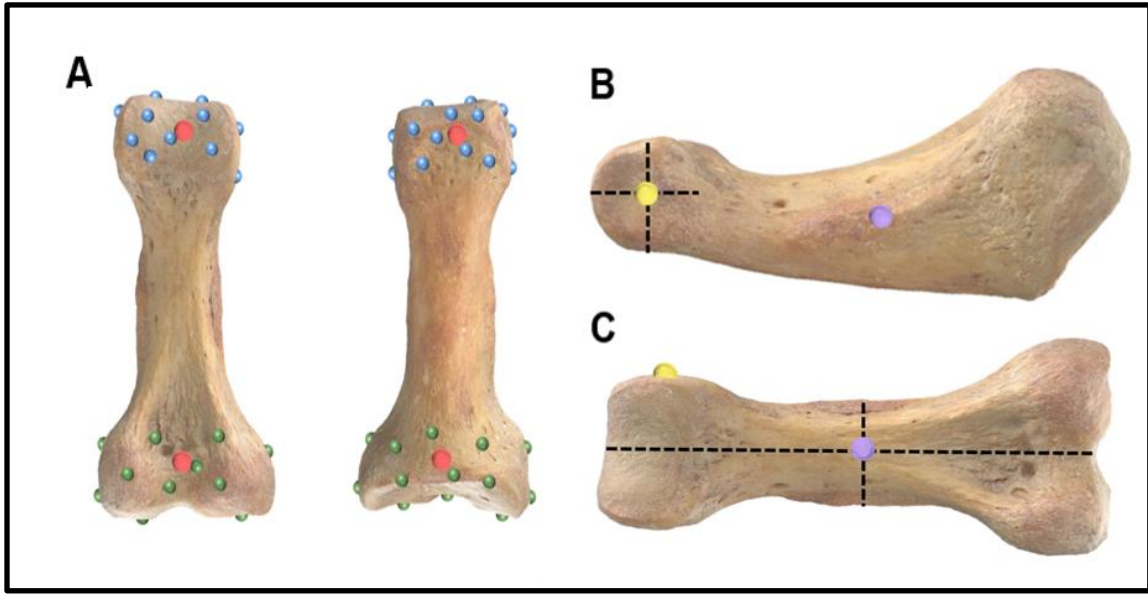
Figure 6.2: Bone Landmark Digitization

Landmarks used for the anatomical frame construction of the proximal phalanx: (A) 15 digitized landmarks on the proximal and distal epiphysis (green and blue, respectively) creating the centroid points MP.B and MP.H displayed in red (calculated as the mean coordinated of all 15 digitized points), (B) MP.HM digitized point displayed in yellow and (C) the origin of the AFs displayed in purple.

Table 6.1: Name and Location of Digitized Landmark

Bone Segment	Palpated Point	Location
Metacarpal Bone	MC.B	Center of the proximal epiphysis of metacarpal
	MC.H	Center of the distal epiphysis of metacarpal
	MC.O	Midpoint between proximal and distal ends
	MC.HM	Medial point of the distal head
Proximal Phalanx	PP.B	Center of the proximal epiphysis of proximal bone
	PP.H	Center of the distal epiphysis of proximal bone
	PP.O	Midpoint between proximal and distal ends
	PP.HM	Medial point of the distal head
Middle Phalanx	MP.B	Center of the proximal epiphysis of middle bone
	MP.H	Center of the distal epiphysis of middle bone
	MP.O	Midpoint between proximal and distal ends
	MP.HM	Medial point of the distal head
Distal Phalanx	DP.B	Center of the proximal epiphysis of distal bone
	DP.H	Center of the distal epiphysis of distal bone
	DP.O	Midpoint between proximal and distal ends
	DP.HM	Medial point of the distal head

6.2.5 Local Frame Definitions and Motion-Based Coordinate System Building

Two sets of frames were constructed for each finger. The landmark definition corresponded to implementation of anatomical frames whereas functional frames included a functional joint axis. The axes' names and conventions were kept consistent for both frames such that:

- $\overrightarrow{X_J}$: The sagittal axis was dorsally oriented [add-abd]

- $\overrightarrow{Y_J}$: The longitudinal axis was proximally oriented [int-ext rot]

- $\overrightarrow{Z_J}$: The transverse axis was radially oriented (along the helical axis direction for the functional frames) [flex-ext]

To construct the MCS, reference finger positions and functional movements were recorded, and one anatomical landmarks was digitized. Prior to performing functional movements, the finger and wrist were placed in a static neutral joint position as described in the ISB recommendations. This position ensured that the third metacarpal was aligned with the longitudinal axis of the forearm and served as a reference, t=0, position for the helical axis transformation calculations performed during active flexion-extension. The first functional movement that was performed was circumduction of the MCPJ. During this movement, the position of tracker S3 was recorded with respect to tracker S4 and the MCP was rotated at the base joint for 10s to find the joint center of rotation (O_{MCPJ}) with respect to S4 (Figure 6.3). Following MCP circumduction, flexion-extension of the finger was performed to find the flexion-extension axis ($\overrightarrow{Z}$) through the DIPJ and PIPJ using helical axis transformations.

For each finger segment, the positions and rotation of the tracker within the segment was recorded with respect to the proximal segment tracker. For each timepoint during the motion, the helical axis transformations were calculated with respect to the reference position (t=0). The mean helical axis unit vector, ($\hat{u}$), was calculated at the DIPJ ($\hat{u}_{S1}^{S2}$) and PIPJ ($\hat{u}_{S2}^{S3}$) and were assigned as the Z-axis of the associated segments ($\overrightarrow{Z_{PIPJ}}$ and $\overrightarrow{Z_{MCPJ}}$, respectively). Subsequently, the point along each of the HA that was closest to the origin

of the respective tracker was assigned as the joint origin (O_j) of the CMCJ, PIPJ, and the DIPJ (Figure 6.3). In addition, a stylus was calibrated to compensate for the magnetic center offset and used to digitize the center of the distal phalanx tip, DIPTip.
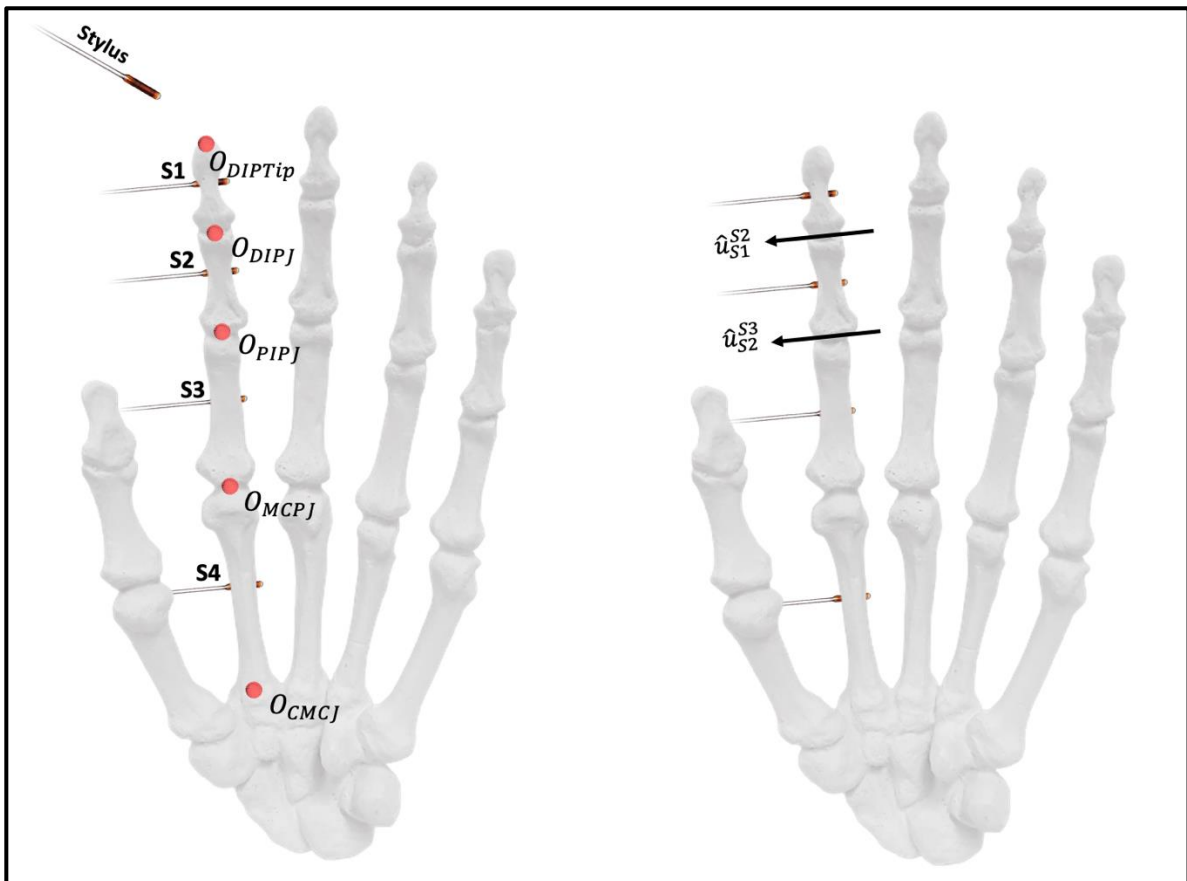
Figure 6.3: Functional Frame Definition

The centers of the CMCJ, MCPJ, PIPJ, DIPJ, and the digitized DIPTip are illustrated using the red dots. Active flexion-extension finger motion was used to derive the HA direction vectors of the PIPJ ($\hat{u}_{S1}^{S2}$) and MCPJ ($\hat{u}_{S2}^{S3}$) (+ve is left for left hand and right for right hand).

6.2.5.1   CMC's Coordinate system

The Z-axis of the CMCJ, defined as $\overrightarrow{Z_{CMCJ}}$, was computed by transforming the Z-axis of the MCPJ from S3 to S4 such that,

$$\overrightarrow{Z_{CMCJ}} = \overrightarrow{Z_{MCPJ}} \times R_{S3}^{S4}$$

A longitudinal line was then computed as the difference in length between the nearby joint centers ($O_{CMCJ} - O_{MCPJ}$) pointing proximally, relative to S4 (Figure 6.4); giving CMC.Line.

To obtain the X-axis,

$$\overrightarrow{X_{CMCJ}} = CMC.Line \times \overrightarrow{Z_{CMCJ}}$$

(where +X is volar for a right hand and dorsal for a left hand)

The Y-axis was computed as the line orthogonal to the ZX plane such that,

$$\overrightarrow{Y_{CMCJ}} = \overrightarrow{Z_{CMCJ}} \times \overrightarrow{X_{CMCJ}} \quad (pointing \ proximally)$$

Lastly, the axes system built for the CMCJ was then transformed into the global reference frame (G$_0$) such that,

$$G_{CMCJ}^{World} = G_{S4}^{World} \times G_{CMCJ}^{S4}$$
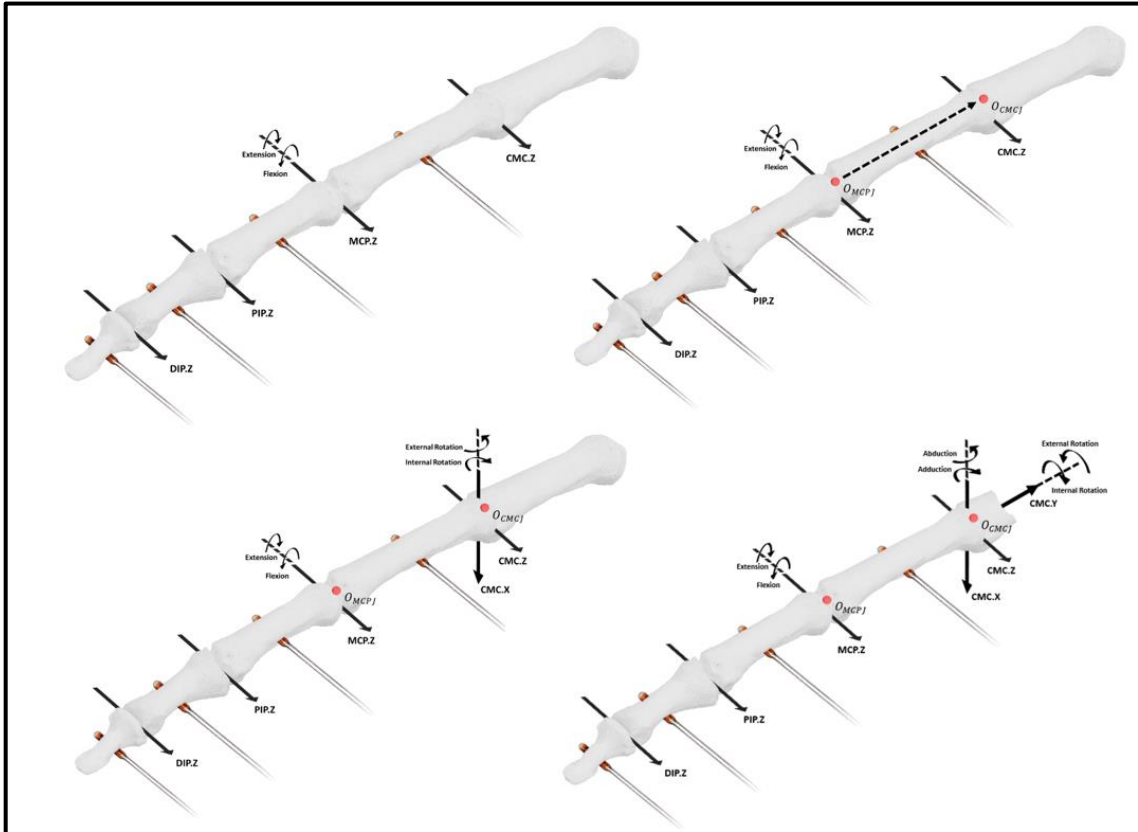
Figure 6.4: JCS Building of CMCJ

This figure illustrated the direction of the derived x-, y-, and z- axes of the CMCJ about the joint's center point, O_{CMCJ}.

6.2.5.2   MCP's Coordinate system

MCP.Line was derived pointing proximally by subtracting O_{PIPJ}, relative to S3, from O_{MCPJ}, relative to S3 (only after first transforming O_{MCPJ} from S4 to S3). In addition, Similar to the CMCJ, the X- and Y- axes were then computed (Figure 6.5) as follows:

$$\overrightarrow{X_{MCPJ}} = MCP.Line \times \overrightarrow{Z_{MCPJ}}$$

$$\overrightarrow{Y_{MCPJ}} = \overrightarrow{Z_{MCPJ}} \times \overrightarrow{X_{MCPJ}}$$

Lastly, the axes system built for the MCPJ was also transformed into the global reference frame (G₀) such that,

$$G_{MCPJ}^{World} = G_{S3}^{World} \times G_{MCPJ}^{S3}$$

6.2.5.3   PIP and DIP's Coordinate system

1. The Z-axis of the DIPJ, defined as $\overrightarrow{Z_{DIPJ}}$, was computed by transforming the Z-axis of the PIPJ from S2 to S1 such that,

$$\overrightarrow{Z_{DIPJ}} = \overrightarrow{Z_{PIPJ}} \times R_{S2}^{S1}$$

1. X-Axes of the two joints were computed as follows:

$$\overrightarrow{X_{PIPJ}} = PIP.Line \times \overrightarrow{Z_{PIPJ}} \text{ (where PIP.Line} = O_{DIPJ} \text{ - } O_{PIPJ}, \text{ relative to S2)}$$

$$\overrightarrow{X_{DIPJ}} = DIP.Line \times \overrightarrow{Z_{DIPJ}} \text{ (where DIP.Line} = O_{DIPTip} \text{ - } O_{DIPJ}, \text{ relative to S1)}$$

2. Y-Axes of the two joints were computed as follows:

$$\overrightarrow{Y_{PIPJ}} = \overrightarrow{Z_{PIPJ}} \times \overrightarrow{X_{PIPJ}}$$
$$\overrightarrow{Y_{DIPJ}} = \overrightarrow{Z_{DIPJ}} \times \overrightarrow{X_{DIPJ}}$$

3. Lastly, the axes system built for the PIPJ and DIPJ were transformed into the global reference frame (G_0) such that,

$$G_{PIPJ}^{World} = G_{S2}^{World} \times G_{PIPJ}^{S2}$$

$$G_{DIPJ}^{World} = G_{S1}^{World} \times G_{DIPJ}^{S1}$$

The Cardan angle sequence adopted for joint decomposition was ZYXr (flexion – pronation – abduction) as proposed by ISB[6] and further validated by Chao *et al*[23]. Ranges of motion and kinematic plots were obtained and proceeded through further analysis. A total of 33 joints were analyzed during 3 motions. Results obtained were stored within a database and used for further statistical analysis related to frame accuracy, motion repeatability, and reproducibility measures.
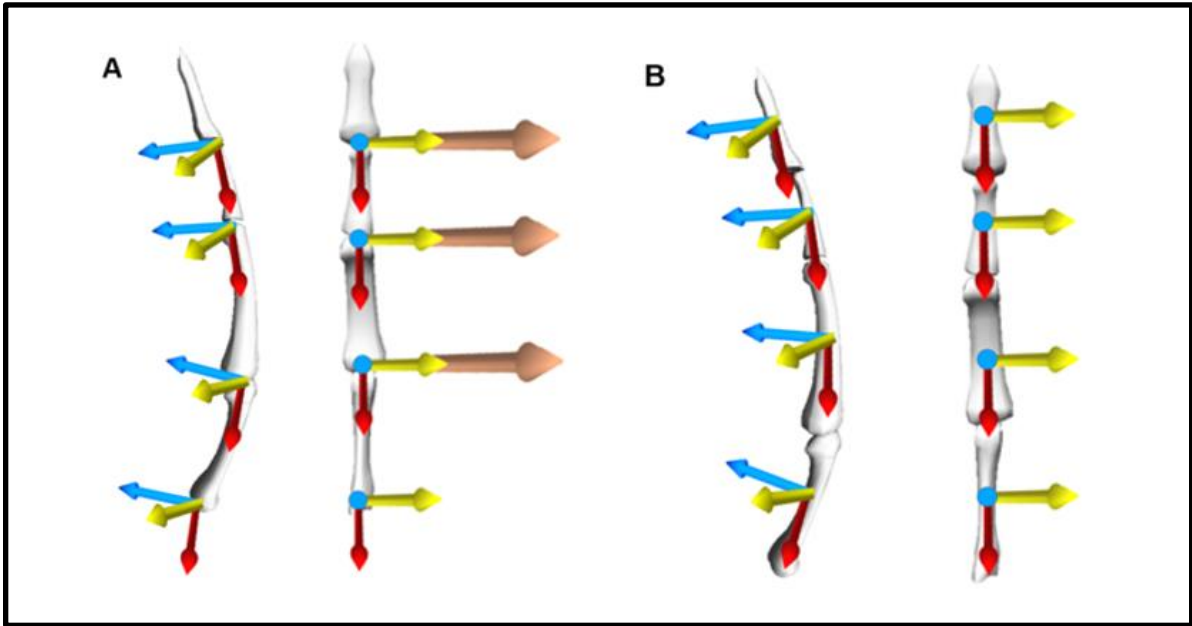
Figure 6.5: Motion-based and ISB Anatomical Coordinate System Frames

The lateral (left) and front (right) views denoting the position and orientation of the anatomical frames constructed for each bone segment using (A) the mean HA (illustrated in orange), and (B) ISB following ISB Recommendation (X-axis, Y-axis, and Z-axis are illustrated in blue, red, and yellow, respectively)

6.3   Data Analysis

6.3.1 Functional Frame Definition Validation

The methodology presented in this study for MCS and ISB were compared with data collected using a goniometer, a standard and widely used clinical range of motion assessment tool[23,24]. Finger joint flexion/extension were measured and mean differences between methodologies were computed for one digit ($\theta_{var} = \theta_{exp} - \theta_{MCS/ISB}$), as well as the deviations measured for all digits. A paired t-test and a linear regression for correlation were also computed for a further validation of the local frame definition in the Z-axis (i.e. flexion/extension).

6.3.2 Deviations between Frame definitions

The two local frame definitions described in this study, MCS and ISB, were compared by calculating the mean angle of each joint measured, along each respective axis, and measuring the deviations between the two frames. A Three-way Repeated Measures ANOVA (factors: Joint (MCP, PIP, DIP); Axes (X, Y, Z); Frame Definition (MCS, ISB)) was conducted to evaluate the differences in each cardan angle obtained during finger motion.

6.3.3 Repeatability and Reproducibility

Repeatability of the helical axes were measured as the deviation in joint angles from all five consecutive motion runs within the same finger. In addition, prior to data collection, an initial active motion test was conducted following the same tracker methodology and frame definitions as previously discussed. Motion data for all joint axes were measured and recorded during this trial. Once concluded, the trackers were removed and subsequently re-installed into the same finger segments. The coordinate frame building protocol was then repeated and the finger was actively flexed with tendon excursion kept consistent with the prior motion test. This protocol was conducted for the sole purpose of measuring the reproducibility of the helical frame axes where reproducibility was quantified as the deviations between all three joint axes between both kinematic motion trials. A paired t-test and a linear regression for correlation were also computed to further validate the reproducibility of the model.

6.4   Results

6.4.1 Comparison of Rotation Angles

The mean joint angle measured using both MCS and ISB local frame definitions for all 33 digits about the X-axis (add-abd), Y-axis (pro-sup), and Z-axis (flex-ext) along one cycle of motion are represented in Figure 6.6 and Table 6.2. Using helical axes, MCP achieved mean flex-ext angles of 92.9±8.4°, a pro-sup angle of 15.9±20.5°, and an abd-add angle of 11.1±17.5°. PIP achieved a flex-ext angle of 105.3±4.9°, a pro-sup angle of 22.5±16.4°, and an abd-add angle of 14.4±18.8°, and DIP achieved a flex-ext angle of 55.2±9.6°, a pro-sup angle of 8.9±9.7°, and an abd-add angle of 10.9±16.5°. In contrast, following ISB frame definition resulted in a MCP flex-ext angle of 89.7±9.5°, pro-sup angle of 16.9±11.9°, and an abd-add angle of 18.0±16.2°. PIP achieved a flex-ext angle of 101.8±9.3°, a pro-sup angle of 20.7±14.8°, and an abd-add angle of 17.5±16.0°, and lastly, DIP achieved a flex-ext angle of 53.2±11.2°, a pro-sup angle of 10.9±13.1°, and an abd-add angle of 10.1±13.5°.

6.4.2 Functional Frame Definition Validation

Tables 6.3 and 6.4 represents the maximum flexion/extension angle for each joint achieved using MCS and ISB in comparison to a goniometer, respectively. For MCS-Goniometer, no significant differences in the measurements were reported at 95% CI for the MCP (p=0.176), PIP (0.104), and DIP (p=0.854). In addition, significant linear correlations (R^2) for the MCP, PIP, and DIP were measured as 0.655, 0.880, and 0.869, respectively. In terms of ISB-Goniometer, no significant differences were either reported at 95% CI for the MCP (p=0.859), PIP (0.486), and DIP (p=0.453) with significant linear correlation of 0.666 for PIP and non-significant correlations of 0.597 and 0.6 for the MCP and DIP, respectively.
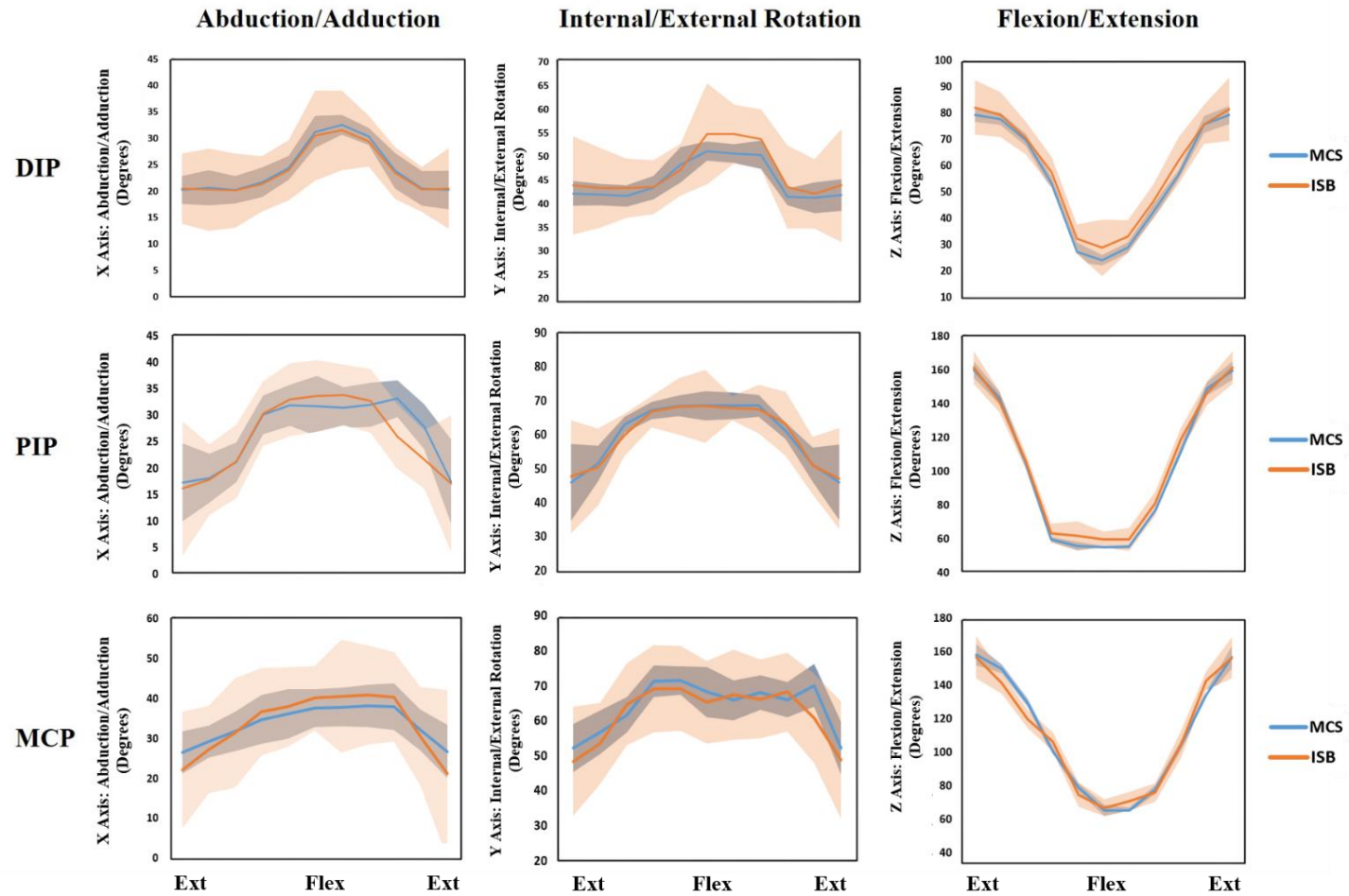
Figure 6.6: Joint Kinematics

The mean angles measured by MCS and ISB local frames for each joint (DIP, PIP, MCP) along its respective X-, Y-, and Z-axes throughout one full active motion cycle are illustrated above. MCS are denoted by blue lines where ISB are denoted by orange lines.

Table 6.2: Joint Angles for MCS and ISB

Joint angles for each individual digit is summarized below.

| | MCP | | | | | | PIP | | | | | | DIP | | | | | |
| | MCS | | | ISB | | | MCS | | | ISB | | | MCS | | | ISB | | |
Axes	X	Y	Z	X	Y	Z	X	Y	Z	X	Y	Z	X	Y	Z	X	Y	Z
Finger 1	39	28	85	39	20	94	59	52	113	39	51	114	28	17	56	28	11	55
Finger 2	31	38	94	37	36	98	15	25	113	44	29	119	5	9	64	11	29	79
Finger 3	41	3	108	36	3	97	-0.3	0.5	108	-0.2	0.4	97	6	2	67	6	2	61
Finger 4	-2	9	91	-2	7	75	14	18	104	11	15	85	51	34	63	42	28	52
Finger 5	3	34	88	3	29	76	1	14	109	1	12	95	7	10	60	6	9	52
Finger 6	5	17	94	7	20	78	10	38	102	15	30	106	18	8	63	10	3	57
Finger 7	-5	-13	79	6	11	90	-3	43	100	4	15	95	-3	4	39	-4	-6	25
Finger 8	2	54	101	34	33	94	5	26	105	23	33	106	-9	-3	39	7	0.2	40
Finger 9	14	4	99	10	4	100	39	16	106	14	28	106	5	6	57	2	34	53
Finger 10	-7	-4	85	4	6	85	17	12	101	37	13	98	9	8	53	2	7	51
Finger 11	4	4	99	24	17	99	3	3	99	4	3	100	2	4	51	1	4	50
Average	11	16	93	18	17	90	15	22	105	17	21	102	11	9	55	10	11	53
SD	18	20	8	20	12	10	19	16	5	16	15	9	17	10	10	13	13	11

Finger Joint

Table 6.3: MCS vs. Goniometer Joint Measurements

The mean MCS rotations vs. Goniometer measurements along the flexion/extension axis

	Joint								
	MCP			PIP			DIP		
Digit	MCS	Goniometer	θ_{var}	MCS	Goniometer	θ_{var}	MCS	Goniometer	θ_{var}
1	85	90	4.92	113	115	2.29	56	60	4.26
2	94	90	-4.38	113	116	2.98	64	61	-2.85
3	108	100	-7.70	108	105	-2.86	67	70	2.58
4	91	85	-6.40	104	100	-3.92	63	60	-3.13
5	88	90	2.37	109	105	-4.29	60	70	10.42
6	94	85	-9.01	102	105	2.67	63	60	-2.69
7	79	85	6.01	100	100	0.44	39	45	6.38
8	101	95	-5.85	105	105	0.06	39	40	0.95
9	99	90	-8.91	106	100	-5.73	53	50	-3.40
10	85	90	-5.46	100	92	-8.42	53	50	-3.39
11	99	95	-2.54	99	95	-4.02	51	45	-5.96
Average	92.9	90.1	2.8	105.3	103.4	1.9	55.3	55.6	-0.2

*θ_{var} = **Angle variation (difference)**

Table 6.4: ISB vs. Goniometer Joint Measurements

The mean ISB rotations vs. Goniometer measurements along the flexion/extension axis

	MCP			PIP			DIP		
					Joint					
Digit	ISB	Goniometer	θ_{var}	ISB	Goniometer	θ_{var}	ISB	Goniometer	θ_{var}
1	94	90	4.92	114	115	2.29	55	60	4.26
2	98	90	-4.38	119	116	2.98	79	61	-2.85
3	97	100	-7.70	97	105	-2.86	61	70	2.58
4	75	85	-6.40	85	100	-3.92	52	60	-3.13
5	76	90	2.37	95	105	-4.29	52	70	10.42
6	78	85	-9.01	106	105	2.67	57	60	-2.69
7	90	85	6.01	95	100	0.44	25	45	6.38
8	94	95	-5.85	106	105	0.06	40	40	0.95
9	100	90	-8.91	106	100	-5.73	53	50	-3.40
10	85	90	-5.46	98	92	-8.42	51	50	-3.39
11	99	95	-2.54	100	95	-4.02	50	45	-5.96
Average	89.7	90.1	-0.4	101.8	103.4	-1.5	53.3	55.6	-2.3

*θ_{var} = **Angle variation (difference)**

6.4.3 Deviations between Local Frame Definitions

The deviations between the two local frames differently defined varied depending on the segment considered. The total deviation reported ranged from 0.8° to 6.9°. On average, the axis deviation in all axes was 2.7°. The largest deviations observed between fingers were between the PIP and DIP joints along the pro-sup and abd-add axes, with flexion-extension axes achieving the lowest deviations in all joints. In addition, A three-way ANOVA resulted in an insignificant mean difference of 0.151° between MCS and ISB (p=0.923)

6.4.4 Repeatability and Reproducibility

The repeatability of the MCS and ISB frame definitions following 5 full flexion-extension cycles were measured to be 0.64° and 0.86°, respectively along the flexion-extension axis. In addition, removing and re-installing the trackers while following the same digitization and frame definition methodologies resulted in angle variances ranging from 0.3 to 23.5° with insignificant mean differences of 2.5° (p=0.137), 2.8° (p=0.060), and 0.8° (p=0.640) in the DIP, PIP, and MCP joints respectively. Finally, linear correlations of 0.962, 0.990, and 0.978 were observed in the DIP, PIP, and MCP joints, respectively.

6.5 Discussion

Currently, the choice of constructing coordinate systems using functional frame for finger joint kinematics is limited by the lack of proper consensus on the validly of the proposed frame definitions. Therefore, the aim of this study was to analyze finger joint kinematics using helical axes in comparison to the frame defined by the International Society of Biomechanics (ISB).

Joint angle measurements reported in this study were in agreement with current literature[7,9]. Each definition resulted in joint orientations with deviations of about 2.7° on average; up to 6.9° among all three different axes. Despite the deviations, both types of frame definitions revealed no statistical differences (p=0.923) in joint rotation angles computed by MCS and ISB. In addition, further validation of the MCS and ISB using a standard

goniometer resulted in insignificant differences of rotation along the flexion-extension axis, with significant linear correlations as high as 0.869 for MCS. However, unlike MCS, ISB did not achieve the same significant correlation between all of its joints and goniometer measurements.

The mean joint kinematic curves, presented in figure 6.6, revealed discrepancies in joint behavior, mainly along the X- and Y-axes with root mean square errors reaching a high of 7.6° and 9.9° in the X- and Y- axes, respectively. The flexion-extension axis (i.e. Z-axis) resulted in the smallest differences between the curves, as expected with the Z-axis being the primary axis of motion[25]. In addition, using MCS to orientate the Z-axis seemed to have an effect on the interpretation of the remaining two axes, as seen in figure 6.6 (i.e the cross-talk effect); especially for the MCP joint. Since the orientation of the X-axis was dependent on specific digitized landmarks and thus, different compared to the MCS, motion around the X and Y axes consequently do not exactly correspond to the classical definitions of the rotations and deviations in the finger[5]. Nonetheless, these findings support the hypothesis made in chapter 1 as discrepancies between both frame definitions were well within the 10° target goal.

Kinematic data reported for the PIP and MCP in all three axes were in agreement with results obtained by Coupier *et al.*[12] and Metcalf *et al.*[26]; two studies in which evaluation of finger joint kinematics were conducted using surface markers. In addition, the MCP joint achieved rotations of 11° and 16° within the X- and Y-axes, respectively that were comparable to those reported in the literature[10]. This is particularly important as the MCP has a higher degree of freedom due to the nature of the joint, unlike other interphalangeal hinge joints. Results reported for the DIP joint however were less conclusive. Our study revealed that the distal phalanx pronates until about 30 degrees of joint flexion, and then supinates until full flexion. This joint pattern is distinctly different from the same motion paths followed by the middle and proximal segment. Nonetheless, a limited number of studies using JCS constructed by CT images and surface markers on skin also reported finger pronation-supination patterns. These studied revealed similar patterns throughout DIP's motion[7,9] with discrepancies thought to result from the simulated repair condition conducted within our study.

There were a few limitations to our study. Although the use of metal was significantly reduced within our setup, the increase in sensitivity to metals of the electromagnetic tracking system maybe have attributed to errors in sensor accuracy and noise throughout testing. Secondly, the creation of the ISB frames were entirely derived from bony landmark digitization and thus, were normally dependent on human errors.

Despite limitations, a few important strengths should be considered within the study. Firstly, the use of an advanced, repeatable, and validated active motion simulator with position and load control of the tendons, in comparison to previously reported in-vitro finger motion simulators. Secondly, the repeatability trial measurement made from 5 finger motion cycles resulted in variations as low as 0.64°; validating the accuracy of the local frames defined, as well as further supporting the hypothesis made in chapter 1 . Thirdly, reproducibility measures were reported to have insignificant differences between tests; further validating the accuracy and validity of the results produced by the MCS across the different fingers tested. In addition, creation of MCS were less dependent on digitization errors; yielding higher reproducibility and repeatability outcomes.

6.6   Conclusion

The need for a standard and accurate definition of joint coordinate systems is necessary for the quantification of joint kinematics. Our findings support the use of the MCS methodology presented in this study in measuring accurate and reproducible finger joint kinematics, compared to ISB Recommendations. In addition, to our author's knowledge, this is the first study that evaluates the accuracy of helical axes during active *in-vitro* finger motion without the use of virtually constructed motion pathways of bone segments in computed tomography (CT) scans.

6.7   References

1.   Carpinella I, Mazzoleni P, Rabuffetti M, Thorsen R, Ferrarin M. Experimental protocol for the kinematic analysis of the hand: Definition and repeatability. doi:10.1016/j.gaitpost.2005.05.001

2.   Ellis B, Bruton A. A study to compare the reliability of composite finger flexion with goniometry for measurement of range of motion in the hand: *http://dx.doi.org/101191/0269215502cr513oa*. 2016;16(5):562-570. doi:10.1191/0269215502CR513OA

3.   Goislard de Monsabert B, Rossi J, Berton E, Vigouroux L. Quantification of Hand and Forearm Muscle Forces during a Maximal Power Grip Task. *Med Sci Sport Exerc*. 2012;44(10). https://journals.lww.com/acsm-msse/Fulltext/2012/10000/Quantification_of_Hand_and_Forearm_Muscle_Forces.11.aspx.

4.   Sancho-Bru JL, ! E Erez-Gonz AP, Vergara-Monedero M, Giurintano D. A 3-D dynamic model of human finger for studying free movements. *J Biomech*. 2001;34:1491-1500.

5.   Brand PW. Clinical mechanisms of the hand. 1985:342-342.

6.   Wu G, van der Helm FCT, Veeger HEJD, et al. ISB recommendation on definitions of joint coordinate systems of various joints for the reporting of human joint motion--Part II: shoulder, elbow, wrist and hand. *J Biomech*. 2005;38(5):981-992. doi:10.1016/j.jbiomech.2004.05.042

7.   Coupier J, Moiseev F, Feipel V, Rooze M, Van Sint Jan S. Motion representation of the long fingers: a proposal for the definitions of new anatomical frames. *J Biomech*. 2014;47(6):1299-1306. doi:10.1016/j.jbiomech.2014.02.017

8.   Coupier J, Hamoudi S, Telese-Izzi S, Feipel V, Rooze M, Van Sint Jan S. A novel method for in-vivo evaluation of finger kinematics including definition of healthy

motion patterns. *Clin Biomech*. 2016;31:47-58.
doi:10.1016/j.clinbiomech.2015.10.002

9. Ishii K, Oki S, Iwamoto T, et al. Quantitative analysis of metacarpophalangeal
    joints during active flexion using four-dimensional computed tomography. *Clin
    Biomech*. 2020;80. doi:10.1016/j.clinbiomech.2020.105188

10. Buczek FL, Sinsel EW, Gloekler DS, Wimer BM, Warren CM, Wu JZ. Kinematic
    performance of a six degree-of-freedom hand model (6DHand) for use in
    occupational biomechanics. *J Biomech*. 2011;44(9):1805-1809.
    doi:10.1016/J.JBIOMECH.2011.04.003

11. Goislard de Monsabert B, Visser JMA, Vigouroux L, Van der Helm FCT, Veeger
    HEJ. Comparison of three local frame definitions for the kinematic analysis of the
    fingers and the wrist. *J Biomech*. 2014;47(11):2590-2597.
    doi:10.1016/j.jbiomech.2014.05.025

12. Marin F, Mannel H, Claes L, D€ U Urselen L. Correction of axis misalignment in
    the analysis of knee rotations. *Hum Mov Sci*. 2003;22:285-296.
    doi:10.1016/S0167-9457(03)00036-8

13. Englander ZA, Cutcliffe HC, Utturkar GM, Garrett WE, Spritzer CE, DeFrate LE.
    A Comparison of Knee Abduction Angles Measured by a 3D Anatomic
    Coordinate System Versus Videographic Analysis: Implications for Anterior
    Cruciate Ligament Injury. *Orthop J Sport Med*. 2019;7(1):2325967118819831.
    doi:10.1177/2325967118819831

14. Grood ES, Suntay WJ. A joint coordinate system for the clinical description of
    three-dimensional motions: application to the knee. *J Biomech Eng*.
    1983;105(2):136-144. doi:10.1115/1.3138397

15. Scherer TP, Hoechel S, Müller-Gerbl M, Nowakowski AM. Comparison of knee
    joint orientation in clinically versus biomechanically aligned computed
    tomography coordinate system. *J Orthop Transl*. 2019;16:78-84.

doi:10.1016/j.jot.2018.07.005

16. Besier TF, Sturnieks DL, Alderson JA, Lloyd DG. Repeatability of gait data using a functional hip joint centre and a mean helical knee axis. *J Biomech*. 2003;36:1159-1168. doi:10.1016/S0021-9290(03)00087-3

17. Coupier J, Hamoudi S, Telese-Izzi S, Feipel V, Rooze M, Van Sint Jan S. A novel method for in-vivo evaluation of finger kinematics including definition of healthy motion patterns. *Clin Biomech (Bristol, Avon)*. October 2015. doi:10.1016/j.clinbiomech.2015.10.002

18. Kontaxis A, Cutti AG, Johnson GR, Veeger HEJ. A framework for the definition of standardized protocols for measuring upper-extremity kinematics. *Clin Biomech (Bristol, Avon)*. 2009;24(3):246-253. doi:10.1016/j.clinbiomech.2008.12.009

19. Haddara MM, Kadar A, Ferreira LM, Suh N. Effect of a Flexor Digitorum Superficialis Hemitenodesis on Reducing Volar Plate Strains for Swan Neck Deformities. *Hand (N Y)*. August 2021:15589447211040876. doi:10.1177/15589447211040877

20. Haddara MM, Byers B, Chinchalkar S, Ferreira LM, Suh N. The Effect of Wrist Position on Finger Tendon Loads Following Pulley Sectioning and Operative Reconstruction. *J Hand Surg Glob Online*. 2019;1(3):154-160. doi:10.1016/j.jhsg.2019.04.002

21. Kadar A, Haddara MM, Fan S, Chinchalkar S, Ferreira LM, Suh N. Use of Thermoplastic Rings Following Venting of Flexor Tendon Pulleys: A Biomechanical Analysis. *J Hand Surg Am*. 2021;46(6):485-492. doi:10.1016/j.jhsa.2020.11.003

22. Haddara MM, Fan S, Matache BA, Chinchalkar SJ, Ferreira LM, Suh N. Development of an In-Vitro Swan Neck Deformity Biomechanical Model. *Hand*. 2020.

23.   Chao EY. Justification of triaxial goniometer for the measurement of joint rotation. *J Biomech*. 1980;13(12):989-1006. doi:10.1016/0021-9290(80)90044-5

24.   Gajdosik RL, Bohannon RW. Goniometry Emphasizing Reliability and Validity Clinical Measurement of Range of Motion: Review of Clinical Measurement of Range of Motion Review of Goniometry Emphasizing Reliability and Validity. *PHYS THER*. 1987;67:1867-1872. http://ptjournal.apta.org/content/67/12/1867. Accessed April 16, 2017.

25.   Cappozzo A, Catani F, Croce U Della, Leardini A. Position and orientation in space of bones during movement: anatomical frame definition and determination. *Clin Biomech (Bristol, Avon)*. 1995;10(4):171-178. doi:10.1016/0268-0033(95)91394-t

26.   Metcalf CD, Notley S V., Chappell PH, Burridge JH, Yule VT. Validation and application of a computational model for wrist and hand movements using surface markers. *IEEE Trans Biomed Eng*. 2008;55(3):1199-1210. doi:10.1109/TBME.2007.908087

Chapter 7

7   The Evaluation of a Novel FDP-to-Volar Plate Zone I Repair Versus Button Repair: An In-Vitro Biomechanics Study

OVERVIEW: Zone I of the finger is the second leading area susceptible to injuries after zone II in the finger. A novel repair technique for zone I tendon avulsions was introduced in 2010, however, biomechanical investigation and evaluation of the effectiveness of the repair remains to be done. Hence, the basis of this chapter is to evaluate joint kinematics and tendon work of flexion (WOF) following flexor digitorum profundus to volar plate (FDP-VP) repair technique relative to the standard pullout.*

7.1   Introduction

Zone I injuries account for 4% of all traumatic tendon injuries in the hand and wrist, and can range from a partial to a full rupture or laceration of the flexor profundus (FDP) tendon[1]. Surgical treatment of the deformity is crucial for preserving fine motor skills and restoring motion of the distal interphalangeal joint (DIPJ). Choice of repair however is highly dependent on the site of injury[2]. Surgeons are often faced with a challenge with injuries distal to the A5 pulley due to an insufficient distal tendon stump to allow for a minimum 7 mm of required tendon purchase[3,4]. The most common approach when faced with an insufficient length of the distal stump is to treat the injury as a tendon avulsion using the button technique[5–7]. However, the button repair can lead to patient concerns and dissatisfaction, and has been associated with complications such as contracture and loss of joint range of motion[4,8,9]. As a result, various techniques involving tendon reinsertion have been reported and later enhanced by other groups in efforts to reduce complications such as infection and nail deformity that were associated with the button repair[10–12].

A recent study proposed in 2010 by Al-Qattan *et al.* introduced a new repair technique using the volar plate (VP) of the DIPJ to augment flexor tendon repair in zone I injuries[13]. The repair was fashioned using three separate figure-of-eight sutures, connecting the VP to the proximal FDP with a 7 mm suture purchase in comparison to the traditional direct tendon-to-tendon repair. Biomechanically, the technique was evaluated in an *in-vivo* animal model load to failure study[14], which reported that the including the VP in the distal tendon purchase significantly increased the tensile strength of the repair at time zero. Furthermore, the same group conducted an anatomical and a prospective clinical study involving 6 patients with clean-cut complete lacerations of the FDP tendon in the distal part of zone I[15] to address complications of using the entire volar plate as a distally-based flap for tendon repair. Anatomical and clinical outcomes both supported the use of the entire VP-based flap as a technique for repairing distal FDP injuries, and ensuring that the repair does not result in joint instability or flexion contracture.

Despite the biomechanically and clinically promising outcomes reported in previous studies, assessment of joint kinematics following the raising of the VP flap are

lacking[16]. Therefore, the primary goal of this study was to evaluate and quantify the *in-vitro* joint kinematics, flexor tendon loads, and work of flexion following treatment of zone I injuries using the proposed FDP-VP repair technique relative to the pullout button repair. The secondary objective was to measure finger-tip forces at full finger flexion.

7.2   Materials and Methods

Fourteen digits comprised of the index, long, and ring fingers, from five freshly frozen cadaveric specimens (age: 63.8±4.9 yrs.) were utilized in this study. Computed tomography (CT) scans of the specimens were evaluated by a surgeon prior to testing and specimens were excluded if any signs of osteoarthritis or other degenerative joint conditions were noted. All screened specimens were amputated 15 cm proximal to the wrist.

7.2.1 Specimen Preparation

Isolation of the FDP, flexor superficialis (FDS), and the extensor digitorum communis (EDC) was performed at the wrist level. Each individual tendon was sutured with a Krackow stitch using a 0-braided Vicryl suture (Ethicon, Somerville, NJ), which was connected to a linear servo-actuator. The second to fifth metacarpals were cross-pinned using two 1.5 mm K-wires, which were anchored to the simulator's base to stabilize the wrist during simulated active finger motions. Finally, a fixed rigid foam block was used to support the dorsum of the hand and the metacarpophalangeal joint (MCPJ) in a neutral wrist position.

7.2.2 In-Vitro Active Finger Motion Simulation

Tendon-driven finger motion trials were conducted using a validated active finger motion simulator[17]. The end-shaft of each servo-actuator was augmented with a uni-axial load cell (Model 34; Honeywell, Charlotte, NC), which measured tendon tensile loads and provided feedback for closed-loop load control. Intact tendon excursions were determined by moving the flexors in position control against a constant 10 N antagonist load on the extensor tendon. Full flexion excursion was defined as the tendon travel required by the flexor tendons to achieve full ROM in all joints (MCPJ: 83±10°, PIPJ: 101±13°, DIPJ:

57±9°). This was repeated for finger extension, with the extensor tendon in position control against a constant 2 N load on each flexor tendon. The intact tendon excursions were subsequently used for testing surgical conditions.

7.2.3 Conditions Tested

Five finger conditions were tested: 1) intact; 2) FDP incised at its insertion; 3) pullout button repair; 4) FDP-VP repair; and 5) 'no slack' FDP-VP repair.

7.2.4 FDP Injury Simulation (FDP Incised)

A 3 cm longitudinal volar midline incision was made over the DIPJ, exposing the flexor tendon sheath to visualize the A5 pulley. The FDP tendon was then sharply incised with a scalpel transversely, detaching it from bone while ensuring that the surrounding collateral ligaments remained intact. Repairs were carried out in the same sequence using 3-0 Polypropylene (Ethicon, Somerville, NJ). Skin was then re-approximated to maintain specimen hydration during motion trials.

7.2.5 Button Repair

For repair using the modified pullout button technique, a two-core modified Kessler suture pattern was performed through the distal edge of the proximal tendon. Two Keith needles were drilled through the middle of the distal phalanx, exiting through the nail plate. The suture ends were then passed through the Keith needle and brought through the distal phalanx dorsally (Figure 7.1). The tendon was then secured by tying the sutures over a 1.3 cm button. The skin incisions were closed for tendon hydration.
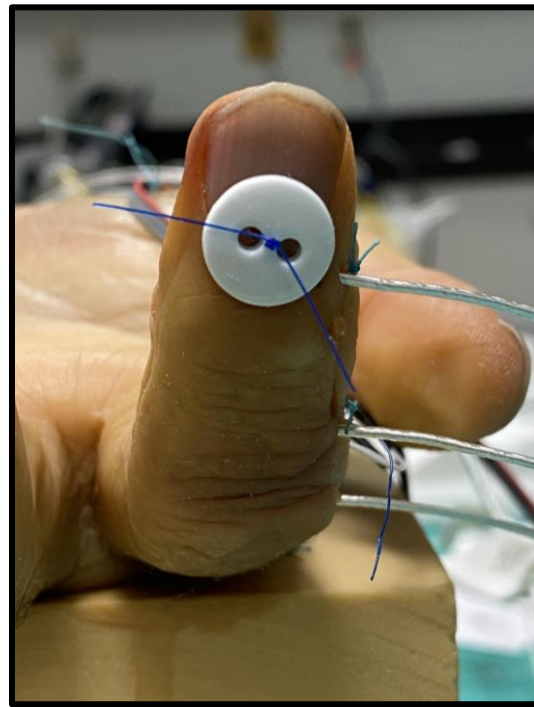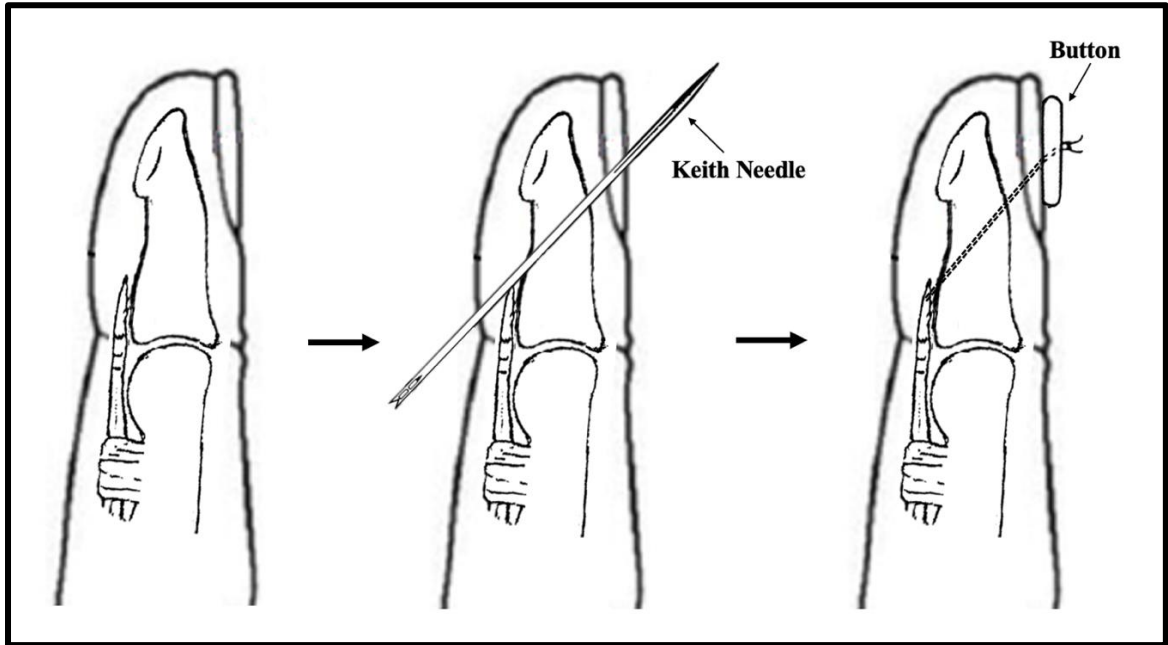
Figure 7.1: Pull-out Button Technique

The stages of a button repair technique. A Keith needle was used to drive the suture through bone and a knot was tied and fixed over the nail plate using a button as illustrated.

7.2.6 FDP-VP Repairs

The flexor sheath was exposed once again, incising through the A5 pulley to visualize the DIPJ VP. The VP was raised as a distally based flap off the middle phalanx while preserving the collateral ligaments. Dimensions of the incised VP were measured using a digital caliper (L=5.9±0.6 mm; W=7.0±0.5 mm; T=1.9±0.2 mm). The proximal end of the VP was then attached to the FDP using two figure-of-eight 3-0 Polypropylene sutures[15](Figure 7.2). With each coaptation, 3 mm of purchase of the VP and 7 mm of purchase in the tendon was obtained, as proposed by Al-Qattan *et al.*[13]. It is conceivable that addition of the VP may result in effectively lengthening the FDP. To account for this, the distance from the FDP insertion site to the proximal aspect of the volar plate was measured (FDP lengthening average: 7.6±0.5 mm). Subsequently, the FDP actuator's starting position was then adjusted by that measured amount and referred to as the 'no slack' condition to correct for the amount the FDP that was effectively lengthened.

7.2.7 Joint Angle Measurement

Joint angles were measured using a trakSTAR® (NDI, Waterloo, ON, Canada) electromagnetic tracking system. Four 2 mm diameter trackers (M180, trakSTAR®, NDI) were installed through drill holes made laterally at the center of each phalanx (distal, middle, proximal, and metacarpal) as previously reported[18,19]. Joint ROMs were recorded using a validated helical axes joint coordinate system to measure rotations along three axes; flexion/extension, abduction/adduction, and internal/external rotation[20,21]. Flexion/extension is the angle generated about the axis going through the joint where abduction/adduction is the angle generated by the long axis in the flexion/extension plane (perpendicular to the joint) and lastly, internal/external are the rotations generated about the long axis. Total joint ROM was denoted as the collective angle achieved by the DIPJ, PIPJ, and MCPJ.
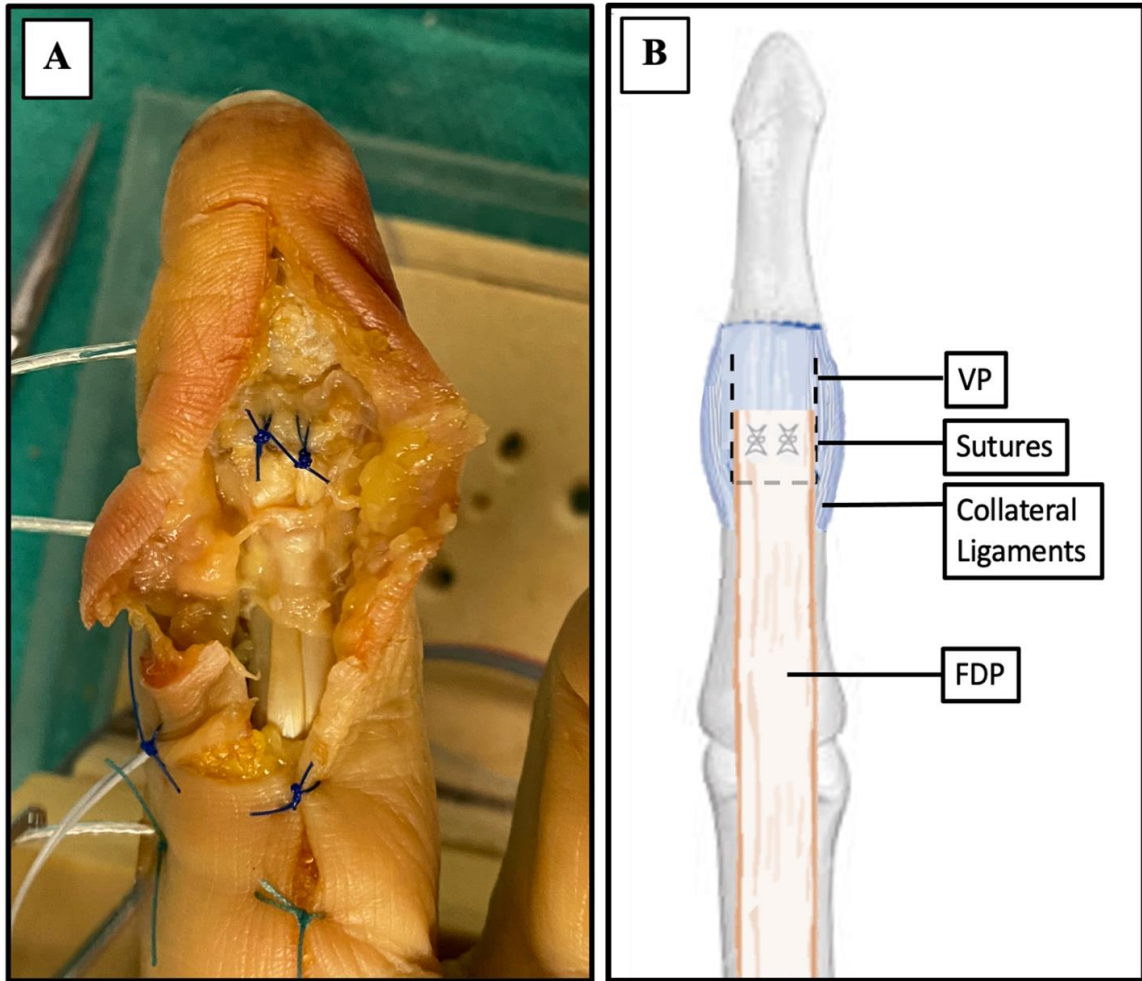
Figure 7.2: FDP-VP Technique

A 3 mm purchase of the proximal end of the VP was attached to a 7 mm purchase of the distal end of lacerated tendon using two figure-of-eight 3-0 Polypropylene sutures in vitro (a) and as illustrated (b).

7.2.8 Tendon Load and Work of Flexion Measurement

Flexor and extensor tendon load feedback was provided by the uni-axial load cells mounted to the end shaft of each linear servo actuator and closed-loop load control was achieved using custom code made in the LabVIEW programming environment (National Instruments, Austin, TX). The work of flexion (WOF) was calculated as the area under the tendon load versus tendon excursion curve[22].

7.2.9 Fingertip Strength

Static fingertip force was measured at full finger flexion against a 6-axis load cell, with the net force magnitude calculated from the Euclidean force vector equation (Figure 7.3). This was achieved with flexor tendons moved to the same excursion point defined in the intact condition, and the load cell's height (21.6 mm) provided interference for resisted flexion. These tests were repeated with each FDP condition.

Figure 7.3: Fingertip Strength Measurement

Resultant forces at the fingertip were measured with a 6-axis load cell. This was achieved with FDS and FDP flexor tendons moved to the same excursion point defined in the intact condition, while the load cell's height (21.6 mm) provided interference for resisted flexion. These tests were repeated with each FDP condition.

7.2.10 PIPJ Volar Plate Strain Measurement

Volar plate strain at the PIPJ was measured using a pre-wired minute strain gauge (Model #:KFH-3-350-C1-11L3M3R, Omega, Norwalk, CT) to investigate the effect of the imbalances in load on the strains induced by the PIPJ as a result of the different conditions tested. Before installing the gauge, modifications to the thickness of the substrate were made to amplify the measurements read by the gauge. A benchmark experiment where various thicknesses of the gauge were individually mounted onto a steel sheet and deflected by the same distance between gauge readings (Appendix B). Sample data was collected where the optimal thickness of the substrate was selected as the thickness that corresponded to the highest strain measurement, before buckling.

Once the gauge was modified, a mid-line incision was made along the length of the volar surface of each digit. Sacrificing of the A3 pulley was necessary for gaining clear access and locating the volar plate overlaying the PIPJ. The distal end of the volar plate was then slightly raised and the gauge was slid underneath the plate and secured using 4-0 Vicryl sutures in a figure of 8 configuration. A small transverse incision was made at the level of the radial skin flap overlying the middle phalanx, and the wire of the strain gauge was passed through this split and secured with 0-Vicryl sutures. The longitudinal skin incision was closed, and the strain gauge wires were further secured to the palm of the hand using Mastisol (Ferndale Laboratories, Inc., MI, United States). Strain measurements were collected with custom code made in the LabVIEW programming environment (National Instruments, Austin, TX, United States) and change in strain was measured using the intact condition as the baseline for all succeeding conditions.

7.2.11 Motion Trial Protocols

All active finger flexion motion trials were simulated with the excursion points and loads of flexors and extensors kept consistent between conditions. Saline solution was used throughout testing to maintain hydration and prevent desiccation. Each finger motion was repeated three times, with the first two trials performed to pre-condition and settle each repair, and with measurements from the third trial recorded for statistical analysis[19].

7.2.12 Statistical Analysis

Multiple One-way repeated-measures ANOVA models, with Bonferroni correction, were performed to analyze the effect of zone I injury and repair settings on tendon load, WOF, joint ROM, and finger-tip forces within all tested conditions. Within-subject effects and pairwise comparisons were also examined, with significance set at $p < 0.05$.

7.3 Results

7.3.1 Flexor Tendon Loads and Work of Flexion

Incising FDP significantly reduced FDP tendon loads at full flexion by 21% (4.3 ± 3.7 N; $p < 0.05$) (Figure 7.4). There was no significant change in FDS loads following incision. Both button and FDP-VP repairs restored FDP and FDS loads to the intact condition with no difference between the two techniques. Following FDP-VP repair, the 'no slack' variation caused a measurable 12% (2.4 ± 3.6 N; $p = 0.229$) increase in FDP load, though not statistically significant. There was negligible change in FDS loads.

The FDP incision significantly decreased FDP WOF by 146 ± 120 N.mm ($p < 0.05$) (Figure 7.5). The button and both FDP-VP repairs restored WOF to intact levels for FDP and FDS ($p = 1.000$). The 'no slack' FDP-VP technique increased WOF compared to the simple FDP-VP repair for both FDP and FDS by 74.1 ± 58.9 ($p < 0.05$) and 64.2 ± 52.8 ($p < 0.05$), respectively. None of the repairs were statistically different from the intact condition, and the button and simple FDP-VP repair was not statistically different from each other.
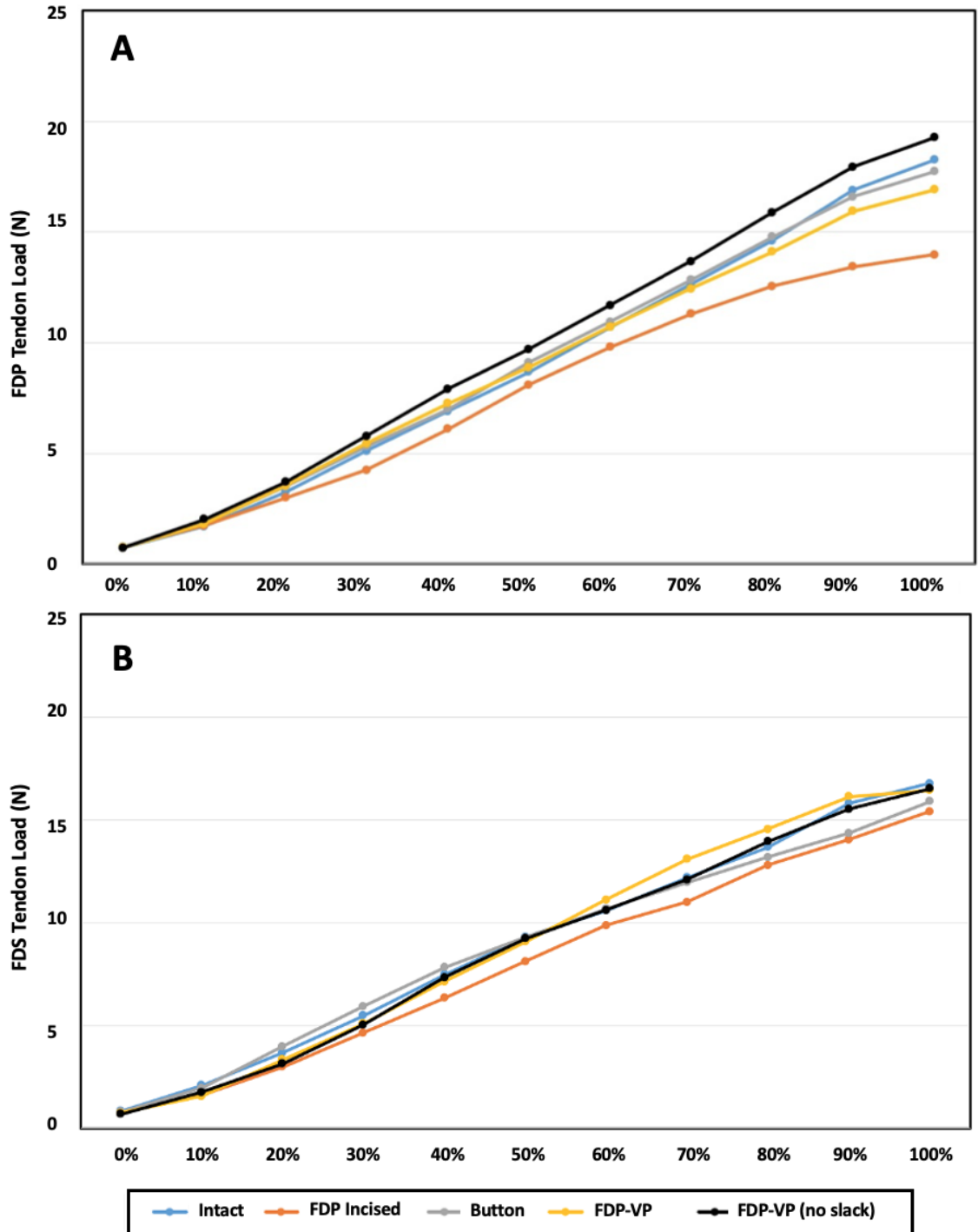
Figure 7.4: Tendon Load vs. Finger Flexion

Flexor tendon loads experienced by a) FDP and b) FDS as a function of percent flexion range. Tendon loads increased with flexion angle for every condition (p<0.001).
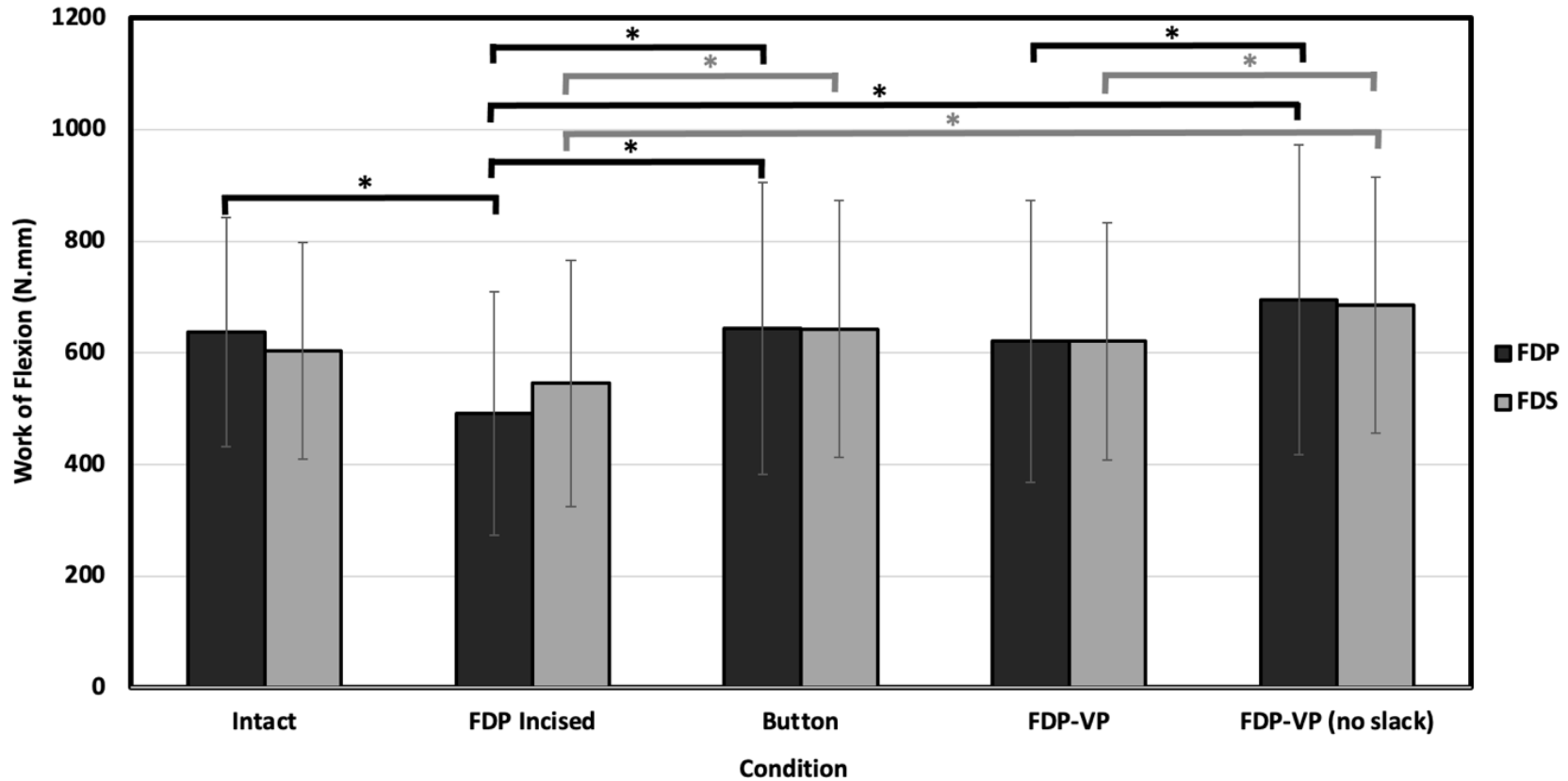
Figure 7.5: Work of Flexion

Work of flexion summed over the full range (WOF) as a function of repair type, where whiskers denote one standard deviation of 14 digits (*p<0.05). All repairs restored lost WOF to the intact condition (p=1.000). Compensating for tendon shortening with the FDP-VP (no slack) repair further increased WOF to the simple FDP-VP. Overall, tendon WOF was not significantly affected by any repair type.

7.3.2 Kinematics

Finger ROM was not altered by the choice of repair. Incision of the FDP reduced DIPJ ROM along the flexion-extension axes by 61.7±11.4° (p<0.001) and reduced the overall finger ROM by 68.6±13.9° (p<0.001) (Figure 7.6). Subsequent correction of the deformity with the button and FDP-VP techniques restored lost total active ROM by 65.1±10.7° (p<0.001) and 62.3±14.4° (p<0.001), respectively.
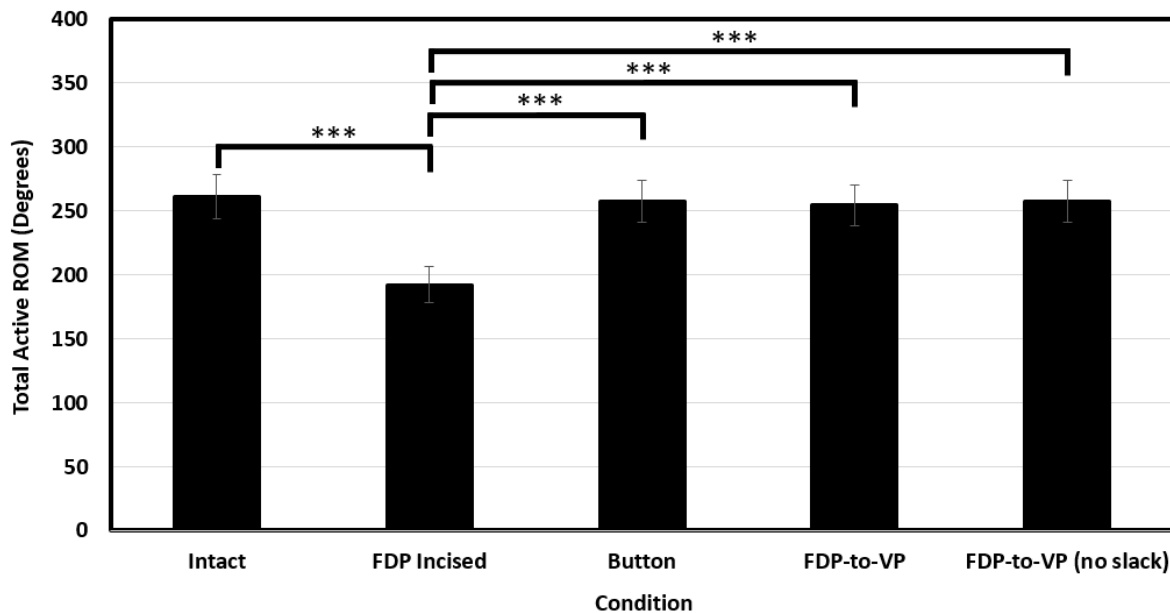
Figure 7.6: Total Active Range of Motion

Total ROM was calculated as the sum of all finger joints DIPJ to MCPJ as a function of finger condition (***p<0.001), where whiskers denote one standard deviation of 14 digits. Following the injured condition, the button and FDP-VP techniques both restored lost ROM, and there was no statistically significant difference between repairs.

Flexion kinematics were consistent with the literature (Figure 7.7)[21,23–25]. Incision of FDP disabled DIPJ ROM as expected, significantly reducing the normal abduction-adduction pathway by 6.1±3.6° (p<0.05) compared to intact. In addition, the PIPJ's normal abduction-adduction pathway by up to 10°, compared to intact. The button and 'no slack' FDP-VP repairs restored kinematics along the abduction/adduction plane to the intact state with no significant difference. Moreover, the simple FDP-VP repair provided 4.8±3.8° of recovery of

abduction/adduction angle in the DIPJ and 4.98±3.5° of recovery in PIPJ. Internal/external rotation kinematics were not affected by any condition.
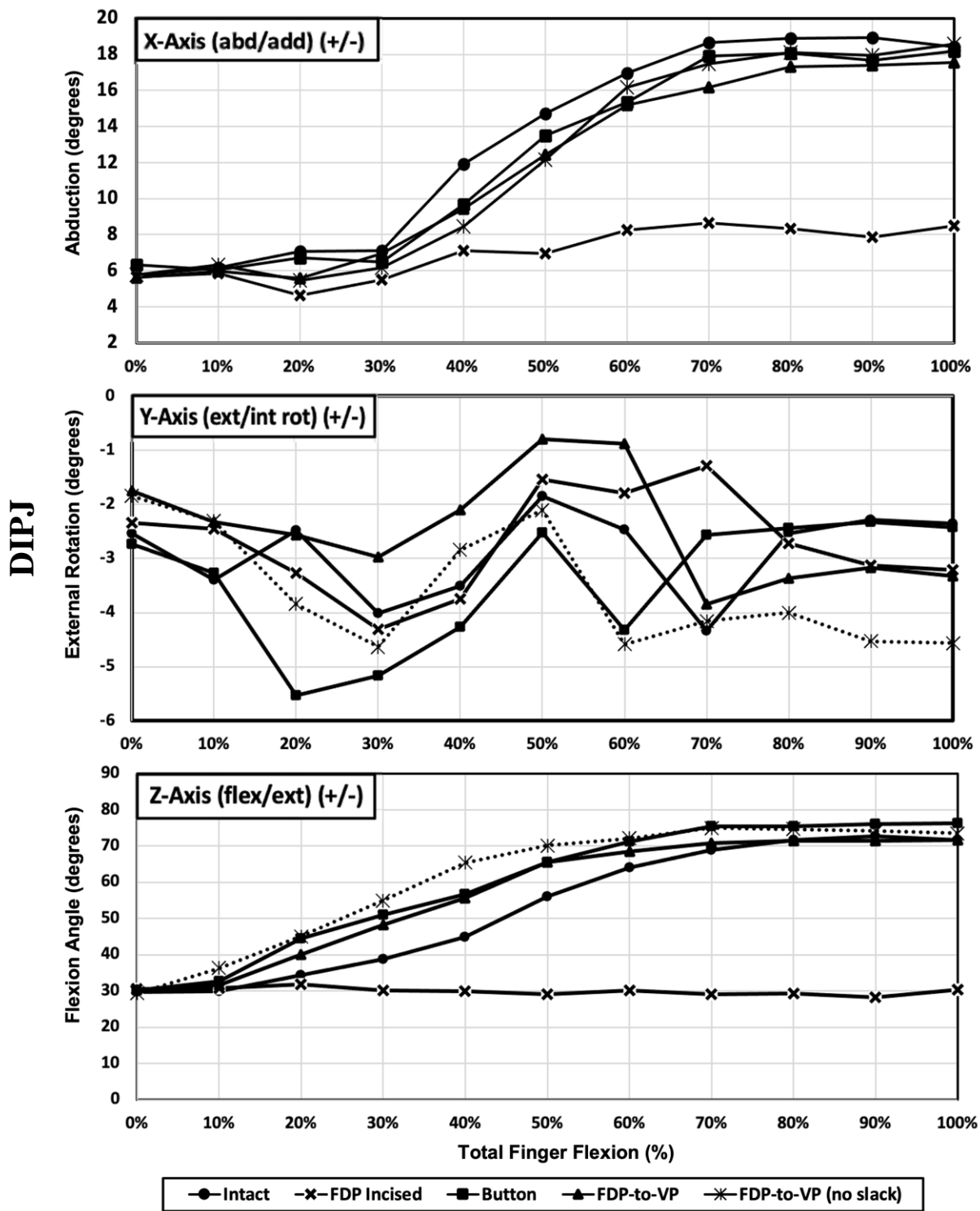
Figure 7.7: Finger Joint Kinematics
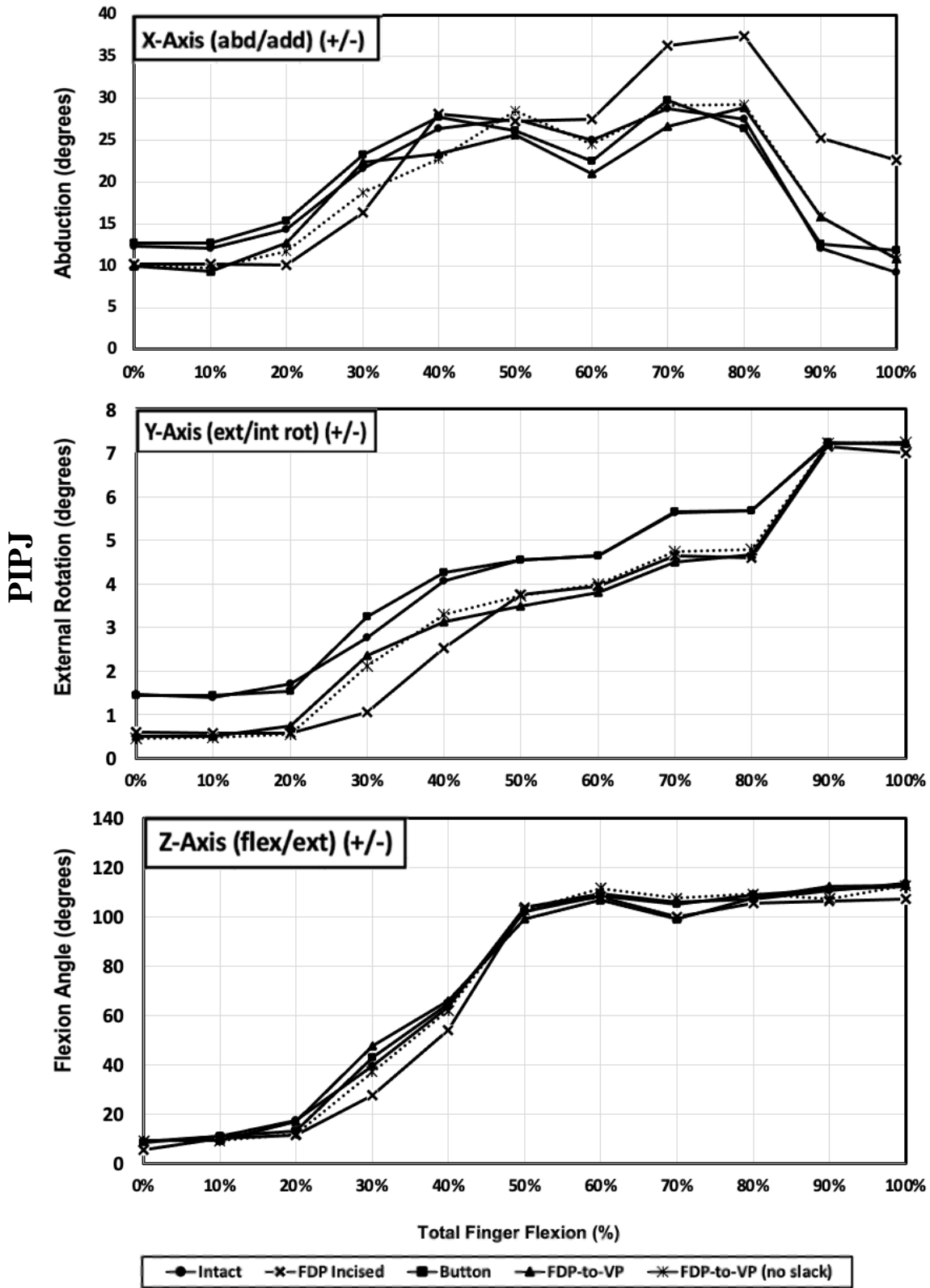
Figure 7.7: continued
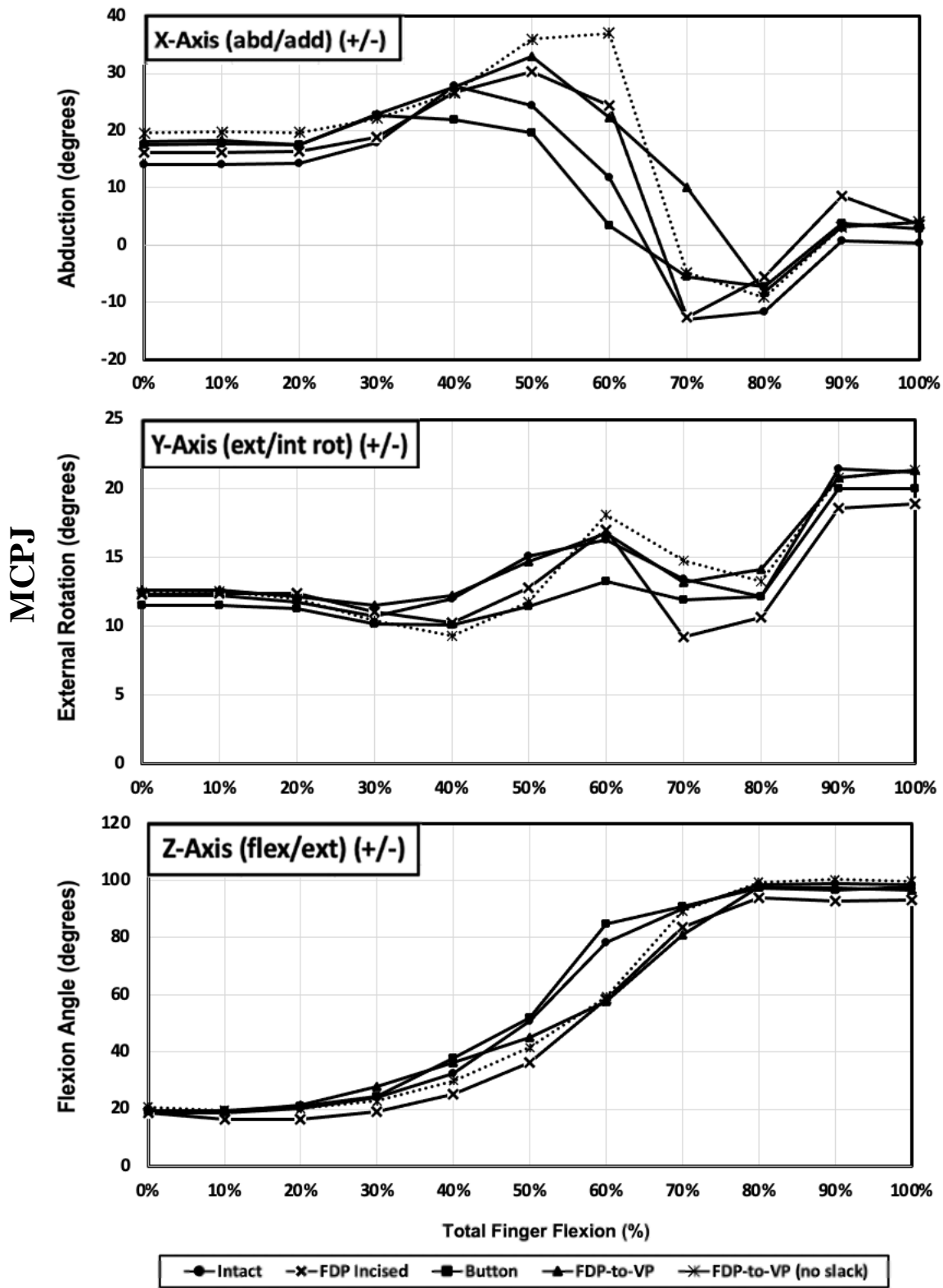
Figure 7.7: continued

7.3.3 Fingertip Strength

Finger condition had an overall significant effect on fingertip strength at full flexion ($p<0.001$) (Figure 7.8). Incision of the FDP tendon resulted in a 65% decrease of 6.4 ± 2.3 N ($p<0.001$). The button repair restored fingertip force with no significant difference from the intact condition. The FDP-VP repair restored forces by 31%, but was still statistically different from intact ($p<0.001$). The 'no slack' adjustment further increased fingertip force by 0.9N, yet still statistically different from intact ($p<0.05$).
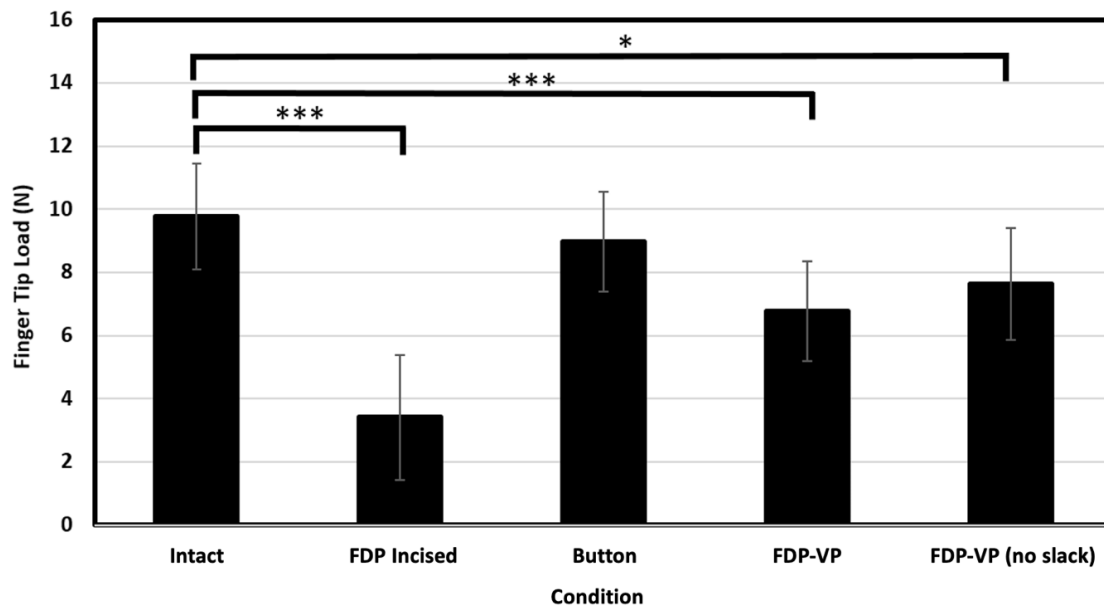
Figure 7.8: Fingertip Strength

Fingertip loads were measured at full tendon flexion excursion with a load cell interposed on the palm (Figure 7.3). Incision of the FDP tendon resulted in a significant decrease in fingertip load compared to the intact condition ($p<0.001$). Surgical correction of the tear using the button and FDP-VP techniques significantly restored loads compared to the FDP incised condition. Adjustment in tendon slack further increased fingertip loads compared to the FDP-VP condition ($p<0.05$), yet still statistically significant from the intact condition ($p<0.05$).

7.3.4 PIPJ Volar Plate Strain

Volar plate strains at the PIPJ were measured at full finger extension where strains were measured with respect to the baseline intact condition across all finger conditions (Figure 7.9). Incision of the FDP resulted in significantly increased volar plate strains by 0.24 ± 0.2 milli-strain (joint hyper-extension) compared to the intact condition (p=0.006). Surgical correction of the tendon through the button technique significantly reduced strains by 0.39 ± 0.3 milli-strain compared to the incised condition (p=0.003). This was a 271% reduction, which restored volar plate strain to within a statistically non-significant difference from the intact condition. Correction of the tendon through a FDP-VP technique also significantly reduced strains by 0.38 $\pm$ 0.3 milli-strain compared to the incised condition (p=0.003). Further correction of the tendon slack caused an additional reduction of 0.02 ± 0.05 milli-strain, which was also a statistically significant reduction from the incised condition (p=0.004), though not significantly different from the FDP-VP condition (p=1.000)
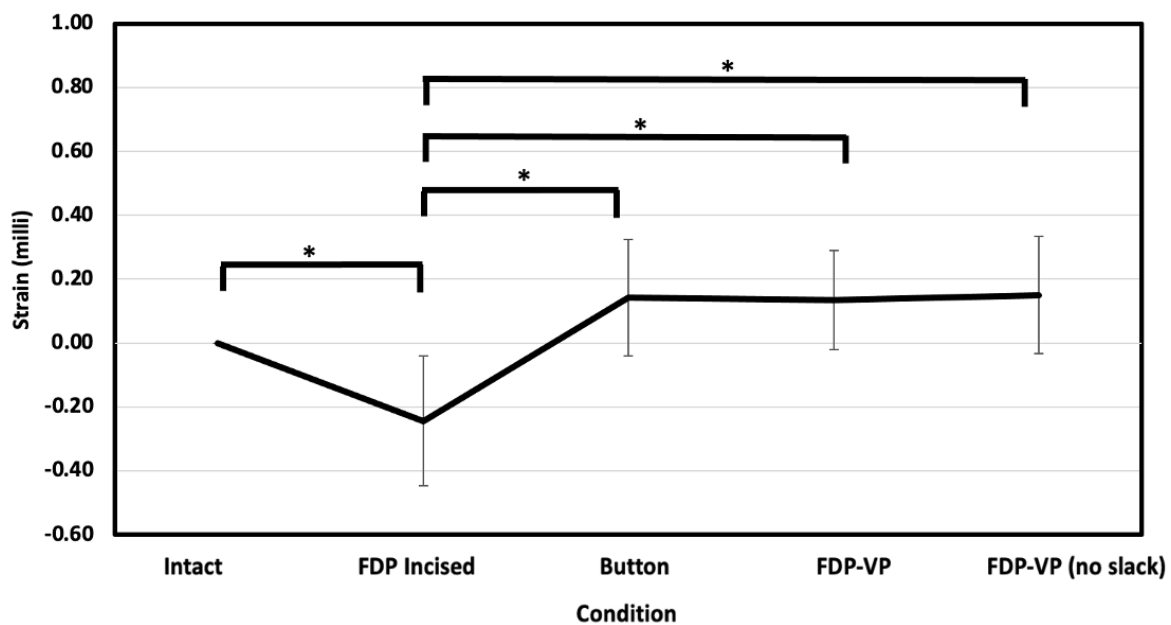
Figure 7.9: PIPJ Volar Plate Strain

*At full finger extension, the volar plate strain at the PIPJ is plotted as a function of finger condition (*p<0.05), where whiskers denote standard deviation of 14 digits.*

7.4   Discussion

The aim of this study was to measure and evaluate the biomechanics and effectiveness of a novel FDP-VP technique compared to the commonly used button repair, following a zone I FDP tendon avulsion. We found that both the pullout button and FDP-VP techniques restored WOF and ROM to within intact levels, with no statistically significant difference. The only difference in performance was detected in fingertip peak strength, in which the button nearly restored intact levels whereas the FDP-VP repairs produced less peak strength at full flexion. It is notable that while the loss was statistically significant, it amounted to only 1-2 N below the button, which is likely not a clinically relevant difference.

Neither repair altered the WOF from the intact condition, and there was no difference between repair both repair types. The 'no slack' variation, of increasing tension over the simple FDP-VP repair, increased WOF by 12% and 10% for FDP and FDS, respectively, but still not significantly higher than the intact or button conditions. Nonetheless, this may indicate that attempting to compensate for the effective tendon lengthening in this manner can increase tendon load, and should be done carefully so as not to increase the chance of post-operative rupture. Further investigation would be needed to determine the balance between effectiveness versus risk (if any) of the 'no slack' variation to the FDP-VP repair.

The kinematic analysis revealed that the DIPJ was significantly altered following FDP avulsion resulting in a minor deviation of up to 4° along the abduction/adduction plane (Figure 7.6). All repairs restored the intact kinematic pattern. Most notable differences between the repairs occurred within the first half of flexion, where higher tension repairs (button and 'no slack' FDP-VP) over-corrected the kinematics while the lower-tension FDP-VP provided less restoring moment to DIPJ. This suggests that, regardless of the technique used, the FDP repair tension can have a significant impact on the overall pathway of the DIPJ. It is unclear how this effect might change with time and healing. Nonetheless, both the button and 'no slack' FDP-VP repairs effectively restored time-zero kinematics without significant deviations from intact.

The reduced fingertip strength of the FDP-VP repairs is explained by the compliance of the volar plate compared to the more rigid anchoring of the button. The tendon excursions were controlled to the same full flexion amounts as in the intact condition; thus, the compliance of the

volar plate would have produced less resistance to flexion and resulted in a lower peak contact force at the fingertip. Even the increased FDP tension of the 'no slack' variation, which was evidence by significantly increased WOF compared to the simple FDP-VP, was not sufficient to reach the fingertip force of the intact condition, although this was a mean loss of only 2 N. The peak fingertip strength was an aggressive test - equivalent to holding 1 kg at the distal phalanx – and it was intended to challenge the repairs. So it is notable that the FDP-VP repairs survived 84 strength trials (2 FDP-VP repairs × 14 fingers × 3 repeated trials) and no rupture or tear was observed, which supports the time-zero robustness of this repair.

Limitations should be considered when interpreting the results: (1) the cadaveric specimens used were previously frozen and of advanced age; (2) amputation of the arm proximal to the wrist was necessary to accommodate the simulator; (3) sacrificing of the tendon sheath and A5 pulley to gain access to the volar plate was unavoidable and may have altered the biomechanics of the finger. However, sacrificing A5 is necessary to perform any repair, and the collateral ligaments were confirmed to be intact; thus, this limitation was still clinically relevant.

Despite its limitations, this study has important strengths. The use of a validated active motion simulator allowed precise measurements in isolated conditions. To the author's knowledge, this is the first biomechanics study to evaluate the proposed FDP-VP repair. Moreover, a repeated-measures experimental design was employed, and thus any changes in the biomechanics due to the amputation, or other limitations, were applied equally to all tested conditions.

7.5   Conclusion

The FDP-VP technique may be an effective alternative to a pullout button repair. Based on its initial strength and its equal biomechanical performance compared to the button repair, the FDP-VP technique is a viable option for treating FDP avulsions. This study provides biomechanical support to the clinical trials that have previously been conducted.

7.6   References

1.   de Jong JP, Nguyen JT, Sonnema AJM, Nguyen EC, Amadio PC, Moran SL. The Incidence of Acute Traumatic Tendon Injuries in the Hand and Wrist: A 10-Year Population-based Study. *Clin Orthop Surg*. 2014;6(2):196-202. doi:10.4055/CIOS.2014.6.2.196

2.   Brar R, Owen JR, Melikian R, Gaston RG, Wayne JS, Isaacs JE. Reattachment of Flexor Digitorum Profundus Avulsion: Biomechanical Performance of 3 Techniques. *J Hand Surg Am*. 2014;39(11):2214-2219. doi:10.1016/J.JHSA.2014.07.054

3.   JB T. Clinical outcomes associated with flexor tendon repair. *Hand Clin*. 2005;21(2):199-210. doi:10.1016/J.HCL.2004.11.005

4.   NS M, D E. Primary flexor tendon repair in zone 1. *J Hand Surg Br*. 2000;25(1):78-84. doi:10.1054/JHSB.1999.0319

5.   Bidwai ASC, Feldberg L. The Button-Over-Nail Technique for Zone I Flexor Tendon injuries. *http://dx.doi.org.proxy1.lib.uwo.ca/101142/S0218810412500323*. 2012;17(3):365-369. doi:10.1142/S0218810412500323

6.   Dovan TT, Gelberman RH, Kusano N, Calcaterra M, Silva MJ. Zone I flexor digitorum profundus repair: an ex vivo biomechanical analysis of tendon to bone repair in cadavera. *J Hand Surg Am*. 2005;30(2):258-266. doi:10.1016/J.JHSA.2004.11.007

7.   Luenam S, Kosiyatrakul A, Prachaporn S. Pullout button suture for the treatment of type IV avulsion of the flexor digitorum profundus tendon: case report. *J Med Assoc Thai*. 2012;95 Suppl 5:S172-6.

8.   Evans RB. A study of the Zone I flexor tendon injury and implications for treatment. *J Hand Ther*. 1990;3(3):133-148. doi:10.1016/S0894-1130(12)80392-9

9.   Huq S, George S, Boyce DE. Zone 1 flexor tendon injuries: A review of the current treatment options for acute injuries. *J Plast Reconstr Aesthetic Surg*. 2013;66(8):1023-1031. doi:10.1016/J.BJPS.2013.04.026

10.   Schultz RO, Drake DB, Morgan RF. A new technique for the treatment of flexor digitorum profundus tendon avulsion. *Ann Plast Surg*. 1999;42(1):46-48.

doi:10.1097/00000637-199901000-00008

11. Sood MK, Elliot D. A new technique of attachment of flexor tendons to the distal phalanx without a button tie-over. *J Hand Surg Br*. 1996;21(5):629-632. doi:10.1016/s0266-7681(96)80146-x

12. Teo TC, Dionyssiou D, Armenio A, Ng D, Skillman J. Anatomical repair of zone 1 flexor tendon injuries. *Plast Reconstr Surg*. 2009;123(2):617-622. doi:10.1097/PRS.0b013e3181956572

13. Al-Qattan MM, Al-Turaiki TM, Al-Zahrani AY, Al-Harbi MS, Al-Kahtani FS. A new technique of flexor profundus repair in the distal part of zone i: Inclusion of the palmar plate. *J Hand Surg Eur Vol*. 2010;35(6):459-463. doi:10.1177/1753193410365631

14. Al-Dubaiban WI, Al-Abdulkarim AO, Arafah MM, Al-Qattan MM. Flexor Tendon–to–Volar Plate Repair: An Experimental Study and 3 Case Reports. *J Hand Surg Am*. 2014;39(11):2222-2227. doi:10.1016/J.JHSA.2014.08.028

15. Al-Qattan MM. Suturing of the flexor digitorum profundus tendon to the entire volar plate in distal zone I injuries. *J Plast Surg Hand Surg*. 2015;50(2):1-6. doi:10.3109/2000656X.2015.1111840

16. Al-Qattan MM. Use of the Volar Plate of the Distal Interphalangeal Joint as a Distally Based Flap in Flexor Tendon Surgery. *J Hand Surg Am*. 2016;41(2):287-290. doi:10.1016/J.JHSA.2015.11.004

17. Haddara M. Development of an Active Finger Motion Simulator: With In-Vitro Assessments of Tendon Loads and Joint Kinematics. 2017:34-44.

18. Kadar A, Haddara MM, Fan S, Chinchalkar S, Ferreira LM, Suh N. Use of Thermoplastic Rings Following Venting of Flexor Tendon Pulleys: A Biomechanical Analysis. *J Hand Surg Am*. 2021;46(6):485-492. doi:10.1016/j.jhsa.2020.11.003

19. Haddara MM, Byers B, Chinchalkar S, Ferreira LM, Suh N. The Effect of Wrist Position on Finger Tendon Loads Following Pulley Sectioning and Operative Reconstruction. *J Hand Surg Glob Online*. 2019;1(3):154-160. doi:10.1016/j.jhsg.2019.04.002

20. Goislard de Monsabert B, Visser JMA, Vigouroux L, Van der Helm FCT, Veeger HEJ. Comparison of three local frame definitions for the kinematic analysis of the fingers and the wrist. *J Biomech*. 2014;47(11):2590-2597. doi:10.1016/j.jbiomech.2014.05.025

21. Coupier J, Moiseev F, Feipel V, Rooze M, Van Sint Jan S. Motion representation of the long fingers: a proposal for the definitions of new anatomical frames. *J Biomech*. 2014;47(6):1299-1306. doi:10.1016/j.jbiomech.2014.02.017

22. Zhao C, Amadio PC, Berglund L, Zobitz ME, An K-N. A new testing device for measuring gliding resistance and work of flexion in a digit. *J Biomech*. 2003;36(2):295-299. doi:10.1016/s0021-9290(02)00300-7

23. Coupier J, Hamoudi S, Telese-Izzi S, Feipel V, Rooze M, Van Sint Jan S. A novel method for in-vivo evaluation of finger kinematics including definition of healthy motion patterns. *Clin Biomech (Bristol, Avon)*. October 2015. doi:10.1016/j.clinbiomech.2015.10.002

24. Degeorges R, Parasie J, Mitton D, Imbert N, Goubier J-N, Lavaste F. Three-dimensional rotations of human three-joint fingers: an optoelectronic measurement. Preliminary results. *Surg Radiol Anat*. 2005;27(1):43-50. doi:10.1007/s00276-004-0277-4

25. Degeorges R, Laporte S, Pessis E, Mitton D, Goubier JN, Lavaste F. Rotations of three-joint fingers: a radiological study. *Surg Radiol Anat*. 2004;26(5):392-398. doi:10.1007/s00276-004-0244-0

Chapter 8

8   Conclusions and Future Work

OVERVIEW: *This chapter revisits the main objectives of the thesis and re-iterates the studies conducted in the context of literature. Important and clinically relevant results and discussions are discussed. Strengths and limitations and future directions of the research are outlined.*

8.1 Summary and Conclusions

Assessment of finger kinematics for biomechanical modelling is valuable for providing the upmost quality of care to a patient suffering from trauma. However, in order to fully understand the biomechanics of the finger, a comprehensive investigation into the influence of different conditions on joint kinematics and load transfers in the finger is essential. The present work discusses the steps taken to develop motion-based coordinate systems for the quantification of joint kinematics, and the advancement and refinement of a previously designed active finger motion simulator for *in-vitro* finger cadaveric studies.

The main objectives first outlined for this work were:

1. Evaluating the rotational and translational accuracy and reliability of using electromagnetic tracking for joint motion tracking and kinematics.

2. Establishing distinct tendon-to-load, work of flexion relationships, and biomechanically driven models *in-vitro* to study the impact of injury on finger biomechanics.

3. Proposal of novel motion derived based frames for finger joint kinematic analysis.

4. Application of the biomechanical innovation developed in this thesis within *in-vitro* cadaveric tests.

Chapter 2: Evaluation and assessment of the translational and rotational accuracy of electromagnetic tracking compared to optical tracking

The first main objective of this thesis was to quantify and directly compare the technical accuracies of the two most widely used tracking modalities using the same accuracy assessment tools and methods within the same setting. This was achieved through a series of tests where the rotational and translational accuracy of the systems were evaluated using two separate motion systems: a coordinate measuring machine and a rotary computer numerical control machine. By driving the trackers to discrete points within the acceptable field of vision of the tested system, the accuracy and repeatability of the trackers were evaluated and quantified using a standard

testing method (ASTM) as a guideline. Moreover, the influence of varying depth levels from the transmitter on the discrepancies in results were evaluated.

Results from this study revealed maximum differences of 0.8 mm and 0.3° in the translational and rotational accuracies of electromagnetic tracking, compared to optical tracking. The translational accuracy of both systems were comparable to the information provided by the manufacturer. Furthermore, unlike optical tracking, different depth levels did not have any significant effect on the accuracy of the system. Therefore, this study concluded that electromagnetic tracking is in fact a reliable and effective tool for the quantification of finger joint kinematics; fulfilling the objective and supporting the hypothesis made in Chapter 1.

Chapter 3: Effect of Flexor Digitorum Profundus Repair Position Relative to Camper's Chiasm on Tendon Biomechanics

The main objective of this cadaveric study was to further enhance the use of the active finger motion simulator for biomechanical modelling through mean of establishing tendon-to-load relationships and work of flexion measures following zone II finger injury (Objective 2). Results obtained in this study revealed a non-linear relationship between tendon load and excursion, refuting the initial hypothesis made. Moreover, repeatability of the simulator and metrics were well within the hypothesized 5% target. Therefore, the goal of this *in-vitro* study was accomplished using the finger motion simulator to measure metrics such as tendon excursion, tendon load, and joint ranges of motion.

Chapters 4 & 5: Development of Swan Neck Model; Effect of FDS Hemitenodesis Repair

Similar to chapter 3, chapters 4 and 5's goal was to further enhance the use of the finger motion simulator by developing a swan neck deformity biomechanical model in chapter 4 followed by chapter 5; a study where the influence of a commonly used repair technique to treat swan neck is evaluated. The biomechanical model was established through the use of minute strain gauges to measure strains induced by the volar plate with the simulation of a mallet finger and swan neck models.

The study in chapter 4 demonstrated results that exhibited an increase in strains at the volar plate with the simulation of the mallet finger and swan neck deformities, respectively. Repair of the deformity in chapter 5 however, restored strains to the native healthy conditions. However, unlike the SND condition, mallet finger condition did not exhibit significant strain changes compared to the native intact condition. Such findings refutes the hypothesis initially made in chapter 1. Nonetheless, the use of a sensitive strain gauges in this study to measure deformation at the volar plate is a novel and effective concept which allowed for the detection of heightened tissue strains, an effect otherwise too small to be measured using kinematic measurement devices at the PIPJ. Furthermore, a strong relationship between volar plate strain and PIPJ hyperextension was observed and established, and the metrics measured were well within the 5% repeatability goal; supporting the use of strain as a surrogate measurement for swan neck.

The application of the finger motion simulator in this study, along with the individual metrics measurement, fulfilled the second objective listed and provided valuable data that was used to develop a model that can be used in future studies to evaluate the influence of different surgical interventions on the strain at the volar plate within a defective digit.

Chapters 6: Evaluation and Comparison of *In-vitro* Joint Kinematics using Motion-Based Coordinate System vs. Anatomical Landmarks

The third objective of this dissertation was to develop reproducible and repeatable finger motion derived coordinate frames (MCS) for joint kinematic quantification. This proposed system was then evaluated and compared to the commonly used coordinate system by means of anatomic landmark definition, as per ISB's recommendations. This objective was accomplished using the electromagnetic tracking and the finger simulator where planar finger flexion-extension was actively simulated to define the primary axes of rotation for the joints.

Results produced from this study supports the hypothesis made in chapter 1 which stated that the MCS and anatomical landmark definitions would result in discrepancies within $10°$ between subjects. Moreover, the repeatability trial measurement from 5 motion cycles results in variations as low as $0.64°$; further validating the accuracy of the local frames defined and the hypothesis made in chapter 1. Thirdly, reliability and reproducibility measures reported insignificant

differences between goniometer measurements and thus, further supporting the validity of the results produced by the MCS.

Chapter 7: The Evaluation of a Novel FDP-to-Volar Plate Zone I Repair Versus Button Repair: An In-Vitro Biomechanics Study

The fourth and final objective of this thesis was to adopt all enhanced and refined methodologies developed through previous chapters and apply them collectively in a clinically relevant *in-vitro* injury model setting. Similar to other cadaveric tests conducted, this study focused on the evaluation of a novel FDP-VP repair technique in the occurrence of a zone I tendon avulsion injury. The use of the motion simulator in quantifying and reporting tendon-load relationships, joint kinematics results, and physiological deformities in the finger, post gauge modifications, are valuable tools for assessing proper finger biomechanics. Such access to advanced tools will aid clinicals and rehabilitation specialists in developing proper patient-specific protocols to enhance future quality of life.

8.2   Strengths and Limitations

The strengths of this body of work is that the active finger motion simulator used is one of the more advanced and refined systems used today for *in-vitro* testing. Its peak performance in terms of its reliability, reproducibility, and overall accuracy increases its credibility as an emerging tools for clinical and biomechanical research purposes. Secondly, the use of a highly sensitive and refined strain gauge is a novel concept that can detect changes in the biomechanics of the finger that other assessment tools lack in reporting. Thirdly, the integration and development of motion based coordinate frames captured real time joint kinematic measurements throughout the entire tested range of motion. Furthermore, the employment of motion based frames allow avoids the need for denuding specimens to locate and digitize unique features on bones, which is a large source of error introducing both intra- and inter-user variabilities that hamper reproducibility across research groups.

Despite the strengths, this work also has limitations that should be considered. Firstly, the in-vitro tests conducted use cadaveric specimens that were previously frozen and of advanced age.

This limitation however was mitigated by having an orthopedic fellow pre-screen specimen CT scans for pathology, prior to testing. Secondly, inability to assess the influence of post-surgical swelling that is expected to occur at time zero *in-vivo* could have affected the work of flexion of tendons and gliding resistance to the surrounding structures; a case that is limited by using cadaveric tissue. Thirdly, amputation of the arm proximal to the wrist is necessary to accommodate the simulator. This loss of tissue and muscles within the forearm is sought to may have minor effects on the trajectory of the fingers during specific motions. Lastly, the need to sacrifice tissues such as tendon sheaths and A3 and A5 pulleys to gain access to volar plate was unavoidable and may have altered the overall biomechanics of the finger. However, sacrificing of the A3 and A5 pulleys are usually necessary to perform any repair and thus, this limitation was still clinically relevant.

A noteworthy strength observed during the in-vitro cadaveric tests is the amount of time taken for full completion of the testing protocol. In light of findings made by Huang *et al.,* Jung *et al.* and Moon *et al.*, chances of significant degradation of peak loads in tendons and the joints within the first 5 freeze-thaw cycles are lowered immensely during such short testing periods; increasing the integrity of the study[1,2,3].

8.3   Future Work

The work included in this thesis has provided considerable improvement in the approach towards kinematic analysis and joint biomechanics in the finger. However, the goals achieved within this thesis have paved more paths that are worth exploring in the future.

Firstly, the simulator is fully CT compatible and therefore, precise 3D joint segmentation and measurements can be analyzed and further used to validate the accuracy of the derived motion based coordinate frames.

Secondly, the incorporation of more muscles and ligaments, such as lumbrical muscles, through loading will allow for a clearer, more refined, pathway of finger motion; mimicking true in-vivo scenarios. This integration would be of clinical significance when carrying out future cadaveric studies.

Implant development for joint arthroplasty is currently in its infancy, but is also a very interesting and draws many exciting clinical questions. Therefore, a possible application of the finger simulator is in invasive finger joint implant studies. The studies would quantify and evaluate the impact of different joint implants on the overall integrity of the finger, both biomechanically and physiologically. Such studies would produces clinically relevant outcomes that can, in the future, result in patient specific finger wearable designs.

Finally, other proposed studies would involve incorporating wrist motion, along with finger motion to examine the effects of a pre-and post-injury and repair condition to understand the influence of trauma on the integrity of the hand.

8.4   References

1. Huang H, Zhang J, Sun K, Zhang X, Tian S. Effects of repetitive multiple freeze-thaw cycles on the biomechanical properties of human flexor digitorum superficialis and flexor pollicis longus tendons. *Clin Biomech (Bristol, Avon)*. 2011;26(4):419-423. doi:10.1016/j.clinbiomech.2010.12.006

2. Jung HJ, Vangipuram G, Fisher MB, et al. The effects of multiple freeze-thaw cycles on the biomechanical properties of the human bone-patellar tendon-bone allograft. *J Orthop Res*. 2011;29(8):1193-1198. doi:10.1002/jor.21373

3. Moon DK, Woo SL, Takakura Y, Gabriel MT, Abramowitch SD. The effects of refreezing on the viscoelastic and tensile properties of ligaments. *J Biomech*. 2006;39(6):1153-1157. doi:10.1016/j.jbiomech.2005.02.012

Appendix A: Glossary

ANOVA	Analysis of Variance, a statistical method for simultaneous comparisons among means
Axial	Plane situated in the central part of the body, separating the head and trunk from the limbs. Also known as the transverse plane
Cadaver	Dead body preserved especially for scientific study or medical use
Computed Tomography (CT)	Medical imaging method used to generate a three-dimensional image of the inside of an object using a series of two-dimensional images
Denude	Stripping soft tissue off bones
Distal	Situated away from the center of the body; opposite to proximal
Extension	Straightening part of a body from a bent to straight position so that the angle of the articulating bones attached to the joint increases; opposite to flexion
Extensor	Muscle responsible for the straightening of the limb
Epiphysis	Expanded end of the long bones which ossifies separately from the bone shaft

Flexion	Movement of body part from a straight to a bent position so that the angle of the articulating bones attached to the joint decrease; opposite to extension
Flexor	Muscle responsible for the bending of the limb
Helical Axes (HA)	Motion of a rigid body broken down into a rotation about, and a translation along, a single axis varying from one moment to the next; also referred to as screw axis
Incise	To cut
In-vitro	Performed outside of a living body
In-vivo	Performed within a living body
Joint	Point where bones make contact
Kinematics	Study of motion without consideration of the forces that caused the motion. Measure of the angles formed in the joints along all planes.
Ligament	Tissue connecting bone to bone
Load cell	Transducer that converts force into a measurable electrical output
Proximal	Situated nearest to the point of reference; opposite to distal

Range of Motion (ROM)	Amount of motion attained during an activity
Radius	Outer bone situated in forearm; viewed with palm in standard anatomical position
RMSE	Root mean square error
Suture	To attach structures to one another
Strain	A measure of deformation, calculated as the change in length over the original length
Tendon	Fibrous tissues that connect muscle to bone
Ulna	Inner bone situated in forearm; viewed with palm in standard anatomical position
Volar	Pertaining to the front or palm; opposite to dorsal
Volar Plate (VP)	Thick tissue that connects bone to bone, overlaying the proximal and distal interphalangeal joints in the finger
Work of Flexion (WOF)	Measure of load required to move the finger

Appendix B: Strain Gauge Modifications

Overview

Volar plate strain was measured using a small pre-wired strain gauge (Model #:KFH-3-350-C1-11L3M3R, Omega, Norwalk, CT) that was inserted under the volar plate, and then sutured down into the plate and further reinforced with surgical tape and Mastisol liquid adhesive.

Rationale

Pilot strain data collected from chapter 4 was found to be inconsistent between trials. More specifically, some strain data trends did not exhibit the same magnitude of increase compared to other data measured under the same conditions for different specimens. In addition, further analysis of the pilot data revealed discrepancies in strain polarity measurements. Cause of data incongruities is hypothesized to be a factor of the gauge's sensitivity to detect changes between injury conditions. Moreover, the slender thickness of the gauge's structure is also hypothesized to be the cause of divergence in strain trends due to inconsistent bending directions of the gauge under the plate during finger motion. Consequently, in contrast to the swan neck condition, the sensitivity of the existing model was not ample enough to detect minor strain changes when a mallet finger was first induced. This drawback in the gauge was a limitation that required addressing and thus, the purpose of this experiment was to enhance the sensitivity of the gauge to allow for better consistency in strain readings between subjects in future tests.

Impact of Substrate on Strain Readings

To further refine the data collected using the strain gauge, the overall thickness of the gauge was altered by adhering a substrate of different material composition than that of the strain gauge. Varying the thickness of the gauge will in return result in an increase in ratio of tensile reinforcement of the gauge's cross-section. Furthermore, this increase in ratio will result in a shift of the location of the neutral axis in the direction of the tension area. Based on the strain-curvature relationship below,

$$\varepsilon_x = -\kappa y, \quad \text{where curvature } \kappa = \frac{1}{\rho} \tag{1}$$

Strain, ε , is proportional to curvature and varies linearly with distance 'y' from the neutral axis. Although ductility of the cross section is impacted, this refinement in the physical model is advantageous as an increase in reinforcement ratio will result in the amplification of strain values recorded under the volar plate.

Experimental Setup

Five 10 mm x 6 mm pieces of electrical tape were constructed; ranging from 0.1 to 0.5 mm in thickness. One pre-wired strain gauge was placed on each piece of electrical tape and adhered using a Mastisol, a non-water soluble liquid adhesive; ensuring that the electrical wire leads are facing away from the adhered surface of the gauge (Figure B.1). Once bonded, the gauge was then mounted onto a 0.8 mm thick steel beam using clear tape. Caution was taken to ensure that the tape doesn't not adhere the gauge to the beam by using a small sheet of paper as a barrier between the gauge and the tape (Figure B.2). Two steel clamps were distanced 14.5 cm apart and then fastened down to hold the steel beam in place. Lastly, a cylindrical tube (Ø 0.7 mm) was used to deflect the beam to allow for strain reading and evaluation (Figure B.3). Such use of a cylindrical tube resulted in same beam deflections between trials and thus, allowed for a more repeatable and reliable evaluation of strain measurement between different gauges tested
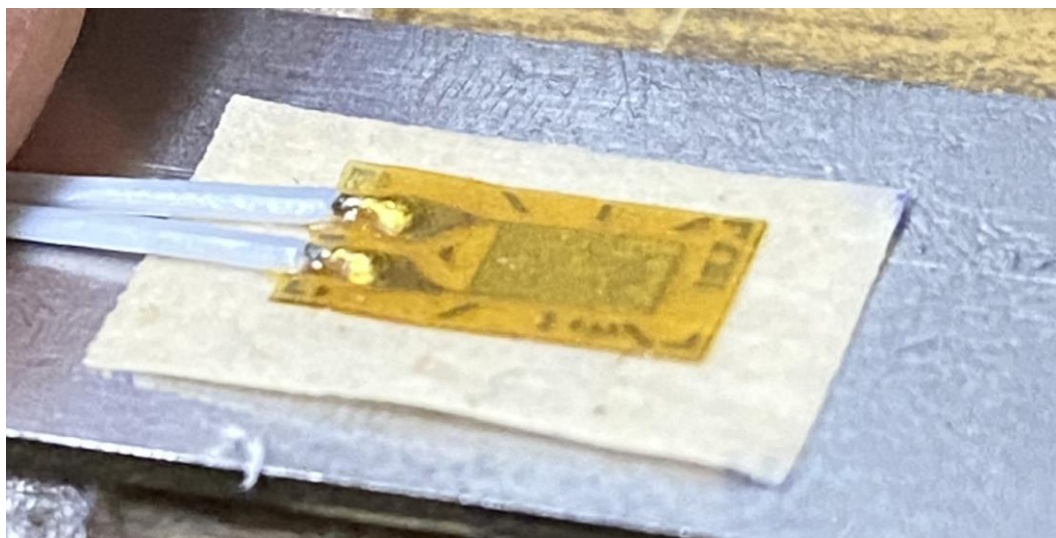
Figure B.1: Strain gauge with the attached 0.1 mm substrate model
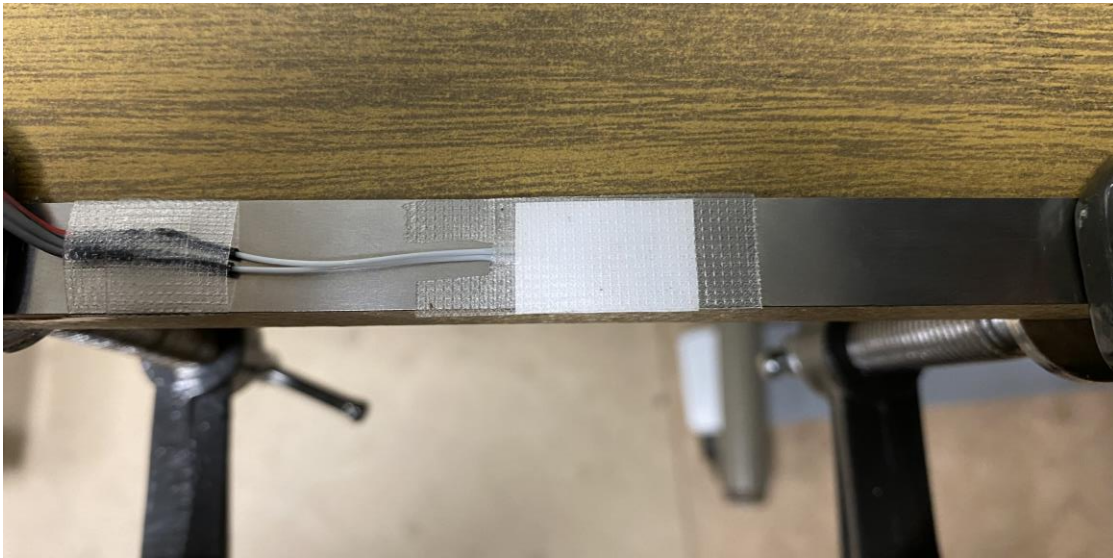
Figure B.2: Fixation of the stain gauge onto beam using surgical tape. Strain-Tape Experimental Setup on Beam

Figure B.3: Beam deflection using a 0.7 mm diameter rod for strain measurement

All strain gauges were properly calibrated and biased prior to testing. Strain readings were measured and recorded using a data acquisition board (DAQx, National Instruments, Waterloo, Canada) where output values were plotted and compared.

To ensure that the degree of sensitivity from the enhanced model is sufficient, the same set of strain data collected in chapter 4 was magnified by the degree of strain amplification achieved with the new model and then statistically re-analyzed to determine if the statistics between conditions was positively influence by the re-modeling of the gauge. Originally, the data collected in chapter 4 reported strain increases of 0.3 and 0.6 milli strain with the simulation of the mallet finger and swan neck conditions, respectively, compared to the intact condition. However, in contrast to the swan neck condition, the repeated-measured ANOVA statistics model did not detect significant change between the mallet and intact conditions.

Results

1. *Strain Sensitivity as a Function of Substrate Thickness*

Strain increased linearly with thickness, reaching a peak reading at 0.2 mm before declining (Figure B.4). Causes of decline is hypothesized to be due to the bulkiness of the gauge as stiffness is increased to a degree where the gauge is no longer following the curvature of the ruler. This is also hypothesized to be the same case with the volar plate as the plate itself is soft so a thicker substrate would result in resistance in bending.
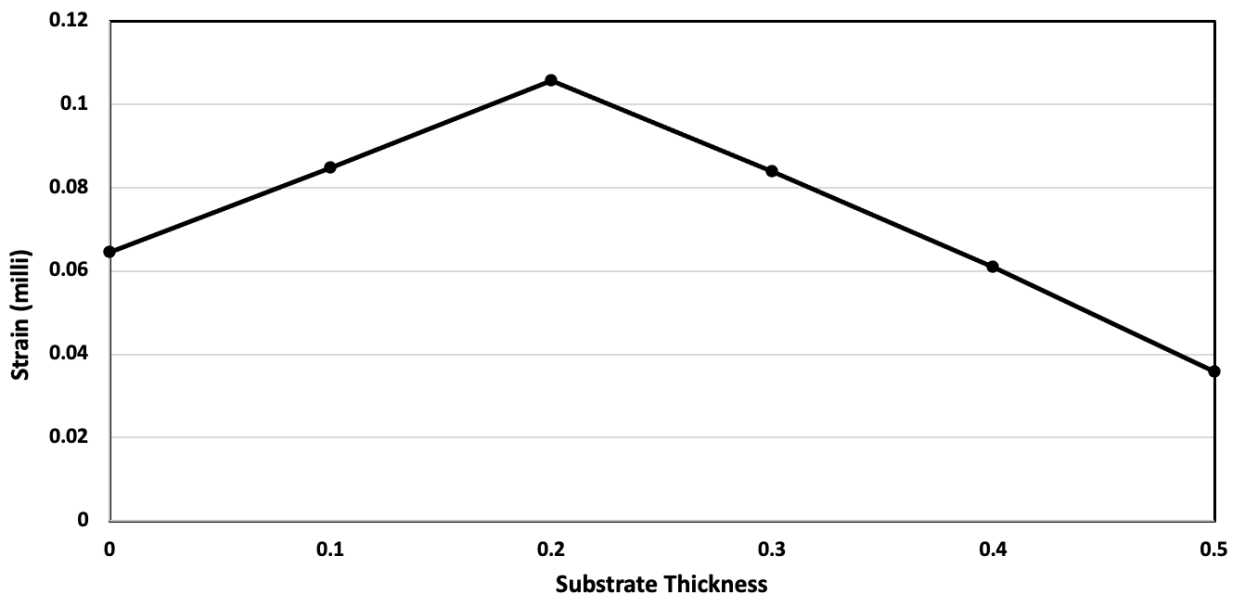
Figure B.4: Influence of increasing substrate thickness on strain readings

2. *Swan Neck Model Re-analysis*

By applying the factor of amplification detected with the re-designed model and manually correcting the set of results from chapter 4, strain changes between conditions was significantly enhanced by approximately 0.6 and 0.9 milli strain for the mallet finger and swan neck conditions, respectively, compared to the intact condition. Moreover, new pairwise significance in the data were found between the intact and mallet finger conditions ($p<0.05$).

Discussion

Modifications to the thickness of the substrate were made to refine and increase the reliability of strain measurements read by the gauge under the volar plate. Increasing the substrate thickness to 0.2 mm resulted in a 164% (factor of 1.64) amplification of strain, compared to the unaltered gauge.

To ensure that the degree of amplification is ample enough for future studies, supplementary evidence using previously analyzed data from the swan neck deformity model chapter (chapter 4) was conducted. Findings from the re-analyzed data revealed new significances between condition that the unaltered gauge failed to initially detect and thus, further validating the influence of increasing thickness on the overall sensitivity of the gauge.

As a result, the modified strain gauges within the finger now allow for more sensitive and reliable detection of changes and load imbalances as a result of different injury conditions. This ultimately enhances the development and quantification of joints and biomechanical modelling.

Appendix C: Copyright Permissions

CCC Marketplace™

This is a License Agreement between Mohammad Haddara ("User") and Copyright Clearance Center, Inc. ("CCC") on behalf of the Rightsholder identified in the order details below. The license consists of the order details, the CCC Terms and Conditions below, and any Rightsholder Terms and Conditions which are included below.

All payments must be made in full to CCC in accordance with the CCC Terms and Conditions below.

Order Date	19-Jan-2022	Type of Use	Republish in a thesis/dissertation
Order License ID	1179511-1		
ISSN	0363-5023	Publisher	W.B./SAUNDERS CO.
		Portion	Chapter/article

LICENSED CONTENT

Publication Title	The Journal of hand surgery	Language	English
		Country	United States of America
Article Title	The Effect of Flexor Digitorum Profundus Repair Position Relative to Camper Chiasm on Tendon Biomechanics	Rightsholder	Elsevier Science & Technology Journals
		Publication Type	Journal
Author/Editor	AMERICAN SOCIETY FOR SURGERY OF THE HAND.		
Date	01/01/1976		

REQUEST DETAILS

Portion Type	Chapter/article	Rights Requested	Main product
Page range(s)	78-92	Distribution	Worldwide
Total number of pages	14	Translation	Original language of publication
Format (select all that apply)	Print, Electronic		
		Copies for the disabled?	No
Who will republish the content?	Academic institution	Minor editing privileges?	No
		Incidental promotional use?	No
Duration of Use	Life of current edition		
Lifetime Unit Quantity	More than 2,000,000	Currency	CAD

NEW WORK DETAILS

Title	The Development of Motion-Based Coordinate System for Finger Modelling	Institution name	Western University
		Expected presentation date	2022-03-21
Instructor name	Mohammad Haddara		

ADDITIONAL DETAILS

Order reference number	N/A	The requesting person / organization to appear on the license	Mohammad Haddara

Craig Myles
Senior Rights Coordinator
SAGE Publications, Inc.
2455 Teller Road
Thousand Oaks, CA 91320
USA

January 19, 2022

Dear Mohammad Haddara,

As you are the author of "Effect of a Flexor Digitorum Superficialis Hemitenodesis on Reducing Volar Plate Strains for Swan Neck Deformities" from the SAGE journal, '*HAND*,' I am pleased to report we can grant your request to include your article as part of your thesis.

Permission is granted for the life of the thesis on a non-exclusive basis, in the English language, throughout the world in all formats provided full citation is made to the original SAGE publication. Permission does not include any third-party material found within the work. Please contact us for any further usage of the material.

If you have any questions, or if we may be of further assistance, please let us know.

Best wishes,

Craig Myles
Senior Rights Coordinator

SAGE Publishing

Mary Ann Price
Rights Coordinator
SAGE Publications, Inc.
2600 Virginia Ave NW, Suite 600
Washington, DC 20037
USA

January 27, 2022

Dear Mohammad Haddara,

As you are the author of " Development of an In Vitro Swan Neck Deformity Biomechanical Model" from the SAGE journal, 'HAND,' I am pleased to report we can grant your request to include your article as part of your thesis.

Permission is granted for the life of the thesis on a non-exclusive basis, in the English language, throughout the world in all formats provided full citation is made to the original SAGE publication. Permission does not include any third-party material found within the work. Please contact us for any further usage of the material.

If you have any questions, or if we may be of further assistance, please let us know.

Best wishes,
Mary Ann Price
Rights Coordinator

Curriculum Vitae

MOHAMMAD M HADDARA

Roth|McFarlane Hand and Upper Limb Centre St. Joseph's Health Care, London, ON
CMHR University Hospital, London, ON.
CIHR Strategic Training Program in Musculoskeletal Health Research and Leadership, London, ON.

EDUCATION

Postgraduate Doctoral Degree of Engineering Science (MESc), Biomedical
Engineering, Biomechanics
Western University   *London, Ontario 2018- Expected Graduation April 2022*
Supervisor: Dr. Louis M. Ferreira
Research Project: Development of Motion-Based Coordinate Finger Frames using a
Refined Active Finger Motion Simulator: With in-vitro Assessment and Quantification of
Finger Biomechanics and Kinematics

Masters of Engineering Science (MESc), Biomedical Engineering, Biomechanics
Western University   *London, Ontario 2015- June 2017*
Supervisor: Dr. Louis M. Ferreira
Research Project: Development of an Active Finger Motion Simulator: With In-Vitro
Assessments of Tendon Loads and Joint Kinematics

Bachelor of Engineering Science (BESc), Mechatronics Engineering
Western University   *London, Ontario 2011- 2015*

RELEVANT RESEARCH EXPERIENCE

Graduate Research Assistant, Biomechanics
Roth|McFarlane Hand and Upper Limb Centre St. Joseph's Health Care, London, ON

Joint Motion Program (JuMP)
University Hospital   *London, Ontario Summer of 2013*
Supervisor: Dr. Louis M. Ferreira, Dr. Timothy Burkhart
Research Project: Tendon Excursion and Adhesion Simulation in Cadaver Hands
Specimens: Comparative Force and Kinematic Analysis.

Work Study
Mechatronics Laboratory,
St. Joseph's Hospital   *London, Ontario   November 2012- 2013*
Western University
Supervisor: Dr. Louis M. Ferreira
Modifying a MotionSation project on LabView; debugging Testing different scripts using a Certus tracking camera Creating codes and functions on LabView
Working with Refman and Reworks databases.

RELEVANT ACADEMIC EXPERIENCE

SunStang Solar Car Project
Western University   *London, Ontario September 2012- April 2015*
Supervisors: Lesley
Mounteer Non-
Technical Manager

Mechatronics Capstone Project
Western University   *London, Ontario September 2014- April 2015*
Supervisor: Dr. Michael Naish
Designing and Building a 5 mm diameter SmartCable for the Davinci surgical instrument that can feedback tensile forces exerted onto them; protecting the patient.

FUNDING AND SCHOLARSHIPS

Joint Motion Program (JuMP)
University Hospital   *London, Ontario*

CMHR Fellowship in Musculoskeletal Health Research and Leadership - $1500
2015 – 2017 Western University

CIHR Fellowship in Musculoskeletal Health Research and Leadership - $6000
Summer of 2013

TEACHING

Graduate Teaching Assistant
ES1050: Engineering Design
Western University   *London, Ontario September 2015 - Present*
Professor: Dr. Jonathan Southen and Dr. John Dickinson
Assisting students with their critical thinking and design development. Evaluating 50 students through presentations, reports, and exams.

MSE 3302: Sensors and Actuators
Western University   *London, Ontario January 2019 - April 2019*
Professor: Dr. Ana Luisa Trejos
Evaluated 54 students through exams and assignment

MSE 4487: Mechatronic Design
Western University   *London, Ontario September 2018 - December 2018*
Professor: Dr. Michael Naish
Evaluated 40 students through exams and assignment

BUS 2299E: Engineering Business
Western University   *London, Ontario September 2015- April 2019*
Professor: Dr. David House
Evaluating 400 students through exams and reports

ENGSCI 4498F: Engineering Ethics
Western University   *London, Ontario Summer 2015*
Professor: Dr. Ayman El Ansary
Evaluated 54 students through exams and assignment

SUPERVISION

Secondary School Students (co-supervised)   *London, Ontario Summer 2015*
James Han, High-School Co-Operative Education Program, *Lucas Secondary School*
 Research Project: Tendon Excursion and Adhesion Simulation in Cadaver Hands
Specimens: Comparative Force and Kinematic Analysis.

ACADEMIC AWARDS

3MT Engineering Competition - $150   *London, Ontario   April 2017*
First Place

PUBLISHED MANUSCRIPTS

Haddara MM, Byers B, Ferreira LM, Suh N. (March 2019) The Effect of Wrist Position on Tendon Loads Following Pulley Sectioning and Operative Reconstruction. Journal of Hand Surgery Global.

Kadar A, **Haddara MM**, Fan S, Chinchalkar S, Ferreira LM, Suh N. (September 2020) Use Of Thermoplastic Rings Following Venting Of Flexor Tendon Pulleys - A Biomechanical Analysis. Journal of Hand Surgery.

Haddara MM, Fan S, Matache B, Chinchalkar S, Ferreira LM, Suh N. (October 2020) Development of an In-Vitro Swan Neck Deformity Biomechanical Model. HAND.

Haddara MM, Kadar A, Ferreira LM, Suh N. (August 2021) Effect of a Flexor Digitorum Superficialis Hemitenodesis on Reducing Volar Plate Strains for Swan Neck Deformities. HAND

Haddara MM, Mitchell EC, Ferreira LM, Gillis J. (Dec 2021) The Effect of Flexor Digitorum Profundus Repair Position Relative to Camper Chiasm on Tendon Biomechanics. Journal of Hand Surgery

ACCEPTED MANUSCRIPTS

Mitchell EC, Haddara MM, Ferreira LM, Gillis J. Strength comparison of fibrin glue and suture constructs in upper extremity peripheral nerve coaptations: an in-vitro study. Journal of Hand Surgery

MANUSCRIPTS UNDER REVIEW

Haddara MM, Mitchel EC, Ferreira LM, Gillis J, Suh N. The Evaluation of a Novel FDP-to-Volar Plate Zone I Repair Versus Button Repair: An In-Vitro Biomechanics Study. Journal of Hand Surgery

PRESENTATIONS & CONFERENCES

*Presenting Author is underlined

Haddara MM, Mitchell EC, Ferreira LM, <u>Gillis J.</u> (September 2021) The Effect of Flexor Digitorum Profundus Repair Position Relative to Camper Chiasm on Tendon Biomechanics. Annual Meeting of the American Society for Surgery of the Han: ASSH. (USA) (Podium) (Grad)

<u>**Haddara MM,**</u> Mitchell EC, Ferreira LM, Gillis J. (May 2021) The Effect of Flexor Digitorum Profundus Repair Position Relative to Camper Chiasm on Tendon Biomechanics. London Health Research Day: LHRD. Virtual Conference. (Canada) (E-Poster) (Grad)

<u>**Haddara MM**</u>, Kadar, A, Ferreira LM, Suh N. (June 2020) The Effect of FDS Hemitenodesis on Reducing Volar Plate Strains for Swan Neck Deformities. Canadian Orthopedic Association: COA. Virtual Conference. (Canada) (E-Poster) (Grad)

Haddara MM, Fan S, Matache B, Chinchalkar S, Ferreira LM, Suh N. (February 2020) Development of an In-Vitro Swan Neck Deformity Biomechanical Model. Orthopedic Research Society. Phoenix, AZ (United Stated) (Poster) (Grad)

<u>**Haddara MM**</u>, Byers B, Ferreira LM, Suh N. (January 2018) The Effect of Wrist Position on Tendon Loads Following Pulley Sectioning and Operative Reconstruction. Canadian Orthopedic Association: COA. Victoria, B.C. (Canada) (Podium) (Grad)

Haddara MM, Byers B, Ferreira LM, Suh N. (January 2018) The Effect of Sequential Flexor Tendon Pulley Sectioning and Reconstruction on Joint Range of Motion and Tendon Load. Canadian Orthopedic Association: COA. Victoria, B.C. (Canada) (Podium) (Grad)

Haddara MM, Byers B, Ferreira LM, Suh N. (January 2018) The Effect of Wrist Position on Tendon Loads Following Pulley Sectioning and Operative Reconstruction. Congress of the Federation of the European Societies for Surgery of the Hand: FEESH. Copenhagen, Denmark. (Europe) (Podium) (Grad)

Haddara MM, Byers B, Ferreira LM, Suh N. (January 2018) The Effect of Sequential Flexor Tendon Pulley Sectioning and Reconstruction on Joint Range of Motion and Tendon Load. Congress of the Federation of the European Societies for Surgery of the Hand: FEESH. Copenhagen, Denmark. (Europe) (Poster) (Grad)

Haddara MM, Byers B, Ferreira LM, Suh N. (January 2018) The Effect of Wrist Position on Tendon Loads Following Pulley Sectioning and Operative Reconstruction. American Association for Hand Surgery: AAHS. Phoenix,Arizona. (U.S.) (Podium) (Grad)

Haddara MM, Byers B, Ferreira LM, Suh N. (January 2018) The Effect of Sequential Flexor Tendon Pulley Sectioning and Reconstruction on Joint Range of Motion and Tendon Load. American Association for Hand Surgery: AAHS. Phoenix, Arizona. (U.S.) (E-Poster) (Grad)

Haddara MM, Ferreira LM. (September 2017) Development of an Active Finger Motion Simulator. Western University Thesis Seminar Presentation. London, ON. (Local) (Podium) (Grad)

Haddara MM, Ferreira LM. (May 2017) Tendon Excursion and Adhesion Simulation: A Cadaveric Force and Kinematic Study. Western University Biomedical Research Day. London, ON. (Local) (Poster) (Grad)

Haddara MM, Ferreira LM. (February 2016) Tendon Excursion and Adhesion Simulation: A Cadaveric Force and Kinematic Study. Western University Thesis Seminar Presentation. London, ON. (Local) (Podium) (Grad)

Haddara MM, Ferreira LM. (April 2015) Kinematics of Tendon Excursion and Adhesion Simulation in Cadaveric Hands. Western University Thesis Presentation. London, ON. (Local) (Podium) (Undergrad)

Haddara MM, Ferreira LM. (April 2015) Use of FBG cables for Force Feedback Analysis on The DaVinci Surgical Tool. Fourth Year Capstone Project. London, ON. (Local) (Poster) (Undergrad)